R-03-24

Modelling of groundwater flow and flow paths for a large regional domain in northeast Uppland

A three-dimensional, mathematical modelling of groundwater flows and flow paths on a super-regional scale, for different complexity levels of the flow domain

Johan G. Holmén and Martin Stigsson
Golder Associates

Niko Marsic and Björn Gylling
Kemakta Konsult AB

December 2003

Svensk Kärnbränslehantering AB
Swedish Nuclear Fuel
and Waste Management Co
Box 5864
SE-102 40 Stockholm Sweden
Tel 08-459 84 00
+46 8 459 84 00
Fax 08-661 57 19
+46 8 661 57 19

ISSN 1402-3091
SKB Rapport R-03-24

Modelling of groundwater flow and flow paths for a large regional domain in northeast Uppland

A three-dimensional, mathematical modelling of groundwater flows and flow paths on a super-regional scale, for different complexity levels of the flow domain

Johan G. Holmén and Martin Stigsson
Golder Associates

Niko Marsic and Björn Gylling
Kemakta Konsult AB

December 2003

Executive summary

Modelling of groundwater flow and flow paths for a large regional domain in Northeast Uppland. A three-dimensional, mathematical modelling of groundwater flows and flow paths on a super-regional scale, for different complexity levels of the flow domain.

General purpose of study

The general purpose of this study is to estimate the groundwater flow for a large regional domain by use of groundwater models; and to do that with such a resolution (degree of detail) that important local properties of the flow system studied is represented in the established models. Based on the results of the groundwater modelling, we have compared different theoretical locations of a repository for nuclear waste, considering length and breakthrough time (advective flow) for flow paths from such a repository.

Area studied

The area studied is located in Sweden, in the Northeast of the Uppland province. The area has a maximum horizontal extension of 90 km by 50 km, and the size of the area is approximately 2000 km^2. The location of the area is given in Figure 3-1 (page 25).

Methodology and detailed objectives

The study is based on a system analysis approach. The studied system is the groundwater flow in the rock mass of Northeast Uppland. To reach the objectives of the study, different mathematical models were devised of the studied domain; these models will, in an idealised and simplified way, reproduce the groundwater movements at the area studied. The formal models (the mathematical models) used for simulation of the groundwater flow are three-dimensional mathematical descriptions of the studied hydraulic system. For establishment of the formal models we used two different numerical codes GEOAN /Holmén, 1992/, which is based on the finite difference method and NAMMU /Cliffe et al, 1998/, which is based on the finite element method.

Considering flow path lengths and breakthrough times from a theoretical repository, we have evaluated the following:

- Importance of the local and regional topography.
- Importance of cell size in the numerical model.
- Importance of depth of domain represented in the numerical model.
- Importance of regional fracture zones.
- Importance of local lakes.
- Importance of areas covered by a clay layer.
- Importance of a modified topography.
- Importance of the shore level progress.

- Importance of density dependent flow.

The results of the study includes:

- Length and breakthrough time of flow paths from theoretical repository positions.
- Properties of the discharge areas for the flow paths from the repository.
- Magnitude and direction of groundwater flow at different depths.

To be able to evaluate the importance of the entities above we have established a chain of models, in which the complexity of the flow domain is increased for each model. For all models a basic set of analyses have been carried out. By comparing the results of these analyses, it is possible to draw conclusions of the importance of different hydrogeological entities and level of hydrogeological complexity. A summary of the properties of the different cases (chain of models) is given in Table 2-1 (page 23).

Methodology for analyses of flow field by use of flow paths

In this study the flow pattern of the groundwater (the flow field) was analysed by the use of flow paths. The applied models create flow paths by use of simulated particles, particles that follow the flow of groundwater through the model (i.e. particle tracking).

The flow paths were released at a depth that corresponds to a possible depth of a repository, i.e. depths between 490 and 540 m below ground surface. Paths were released in a regular pattern, one or several paths in each volume (cell or element) studied, regardless of the flow through the volume studied. Paths were released in a regular pattern considering (i) the whole model or (ii) areas inside of the shoreline (not below the Sea). The flow paths were analysed considering length and breakthrough time. Release positions that produced the longest path lengths and the longest breakthrough times were identified.

Only advective flow paths were studied in the flow path analyses, diffusion, mechanical mixing and retardation were not included in the flow path analyses.

Conclusions

The topography of the area studied is not very dramatic; it is a smooth lowering of the elevations of the ground surface, with some local topographic undulation, towards the shoreline (the topography is given in Figure 3-2, page 27). A simplification of the studied system by ignoring, or strongly reducing, the local topographic undulation may not seem like a change that is very important for the groundwater flow – but it is. Without the local topographic undulation the topography will follow the regional topographic gradient and the topography will be like that of an inclined plane (Case 1). And for such a situation the groundwater flow field is primarily controlled by the regional topographic gradient, and with little regard for the complex horizontal shape of the area studied, most flow paths (about 70%) from repository depth will flow towards the shoreline and discharge below the Sea or close to the shoreline. For such a situation, the repository positions with the longest flow paths and breakthrough times are positions as far as possible from the shoreline, because on the average flow paths length (and breakthrough time) increases with distance from the Sea (see Figure 5-3, page 49).

With inclusion of the local undulation of the topography (Case 2) the groundwater flow situation changes dramatically, the groundwater flow field at repository depth and above it (above a depth of approximately 500 m) will primarily be controlled by the local

topographic undulation. Regardless of distance to the Sea, most flow paths will be shorter than 3 km (90% of the paths are shorter than 3 km and 99% of the paths are shorter than 10 km, see Figure 5-5, page 51). The flow field is illustrated in Figure 5-6 (page 52), it is demonstrated by the figure that it is the local topographic undulation that controls the flow paths from repository depth.

With inclusion of the local topographic undulation, the repository positions with the longest flow paths are not necessarily far away from the Sea. Repository positions with long flow paths are found at many different positions within the domain studied and at different distances to the Sea (see Figure 5-7, page 54). The positions with long flow paths are however all located below local topographic heights. Considering breakthrough time, a more complex situation arises. If flow paths are released both inside of the shoreline and outside of the shoreline, the longest breakthrough times will take place for the flow paths released outside of the shoreline (below the sea), because of the small hydraulic gradient below the Sea (see Figure 5-8, page 56). If only release positions inside of the shoreline are considered, repository positions with long breakthrough times are found at many different positions within the domain studied and at different distances to the Sea (Figure 5-9, page 57). Nevertheless, many of the repository positions with long breakthrough times are close to the shoreline or outside of the shoreline, below islands, because of the small hydraulic gradient below the Sea. By comparing the repository positions with the longest paths and the positions with the longest breakthrough times we note that these positions are not the same. Positions below local heights will produce long flow paths, but the gradients could be large at such places, which may produce short break through times.

The importance of the topography was also demonstrated by a sensitivity analysis of the relationship between the regional and the local topographic gradients (Cases 7 and 8). If the regional gradient is increased, but the local undulation is not changed, the resulting distribution of flow path lengths will converge towards the distribution produced by the model without any local undulation. If both the regional gradient and the local gradients are increased in proportion, the local flow cells will remain in the flow system and continue to dominate the flow system; and if the increases in gradients are within reasonable values, the lengths of the flow paths from repository depth will not change much. For both sensitivity cases, the breakthrough times will decrease, because of the increase in gradients and flow velocities.

Addition of the vertical fracture zones (Case 3) will not cause a large change in the regional flow pattern; because fracture zones typically takes place along low lying parts of the topography, i.e. along valleys; and these areas are, with or without the fracture zones, discharge areas for the flow paths from repository depth. With or without fracture zones, the groundwater flows towards the lowest potential. Keeping the vertical fracture zones in the model and adding a continuous sub-horizontal fracture zone at a depth of 250 m (Case 5), will produce path lengths from repository depth that are somewhat longer and breakthrough times that are shorter, compared to situation without the sub-horizontal zone. However, the model with vertical zones and the model with both vertical zones and a sub-horizontal zone produce approximately the same repository positions as a model without fracture zones, when considering the longest flow paths or the longest breakthrough times.

The overall flow path distribution will also remain approximately the same after addition of lakes and areas covered with clay. The lakes will not cause a large change in the regional flow pattern because (as for the fracture zones) lakes typically takes place along low lying parts of the topography; and these areas are, with or without the lakes, discharge areas for the flow paths from repository depth. The addition of areas covered with clay will have a somewhat larger influence on the regional flow pattern, because in the model the ground-water flow cannot penetrate the clay; but the clay areas are discontinuously distributed over

the area represented by the model and therefore (on a regional scale) the influence of the clay areas is limited. The model containing regional fracture zones, lakes and some areas covered by clay (Case 6), produce approximately the same repository positions as a homogeneous model with undulating topography (Case 2), when considering the longest flow paths or the longest breakthrough times (Compare Figure 5-7, page 54 and Figure 5-20, page 76).

The shoreline will not stay the same in the future. Due to the shore level progress, the Sea will retreat and repository positions that today are outside of the shoreline or close to the shoreline may in the future be inside of the shoreline; and this will change the flow paths from these repository positions. Hence, repository positions close to the present shoreline, which for the present situation may not produce the longest flow path lengths and longest breakthrough times, may in the future be among the repository positions that produce the longest paths and longest breakthrough times; this is due to the changed flow field that will be created by the retreat of the shoreline (see Case 9).

When analysing the regional flow pattern and the spatial distribution of flow paths from repository depth, it is also of interest to study the variation of size of groundwater flow with depth. Only a very small part of the potential groundwater recharge will, on the average, infiltrate into the fractured rock and create deep groundwater. For the domain studied, the model calculates the actual groundwater recharge to the rock mass as a part of the solution of the flow field. Considering a model that includes fracture zones, lakes and areas covered with clay (Case 6), and considering an average value of the whole model (including the Sea), the actual groundwater recharge is 1.6 mm/year. In the fractured rock, on the average, the size of the groundwater flow decreases with depth. At great depth, the average specific groundwater flow is only a small fraction of the potential groundwater recharge, and an even smaller fraction of the precipitation. This is demonstrated in Figure 5-23 (page 80). Considering a model with fracture zones, lakes and areas covered with clay (Case 6), the amount of water that infiltrates into the fractured rock is 0.25% of the precipitation and 0.64% of the potential recharge. The groundwater flow decreases with depth. At a depth of 500 m, the downward component of the groundwater flow is close to 0.3 mm/year, which is: (i) 0.05% of the precipitation, (ii) 0.12% of the potential recharge and (iii) 19% of the groundwater recharge at ground surface. These results were obtained for a model in which the conductivity is constant with depth; a model with decreasing conductivity with depth will produce much smaller groundwater flows at great depth. It should also be noted that at a local point the vertical component of the groundwater flow (and the average actual recharge) might diverge significantly from the average values discussed above. The specific groundwater flow is defined as a flow per unit area; and because of the heterogeneous properties of the rock mass (i.e. the highly permeable fracture zones), and the undulating topography, the specific flow will vary in the model; this is illustrated in Figure 5-12 (page 60).

Flow paths from repository depth discharges into different types of environment. Based on the boundary conditions of the model, we have divided discharge areas into three different types: (i) the lakes, (ii) the Sea and (iii) the rest (the rest includes all land above shoreline that is not defined as lakes). The analyses was carried out for Case 6, which is the model with the most realistic properties at ground surface (lakes and clay is included) When considering all flow paths from repository depth, but only release positions inside of the shoreline (no release positions below the Sea), the following result was obtained: 23% of the paths discharged into lakes, 6% of the paths discharged into the Sea and 71% of the paths discharged on land (but not directly into areas defined as lakes). Of the 100 repository positions with the longest path lengths, 35% discharged into lakes and 11% into the Sea. Considering the 100 repository positions with the longest path breakthrough times, 21% discharged into lakes and 36% into the Sea.

The addition of density dependent flow (Case 10) will not cause any large and dramatic effects on the regional flow field. Considering flow paths from repository depth, density dependent flow will increase both path lengths and breakthrough times, the increase will however primarily take place for the longest flow paths, the median value is not affected to the same degree. Repository positions with large flow path lengths and large breakthrough time can be found at many different places within the domain studied; this conclusion is not changed by the introduction of the transient and density dependent solution. However, when considering the repository positions with the longest path lengths and the longest breakthrough times, the distribution of the positions in the density dependent model is not the same as for the other cases studied. Compared to the other cases studied, the density dependent model predicts that a large amount of the positions with long path lengths are located in the Northwest part of the domain studied (see Figure 8-14. page 126).

The analysis of the flow situations with local topographic undulation demonstrates that above the shoreline, the local undulation of the topography creates local flow cells for groundwater, and these local flow cells will come to dominate the general flow pattern of the groundwater, even below repository depth. It should however be noted that this flow situation (as seen in Figure 5-6, page 52) follows not only from the local undulation of the topography, but also from the size of the permeability of the flow medium and the size of the groundwater recharge. For this flow situation to occur it is necessary that: (i) the permeability (length/time) of the flow medium is small compared to the potential groundwater recharge (length/time), or that (ii) the potential recharge is large compared to the permeability. Considering a fractured crystalline rock mass and the climate of North Europe, both the above discussed conditions are fulfilled: the permeability is small and the potential recharge is large.

The hydrogeological complexity of the models representing the domain studied was increased gradually; step by step different hydrogeological entities were added to the model: local topographic undulation, regional fracture zones, lakes, clay-areas, shore-level progress, and density dependent flow. For all the studied cases, the conductivity and the porosity of the rock mass between fracture zones were the same and not changed. Considering flow paths from repository depth, the result of this procedure is presented in Figure 9-1 (page 157), as well as in Table 9-1 (page 158). As a reference case we have selected a homogeneous model that includes the local topographic undulation (Case 2). The reference case model is based on the present topography and includes the present shoreline (2000 AD). Table 9-1 presents a comparison between (i) path lengths and breakthrough times produced by the reference case, and (ii) path lengths and breakthrough times produced by other cases with increasing complexity. It is well demonstrated by Table 9-1 that the most important parameter is the local topographic undulation; without the local topographic undulation the simulated groundwater flow field will be very different. The addition of the other hydraulic entities will in comparison be of less importance.

The case without local topographic undulation is very different from the other cases, therefore in the following discussion it is not considered as a part of the chain of cases representing increasing complexity. Considering the cases with undulating topography, the path lengths tend to increase with increasing model complexity. The largest lengths take place with density dependent flow. With density dependent flow and considering the median of the flow path length distributions, the increase in median value, compared to the reference case, is within a factor of 2.0. Considering the cases with undulating topography and the models with a larger complexity than the reference case, the breakthrough times tend to be smaller than the times produced by the reference case; except for the model that includes density dependent flow. With density dependent flow and considering the median of the breakthrough time distributions, the increase in median value, compared to the reference case, is within a factor of 1.5. A comparison between the results produced by the density

dependent case and an identical case solved without density dependence (both models were defined with the NAMMU code) produces an increase in the median path length by a factor of 1.5 and an increase in the median breakthrough time by a factor of 1.2 (the increase took place for the density dependent model). It should be noted that the models studied are regional models, and they do not include parameter heterogeneity on a detailed scale, such heterogeneity will increase the variance presented in Table 9-1.

When studying the variation in path lengths and breakthrough times presented in Table 9-1, it is necessary to keep in mind the uncertainty in the parameters defining the system studied, (e.g. the uncertainty in conductivity and in porosity). The range of variation given in the table is not necessarily significant when considering the combined uncertainty of the parameters defining the system studied.

Thus, considering a regional scale and the spatial distribution of flow paths from repository depth, the most important parameters are the topography and the position of the Sea. A model used for prediction of flow path distribution needs to include the local topographic undulation, and the topography needs to be included in such detail that the model is capable of reproducing the influence that the local topographic undulation has on the groundwater flow field.

The studied models also demonstrate that repository positions at a depth of about 500 m below ground surface, with long flow path lengths and long breakthrough times for the groundwater flow from the repository to the ground surface, such repository positions may be found at many different places within the domain studied. This conclusion is based on all the different cases studied. There is no general trend that the positions with the longest paths or the longest breakthrough times are found as far as possible from the Sea.

Contents

1 Introduction and purpose

Modelling of groundwater flow and flow paths for a large regional domain in Northeast Uppland. A three-dimensional, mathematical modelling of groundwater flow and flow paths on a super-regional scale, for different complexity levels of the flow domain and the flow regime.

1.1 General purpose of study

The general purpose of this study is to estimate the groundwater flow for a large regional domain by use of groundwater models; and to do that with such a resolution (degree of detail) that important local properties of the flow system studied is represented in the established models. The area studied is located in Sweden, in the Northeast of the Uppland province. Based on the results of the groundwater modelling, an analysis will be carried out that compares different theoretical locations of a repository for nuclear waste, considering length and breakthrough time for flow paths from such a repository. Considering the groundwater flow only, and based on calculated flow paths from different repository positions, we will present some general conclusions on where flow path length and transportation time are optimal in relation to the local topography and distance to the shoreline.

1.2 Method

The study is based on a system analysis approach, and the studied system is the groundwater flow in the rock mass of Northeast Uppland. To reach the objectives of the study, different mathematical models were devised of the studied domain; these models will, in an idealised and simplified way, reproduce the groundwater movements at the area studied. The formal models (the mathematical models) used for simulation of the groundwater flow are three-dimensional mathematical descriptions of the studied hydraulic system. To set up the formal models we used two different numerical codes GEOAN /Holmén, 1992/, which is based on the finite difference method and NAMMU /Cliffe et al, 1998/, which is based on the finite element method.

1.3 Detailed objectives

The results of the study include:

- Magnitude and direction of groundwater flow.
- Length of flow paths from theoretical repository positions.
- Breakthrough times of flow paths from theoretical repository positions.
- Properties of the discharge areas for the flow paths from the repository.

Considering flow path lengths and breakthrough times from a theoretical repository, the following have been analysed:

- Importance of the local and regional topography.
- Importance of regional fracture zones.
- Importance of local lakes.
- Importance of areas covered by a clay layer.
- Importance of cell size in the numerical model.
- Importance of depth of domain represented in the numerical model.
- Importance of the shore level progress and the transient behaviour of the regional flow.
- Importance of density dependent flow.

2 Methodology

2.1 The system analysis approach

In this study the limited part of the reality that we are investigating is called *the system*. *The model* is an idealised and simplified description of the studied system. This study is based on *the system analysis approach*. This is a method for solving complicated problems by: (i) establishing a model of the studied system, (ii) using the model for simulations which imitate the behaviour of the studied system and (iii) based on the results of the simulations, determine a solution to the investigated problem.

Based on the objectives, and on available information of the system studied, a conceptual model is established. *The conceptual model* includes information of the studied media (rock mass etc) and the physical processes governing the groundwater flow, but it includes only information relevant as regards the objectives of the study. Based on the conceptual model a formal model is established. *The formal model* is a mathematical description of the conceptual model, it is established by the use of a computer code. The formal model is used for simulations.

2.2 Original flow equations

The formal model is a three-dimensional, time-dependent mathematical description of the studied hydraulic system. Groundwater flow will be calculated with by use of different formulations of Darcy´s law /Darcy, 1856/, and the continuity equation. Darcy's law assumes a non-deformable flow medium and that the inertial effects and the internal friction inside the fluid are negligible; these generalisations are applicable, considering the flow system studied. For the cases with constant density, the governing equation for groundwater flow in a continuous medium is the following differential equation (presuming constant fluid density, the X-direction and the Y-direction is in the horizontal plane, the Z direction is in the vertical plane).

$$\frac{\partial}{\partial x}\left(K_x \frac{\partial \phi}{\partial x}\right)+\frac{\partial}{\partial y}\left(K_y \frac{\partial \phi}{\partial y}\right)+\frac{\partial}{\partial z}\left(K_z \frac{\partial \phi}{\partial z}\right)- VF = Ss \frac{\partial \phi}{\partial t} \qquad (2\text{-}1)$$

Where

K_x , K_y , K_z = *Hydraulic conductivity along axes [L* t^{-1}*]*
ϕ = *Hydraulic head (Piezometric head, Groundwater head) [L]*
VF = *Volumetric flow (flow per unit volume, inflow and outflow of water) [*T^{-1}*]*
Ss = *Specific storage of medium [*L^{-1}*]*
t = *Time [T]*

The head (hydraulic head) is defined as the sum of pressure and elevation. The development of Equation 2-1 from Darcy's law and from the continuity equation is well known, see for example /Bear and Verruit, 1987/.

Equation 2-1 constitutes, together with initial conditions and boundary conditions, a mathematical representation of a flow system. Analytical solutions to the equation normally exist only for very idealised and simplified cases. Consequently, we need to use numerical models.

Description of density driven flow, induced by a variable salinity of the groundwater, requires both flow, continuity and transport equations. The following formulations are implemented in the NAMMU computer code /Cliffe et al, 1998/.

Darcys law (flow equation):

$$\bar{q} = -\frac{\bar{k}}{\mu}\left(\nabla p^R - (\rho - \rho_0)g\right)$$

Where
$\bar{q}$ = Darcy velocity
$\bar{k}$ = Intrinsic permeability tensor
μ = *Fluid viscosity*
p^R = *Residual pressure with:* $p^R = p + p_0\, g(z - z_0)$
ρ = *Fluid density*
ρ_0 = *Reference density of fluid*
z = *Elevation*
z_0 = *Reference elevation*
g = *Gravitational acceleration*

The continuity equation:

$$\frac{\partial}{\partial t}(\eta\rho) + \nabla\cdot(\rho\bar{q}) = 0$$

Where
η = *porosity*

Introducing the specific storage coefficient:

$$S = \rho g\left(\frac{\partial \eta}{\partial p} + \alpha\eta\right)$$

Where
S = *Specific storage coefficient.*
α = *Fluid compressibility*

Using the specific storage coefficient in the continuity equation yields:

$$\frac{S}{g}\frac{\partial p^R}{\partial t} + \nabla\cdot(\rho\bar{q}) + \eta\frac{\partial\rho}{\partial c}\frac{\partial c}{\partial t} = 0$$

Where
c = Concentration of solute as a mass fraction of the reference concentration

The advection-dispersion equation (transport equation)

$$\frac{\partial}{\partial t}(\eta \rho c) + \nabla \cdot (\rho \bar{q} c) = \nabla \cdot (\rho \bar{q} \bar{D} \cdot \nabla c)$$

Where
$\bar{D}$ = *Hydrodynamic dispersion tensor*

The relationship between density and solute concentration is given by the following relationship:

$$\rho = \left(\frac{1-c}{\rho_0} + \frac{c}{\rho_s} \right)^{-1}$$

Where
ρ_s = *Saturation density of fluid*

2.3 Numerical and analytical approach, computer codes

The formal models are mathematical descriptions of the studied hydraulic system. The formal models are based on a numerical approach and established by use of the GEOAN computer code, except for the case with density dependent flow that was established by use of the NAMMU computer code. GEOAN is a computer code based on the finite difference numerical method. The finite difference method and the GEOAN code are briefly presented in /Holmén, 1997/; the code was first presented by /Holmén, 1992/. NAMMU (Numerical Assessment Method for modelling Migration Underground) is a finite-element software package for modelling groundwater flow and transport in porous media /Cliffe et al, 1998/.

2.4 Mathematical approach to the flow media – the heterogeneity of the flow media and the models

The established models represent a fractured crystalline rock mass. Groundwater flow in such a rock occurs in fractures and in fracture zones of different size and significance. These fractures and fracture zones determine the heterogeneous and anisotropical hydraulic properties of the rock mass.

There are different approaches available when establishing a mathematical description of a fractured medium. In this study we will use the continuum approach, which replaces the fractured medium by a representative continuum in which spatially defined values of hydraulic properties can be assigned to blocks of a given size. A large number of blocks represent the studied media. We will in this study not discuss in detail the concept of the continuum method; for a detailed presentation of the continuum method we refer to /Bear and Verruit, 1987/ and /Bear and Bachmat, 1990/.

Properties may be assigned to the blocks in a deterministic way, if the detailed information is available i.e. *a deterministic continuum model*. If we replace a heterogeneous property (e.g. the conductivity) with an average value and assign that value to the blocks of a model,

we will get a model that we will call *a uniform continuum model*. If detailed information of the hydraulic properties are unknown and we want to include the heterogeneity into the model, we can use *a stochastic continuum model*. In a stochastic continuum model the hydraulic properties of the blocks are described by probability distributions, selected to fit the size of the studied blocks. The different methods should be regarded as different ways of idealising and simplifying the system studied, when establishing a mathematical model representing the system.

For the system that we will study, it is possible to identify two different types of flow media: the rock mass between large fracture zones and the large fracture zones. We will use the following approach considering the continuity and the conductivity of the different identified flow media:

- The rock mass between large fracture zones will be defined as continuous, having a homogeneous conductivity by use of representative averages values of conductivity.
- Large fracture zones will be defined as separate continuous structures, by use of an implicit formulation as regards the conductivity of the different volumes defining the geometry of the models (the cells). The conductivity of the zones is defined as being homogeneous, by use of representative average values of conductivity.

Our specific knowledge of the local heterogeneity of the fractured crystalline rock mass between the regional fracture zones is limited. However, we can assume that in principle it will be similar to the heterogeneity of the fractured crystalline rock mass at Äspö Hard Rock Laboratory, which has been investigated in several studies, see e.g. /Gustafson et al, 1989; Wikberg et al, 1991/. Investigations at Äspö HRL have demonstrated that the heterogeneity of a fractured rock mass is scale dependent. At small scales the heterogeneity is large and at large scales the heterogeneity is small.

In a numeric model, the properties of the model are defined at the cells (elements) of the model grid (model mesh). Heterogeneity in the properties of a domain studied is included in a numerical model by assigning different properties to different cells of the model grid. However, as the heterogeneity of a fractured rock is scale dependent, the variation in properties assigned to the cells of the grid should depend on the size of the cells.

This study aims at estimating the groundwater flow for a very large domain. As a consequence the cell sizes (element sizes) needs to be large because of computational restrictions. The smaller the cells the larger the number of cells in the grid, and the larger the computational times etc. The base case model of this study uses cells that in the horizontal plane has a size of 330 m × 330 m, in the vertical plane the size varies between 50m and 150 m (this is discussed in more detail in Section 4.2). For cells of this size, and for larger cells, the local heterogeneity of the rock mass between large fracture zones is probably not very large, see /Gustafson et al, 1989; Wikberg et al, 1991/. Therefore we have not included any local heterogeneity in the properties of the rock mass between the fracture zones. The average conductivity of the rock mass may in reality vary between different regions of rock mass; this is however not the same thing as the local heterogeneity. For simplicity reasons, we have in the models of this study used a single value of average conductivity for the whole domain studied.

For some of the objectives of this study, the unknown and not included heterogeneity of the rock mass (the heterogeneity that is not represented by the regional fracture zones), is of less importance – these objectives are the predictions of the average flow directions. For other objectives, the unknown and not included heterogeneity might be of more importance. For example the estimated distribution of lengths of flow paths from the repository to the discharge areas and the estimated distribution of breakthrough times will demonstrate a larger variation if the local heterogeneity is included in the model.

Considering the results of the flow path analysis, the calculated variation in length of flow paths and breakthrough times are probably smaller than the actual variation. This is because the local heterogeneity of the rock mass and especially the heterogeneity inside the fracture zones are not included in the models of this study. To produce better estimations also the heterogeneity of the rock mass and the fracture zones need to be included, however such heterogeneity has not been included in this study because of the scale of the studied domain.

2.5 Salt water and the importance of variable density flow

The groundwater at the domain studied is of different origin, and partly dependent on its position in the flow system it is of different age. It is possible to distinguish four different types of groundwater: (i) Fresh water, (ii) Relict glacial meltwater with low levels of salinity, (iii) Relict seawater with a salinity close to that of the present Baltic Sea, and (iv) Shield brine with large levels of salinity (larger than the levels of the Sea).

The fresh water is generally found at shallow depths, but may occur at great depth at some distance from the shoreline. The distribution of the relict glacial water is not well known. Relict seawater is likely to be found anywhere in the domain studied; as the whole of the domain studied was below the Sea at about 8000 years before present /Påsse, 1996/, because of the shore level progress.

Shield brine is generally found at great depth, below the fluids described above. The processes that create the shield brine are not very well understood.

The groundwater models of this study include the area that surrounds the SFR repository. SFR is a repository located about 50 m below the Sea floor and about one kilometre off the shoreline, outside of the Forsmark nuclear power plant. /Stigson et al, 1998/ investigated the importance of variable density flow at SFR, by use of two-dimensional models (SUTRA), representing a large vertical cross-section. A large number of different cases were studied. The changed parameters were:

- Permeability.
- Porosity.
- Change in long term evolution of the salinity in the seawater.
- Presence of vertical and/or horizontal structures.

The most important conclusions were:

- The porosity has a large impact on the results since higher porosity means that the transport time is longer and that more saline water has to be flushed out.
- As the model becomes more complex (i.e. incorporating heterogeneity structures, etc) the spatial differences in salinity and the difference in flow through the SFR, between variable-density and uniform-density flow, becomes less significant.
- Differences are negligible between: (i) modelling groundwater as a variable-density flow or (ii) modelling a uniform-density flow with salt (chloride) as a tracer.

It should however be noted that the SFR is a repository located at depth of only 50 m below the Sea floor. At greater depths, where heavy shield brine may occur, the salinity of the groundwater is more important for the flow of the groundwater.

The following is stated in /Voss and Andersson, 1993/: “Because of the large density contrast between fresh water and shield brine, circulation of shield brine is likely driven by both fluid density differences and topographic forces, whereas flow of the more dilute fluids, including relict seawater, is driven primarily by topographic forces”.

For a flow system that includes variable-density flow and carries shield brine at great depth, the shield brine will limit the vertical extension of the flow of the less heavy groundwater above the shield brine, including the flow of relict seawater. The heavy shield brine will to a large extent act as a confining layer, which creates an upper flow system with less saline groundwater and a lower system with heavy saline water (shield brine). Because of the density difference between the shield brine and the groundwater above it, the less heavy groundwater (above the shield brine) will not penetrate into the domain of the shield brine.

In this study we have used an approach in which density dependent flow is studied in special cases. For the other cases we have not included density dependent flow, consequently the models of these cases (the freshwater cases) do not include the shield brine, instead these models are defined with a limited depth (between 1100 m and 4000 m). The limited depth of the fresh water models is a simplified method of representing the confining effects of the shield brine. Such an approach could be motivated by the study of /Stigson et al, 1998/, which demonstrates that the flow in the domain above the shield brine can be simplified to a non-density dependent flow system; and as it is primarily not an objective of this study to simulate the very deep and slow groundwater flow at very large depths inside the shield brine domain.

2.6 The shore level displacement – the land uplift

During the latest glacial period large amounts of water were tied to the ice mass, which had a maximum thickness of about 3 km. When the ice began to melt both the levels of the land and the water levels of the Seas became higher. The interplay between land, ice and the water has resulted in different water levels and different types of water in the Baltic Sea as well as in the Baltic shield rock. In some periods the Baltic Sea was a freshwater lake while in others it was a saline Sea. The sum of the ground level changes and the Sea level changes is called shore level displacement. The shore level displacement will be considered in the models solved for transient conditions, presented in Section.7.

2.7 Representation of quaternary deposits

Quaternary deposits have not been explicitly included in the formal models, except for low permeable clay layers. At the area studied, a glacial till occurs above the fractured rock with a varying thickness and continuity. We have assumed that on the average this material is more permeable or has approximately the same permeability as the fractured rock. Consequently, in the models, the glacial till is represented in the models as a part of the fractured rock. At some areas a low permeable clay layer occurs above the glacial till, this clay-layer is explicitly included in the models (see Sections 3.6 and 4.2.3).

2.8 Calibration

The models are not calibrated, as no applicable data is available for calibration at the scale of the models. However, the properties of the models are according to observed and measured values and the calculated actual recharge of the models are in line with empirical estimations. The properties of the models are given in Chapter 3 and Chapter 4.

2.9 Methodology for calculation of flow paths

In this study the flow pattern of the groundwater is analysed by the use of flow paths. The GEOAN and NAMMU models create flow paths by the use of simulated particles, particles that follow the flow of groundwater through the model (i.e. particle tracking).

For calculation of flow paths the GEOAN model provides the user with both a semi-analytical method /Pollock, 1989/ and an iterative numerical method. For Cases 1 through 9 we have used the GEOAN model and the semi-analytical method for calculation of flow paths; and for Case 10 we have used the NAMMU model and an iterative approach.

The flow fields of the models were analysed by use of flow paths released at a depth that corresponds to the possible depth of a repository, i.e. depths between 490 and 540 m below ground surface. In this study the flow paths are not released based on the size of the groundwater flow through a given volume, a flow path does not represent a given amount of flow. Paths are released in a regular pattern, one or several paths in each volume (cell or element) studied, regardless of the flow through the volume studied.

In the models, the flow paths will develop inside a flow field that controls the movements of the paths. For a time-independent flow path, the path will develop inside a flow field that will not change with time. Hence, the flow field is constant during the movement of the simulated particle that gives the flow path. For a time-dependent flow path, the flow field will change with time during the movement of the simulated particle that gives the flow path. Theoretically, the actual movement of a particle should take place in a changing flow field, because the flow field will change while the particle moves through the flow medium (the flow field will change due to the shore level progress). The GEOAN and NAMMU models can simulate both time-dependent and time-independent flow paths. In this study we have generated flow paths that are time-independent. Such flow paths represent the flow field for the studied moment in time.

The flow paths were analysed considering length and breakthrough time. Different distributions were obtained for the parameters studied, e.g. breakthrough times for the flow paths from all studied cells inside the shoreline, or breakthrough times for the flow paths from all studied cells at a certain distance from the shore line, etc. For the different cases studied, the properties of these distributions were compared.

2.9.1 Transport processes – dispersion and retardation

Dispersion is the tendency for a solute, dissolved in the groundwater, to spread out from the path that it would be expected to follow according to the advective hydraulics of the flow system. Dispersion is caused by molecular diffusion and mechanical mixing during fluid advection. Molecular diffusion is the process of spreading of a solute of higher concentration to a region of lower concentration, as a result of thermal movement of the molecules of the solute. The mechanical mixing, often called mechanical dispersion, is

caused by the heterogeneous properties of a flow medium. Mechanical dispersion is scale dependent and will occur both at a microscopic scale and at a macroscopic scale.

Because of sorption processes, some solutes will move much more slowly through the flow medium than the groundwater that is transporting them, this effect is called retardation.

Additionally, in a mathematical model an unwanted numerical dispersion may also take place, due to the method used for representation of the transport process.

This study includes the simulation and analyses of flow paths; and as previously stated the GEOAN and NAMMU models create flow paths by the use of simulated particles. Considering the simulated flow paths (particles):

- *Molecular diffusion* is not considered.
- *Mechanical dispersion.* In the models we have not included mechanical dispersion as a tendency for the flow paths to spread out from the advective path.
- *Numerical dispersion*. Considering the simulated flow paths, the model of this study uses the approach of tracking of particles and for this approach there is no numerical dispersion.
- *Retardation.* No retardation is included in the models.

Hence, for the flow paths we have examined advective transport only.

For some of the cases of this study we have included density dependent flow, for these cases the density of the groundwater depends on the salinity of the groundwater. The density dependent cases include the migration of ground water having different levels of salinity (and the corresponding different values of density). Considering the migration of saline water and the dissolved solute (salt):

- *Molecular diffusion and mechanical dispersion* is included in the models by use of the concept of dispersivity /e.g. Fetter, 1993/.
- *Numerical dispersion*. Migration of saline water is calculated by use of a fixed mesh and the solution of the advection-dispersion equation, if follows that numerical dispersion will be included in the calculations (the size of the numerical dispersion is approximately given by the cell/element size of the computation grid).
- *Retardation.* No retardation is included in the models.

2.10 Chain of models

Considering flow path lengths and breakthrough times from a theoretical repository, it is a purpose of this study to evaluate the following:

- Importance of the local and regional topography.
- Importance of regional fracture zones.
- Importance of lakes.
- Importance of areas covered by a clay layer.
- Importance of cell size in the numerical model.

- Importance of depth of domain represented in the numerical model.
- Importance of the shore level progress and the transient behaviour of the regional flow.
- Importance of density dependent flow.

To be able to evaluate the importance of the entities above we have established a chain of models, in which the complexity of the flow domain is increased for each model. For all models a basic set of analyses have been carried out. By comparing the results of these analyses, it is possible to draw conclusions of the importance of different entities. For example if models with and without lakes (everything else being equal) produce the same results, considering a certain analysis e.g. flow path lengths from a theoretical repository; for such a situation, lakes are not important considering flow path lengths from a theoretical repository.

The basic model chain is as follows (see Table 2-1), given with increasing complexity. All models are solved for steady state conditions and uniform density, unless otherwise specified:

Table 2-1. Chain of models.

Primary chain	
1.	Uniform flow medium, topography as an inclined plane.
2.	Uniform flow medium and an undulating topography.
2A	Uniform flow medium with undulating topography, and cells of different horizontal sizes.
2B	Uniform flow medium with undulating topography, and models of different depth.
3.	Uniform rock mass plus regional vertical fracture zones and undulating topography.
4.	Uniform rock mass plus regional vertical fracture zones, undulating topography and Lakes.
5.	Uniform rock mass plus regional vertical fracture zones and a regional sub-horizontal zone everywhere in the model at a depth of 250 m. Undulating topography.
6.	Uniform rock mass plus regional vertical fracture zones, undulating topography, Lakes and Clay layers.
Special cases	
7.	Uniform rock mass plus regional vertical fracture zones and undulating topography. For Case 7, the topography is enhanced by increasing the topographic gradients. Relation between local and regional gradients is not changed.
8.	Uniform rock mass plus regional vertical fracture zones and undulating topography. For Case 8, the topography is enhanced by increasing the regional topographic gradient.
Transient models	
9.	Uniform rock mass plus regional vertical fracture zones and undulating topography. Initial condition at –4000 A.D. Uniform density flow. Analysis of flow field at 2000 AD and at 5000 AD.
10.	Uniform rock mass plus regional vertical fracture zones and undulating topography. Initial condition at –4000 A.D. Density dependent flow. (NAMMU)

3 Properties of the domain studied

3.1 Location of area studied

The area studied is located in Sweden, in the Northeast of the Uppland province, approximately 50 km North of Stockholm. In Figure 3-1 (below) the area studied is marked with green colour. The area studied has a maximum horizontal extension of 90 km by 50 km, and the size of the area is approximately 2000 km^2

In Figure 3-1, blue lines denote the regional topographic water divides and the shoreline is denote by black lines.

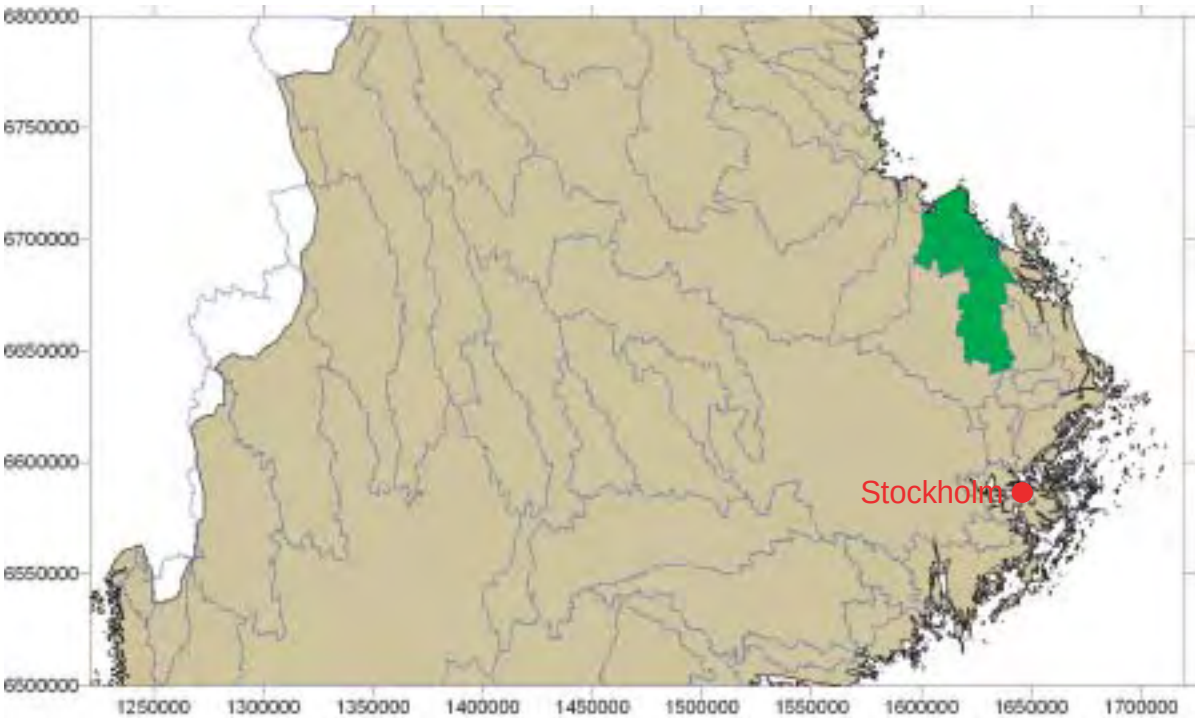

Figure 3-1. *Location of area studied. The area studied is located in Sweden, in the North East of the Uppland province, approximately 50 km North of Stockholm. In the figure above, the area studied is marked with green colour. The regional topographic water divides are denoted by blue lines and the shore line is denote by black lines.*

3.2 Topography

The database used for describing the topography was supplied by SKB from the SICADA database. The data comes from two different files, one is called “tierp_ost_hojd.asc” and covers the area 1569975, 6649975 to 1699975, 6749975. The other file is called “m3680.g” and covers the small area to the south-east, 1610000, 6640000 to 1650000, 6650000. Both topography files uses the co-ordinate system RT90 2.5^{g}V – RH70 and the grid is 50 m in both x and y direction. The topography of the studied area is given in Figure 3-2.

The elevation of the Sea floor (depths) is also taken from the SICADA database, this data was also used in the feasibility study of the Östhammar municipality. Originally the data comes from the Swedish Maritime Administration. The data is coarse and represents two depth curves, the 6 m and 20 m depth curves. The small volume of data, describing the elevation of the Sea floor, is a minor problem for this modelling, since in the model the specified head condition will by used along the Sea floor, a head value given by the average level of the Baltic Sea. There is very little data for the 6 m curve north of 6720000, but as mentioned before this is if minor importance. The 6 m and 20 m depth curves are shown as lines in Figure 3-2

The topography of the area studied, and its surroundings are shown in Figure 3-2

The topography is not very dramatic. North and East of the regional water divides it is a smooth lowering of the elevations of the ground surface, with some local topographic undulation, towards the shoreline.

The lowest elevations within the area studied are below the Sea; the lowest elevation of the Sea floor is below –20 masl. The highest elevation is about 70 masl, and it takes place about 40 km from the shoreline, which produces a regional topographic gradient (above the shoreline) of approximately 0.17%

3.3 Topographic water divides

An area bounded by topographic surface water divides is often called a catchment area, or a drainage basin, or a watershed. According to Nordic Glossary of Hydrology (1984) such an area is defined as: “The whole area having a common outlet for its surface runoff”. A surface water divide is a theoretical line separating surface water flowing into different rivers, catchment areas or drainage basins. The regional topographic water divides for the surface water runoff is used as the models horizontal boundaries.

The regional water divides are presented in Figure 3-1 and in Figure 3-2. Figure 3-1 presents the regional water divides and catchment areas considering a large part of Sweden, in the figure the area studied is denote by green colour. Figure 3-2 presents the studied area in more detail, the area has a horizontal extension of 90 km by 50 km and it is bounded by regional water divides. The water divides are the major surface water divides according to SMHI, 1995. (Personal communication with Sten Lindell, SMHI, 2002-04-17 confirmed that no revisions have been made to this data.)

The following discussion is based on the capital letters denoted in Figure 3-2.

- The water divide between A and B is a regional divide separating: (i) flow into the studied area and (ii) flow towards catchments areas connecting to the river Dalälven catchment area.

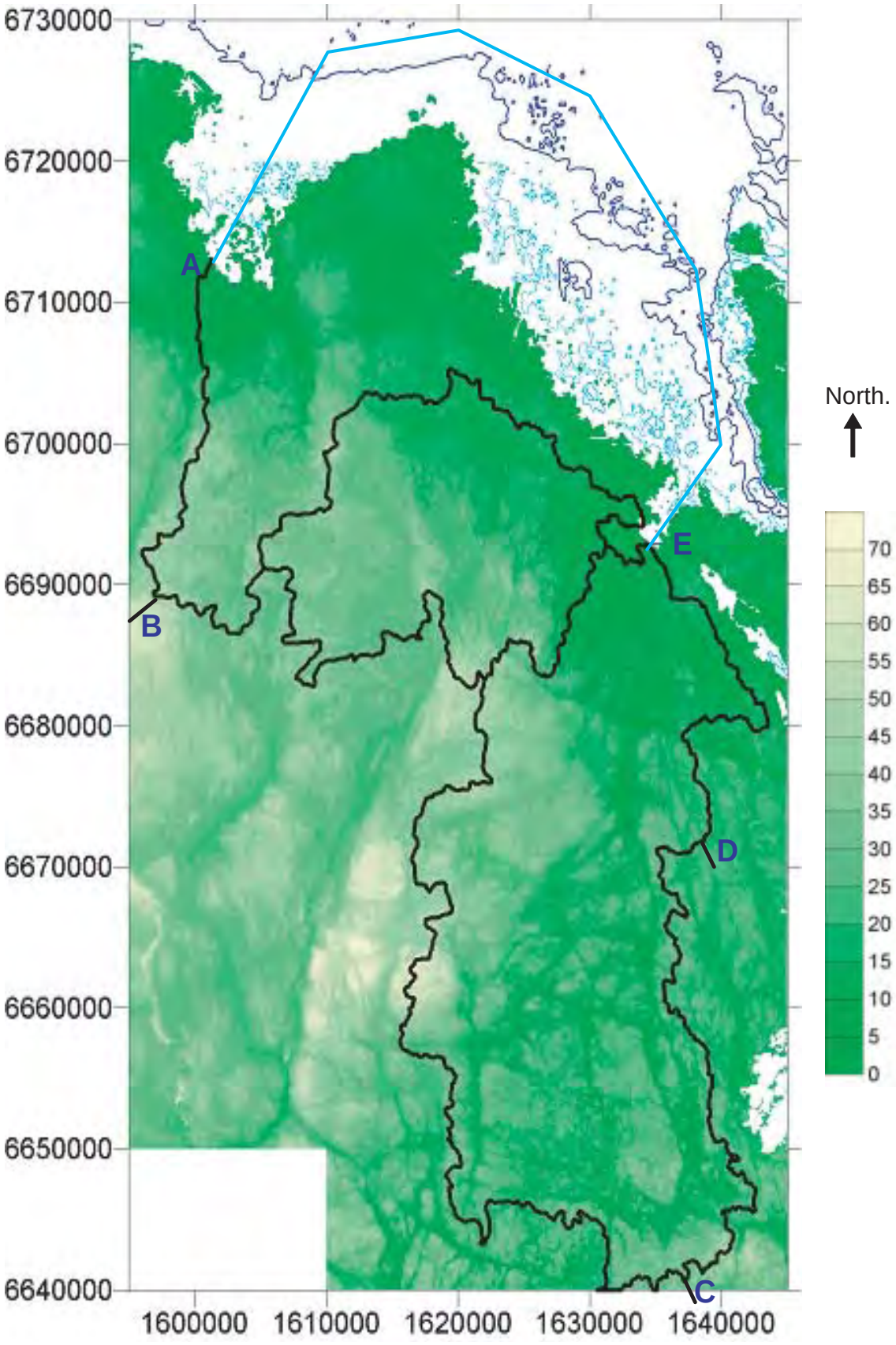

Figure 3-2. *Topography of the area studied. The black lines denote the regional surface water divides. The colour scale refers to the elevation given in metres above Sea level.*

- The water divide between B and C is the regional divide separating: (i) flow into the studied area and (ii) flow towards the Fyrisån river and lake Mälaren catchment areas.
- The water divide between C and D is a regional water divide separating: (i) flow into the studied area and (ii) flow towards East and further on to the Baltic Sea.
- The water divide between D and E is a divide separating: (i) flow into the studied area and (ii) flow towards Northeast and further on to the Baltic Sea.

The established groundwater model represents an area bounded by regional water divides, from A-B-C-D-E.

It is likely that for the studied area the regional surface water divides (A-B-C-D-E) are not only surface water divides, but also groundwater divides, as there are no large hills close to the area studied; and the surface water divides are along major topographic heights. (The boundaries of the established model are also discussed in Section 4.1 and in Appendix A.).

3.4 Fracture zones

The regional lineaments (regional fracture zones) are taken from a couple of different reports, but all data comes primarily from SGU. For the Northern part of the model, between co-ordinates 1595000, 6679000 and 1645000, 6732000, the data are taken from the file “sprickzon_r99_53fig8_4.shp”. The data for the middle part, between 1615000, 6640000 and 1645000, 6681000 of the model is taken from the file “zon_land.shp”. In the most southern part, south of 6640000, the zones are digitised from figure 13 in R-98-32.

The provided definitions of the zones were simplified to a large number of straight lines. The maximum allowed deviation from the provided zone definition and the simplified zone definition was set to 100 m. Duplicate zone definitions were also removed from the data. Finally, about 600 zone segments defines the regional fracture zones.

The extension of the regional zones, as defined in the model, is shown in Figure 3-3. Details of the inclination and depths of the regional zones are not known, in the model all zones are defined as vertical

The presence and extension of sub-horizontal zones are not well known at the regional scale studied. Therefore such zones were not included in the base case of this modelling, but in a special case.

As can be seen in Figure 3-3, below, most of the regional fracture zones are located along low-lying parts of the topography.

3.5 Lakes

The data describing the extension of the lakes are taken from the general map over Uppsala county from a file called SJO1_C.shp provided by Lantmäteriverket. Figure 3-4 presents the lakes within the domain represented by the model.

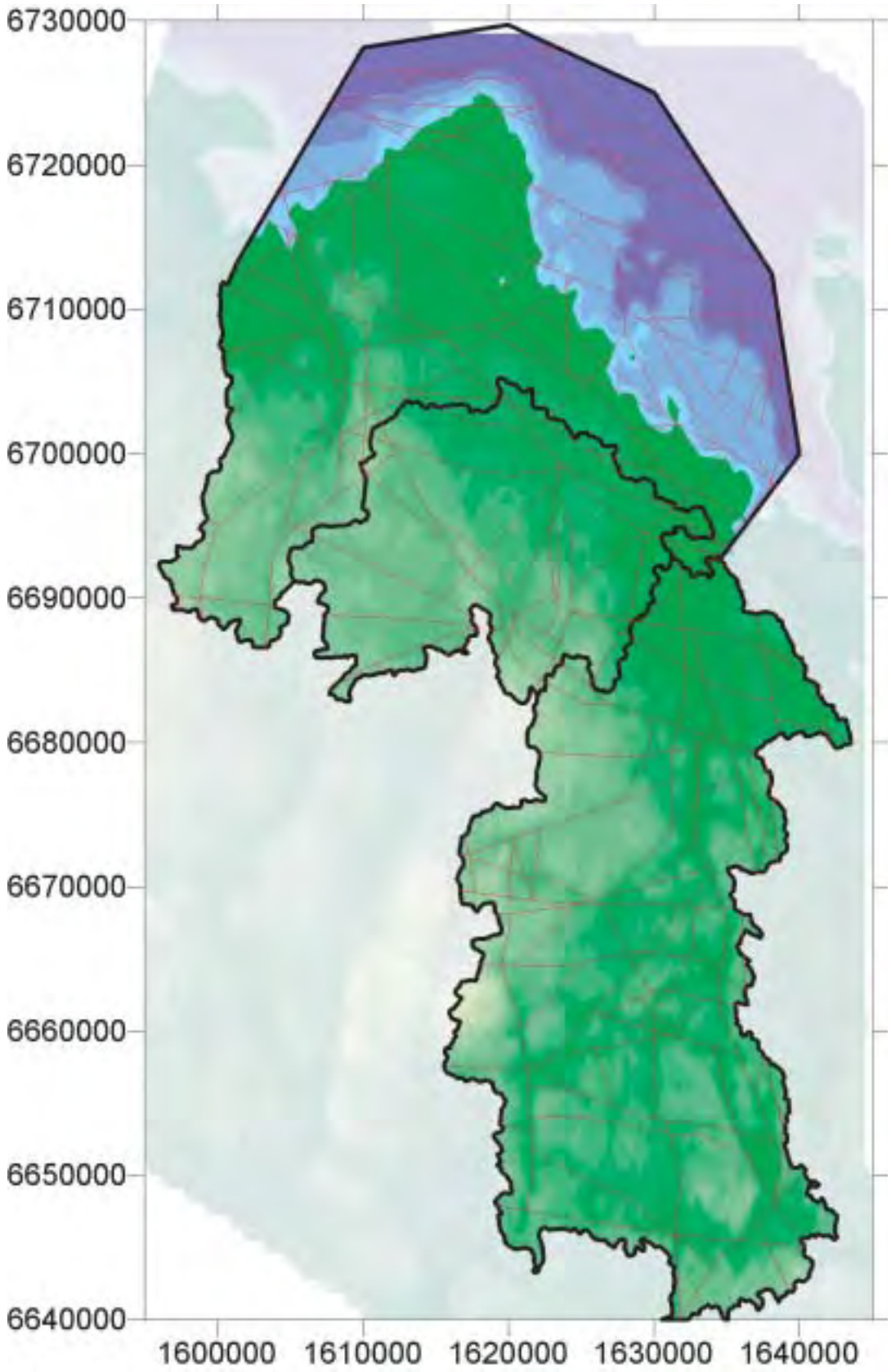

Figure 3-3. *Topography, surface water divides and regional fracture zones. Orange lines denote the horizontal extensions of the zones.*

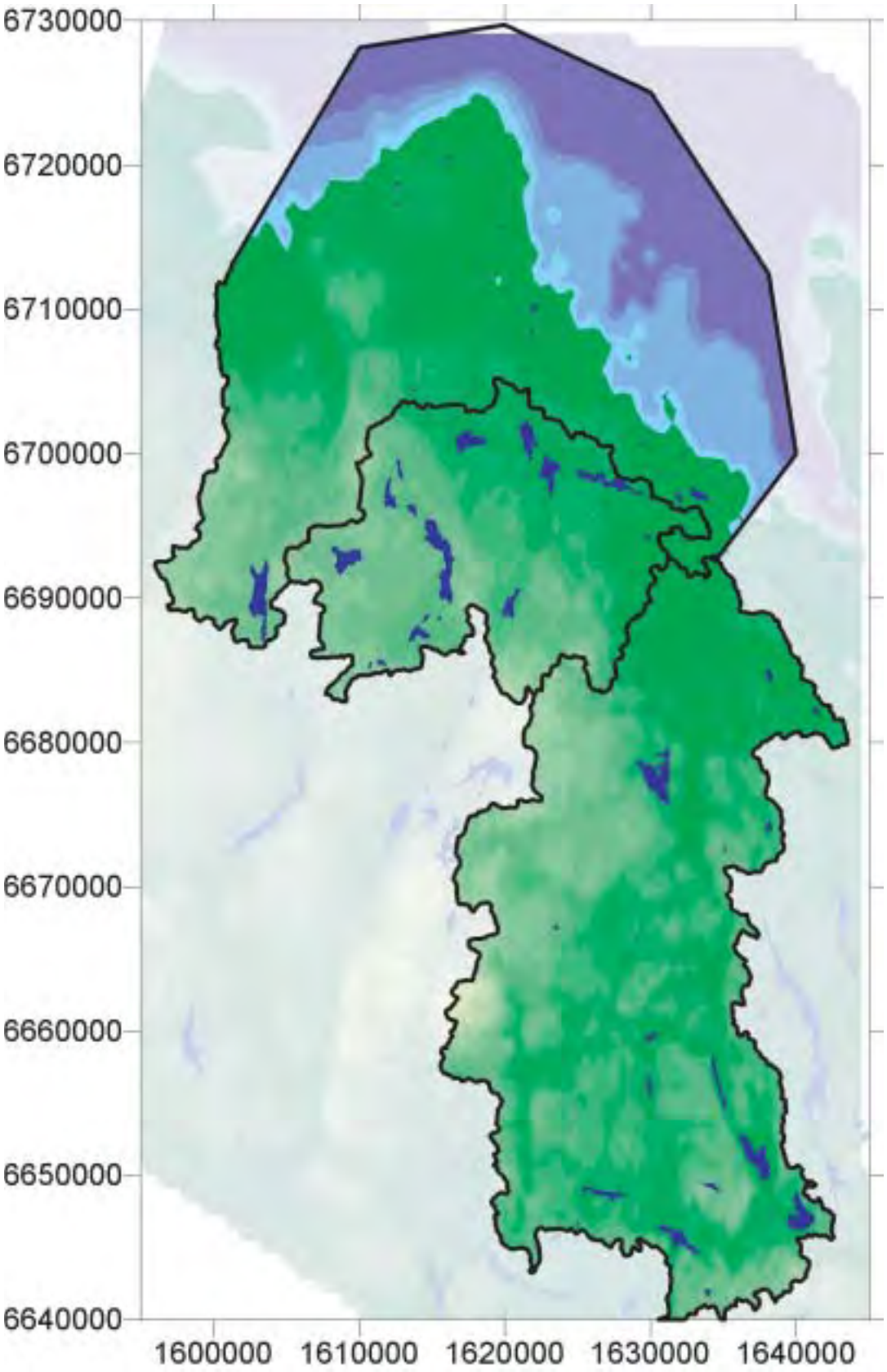

Figure 3-4. *Topography, surface water divides and lakes.*

3.6 Clays

Only the low permeable quaternary deposits, i.e. the clays are taken into account in the model since these may be a discriminative factor for water to enter or leave the groundwater system of the model. The distribution of the clays is taken from the map over the quaternary deposits provided by the Lantmäteriverket. The data was delivered in 6 different files called, j1211i_lera.shp, j12hno_lera.shp, j12ino_lera.shp, j12inv_lera.shp, j13iso_lera.shp and j13siv_lera.shp. The distribution in the domain represented by the model is shown in Figure 3-5. It should be noted that the local continuity of the clay layers is not known in detail. Investigations of the seabed at SFR have revealed that the fractured rock is mainly covered by a glacial till (morain) of varying thickness with a large amount of boulders and a small amount of fine grained material; at present, no continuous layer of fine-grained sediments, e.g. clay, occur at the seabed above the SFR.

3.7 Surface properties of domain studied

A superposition of topography, zones, lakes and clays are shown in Figure 3-6.

3.8 Hydro-meteorology – precipitation and run off

According to /Brandt et al, 1994/, for the period 1961–1990, the average precipitation in the Östhammar municipality, which includes the Forsmark area, is 600–700 mm/year; the average run off is 200–300 mm/year. For the province of Uppland, which includes the domain studied, Figure 3-7 presents the average run off, as measured and estimated by /SMHI, 1999/; in the figure the area studied is denoted by blue lines. The average run off is used in the models as the potential recharge. The average run off, for the domain studied, is approximately 250 mm/year.

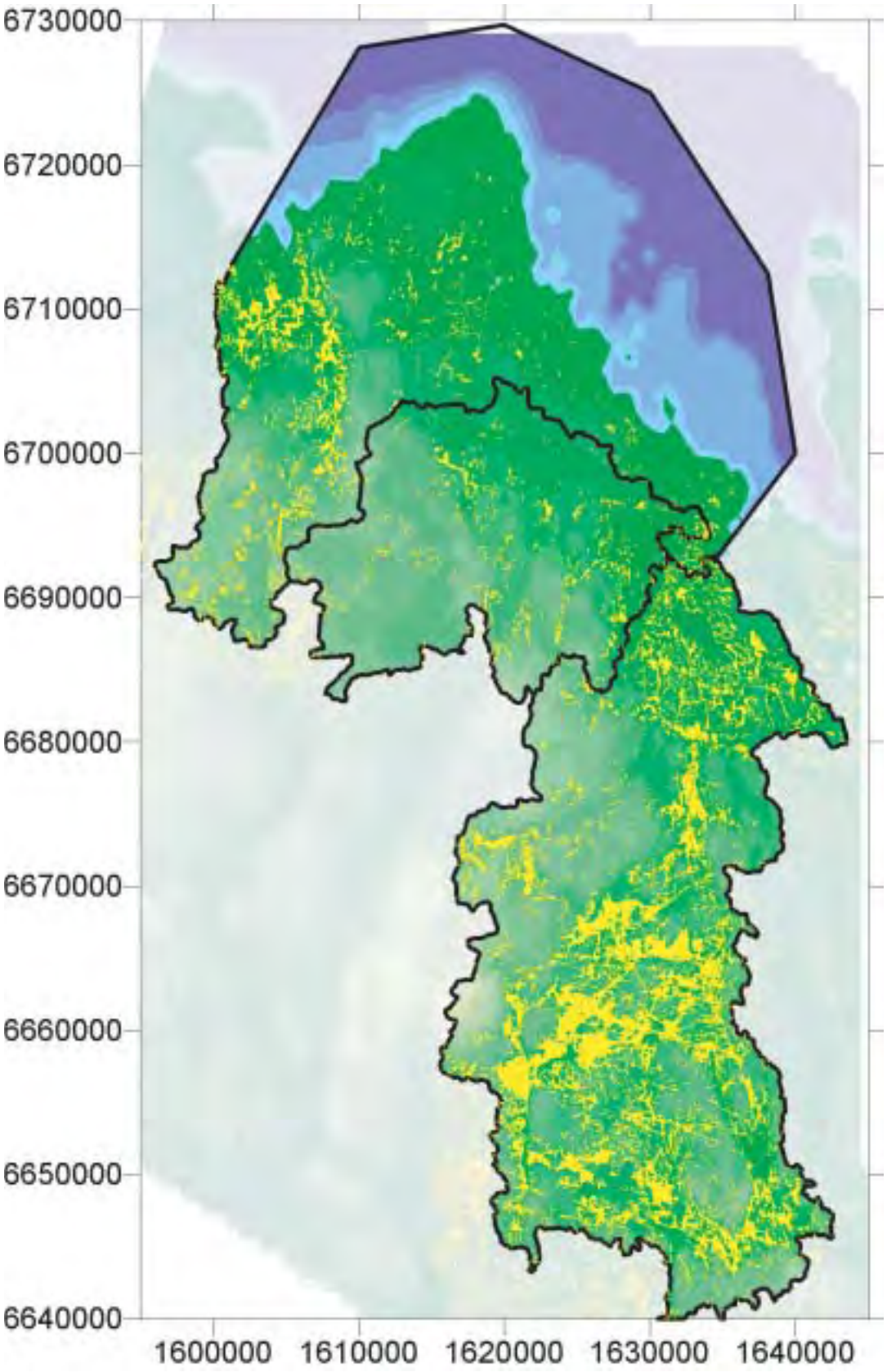

Figure 3-5. *Topography, surface water divides and areas covered by a low permeable clay.*

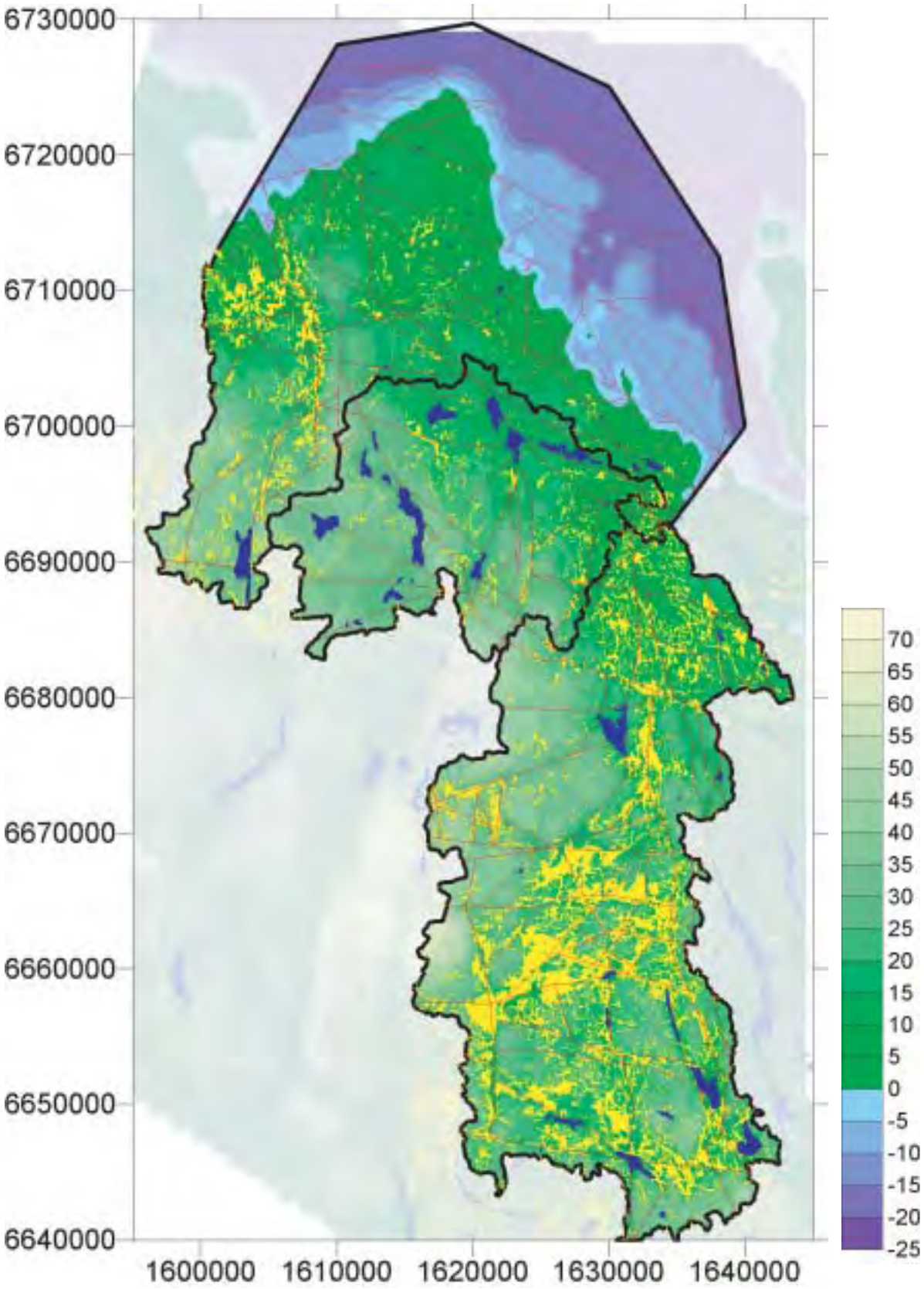

Figure 3-6. *Surface properties of the domain studied.*
Shades of green = topography above shoreline. Shades of blue = topography below shoreline.
Yellow = clay Dark blue = lakes. Orange lines = regional fracture zones.

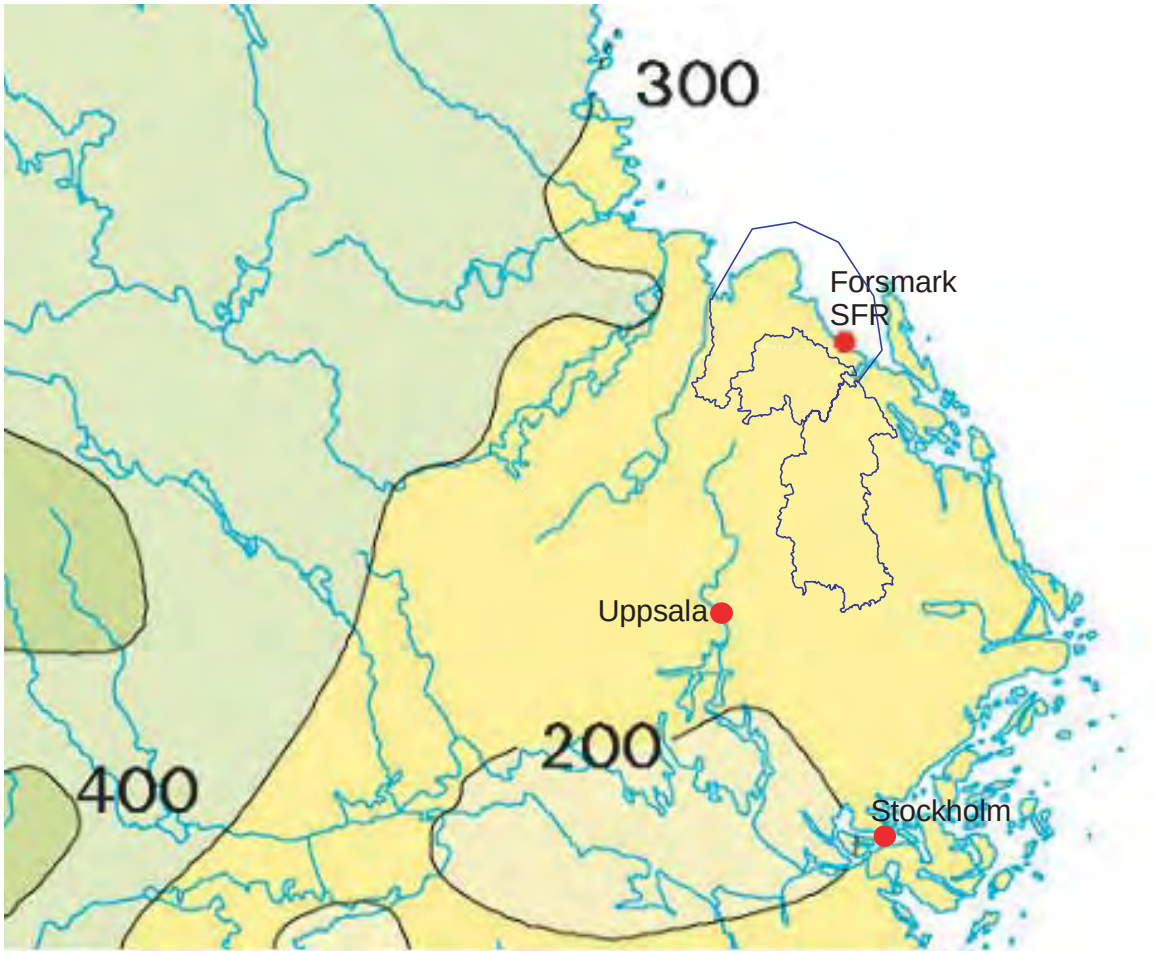

Figure 3-7. *The average run off (the potential recharge) for the province of Uppland /SMHI, 1999/. The position of area studied is denoted in the figure by use of blue lines. The average run off, for the area studied, is approximately 250 mm/year.*

4 Properties of the models

4.1 Size of model and boundary conditions

4.1.1 Size of model

The outer vertical boundary of the model coincides with regional water divides as given in Figure 3-2. These boundaries give the model a length in a north-south direction that is close to 90 km, and in the west-east direction the maximum length of the model is close to 50 km. The model represents an area of 2358 km^2. The upper boundary of the model is an undulating surface, the outer boundaries of the model are vertical and the lower boundary is an undulating surface.

4.1.2 Outer vertical boundary

As stated above, the outer vertical boundary of the model coincides with regional water divides (see Figure 3-2). These boundaries are surface water divides; hence no surface water flow takes place across these boundaries. In the model we assume that these boundaries are groundwater flow boundaries as well, accordingly in the model these boundaries are no-flow boundaries and in the model no groundwater flow will pass through these boundaries. This assumption is based on the observation that the regional surface water divides are along the highest regional topography and no larger hills occur in the surroundings. Hence, there is no area close to the domain studied where higher groundwater potentials may take place than along the regional surface water divides. Nevertheless, it is possible that some groundwater flow may take place across the regional surface water divides, due to regional fracture zones that may create a path across the boundary. Such, flows are probably very limited; this is demonstrated in Appendix A. It should be noted that the established model includes regional water divides that are entirely within the area studied (within the model); these water divides are not assigned any special boundary condition.

4.1.3 Boundary at base of model

The base level of the model is defined at a certain depth below the ground surface. Different vertical extensions have been analysed. Along the base of the model, the no-flow boundary condition is applied.

4.1.4 Boundary condition along the top of the model

The top boundary condition used for the model is either: (i) the specified head condition, representing the seawater table or (ii) a non-linear boundary condition, representing the ground surface above the Sea and the varying actual groundwater recharge. By use of the non-linear boundary condition we will **not** force a certain value of recharge or head condition upon the model. The model will calculate the actual recharge and the position of the groundwater surface as a part of its solution of the flow field (and these properties may vary with time). The extensions and positions of recharge and discharge areas will also be calculated by use of the non-linear boundary condition.

At the area studied the precipitation and the evapotranspiration produces a potential recharge that is much larger than the amount of recharge that can, on the average, infiltrate into the bedrock. The actual recharge varies depending on, potential recharge, topography, conductivity and the state of the groundwater system. For the areas not covered by the Sea, the non-linear boundary condition used by the GEOAN model reproduces closely the interaction between, the state of the groundwater system, the potential groundwater recharge and the ground surface topography. The non-linear boundary condition calculates the actual recharge and the position of the groundwater surface by the use of an iterative algorithm.

The iterative algorithm
First step: The model calculates the position of the groundwater surface and compares it to the topography, thereby estimating the extension of recharge and discharge areas.

Second step: The model estimates the actual recharge.

- Discharge areas: the model will use the specified head boundary condition at discharge areas. The head is set equal to the ground elevation and the model calculates the recharge-discharge components. The maximum recharge is equal to the potential recharge. The discharge is larger than zero.
- Recharge areas: the model will use a continuous boundary condition at recharge areas. The recharge is set equal to the potential recharge and the model calculates the head. The maximum head is equal to the ground surface. The discharge is equal to zero.

The steps are repeated.

For the areas covered by the Sea, the model will use the specified head boundary condition, representing the seawater table (assigned to the cells along the Sea floor). For the model representing the transient regional flow, the shore level displacement will not be simulated as an uplift of the land, but as a lowering of the level of the seawater table, a lowering in relation to a reference co-ordinate system. For each time step taken by the model, the seawater level is lowered, the topography is checked and areas above the new Sea level will be assigned the non-linear boundary condition. For the areas defined as lakes, the model will use the specified head boundary condition and a continuous confined condition (see below). For the areas defined as carrying a surface clay layer, a confined condition is used (see below).

4.1.5 Boundary at lakes

In the model lakes are defined on the models upper surface. The lakes of the model are in partial contact with the underlying groundwater system (see the figure below). The partial contact between the lake and the groundwater system is defined as follows. Along the perimeter (outer boundary) of a lake, the lake is defined as in full contact with the groundwater system, the lake perimeter is therefore defined with the specified head boundary condition, and the specified head corresponds to the surface water level of the lake. Inside of the perimeter, the lake is defined as isolated from the groundwater system. In reality this takes place because of low permeable lake bottom sediments. Consequently, the groundwater system below the lake (and inside of the lake perimeter) is defined as a continuous and confined flow system. The elevation of the lake bottom is defined as 0.5 m below the water level of the lake. Inflow and outflow of groundwater to a lake will only take place along the lake perimeter.

4.1.6 Boundary at clay layers

In the model some areas are defined as carrying a surface clay layer. The groundwater system below such areas is defined as confined and fully isolated from the surface water system. Consequently, the groundwater system below areas covered by clay is defined as a continuous and confined flow system. The lower elevation of the clay is defined in accordance to the topography. In the model, no inflow and outflow of groundwater will take place at cells below an area covered by clay. It should be noted that the local continuity and permeability of the clay layers is not known in detail. In this model we have however assumed that the clay is impermeable and that it is homogeneous and without any disruptions.

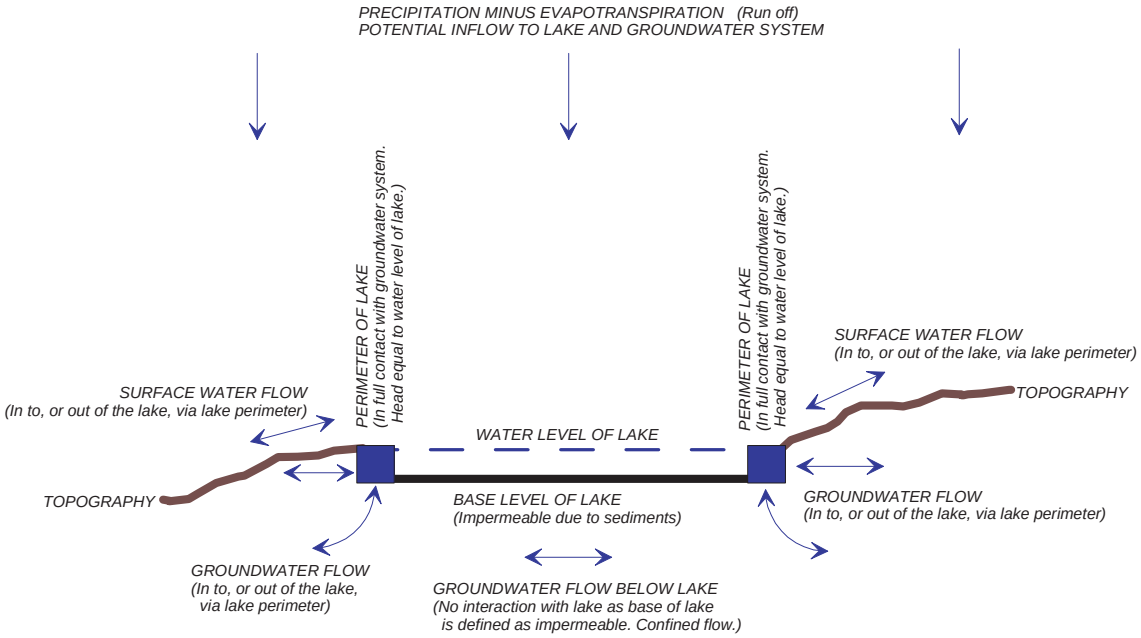

Figure 4-1. *A lake, as defined in the models.*

4.2 Discretization of domain studied

4.2.1 The Grid

A three-dimensional grid (mesh) of cells (elements) represents the domain studied. Several different grids have been analysed.

Horizontal discretization. The analysed grids are regular in the horizontal plane, i.e. all cells are of equal horizontal size. Models with different cell sizes have however been analysed. The smallest cell size analysed, is a model with cells of size: 330 m × 330 m; the model with the largest cells has a cell size of 10 km × 10 km. For the base case, the horizontal extension of a cell is 330 × 330 m.

Vertical discretisation. The models contain a number of different layers of cells. The elevation of the layers are defined in relation to the surface topography, hence all cells of a layer has the same vertical extension, but its elevation varies with the topography. The grids used are not regular in the vertical plane. The vertical extension of cells of the different layers varies with depth. The number of layers have been varied as have the vertical extension of the models, the base case has a depth of 1 100 m below ground surface and contains 11 layers. The vertical extension of the layers in the model of the base case are as follows: Layer 11 (upper layer)= 50 m, Layer 10= 70 m, Layer 9= 100 m, Layer 8= 100 m, Layer 7= 100 m, Layer 6= 70 m, Layer 5= 50 m, Layer 4= 70 m, Layer 3= 100 m, Layer 2= 150 m, Layer 1 (layer at base of model)= 240 m.

The horizontal discretization of the base case model (cell size 330 m × 330 m) is given below in Figure 4-2. The total number of cells in one layer is 21 651. For the 11 layers of the model, the total number of cells is 238 161. A vertical cross section of the grid is given in Figure 5-4.

4.2.2 Discretization of the lakes

The model will calculate which parts of the grid that represents a lake. For these calculations we have applied the condition that all cells that contains a part of a lake will be assigned as lakes. This will lead to an overestimation of the lake area, but as the lakes are limited in size and do not have many “fingers”, the method will produce an acceptable result. The extension of the lakes as defined in the base case is given below in Figure 4-3. The boundary condition on top of the model, applied along areas covered by lakes is presented in Section 4.1.5

4.2.3 Discretization of the areas that carries a surface clay layer

The model will calculate which parts of the grid that represents an area covered by clay. For these calculations it is not possible to apply the condition that all cells that contains a part of the clay areas will be assigned as clay-cells, because this will lead to a huge overestimation of the extension of the clay areas. This is because of the complicated geometry of the clay areas with many “fingers”. Instead a method was applied in which certain conditions regarding amount of clay in a cell studied and the shape of the clay areas were considered before assigning a cell as covered by clay. A trail and error procedure was carried out until an acceptable match with the actual extension of the clay areas was reached. This match is however an overestimation of the extension of the clay areas. The extension of the clay areas as defined in the base case model is given below in Figure 4-4. The boundary condition applied along areas covered by clay is presented in Section 4.1.6.

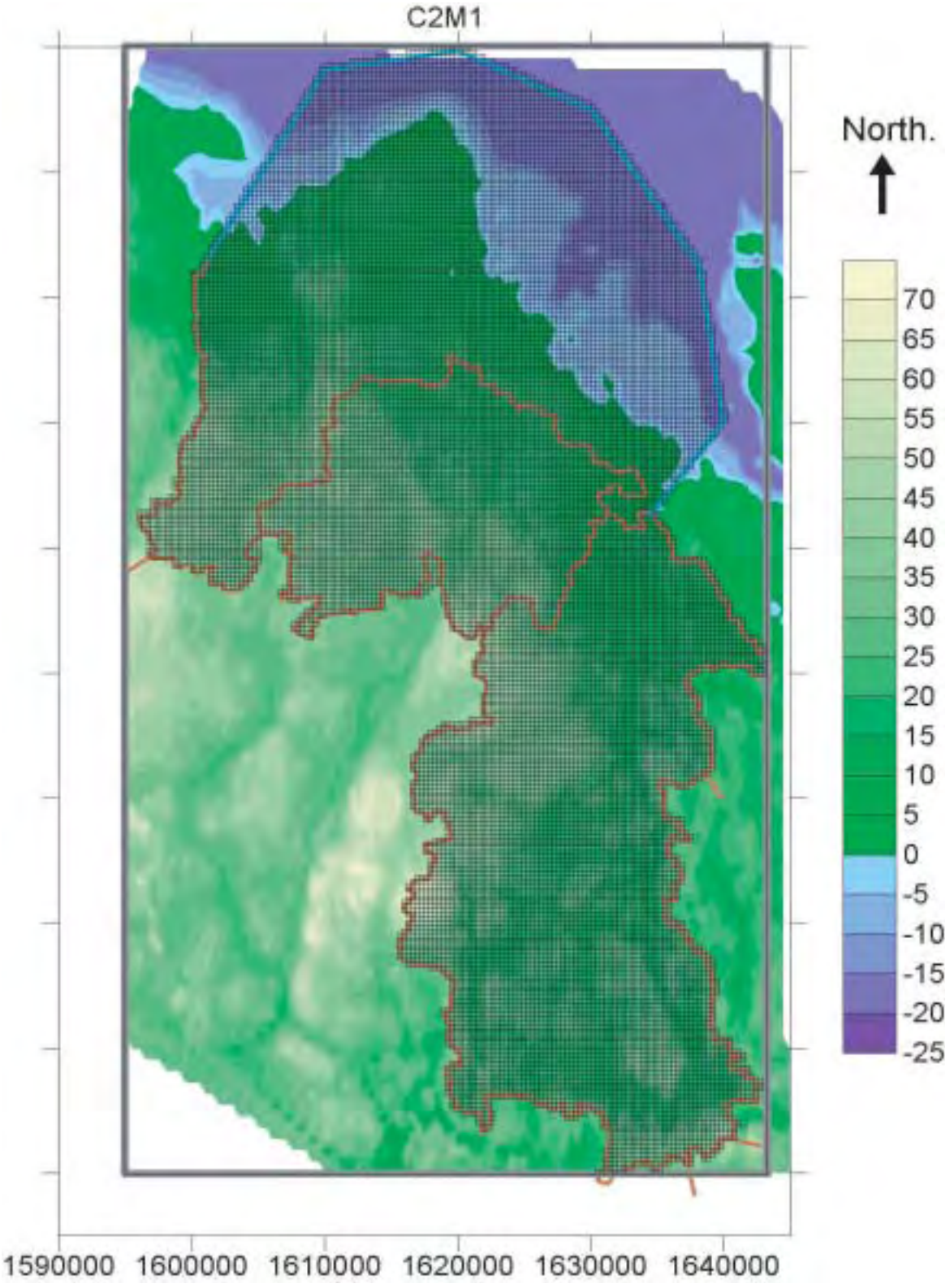

Figure 4-2. *Horizontal discretization of the base case. Cell size in horizontal plane is 330 m × 330 m.*

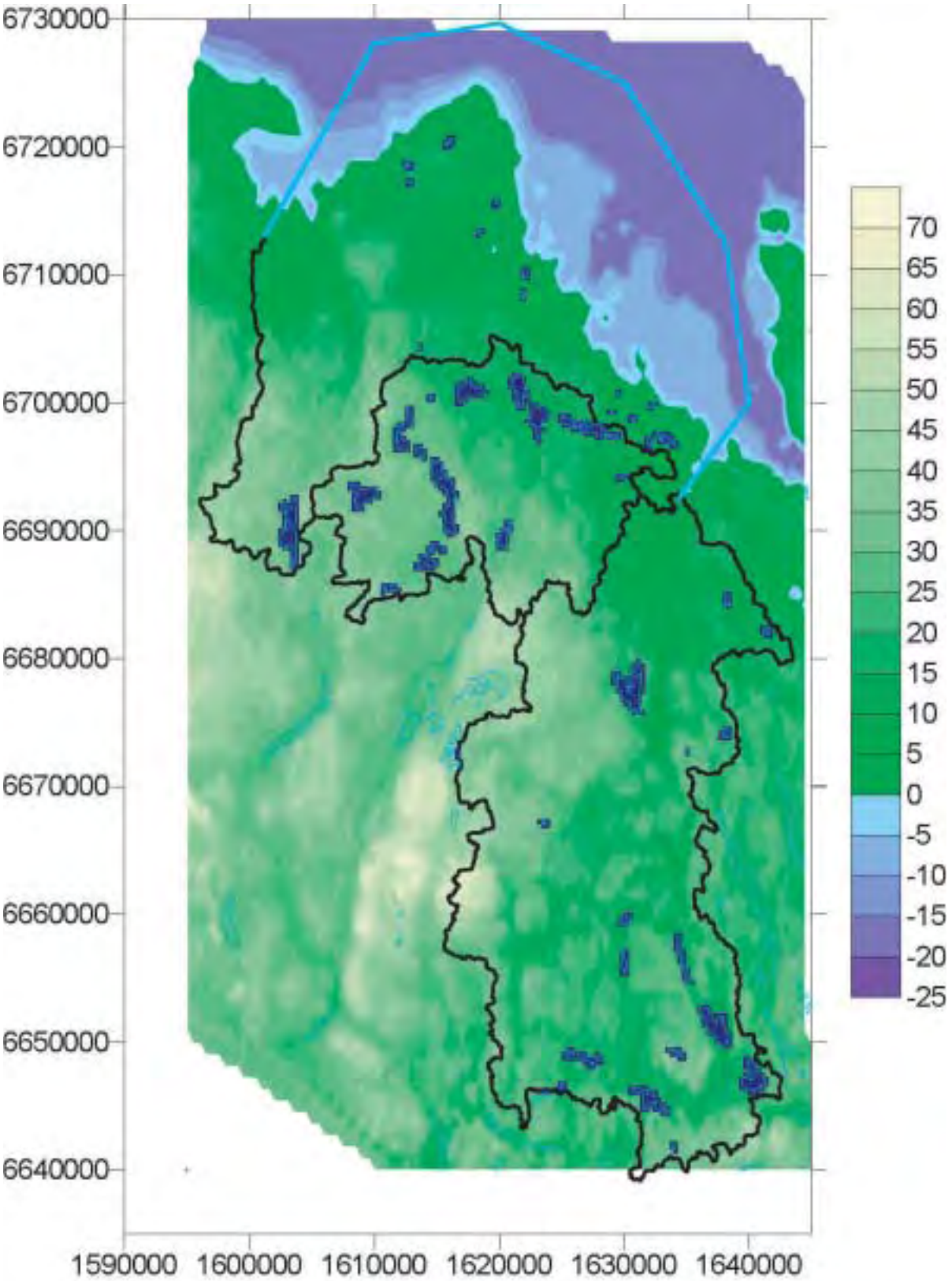

Figure 4-3. *Extension of lakes in base case model. The lakes of the model are denoted by squares.*

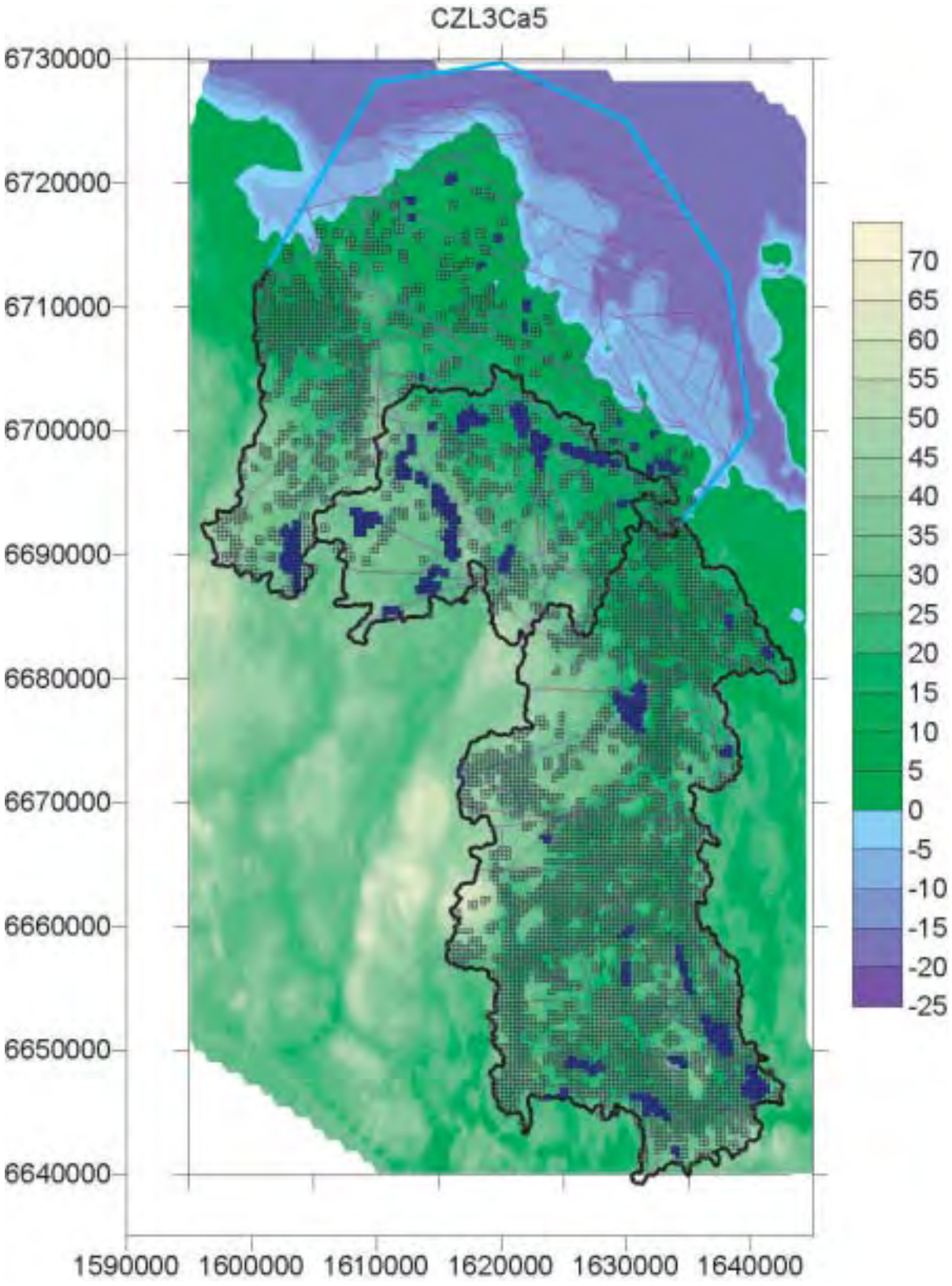

Figure 4-4. *Extension of clay areas and lakes in base case model. The clay areas are denoted by shaded squares. The lakes are denoted by dark blue squares. The purple lines denote the surface extension of the regional fracture zones.*

4.2.4 Discretization of the fracture zones

The model will calculate which cells the regional fracture zones intersect. In the models, the fracture zones are defined as separate continuous structures, by use of an implicit formulation as regards the conductivity of the cells intersected by the fracture zones.

Hence, a cell that represents a zone will also partly represent the surrounding rock mass. The calculation of the properties of such a cell is based on the condition that the transport capacity of the cell should include both the transport capacity of the zone and that of the surrounding rock mass. If the cell is small its properties will be dominated by the properties of the zone. If the cell is large and the zone is small, the properties of the cell will be dominated by the properties of the rock mass.

Cells intersected by a fracture plane will get an anisotropic conductivity formulation, in which some faces of the cells represent the rock mass only, and other faces represent both the zone and the rock mass. Even if the defined fracture zones forms a complicated geometry in three dimensions, by use of the implicit formulation the mesh can be defined as regular and the geometry of the mesh will not cause numerical difficulties.

Cells intersected by regional fracture zones are denoted below in Figure 4-5. In the model the fracture zones are defined all the way down to the base of the model.

4.2.5 Representation of the topography

The topography above shoreline given in the Figure 3-2 is based on a data-grid of size 50 m × 50 m. By use of a non-linear spatial interpolation this data-grid was transferred to the grid (mesh) of the models. The method for the spatial interpolation was based on the inverse distance between data points and by use of a weighting power equal to 2.0. The same method was used for the more sparse data below shoreline.

In the GEOAN model, the topography is defined at the centre of each cell of the grid. Hence, the exactness of the representation of the topography depends on the cell size; a grid with small cells will produce a better representation of the actual topography than a grid with large cells.

4.3 Permeability and porosity of flow domain

4.3.1 Permeability of rock mass

In the models the conductivity of the rock mass between the regional fracture zones was set to 5×10^{-9} m/s. This represents the conductivity of a rock mass without large fracture zones. It is the same value as the value used by /Holmén and Stigsson, 2001/ for the conductivity of the rock mass without fracture zones, in their model of the future groundwater flow at SFR (Forsmark). The value was derived based on the measured groundwater inflow to the tunnels at SFR /see, Holmén and Stigsson, 2001/. No depth trend is introduced to the hydraulic conductivity of the flow media. This decision is based on observations at different sites in Sweden, see /Walker et al, 1997/. It is however possible that rock permeability is reduced at extreme depths, i.e. depths below approximately 8 km. The vertical extension of the models (<= 4000 m) is not so large that it is necessary to reduce the permeability of the rock mass due to extreme depth.

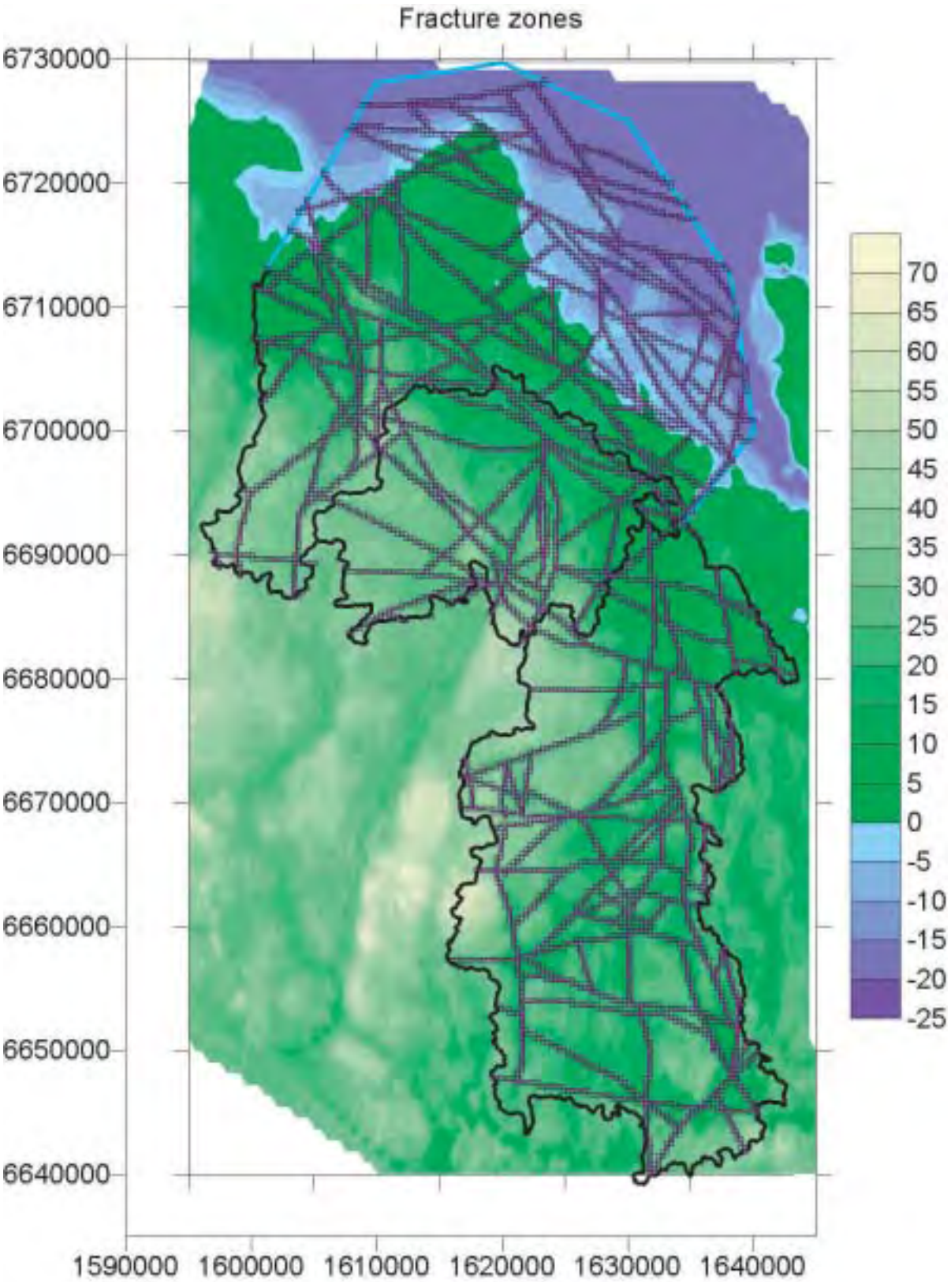

Figure 4-5. *Regional fracture zones (denoted by purple lines) and the cells at ground surface of the base case model intersected by the fracture zones (denoted by black squares). In the model the fracture zone are defined by use of an implicit formulation. Hence, only a part of the cells intersected will represent regional fracture zones.*

4.3.2 Permeability of regional fracture zones

In the model, the regional fracture zones are assumed to have the same properties as the Singö zone, which is a regional zone just off the coast, close to Forsmark. Hence, in the model the conductivity and width of the regional fracture zones are defined in accordance to the measure and estimated properties of the Singö zone.

According to the SFR safety report /SKB, 1993/ the Singö zone is assumed to consist of three parts: a core with a large conductivity and two outer parts with a somewhat smaller conductivity (this assumption goes back at least to /Carlsson, 1986/. The thickness of the different parts are: 14 m (outer part), 2.4 m (core) and 14 m (outer part), which together gives a thickness of 30.5 m. All together the three parts produces a total transmissivity of 2.4×10^{-5} m^2/s. The corresponding conductivity becomes 7.87×10^{-7} m/s.

In the models of this study, the regional zones are defined with a width of 30 m and a conductivity of 8.0×10^{-7} m/s. No depth trend is introduced to the hydraulic conductivity of the flow media. This principle is based on observations at different sites in Sweden, see /Walker et al, 1997/.

4.3.3 Porosity, yield and storativity

Effective porosity

The effective porosity (kinetic porosity or transport porosity) is defined as the ratio of the volume of interconnected pore-space available for fluid transmission to bulk volume of the soil or the rock. The calculated advective breakthrough times are directly proportional to the effective porosity. In the models a single value of the effective porosity was used for the whole domain studied, both for the rock mass and for the fracture zones. This value is equal to **0.001**. The value should be looked upon as a possible value; it was partly chosen to facilitate a comparison with other studies in which this value is used. The calculated breakthrough times are directly proportional to the effective porosity, and as the effective porosity is set as constant in the whole of the model, the breakthrough times for other values of the effective porosity are easily calculated based on the following formula:

$t_{new} = (n_{new} / 0.001) t_{given}$

t_{new} = *Breakthrough time with new value of effective porosity.*

n_{new} = *New value of effective porosity*.

t_{given} = *Breakthrough time given in this study*.

Specific yield and the storativity

The specific yield and the storativity are properties that should be included in a time-dependent model. The specific yield defines the amount of water that is released/stored in the flow medium when the groundwater surface moves. This property is mainly related to the porosity, we have assumed a value equal to 0.005 (m^3/ m^3), which is the same as 0.5%. The storativity defines the amount of water that is released/stored in the flow medium when the groundwater head changes. This property is related to the rock stresses, we have calculated a value equal to $5 \cdot 10^{-6}$ (1/m), based on the following equation /Carlsson and Gustafsson, 1984/.

$S_s = \rho_w \cdot g \cdot (n \cdot \beta_w + \beta_s)$

S_s = *Storativity (1/m)*

ρ_w = *density of water, 1000 kg/m^3*

g = *acceleration of gravity, 9.81m/s^2*

n = *porosity 0.5%*

β_w = *compressibility of water $4 \cdot 10^{-10}$ m^2/N*

β_s = *compressibility of rock $5 \cdot 10^{-10}$ m^2/N*

5 Results of primary model chain

5.1 General conditions for solution and analyses

The models presented in this chapter were all solved for steady state conditions. Density dependent flow was not included in the flow solution. The flow fields of the models were analysed for flow paths from a depth that corresponds to the possible depth of a repository, i.e. depths between 490 and 540 m below ground surface. The flow paths were derived through particle tracking (see Section 2.9). Several flow paths were analysed for each cell at the elevation studied, The total number of analysed flow paths, for each case studied, were approximately 65 000. The flow paths were analysed considering length and breakthrough time. Different distributions were obtained for the parameters studied, e.g. breakthrough times for the flow paths from all studied cells inside the shoreline, or breakthrough times for the flow paths from all studied cells at a certain distance from the shore line, etc. For the different cases studied, the properties of these distributions were compared.

5.2 Case 1 – Uniform rock mass, topography as inclined plane

This is the most simplified of all the models studied. It is not a realistic case, but a case that demonstrates the flow field of a homogeneous model, having topography without local undulation. In comparison with the other models, this model will demonstrate the importance of the undulation of local topography. The topography of the model is given in Figure 5-2, below.

A vertical cross-section through the grid of the model with an inclined plane as the topography is given in Figure 5-1, below. Note that the scale in the vertical direction is 10 times larger than the scale in the horizontal direction. The blue cells denote the Sea floor. The maximum topographic elevation is 120 masl, the minimum topographic elevation is –25 masl.

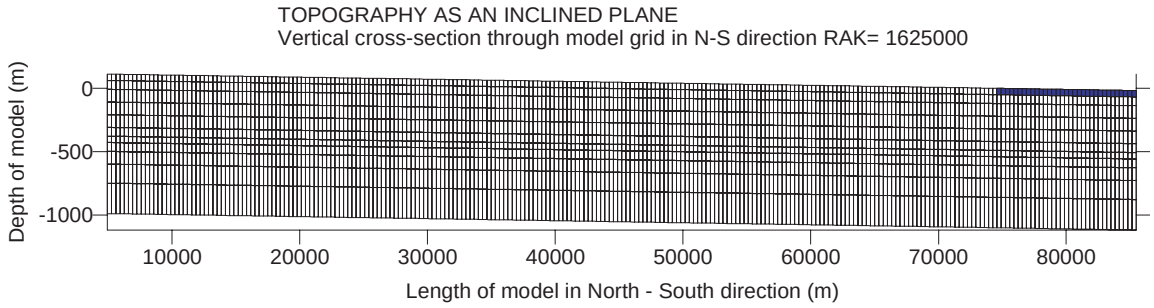

Figure 5-1. *Vertical cross section through the grid of the model (Case 1) with an inclined plane as the topography (only the active cells are plotted). Note that the scale in the vertical direction is 10 times larger than the scale in the horizontal direction.*

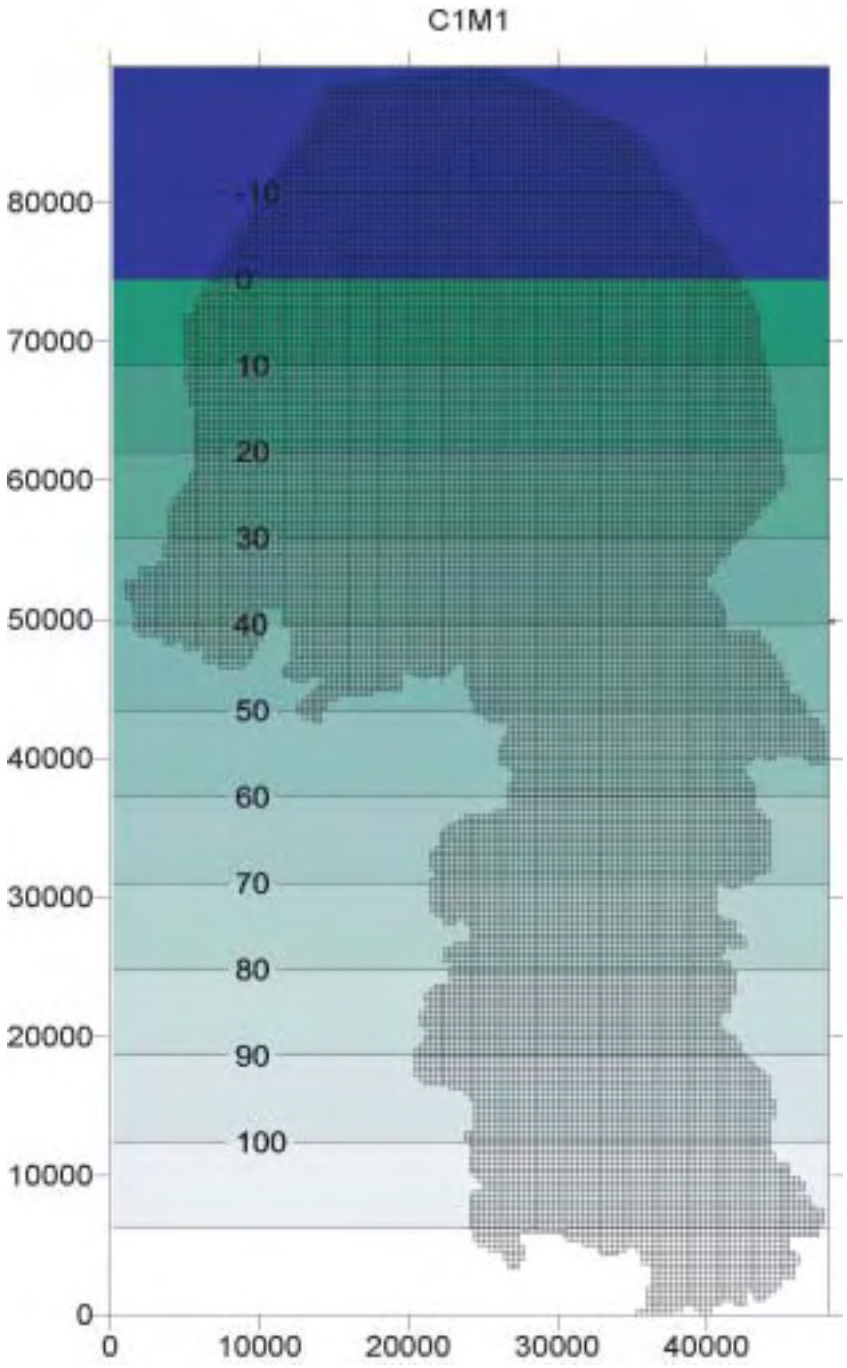

Figure 5-2. *Topography and grid of the model with an inclined plane as the topography. The blue colour denotes the position of the Sea.*

The flow field of the model was investigated by use of flow paths; these were released inside the shoreline between a depth of 490 m and 540 m. Considering different distances to the shoreline, different distributions of flow path length were obtained. Figure 5-3 demonstrates how the shapes of these distributions vary with distance to the shoreline. It is demonstrated by the figure that most flow paths will flow towards the Sea, regardless of release point, i.e. for most flow paths the length of the path is close to the distance to the Sea. At large distances from the shoreline, a certain amount of the flow paths will discharge at ground surface at different distances from the release point. This is because of the complex shape of the models outer boundaries; these boundaries follow water divides that are not present in this model, as the topography of the model is given by an inclined plane. For all flow paths in one sample, the following distribution of path lengths was obtained (see Table 5-1).

We conclude: This is the most simplified of all the models studied. It is not a realistic case, but a case that demonstrates the flow field of a homogeneous model, having topography without local undulation. Without any local topographic undulation, the flow field is primarily controlled by the regional topographic gradient, and with little regard for the complex horizontal shape of the model, most flow paths (about 70%) will flow towards the shoreline and discharge below the Sea or close to the shoreline. For such a situation, the repository positions with the longest flow paths and breakthrough times are positions as far as possible from the shoreline, because on the average flow paths length (and breakthrough time) increases with distance from the Sea.

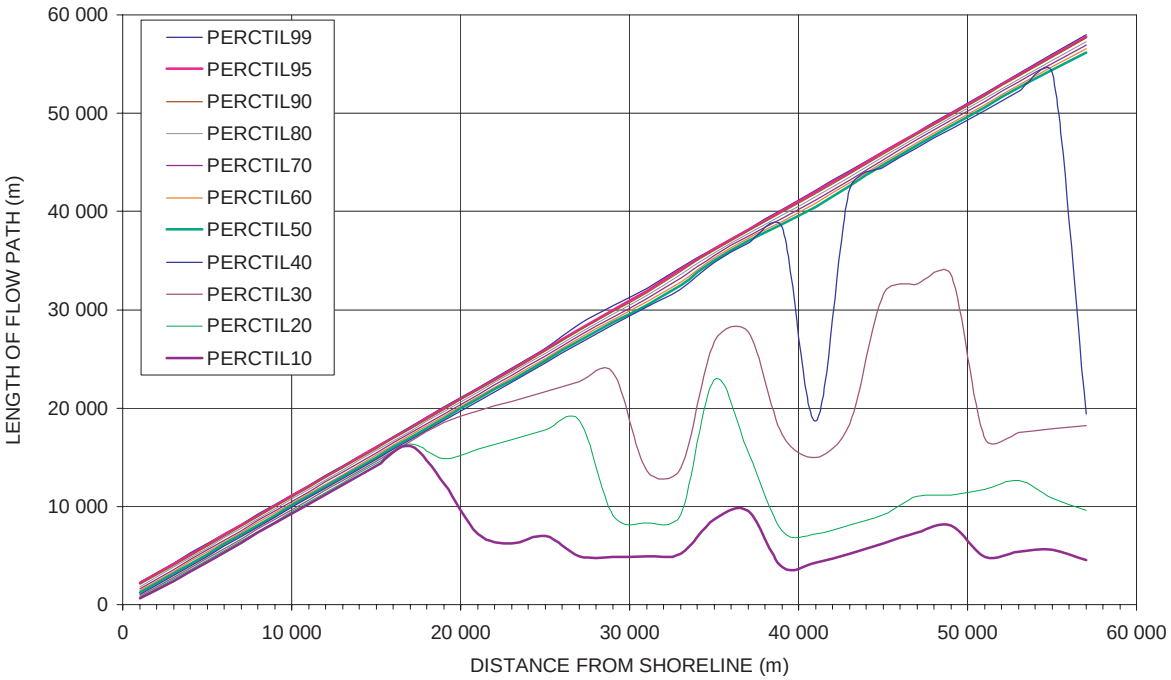

Figure 5-3. *Case 1. Flow path length versus the distance between the release point and the Sea. Flow paths were released at repository depth (depth= 490–540m), and inside shoreline.*

Table 5-1. Case 1. Percentiles of flow path length, all paths in one sample. Paths are from repository depth, no paths are released below the Sea.

Case	Percentiles of flow path length (m)				
	90th	70th	50th	30th	10th
C1	54900	28200	17500	9400	3000

5.3 Case 2 – Uniform rock mass and an undulating topography

The only difference between this model and the previously presented model is the topography; this model carries the actual topography on top, with the local topographic undulation. In comparison with the previous model, this model will demonstrate the importance of the undulation of local topography. The topography of the model is given in Figure 3-2, above. The horizontal discretisation of the model studied is that of the base case, as given in Figure 4-2, above. A vertical cross-section through the grid of the base-case model (with the undulating topography) is given in Figure 5-4, below. Note that the scale in the vertical direction is 10 times larger than the scale in the horizontal direction. The red dot denotes the layer of cells that are between 490 m and 540 m below ground surface; this is the repository depth. The blue cells denote the Sea floor. The maximum topographic elevation is approximately 60 masl, the minimum topographic elevation is –25 masl.

The flow field of the model was investigated by use of flow paths; these were released inside the shoreline between a depth of 490 m and 540 m. Considering different distances to the shoreline, different distributions of flow path length were obtained. Figure 5-5 demonstrates how the shapes of these distributions vary with distance to the shoreline, figure (i) has the same Y-scale as Figure 5-3, and figure (ii) is given in a scale adjusted to the distributions produced. A comparison of Case l (Figure 5-3) and Case 2 (Figure 5-5) demonstrates that the flow field of Case 2 is very different from that of Case 1. The flow paths of Case 2 are much shorter than those of Case 1, and in Case 2 there is no general trend of increasing flow path lengths with distance from shoreline. The reason for this is that in Case 2 the local undulation of the topography creates local groundwater flow cells, and these local flow cells dominates the flow pattern of the groundwater. Examples of flow paths are given in Figure 5-6, below.

For all flow paths in one sample, the following statistical distribution was obtained (see Table 5-2).

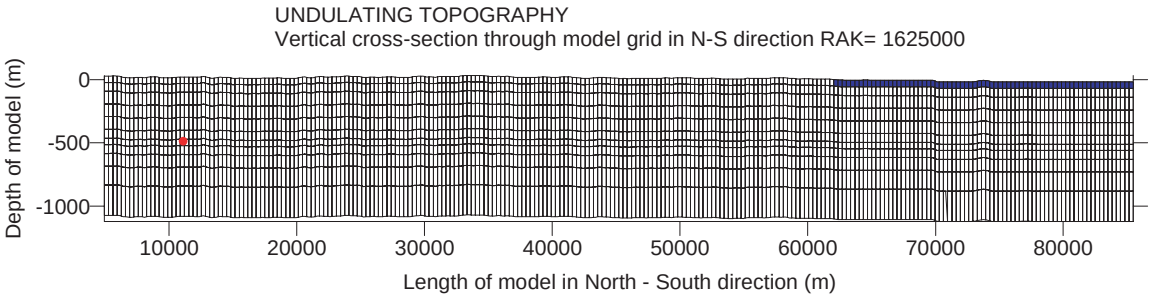

Figure 5-4. *Vertical cross section through the grid of the base-case model (only the active cells are plotted). Note that the scale in the vertical direction is 10 times larger than the scale in the horizontal direction.*

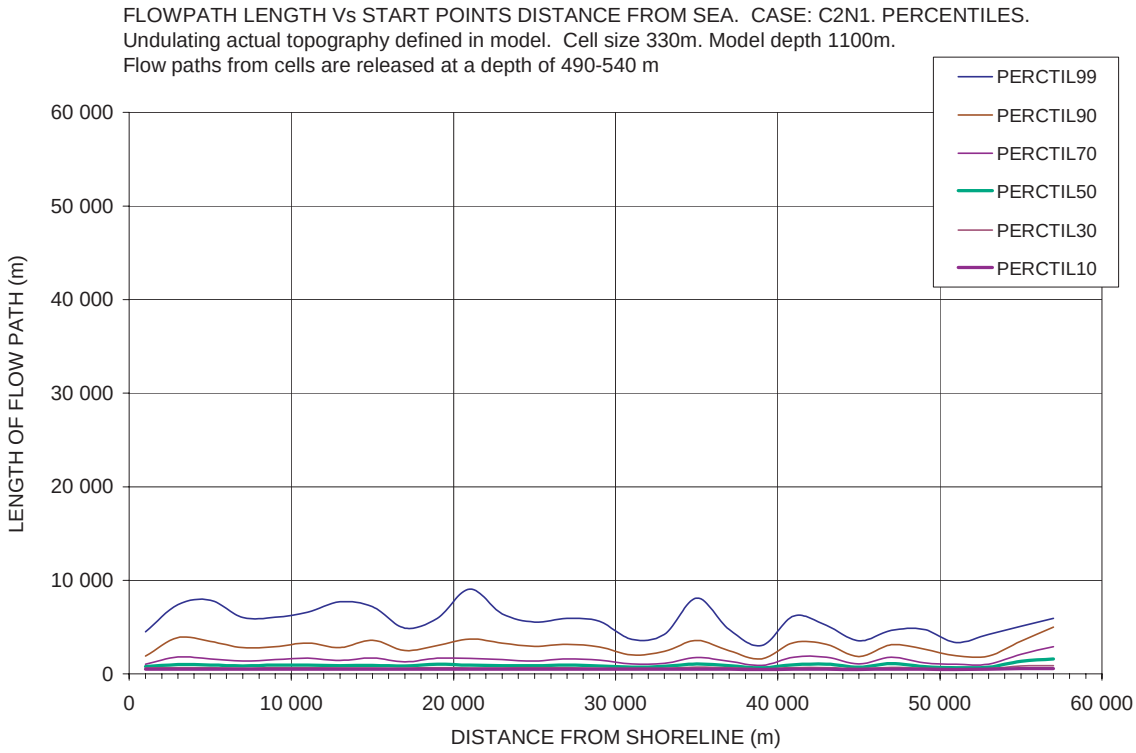

Figure (i)

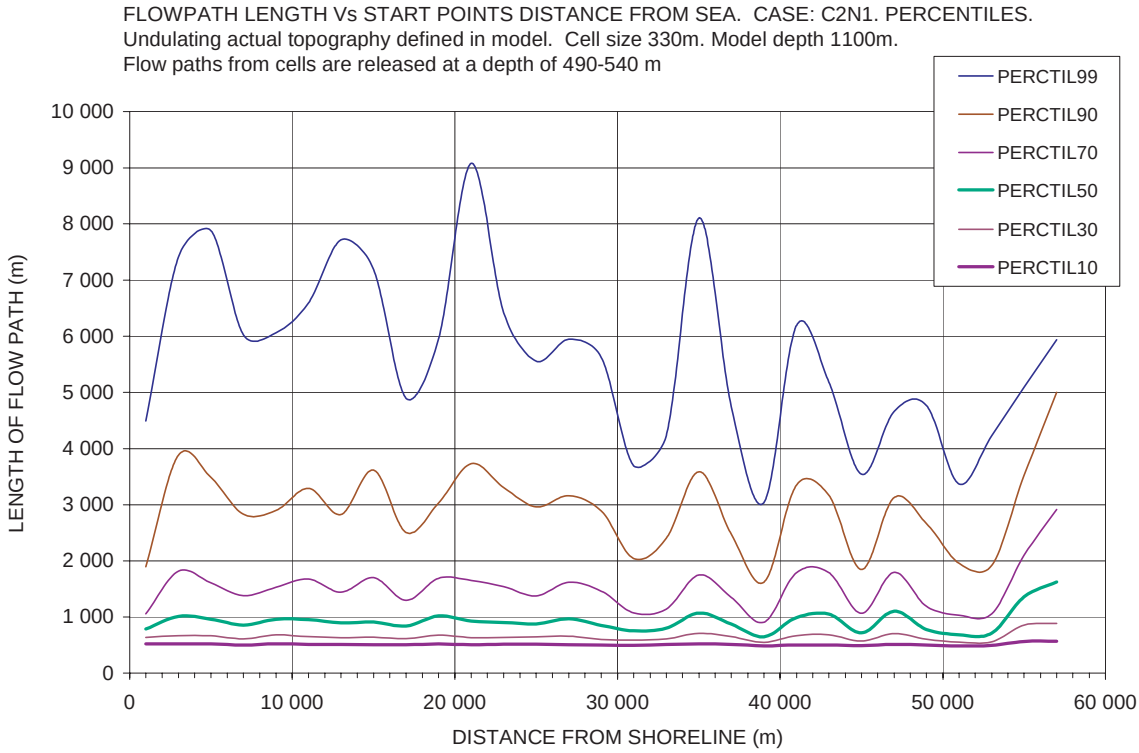

Figure (ii)

Figure 5-5. *Case 2. Flow path length versus the distance between the release point and the Sea.*

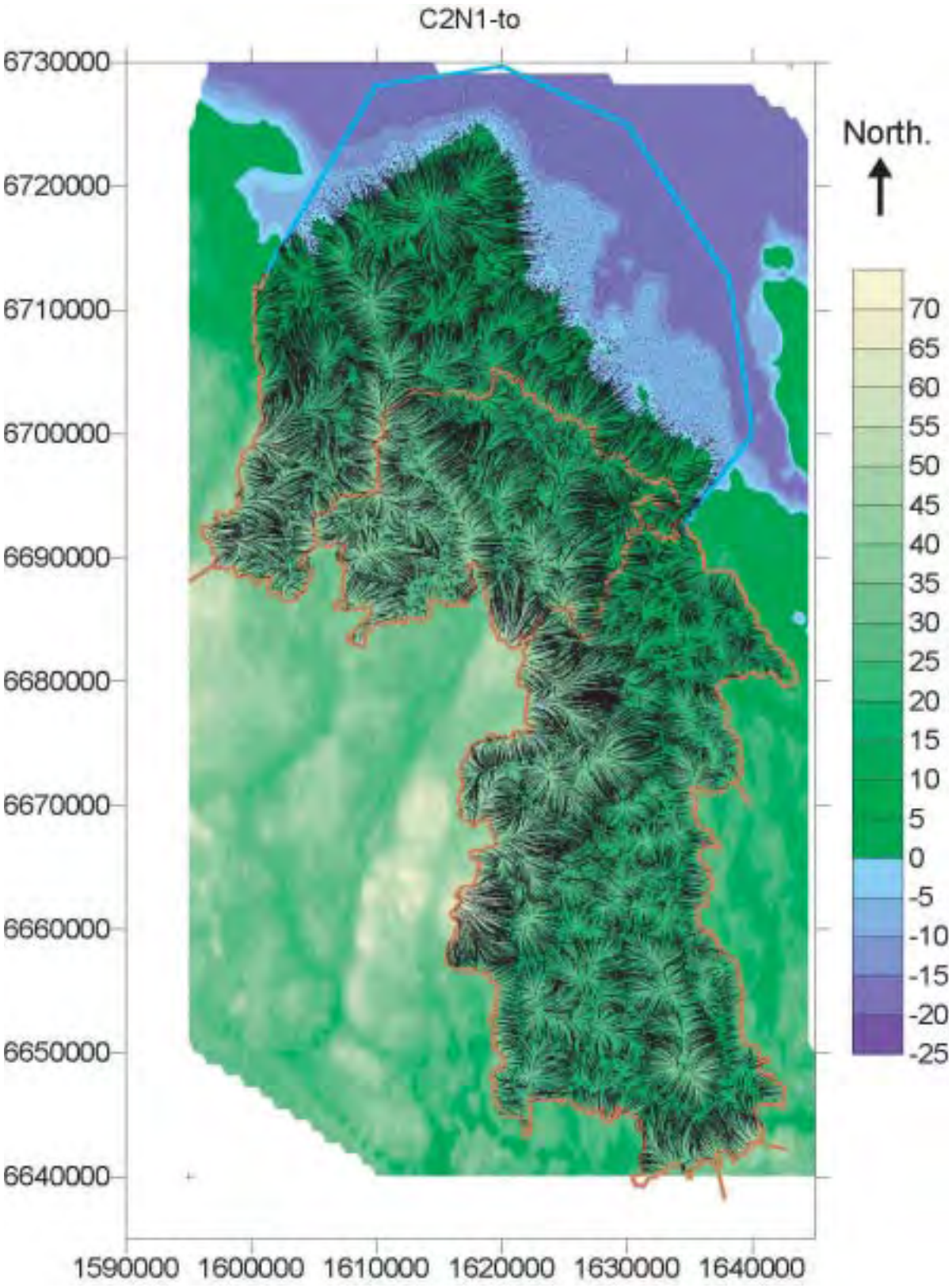

Figure 5-6. *Case 2. Flow paths released at repository depth (depth=490–540m). The figure presents one path for each cell of the layer that represents repository depth, which gives 21 000 paths, plotted in the figure above.*

Table 5-2. Case 2. Percentiles of flow path length, all paths in one sample. Paths are from repository depth, no paths are released below the Sea.

Case	Percentiles of flow path length (m)				
	90th	70th	50th	30th	10th
C2	3020	1490	930	680	560

Most flow paths will discharge on the ground surface relatively close to their start positions, 90% of the paths are shorter than 3 km. Regardless of distance to the Sea, the 50th percentile of flow path lengths is close to 1000 m.

Repository positions with long flow path lengths can be found at many different places within the domain studied. There is no general trend that the positions with large path lengths are located as far as possible from the shoreline. The 500 positions (cells) with the longest paths are given in Figure 5-7, above. Each position corresponds to an area of 330 m × 330 m. Based on the figure above we note that repository positions with long flow path lengths are located below local topographic heights. The heights are recharge areas hence, below the heights in the rock mass, the groundwater flow is to a large degree directed downwards. Flow paths from such positions will be long as such positions are at the upstream part of a groundwater flow-tube.

The 500 positions (cells) with the longest paths corresponds to the very upper part of the distribution of all flow path lengths, it corresponds approximately to the flow paths above the 97th percentile. These paths demonstrate lengths between 13 200 m and 4600 m. For the 100 positions with the longest paths, the path length varies between 13 200 m and 6 700 m.

Breakthrough times are not only dependent on length of flow paths, but also on the groundwater velocity. A long flow path with large velocity may have a shorter breakthrough time than a short path with a small velocity. Considering repository positions at depths between 490 m and 540 m and the whole domain studied, including repository positions outside the shoreline (below the sea), for such a situation the repository positions with the longest breakthrough times are given in Figure 5-8, below (breakthrough times for flow paths from repository positions to ground surface or Sea floor). As can be seen in the figure all positions are below the Sea.

Interesting information provided by Figure 5-8, is the general location of the repository positions – they are all below the Sea and as far away as possible from the shoreline. Below the Sea the gradients of the groundwater flow field are very small and consequently the breakthrough times are large (see also Figure 5-11). However, for the repository positions below the Sea, the lengths of the flow paths are short; they are more or less straight upwards to the Sea floor, which produces lengths in the range of 500 m; nevertheless the breakthrough times are large due to the very small velocities. Considering the 500 positions with the largest break through times (all located below the Sea), the breakthrough times varies between $4x10^{11}$ years and $3x10^{9}$ years.

Introducing the condition that only repository positions inside the shoreline should be considered in the analyses will produce the repository positions given in Figure 5-9. For the 500 positions with the longest breakthrough times, the breakthrough times varies between 1 342 000 years and 70 500 years. For the 100 positions with the longest breakthrough times, the breakthrough times varies between 1 342 000 years and 134 000 years. For this situation many of the positions with long breakthrough times are located close to the shoreline. The 10 positions with the largest break through times are all located close to the shoreline or below islands. The paths from these positions extend below the Sea where the velocities are small, which produces large breakthrough times.

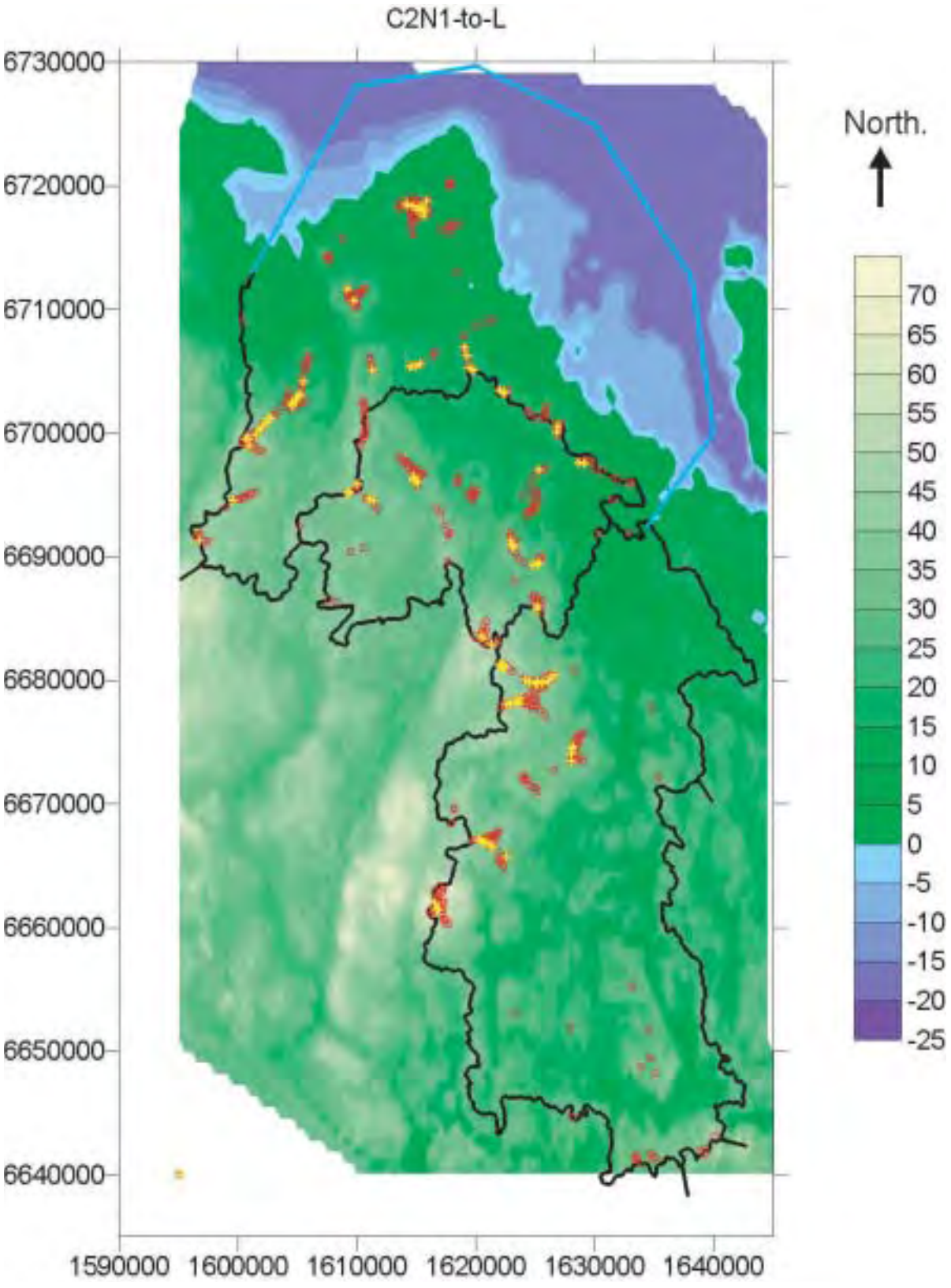

Figure 5-7. *Case 2. The 500 repository positions (Red dots) and the 100 positions (yellow dots), with the longest flow path length from repository to ground surface (one position corresponds to an area of 330 × 300 m). All flow paths are released inside of the shoreline (or below an island).*

Even if off-shore positions seem ideal with respect to breakthrough times, this situation may change due to the ongoing shore level progress (land rise). Positions that are today close to the shoreline or below the Sea may in the future be above the Sea and at some distance from the shoreline; and the flow paths for these positions will no longer be the same for such a situation. /Holmén and Stigsson, 2001/ have predicted the change in local groundwater flow conditions for the SFR area, considering a shoreline that passes over a repository located at shallow depth (50 m below the Sea flow). They concluded that both direction and size of the groundwater flow changes as the shoreline retreats and passes above the repository; and a situation similar to the present situation above the shoreline will develop within a few thousands of years. It follows that the shore level progress is fast compared to the very slow velocities of the flow paths at great depth below the Sea. Hence, assuming that the shore level progress will continue in the future, the breakthrough times of the flow paths that are at present at great depth below the Sea may in the future be shortened, if the shore level progress continues.

Breakthrough time for flow paths from repository depth is given below in Table 5-3. The table is based on repository positions inside the shoreline (flow paths that start outside of the shoreline, below the Sea, were not considered when the statistics were calculated).

Case 2 demonstrates that above the shoreline, the local undulation of the topography creates local groundwater flow cells, and these local flow cells dominate the flow pattern of the groundwater. It should however be noted that this flow situation (as seen in Figure 5-6) follows not only from the local undulation of the topography, but also from the size of the permeability of the flow medium and the size of the groundwater recharge. For this situation to take place it is necessary that (i) the permeability (length/time) of the flow medium is small compared to the potential groundwater recharge (length/time), or that (ii) the potential recharge is large compared to the permeability. Considering a fractured crystalline rock mass and the North European climate, both the above discussed conditions are fulfilled: the permeability is small and the potential recharge is large.

A comparison of repository positions inside the shoreline, considering both longest path lengths (Figure 5-7) and longest breakthrough times (Figure 5-9), demonstrates that the positions are not the same. Positions below local heights will produce long flow paths, but the gradients could be large at such places, which may produce short break through times.

Table 5-3. Case 2. Percentiles of breakthrough time for flow-paths from repository depth (490–540 m), all paths in one sample. *No* paths are released below the Sea.

Case	Percentiles of breakthrough time (years)				
	90^{th}	70^{th}	50^{th}	30^{th}	10^{th}
C2	6840	2670	1480	880	480

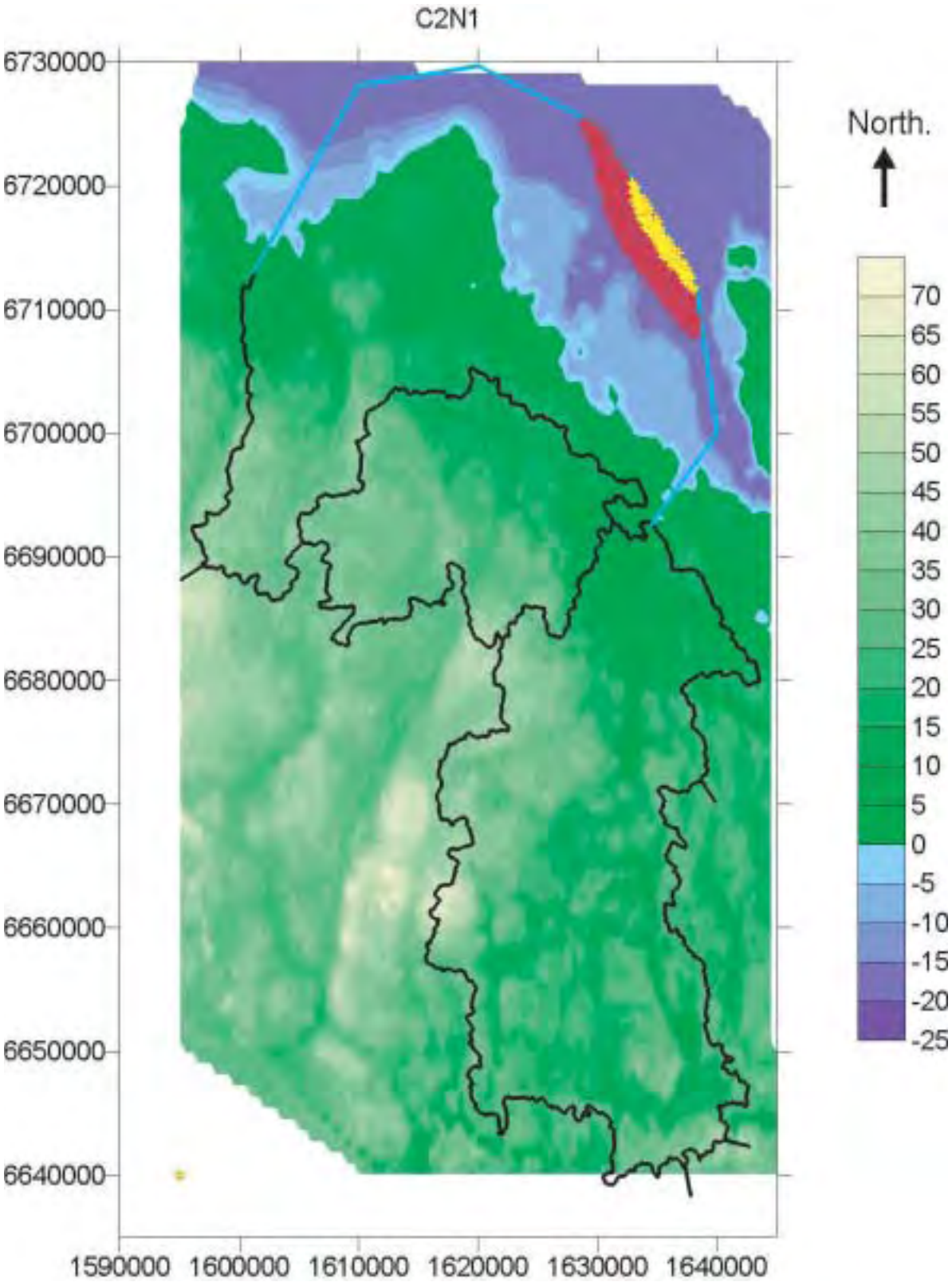

Figure 5-8. *Case 2. The500 repository positions (Red dots) and the 100 positions (yellow dots) with the longest breakthrough times, from repository to ground surface. One repository position represents an area of 330 m × 330 m. Repository positions both inside and outside the shoreline were considered.*

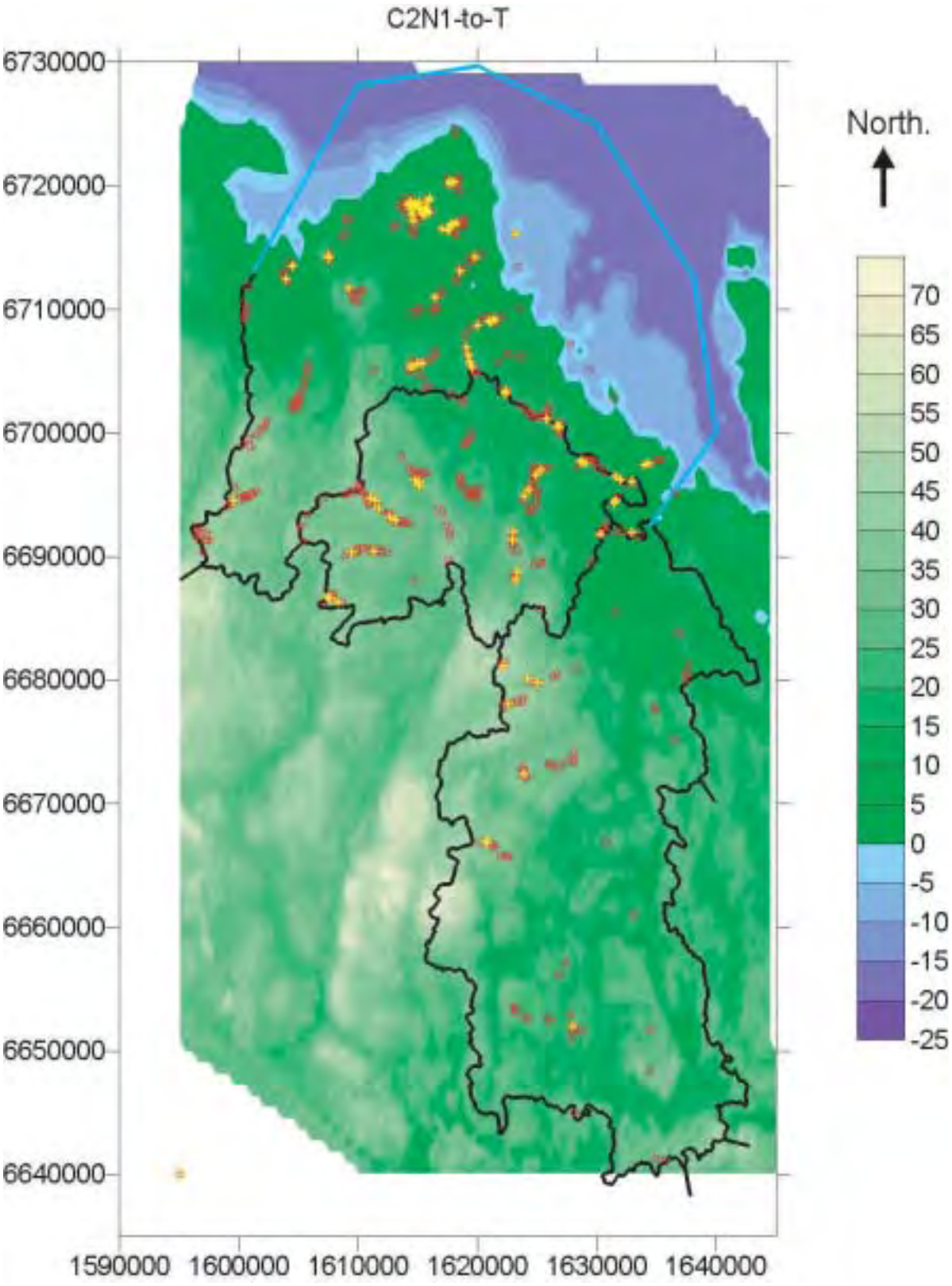

Figure 5-9. *Case 2. The 500 repository positions (Red dots) and the 100 positions (yellow dots) with the longest breakthrough times, from repository to ground surface. One repository position represents an area of 330 m × 330 m. All flow paths are released inside the shoreline (or below an island).*

We conclude: The groundwater flow field at repository depth and above it (above a depth of approximately 540 m) is primarily controlled by the local topographic undulation. Regardless of distance to the Sea, most flow paths will be shorter than 3 km (90^{th} percentile). Repository positions with the longest flow path lengths are not necessarily located far away from the Sea. Repository positions with long flow paths lengths are found at many different positions within the domain studied and at different distances to the Sea. The positions are however all located below local topographic heights. Considering breakthrough time, a more complex situation arises. Many of repository positions with long breakthrough times are close to the shoreline or outside of the shoreline (below the Sea), because of the small hydraulic gradient below the Sea. However, the shoreline will not stay the same in the future. Due to the shore level progress, the Sea will retreat and positions that today are below or close to the Sea may in the future be above the Sea, and this will change the flow paths from these repository positions. A comparison of repository positions inside the shoreline, considering both longest path lengths and longest breakthrough times, demonstrates that the positions are not the same. Positions below local heights will produce long flow paths, but the gradients could be large at such places, which may produce short break through times.

5.4 Distribution of specific flow for three different cases

Size of groundwater flow may be characterized by use of the specific flow concept. The specific flow [m/s] is the flow per unit area at right angle to the direction of flow. The distributions of specific flows in three different models are given in Figure 5-10, Figure 5-11 and Figure 5-12 (below). The importance of the local topography and the heterogeneity of the rock mass is well demonstrated by these three figures. The different cases presented in the figures are:

- Case 1: homogeneous flow medium with topography as an inclined plane,
- Case 2: homogeneous flow medium with undulating topography and
- Case 6: heterogeneous flow medium, uniform rock mass plus regional vertical fracture zones, with undulating topography, lakes and a discontinuous clay layer (Case 6 is presented in more detail in Section 5.11).

The figures use three-dimensional views (with a very exaggerated vertical scale) and a logarithmic colour scale for representing the specific flow of the rock mass. Size of specific flow varies in the models of all three cases, as demonstrated by the figures, but in Case 1 the variation is not large upstream of the shoreline. A much more complex distribution and larger variation of the specific flow takes place in Case 2, this is a result of the undulating topography. The inclusion of the fracture zones etc in Case 6 produces an even more complex distribution and variation of the specific flow. It is well demonstrated by the figures that for the cases with undulating topography the specific flow (the velocity) is the smallest below the Sea.

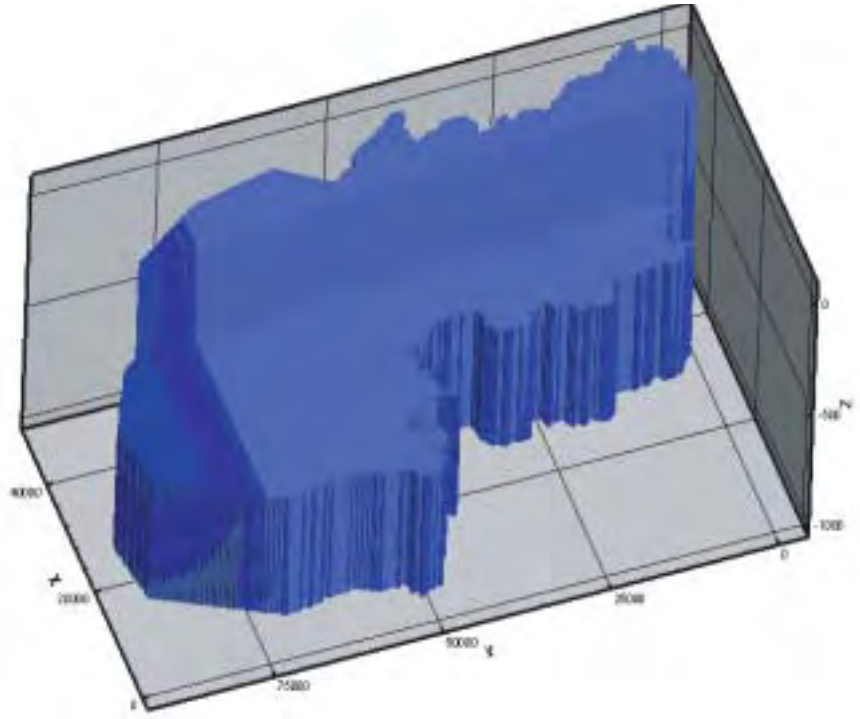

Figure 5-10. *Case 1: distribution of specific flow (homogeneous flow medium with topography as an inclined plane).*

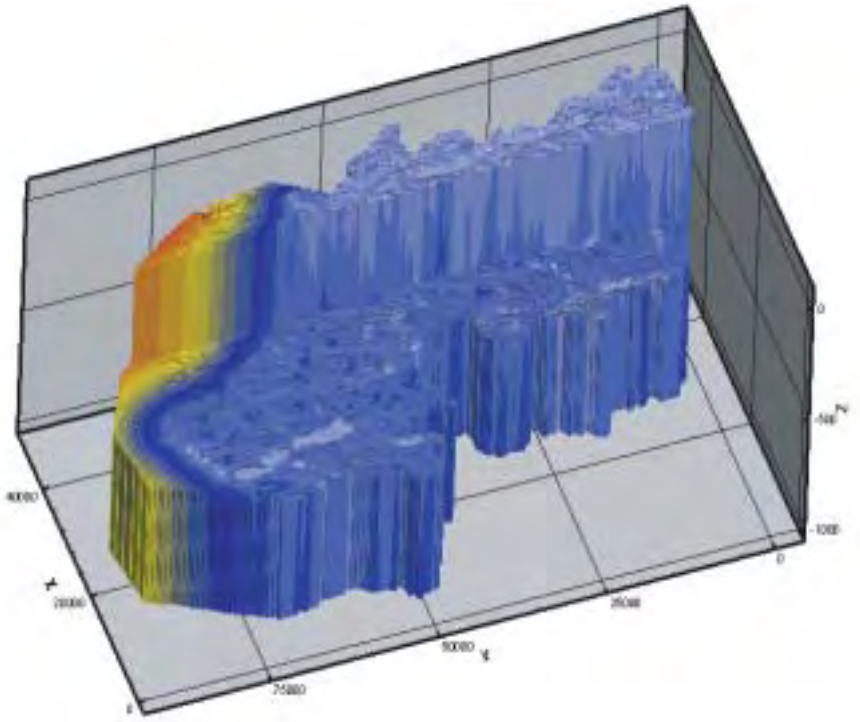

Figure 5-11. *Case 2: distribution of specific flow (homogeneous flow medium with undulating topography).*

The colours scale corresponds to the logarithms of the specific flow (the same colour scale is used in all three figures presenting the specific flow): Red (smallest flow) – Yellow – Blue – White (largest flow). The model presents two near horizontal steps, the upper surface corresponds to the topography (as defined in the model), the lower surface corresponds to a depth of 550 m (repository depth). Note that the scale in the vertical direction is extremely large compared to that of the horizontal direction.

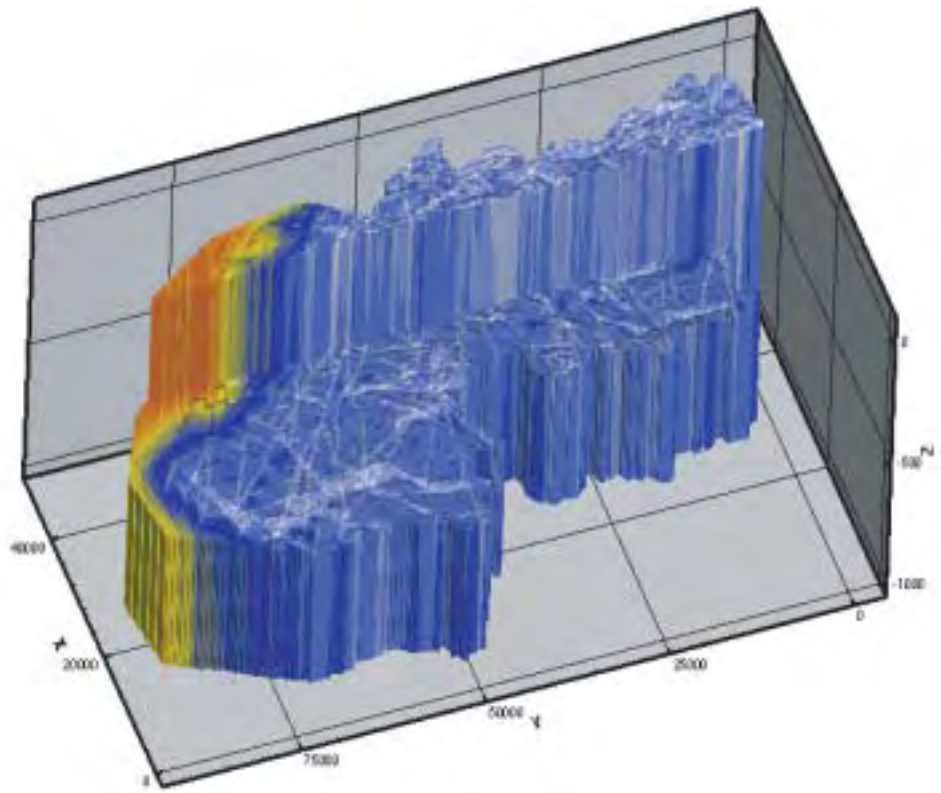

Figure 5-12. *Case 6: distribution of Specific flow (heterogeneous flow medium, uniform rock mass plus regional vertical fracture zones, with undulating topography, lakes and a discontinuous clay layer (Case 6 is presented in more detail in Section 5.11).*

The colours scale corresponds to the logarithms of the specific flow (the same colour scale is used in all three figures presenting the specific flow): Red (smallest flow) – Yellow – Blue – White (largest flow). The model presents two near horizontal steps, the upper surface corresponds to the topography (as defined in the model), the lower surface corresponds to a depth of 550 m (repository depth).

Note that the scale in the vertical direction is extremely large compared to that of the horizontal direction.

5.5 Case 2 – Comparison between Geoan and Nammu

Case 2 have been solved by use of two different computer codes. The finite difference code GEOAN and the Finite element code NAMMU. Two models were established; one for GEOAN and one for NAMMU, both models were based on the same data. As far as possible both models used the same mesh, in GEOAN as a finite difference grid with one node at the centre of each cell/element, in NAMMU as a finite element net with one node at each corner of the cells/elements. The shape and size of the cells/elements were the same in both models. Nevertheless there are some differences between the two models. The topography is defined at the centre of the cells/elements in GEOAN, but at the corners of the cells/elements in NAMMU. The topography of both models is however based on the same topographic database. The top boundary condition in GEOAN is a combined specified flow/specified head condition, see Section 4.1.4, and in NAMMU the top boundary is the specified head condition (the topography as a given head). In both models, the Sea is defined as an area with a specified head condition on top of the models (head equal to

the level of the Sea). All other boundaries – the vertical faces of the model and the base of models – were defined as no-flow boundaries in both models. The conductivity and the effective porosity are the same in both models.

Both models predict a groundwater flow pattern that is very much the same. The flow field was analysed by releasing one flow path (particle) at the centre of each cell in layer 5, (at a depth of 515 metres), both inside and outside of the shoreline. In GEOAN the particle tracking was performed by use of an analytical method (see Section 2.9) and in NAMMU an iterative approach was used. The comparison between the two models is presented below in Figure 5-13 and Figure 5-14, as well as in Table 5-4 and Table 5-5. The figures present the lengths of the flow paths and the breakthrough time, as produced by the two models.

It is well demonstrated by the two figures that both the lengths and the breakthrough times produced by the NAMMU model are somewhat larger than the values produced by the GEOAN model. The differences between the estimates of the two models can be expressed as an error percentage or as a difference percentage. Such values are given below in Table 5-4 and Table 5-5. The agreement of two models is acceptable.

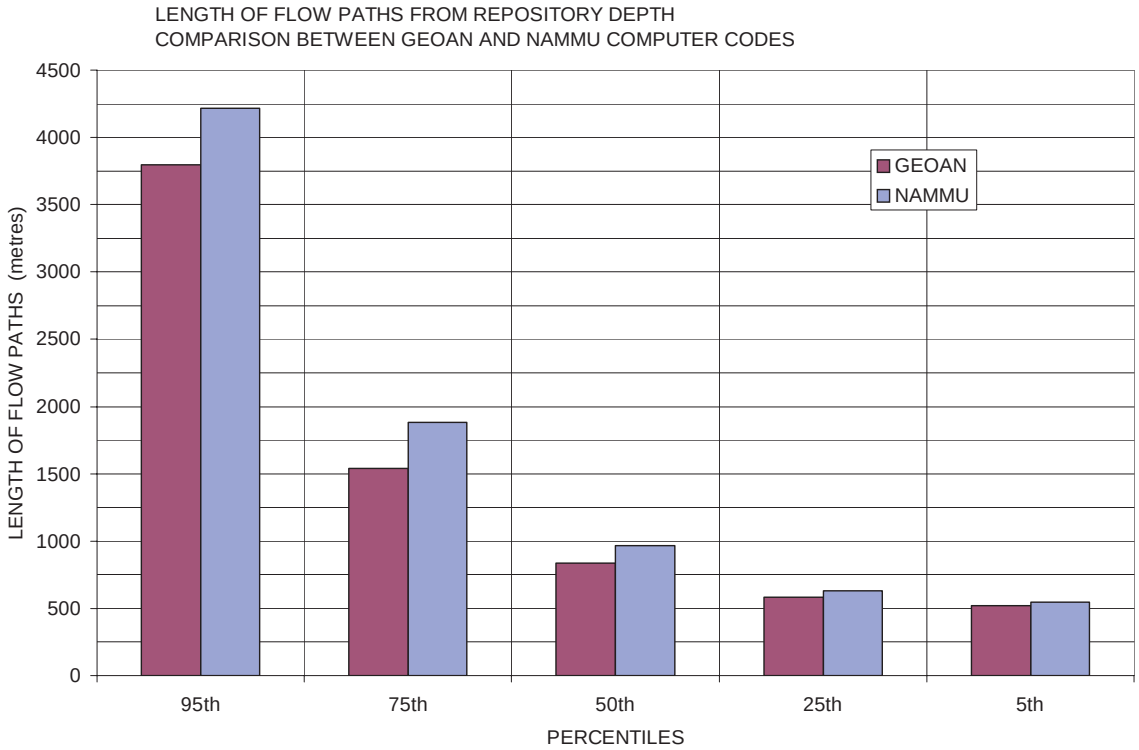

Figure 5-13. *Geoan and Nammu. Length of flow paths from repository depth.*

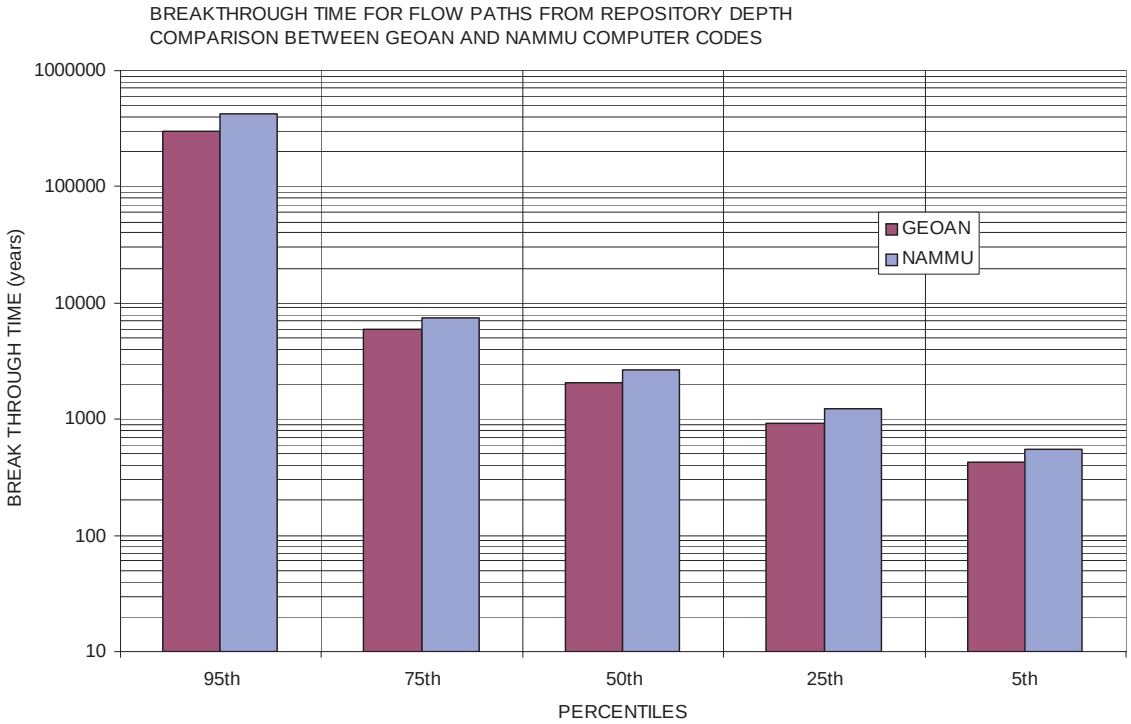

Figure 5-14. *Geoan and Nammu. Breakthrough time for flow paths from repository depth.*

Table 5-4. Geoan and Nammu. Comparison of estimated distributions of flow path length.

Percentiles	Length of flow paths Length Nammu (m)	Length Geoan (m)	Quota Nammu/Geoan	Errror % (1)	Difference % (2)
95th	4217	3798	1.11	5.2	10.4
75th	1885	1540	1.22	10.1	20.1
50th	965	836	1.15	7.2	14.4
25th	630	584	1.08	3.9	7.7
5th	549	523	1.05	2.4	4.9

(1) Error % = ABS[100 * (Nammu – Geoan) / (Nammu + Geoan)]

(2) Difference % = ABS[100 * (Nammu – Geoan) / ((Nammu + Geoan) / 2)]

Table 5-5. Geoan and Nammu. Comparison of estimated breakthrough times.

Percentiles	Break through times Break through Nammu (m)	Break through Geoan (m)	Quota Nammu/Geoan	Errror % (1)	Difference % (2)
95th	421988	298148	1.42	17.2	34.4
75th	7470	5896	1.27	11.8	23.5
50th	2655	2047	1.30	12.9	25.9
25th	1216	927	1.31	13.5	27.0
5th	552	424	1.30	13.1	26.1

(1) Error % = ABS[100 * (Nammu – Geoan) / (Nammu + Geoan)]

(2) Difference % = ABS[100 * (Nammu – Geoan) / ((Nammu + Geoan) / 2)]

5.6 Case 2B – Uniform rock mass, undulating topography and models with cells of different horizontal sizes

The models that are presented below are identical to the previous presented model (Case 2), except for the horizontal discretisation of the domain studied. We have increased the horizontal sizes of the cells of the grid, and thereby reduced the number of cells in the grid. The vertical discretication is the same as for the previous models. The horizontal extension of the domain studied is approximately the same as for Case 2, but somewhat larger dependent on the changed cell size. We have analysed models with the following cells, quadratic cells with a horizontal extension of: (i) 330 m × 330 m, (ii) 660 m × 660 m, (iii) 1 km × 1 km, (iv) 3 km × 3 km and (v) 10 km × 10 km.

The exactness of the representation of the topography depends on the cell size; a grid with small cells will produce a better representation of the actual topography than a grid with large cells. If the cell size is very large, the local topographic undulation will not be well represented. For such a case, the topography of the model will be dominated by the regional topographic trend; and as demonstrated by a comparison between Case 1 and Case 2, the local topographic undulation could be very important for the groundwater flow field. The purpose of the models with large cells is to evaluate the negative effects of using a grid with large cells, when estimating flow paths from repository depth.

As for the previous cases the flow fields of the models are investigated by use of flow paths; these were released between a depth of 490 m and 540 m. For each model all flow paths (from the entire domain studied) are put in one sample, and for the samples percentiles are calculated. To demonstrate the importance of horizontal cell size, percentiles (which represent different models) are plotted versus the cell size of the models. If the cell size is of no importance, the percentiles of all models should be the same. If the cell size is important, the percentiles should move towards the values given in Table 5-1 (Case 1) as the cell size gets larger.

This type of analysis is presented in Figure 5-15. Based on the figure we conclude the following: the larger the cell size, the longer the flow paths. The smallest changes takes place for the lower part of the distributions (the short flow paths), this is because the minimum path length is given by the repository depth, and the depth is the same regardless of cell size. The largest changes take place for the upper part of the distribution (the long flow paths).

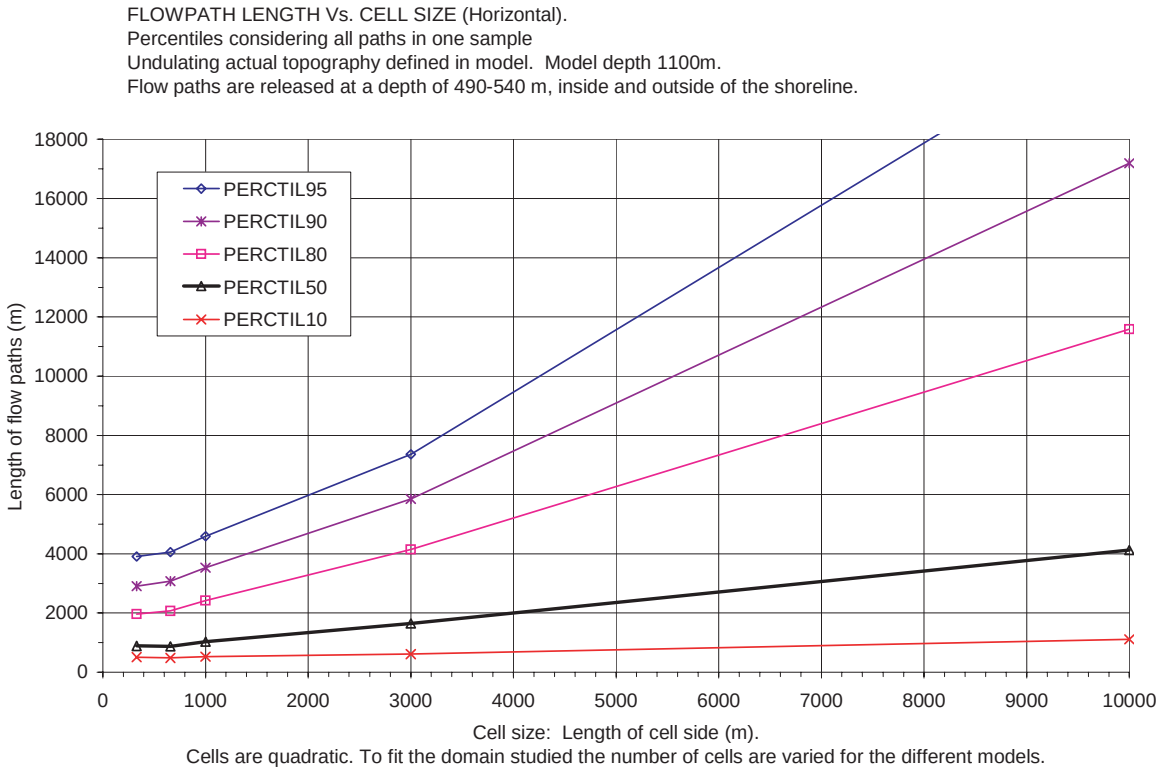

Figure 5-15. *Length of flow paths from repository depth, versus cell size. The vertical dicretisation is the same in all models studied, the horizontal discretisation differs.*

The 90th percentile of flow path length will increase from 3 km at a cell size of 330 m × 330 m and up to 6 km with a cell size of 3 km × 3 km, and at a cell size of 10 km × 10 km the 90th percentile is equal to 17 km. The increase in flow path length, as the horizontal cell size is increased, is limited by the fact that the vertical discretisation is the same in all models.

We conclude: The smaller the cells the better the representation of the local topography. It follows that the cell size is important, and that it will influence the lengths of the calculated flow paths. The larger the cell size, the longer the flow paths. The largest acceptable cell size depends on the amount of local topographic undulation and the purpose of the study. For the analyses carried out in this study (modelling on a super regional scale), Figure 5-15 demonstrates that the horizontal cell size should be smaller than about 700 m.

5.7 Case 2C – Uniform rock mass, undulating topography and models with different depths

The models presented below are identical to the previous presented model (Case 2), except for the vertical extension and discretisation of the domain studied. We have increased the vertical extension of the grid, and thereby increased the number of layers and cells in the grid. The horizontal discretication is the same as for Case 1 and Case 2, the models have quadratic cells with a horizontal extension of: (i) 330 m × 330 m. We have analysed models with the following vertical extension: (i) 1100 m with 11 layers, (ii) 2200 m with 13 layers and (iii) 4000 m with 15 layers.

The quality of the representation of the actual flow field, as produced by the models, depends on the vertical disretication and extension of the models. Considering the cell size in the vertical direction and the representation of the flow field, the smaller the cells the better the representation. However, when it comes to the model's total vertical extension it becomes more complicated. If the model has a large vertical extension, we need to consider the density of the heavy saline groundwater at great depth, as well as the properties of the rock masses at great depth. At great depth we will find Shield brine with large levels of salinity (larger than the levels of the Sea), and at great depth the properties of the rock mass is not well known. There are although some indications that the permeability may be about the same at a depth of a kilometre, as at more shallow depths /Walker, 1997/

For cases presented below, we have not included density dependent flow, density dependent flow is analysed in a special case. The motivation for this is given in Section 2.5, as follows: "In this study we have used an approach in which density dependent flow is studied in special cases. For the other cases we have not included density dependent flow, consequently the models of these cases (the freshwater cases) do not include the shield brine, instead these models are defined with a limited depth (between 1100 m and 4000 m). The limited depth of the fresh water models is a simplified method of representing the confining effects of the shield brine. Such an approach could be motivated by the study of /Stigson et al, 1998/, which demonstrates that the flow in the domain above the shield brine can be simplified to a non-density dependent flow system; and as it is primarily not an objective of this study to simulate the very deep and slow groundwater flow at very large depths inside the shield brine domain."

Hence, the purpose of the models presented below is to determine the importance of the thickness of the zone between the repository depth and the depth of the confining shield brine.

As for the previous cases the flow fields of the models are investigated by use of flow paths; these were released between a depth of 490 m and 540 m. For each model flow paths from the entire domain studied (inside as well as outside of the shoreline) are put in one sample, and for the samples percentiles are calculated. To demonstrate the importance of the vertical extension of the models, a figure is created in which percentiles (which represent different models) are plotted versus the vertical extension of the models. If the vertical extension of the model is of no importance, the percentiles of all models should be approximately the same. If the vertical extensions of the models are important, the percentiles should be different for the different models as the vertical extension of the models is increased.

This type of analysis is presented in Figure 5-16, below. Based on the figure we conclude that most flow paths from repository depth are not much influenced by the vertical extension of the model below a depth of 1.1 km. Flow paths shorter than the 80^{th} percentile are very much the same for the different values of model vertical extension (1.1 km up to 4 km). This is because most flow paths from repository depth are controlled by the local topography and will not flow very much deeper than repository depth. There are however a certain amount of flow paths from repository depth, especially the longest 5 percent, that flows deep into the rock mass and these paths are influenced by vertical extension of the model. The 90^{th} percentile of flow path lengths (from repository depth) increases from 3000 m to 3750 m, which is not very much, but the 95^{th} percentile increases from 3900 m to 6400 m, which is somewhat more; as the vertical extension of the model is increased from 1.1 km and up to 4 km.

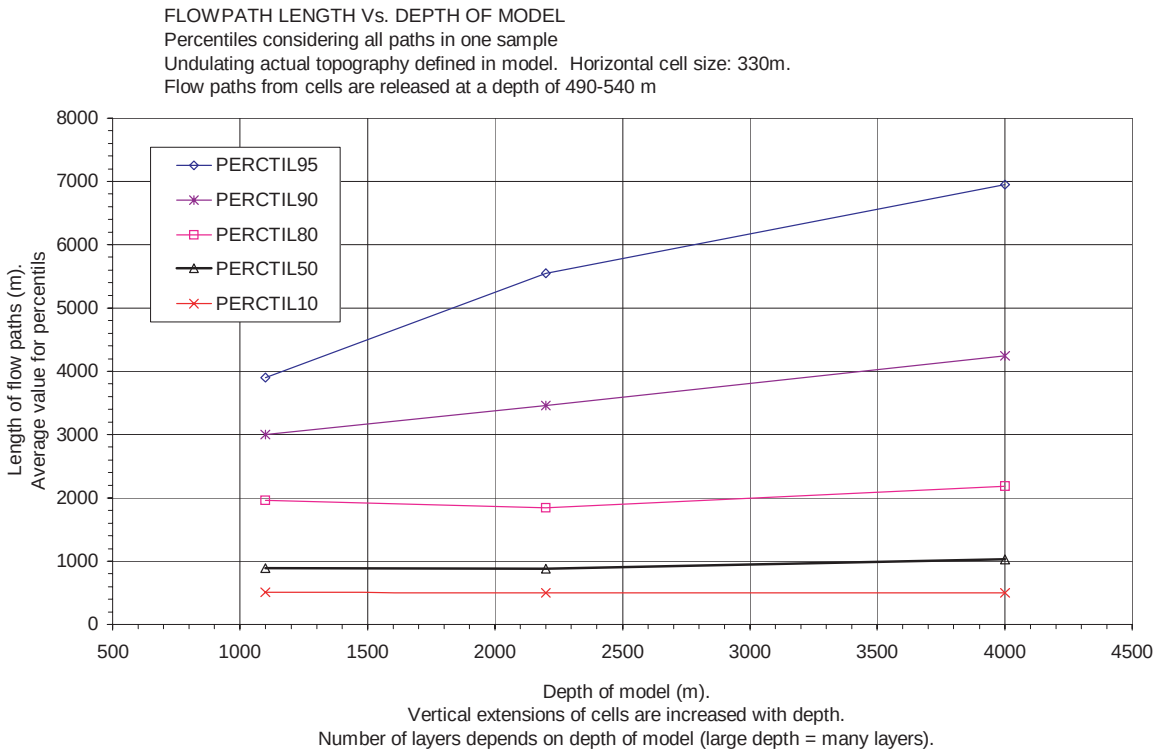

Figure 5-16. *Length of flow paths from repository depth, versus vertical extension of model. The horizontal dicretisation is the same in all models studied (horizontal cell size= 330 m × 330 m), the vertical discretisation differs.*

The discharge points for the flow paths of large lengths are in general the same for the different models (with different vertical extensions), because the increase in path length is mainly attributed to an increased vertical movement of the paths and not very much caused by a changed horizontal movement, even if that occur for some paths. Consequently, when comparing the models with different vertical extensions, the 500 repository positions with the longest path lengths and breakthrough times are generally the same for the different models with different vertical extensions , even if the absolute values of lengths and breakthrough times are different (larger for the models with larger extension).

We conclude: Considering flow paths from repository depth; it is only the flow paths with very large lengths that are influenced by the vertical extension of the model, in general only the longest 10%. The models presented in this section simplify the actual flow regime and use an approach with uniform density flow. Therefore, the models should not include the heavy saline groundwater at great depths (i.e. the Shield brine), and the vertical extension of the model should represent the rock mass above the heavy saline groundwater. It is not possible to conclude if a model of depth 1100 m is a better representation than a model of depth 2200 m (or even 4000 m). However, the uncertainty in depth of model will only influence length and breakthrough time for the longest flow paths, but it will not influence the localisation of the 500 or the 100 repository positions with the longest flow paths or longest breakthrough times, which are in general the same regardless of vertical extension of model.

5.8 Case 3 – Uniform rock mass plus regional vertical fracture zones, and undulating topography

The model of Case 3 that is presented below is identical to the previous presented model of Case 2, except for the addition of vertical regional fracture zones, which are included in the Case 3 model. (Cell size is 330 m × 330 m and model depth is 1100 m.) The regional fracture zones are discussed in Sections 3.4 and 4.2.4, the location of the vertical fracture zones are given in Figure 3-3 (above). In the model, the fracture zones are defined all the way down to the model base.

The flow field of the model was investigated by use of flow paths; these were released inside the shoreline between a depth of 490 m and 540 m. Putting all flow paths from repository depth in one sample, the following distribution was obtained (see Table 5-6).

Compared to the model of Case 2, the path lengths are somewhat longer. This is because of the small flow-resistance in the highly permeable fracture-zones. The flow field will change somewhat with the introduction of the zones, the new flow field will on the average create longer flow paths, but these paths will have a smaller total flow-resistance than the paths of Case 2, because the paths of Case 3 will to a large extent use the zones. Approximately 75% of all flow paths will on their route to the ground surface use one or more of the fracture zones (for a shorter or longer part).

Breakthrough time for the flow paths from repository depth is given below in Table 5-7. The breakthrough times are shorter than for the model of Case 2. This is because of the large flow velocities in the fracture zone (caused by the large permeability of the zones).

Regional fracture zones, which can be observed on the ground surface, are in general found along low-lying parts of the topography – often along valleys. Low-lying parts of the topography are in general discharge areas for the groundwater coming from great depth. Therefore, as the fracture zones occur along valleys, they will provide efficient flow routes for the flow paths from a repository to ground surface. However, as the fracture zones commonly occur in areas that with or without the fracture zone will be discharge areas, the introduction of the fracture zones will not radically change the flow field of the domain studied.

Table 5-6. Case 3. Percentiles of flow path length, all paths in one sample. Paths are from repository depth, no paths are released below the Sea.

Case	Percentiles of flow path length (m)				
	90th	70th	50th	30th	10th
C3	3302	1827	1132	773	571

Table 5-7. Case 3. Percentiles of breakthrough time for flow-paths from repository depth (490–540 m), all paths in one sample. *No* paths are released below the Sea.

Case	Percentiles of breakthrough time (years)				
	90th	70th	50th	30th	10th
C3	6494	1542	731	198	14

We conclude: With the addition of vertical fracture zones, the path lengths gets somewhat longer and the breakthrough times get somewhat shorter (compared to situation without zones). Repository positions with large flow path lengths or large breakthrough time can be found at many different places within the domain studied. This conclusion is not changed by the introduction of the fracture zones. The Case 3 models produce approximately the same repository positions as the model of Case 2, when considering the longest flow paths or the largest breakthrough times.

The introduction of the vertical fracture zones will not cause a large change in the overall flow paths distribution (considering paths from repository depth); because fracture zones typically takes place along low lying parts of the topography, i.e. along valleys; and these areas are, with or without the fracture zones, discharge areas for the flow paths from repository depth. With or without fracture zones, the groundwater flows towards the lowest potential.

5.9 Case 4 – Uniform rock mass plus regional vertical fracture zones and undulating topography and Lakes

The model of Case 4 that is presented below is identical to the previous presented model of Case 3, except for the addition of lakes, which are included in the Case 4 model. (Cell size is 330 m × 330 m and model depth is 1100 m.) The lakes are discussed in Sections 3.5, 4.1.5 and 4.2.2 and, the locations of the lakes are given in Figure 4-3 (above).

Lakes are surface water bodies normally located at low laying parts of the topography. In the model the lakes are in partial contact with the groundwater system, as follows, the perimeter of the lake is defined as in full contact with the groundwater system and the inner part of the lake is fully isolated from the groundwater system (see Figure 4-1). Due to the discretisation of the lakes and the domain studied as defined in the model, the lakes are defined as somewhat larger than their actual size.

The flow field of the model was investigated by use of flow paths; these were released inside the shoreline between a depth of 490 m and 540 m. Putting all flow paths from repository depth in one sample, the following distribution was obtained (see Table 5-8). Compared to the model of Case 3, the path lengths are approximately the same.

Breakthrough time for the flow paths from repository depth is given below in Table 5-9.

Table 5-8. Case 4. Percentiles of flow path length, all paths in one sample. Paths are from repository depth, no paths are released below the Sea.

Case	Percentiles of flow path length (m)				
	90^{th}	70^{th}	50^{th}	30^{th}	10^{th}
C4	3280	1860	1170	800	580

Table 5-9. Case 4. Percentiles of breakthrough time for flow-paths from repository depth (490–540 m), all paths in one sample. *No* paths are released below the Sea.

Case	Percentiles of breakthrough time (years)				
	90th	70th	50th	30th	10th
C4	4050	1590	770	225	19

The distribution of breakthrough times demonstrates a smaller spread than for the model of Case 3. Especially the 90th percentile is much shorter with lakes than without lakes. The reason for the smaller value of the 90th percentile is probably that the lakes are often above fracture zones. The hydraulic contact between the lake perimeter and the flow system in the fracture zone makes the fracture zone to a stronger sink, which intercepts flow at greater depths with a lake on top than without a lake. This effect is probably enhanced by the overestimation of the extension of the lakes that takes place in the model (due to the discretisation of the lakes).

We conclude: Considering groundwater flow from repository depth, the analyses of the cases with and without lakes demonstrate that the addition of lakes will in general not cause a large change in magnitude and direction of the groundwater flow. Repository positions with large flow path lengths or large breakthrough time can be found at many different places within the domain studied. This conclusion is not changed by the introduction of the lakes. The Case 4 models produce approximately the same repository positions as the model of Case 2, when considering the longest flow paths or the largest breakthrough times.

5.10 Case 5 – Uniform rock mass plus regional vertical fracture zones, undulating topography, with lakes and a continuous horizontal zone at depth=250m

The model of Case 5 that is presented below is identical to the previous presented model of Case 4, except for the addition of continuous sub-horizontal fracture zone at a depth of 250 m. (Cell size is 330 m × 330 m and model depth is 1100 m.) The sub-horizontal zone is defined everywhere in the model. As the zone is at a depth of 250 m, it is located between the repository depth and the ground surface. The purpose of the model of Case 5 is to demonstrate the importance of such a zone.

The flow field of the model was investigated by use of flow paths; these were released inside the shoreline at a depth of 490 m and 540 m. Putting all flow paths from repository depth in one sample, the distribution the table below was obtained as regard lengths

Table 5-10. Case 5. Percentiles of flow path length, all paths in one sample. Paths are from repository depth, no paths are released below the Sea.

Case	Percentiles of flow path length (m)				
	90th	70th	50th	30th	10th
C5	3760	2260	1520	1020	650

Compared to the model of Case 4, the flow paths are somewhat are longer for Case 5, the lengths are increased with about 15% to 30%. For the groundwater flow below the sub-horizontal zone, the zone has a tendency to average-out and weaken the influence of the local topography. It follows that the length of the flow paths from repository depth (below the zone) will be longer as it will be more influenced by the regional flow.

Breakthrough time for the flow paths from repository depth is given below in Table 5-11. Compared to the model of Case 4, the breakthrough times are larger for Case 5, the times are increased with about 35% (except for the 10th percentile for which the increase is 12%). This is partly an effect of longer paths, but also of somewhat smaller gradients in connection to the zone.

Approximately 85% of all flow paths from repository depth will on their route to the ground surface use one or more of the vertical fracture zones (for a shorter or longer part), and 30% will use the horizontal zone. For these calculations we have assumed that if a flow path crosses a horizontal zone along a vertical zone, the path is in the vertical zone only.

We have for this case estimated the localisation of the repository positions with the longest flow paths. (Flow paths were released at a depth between 490 m and 540 m.) Because of the fracture zones we have added an additional condition for the repository localisation: The distance between a repository position and a vertical fracture zone has to be 660 m, or larger. The 500 and 100 positions with the longest flow paths or largest breakthrough times are given in Figure 5-17 and Figure 5-18.

Repository positions with large flow path lengths or large breakthrough times can be found at many different places within the domain studied. There is no general trend that positions with large lengths or breakthrough times are located as far as possible from the shoreline. For Case 5, the lengths of the flow paths from the repository positions with the longest paths (the 500 and 100 positions with the longest paths) are nearly the same as to those of Case 2 (see Section 5.3). For Case 5, the breakthrough times of the flow paths from the repository positions with the largest times as follows: For the 500 positions with the longest times, the breakthrough times are between 650 000 and 41 000 years; and for the 100 positions with the longest times, the breakthrough times are between 650 000 and 130 000 years. The ten positions with the longest break through times are all located close to the shoreline, or below islands. The paths from these positions extend below the Sea where the velocities are small, which produces large breakthrough times.

We conclude: With the addition of a continuous sub-horizontal zone, the path lengths gets longer (15–30%) and the breakthrough times get larger (approximately 35%), compared to situation without the sub-horizontal zone. As demonstrated by the previous models (e.g. Case 2), repository positions with large flow path lengths or large breakthrough time can be found at many different places within the domain studied. This conclusion is not changed by the introduction of the sub-horizontal fracture zone. The Case 5 models produce approximately the same repository positions as the model of Case 2, when considering the longest flow paths or the largest breakthrough times. A very large sub-horizontal fracture zone will not separate the groundwater flow system into a lower system with long flow paths (below the sub-horizontal zone), and an upper system with short paths (above the zone).

Table 5-11. Case 5. Percentiles of breakthrough time for flow-paths from repository depth (490–540 m), all paths in one sample. *No* paths are released below the Sea.

Case	Percentiles of breakthrough time (years)				
	90th	70th	50th	30th	10th
C5	5510	2160	1010	300	21

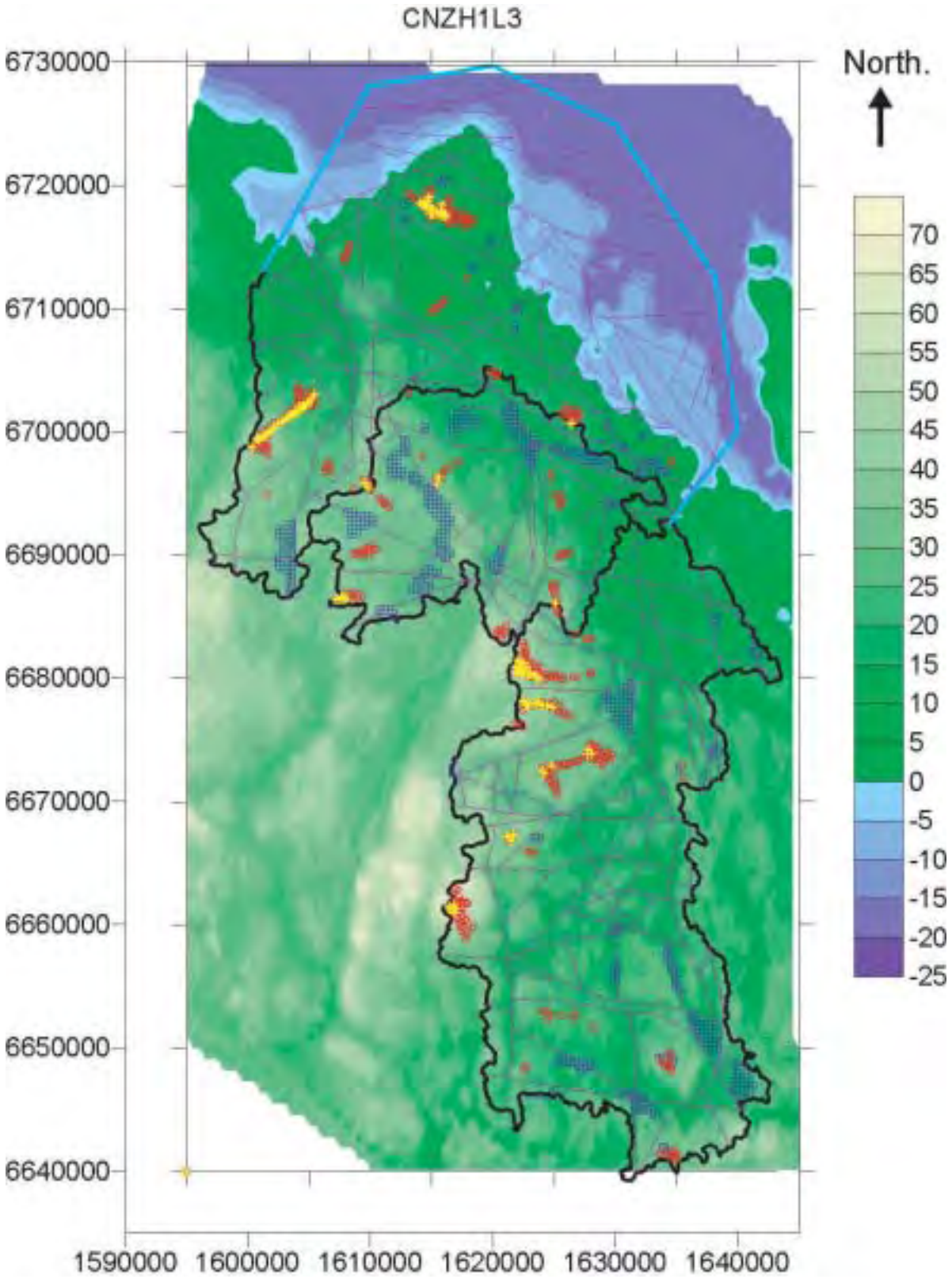

Figure 5-17. *Case 5. The 500 repository positions (Red dots) and the 100 positions (yellow dots) with the longest flow path lengths, from repository to ground surface (one position corresponds to an area of 330 × 300 m). All flow paths are released inside the shoreline. The model includes: Undulating topography, vertical fracture zones, lakes, and a continuous sub-horizontal fracture zone at a depth of 250 m.*

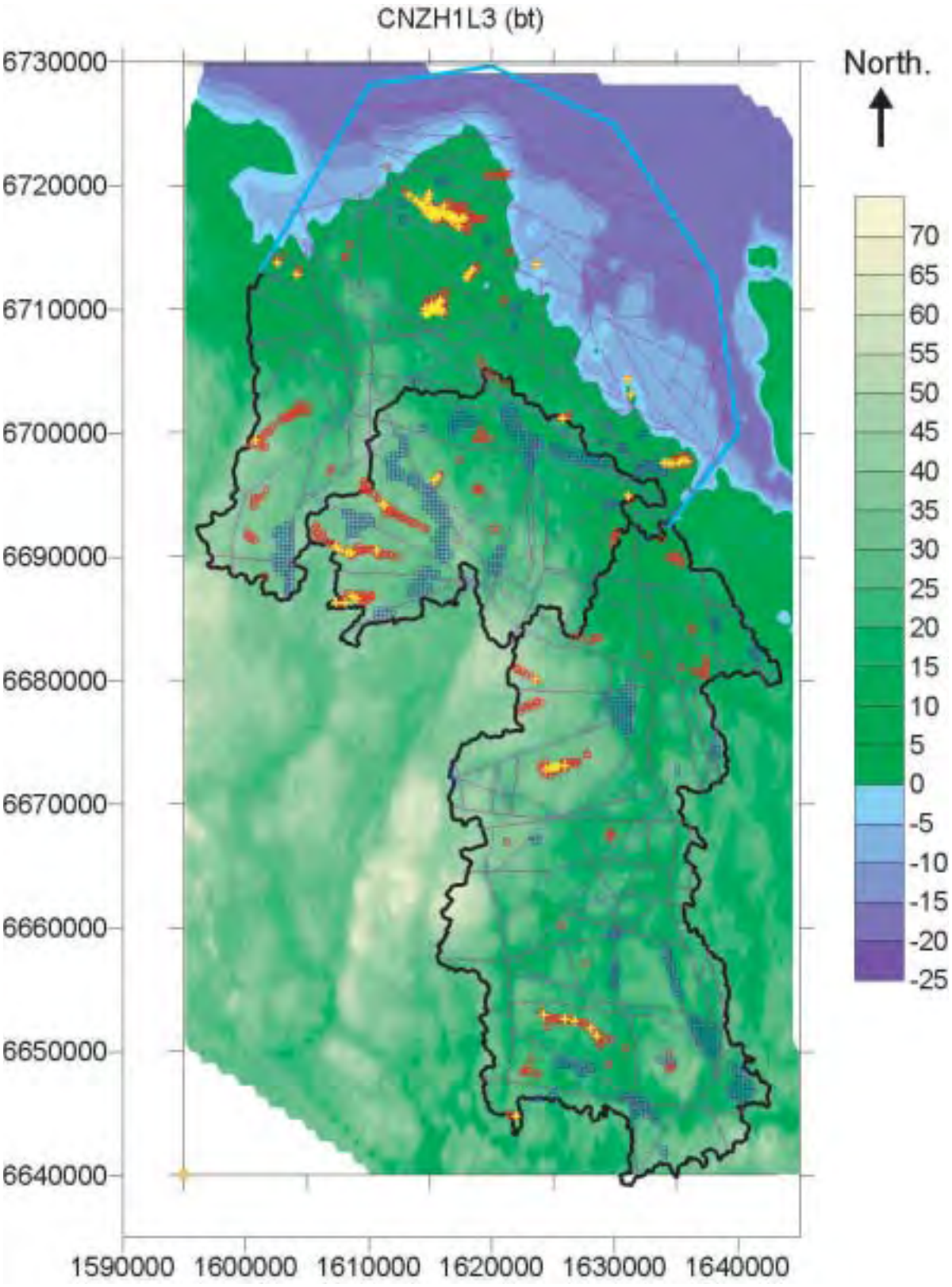

Figure 5-18. *Case 5. The 500 repository positions (Red dots) and the 100 positions (yellow dots) with the longest breakthrough times, from repository to ground surface. One repository position represents an area of 330 m × 330 m. All flow paths are released inside the shoreline (or below an island). The model includes: Undulating topography, vertical fracture zones, lakes, and a continuous sub-horizontal fracture zone at a depth of 250 m.*

5.11 Case 6 – Uniform rock mass plus regional vertical fracture zones, undulating topography, with lakes and a discontinuous clay layer

5.11.1 Introduction

The model of Case 6 is identical to the previous presented model of Case 4, except for the addition of a clay material at the ground surface, which covers some areas of the domain studied. (Cell size is 330 m × 330 m and model depth is 1100 m.) Note that the sub-horizontal zone of Case 5 is not included in any other model than that of Case 5. The definition of the clay layer is presented in Section 3.6, Section 4.1.6 and Section 4.2.3.

Of all the fresh water models studied, Case 6 is the model that includes most informati on of the system studied and it is probably the freshwater model that best represents the domain studied (based on available data). Therefore we have made an extended analysis of this case.

5.11.2 Analysis of flow field by use of flow paths

The flow field of the model was investigated by use of flow paths. Examples of such paths are given in Figure 5-19. Flow paths were released between a depth of 490 m and 540 m. Putting all flow paths released inside the shoreline in one sample, the following distributions were obtained as regard length of flow paths (see Table 5-12). Compared to the model of Case 4, the flow paths are longer for Case 6, the lengths are increased about 10 to 25 percent. The clay-material will act as a confining layer (see Section 4.1.6), therefore in Case 6 groundwater discharge can only occur at areas without clay, hence on the average the flow paths will be longer than in Case 4.

Breakthrough time for the flow paths from repository depth is given below in Table 5-13. Compared to the model of Case 4, the breakthrough times are larger for Case 6, the times are increased between 30 to 80 percent. This is partly an effect of longer paths, but also of small gradients in connection to the clay layer. The largest change takes place when comparing the paths with the shortest breakthrough times.

Table 5-12. Case 6. Percentiles of flow path length, all paths in one sample. Paths are from repository depth, no paths are released below the Sea. Case 4 and Case 6.

Case	Percentiles of flow path length (m)				
	90th	70th	50th	30th	10th
C4	3280	1860	1170	800	580
C6	4050	2330	1480	960	630
C6 in % of C4	124	125	126	120	109

Table 5-13. Case 6. Percentiles of breakthrough time for flow-paths from repository depth (490–540 m), all paths in one sample. No paths are released below the Sea. Case 4 and Case 6.

Case	Percentiles of breakthrough time (years)				
	90^{th}	70^{th}	50^{th}	30^{th}	10^{th}
C4	4050	1590	770	225	19
C6	5135	2144	1039	373	34
C6 in % of C4	127	135	135	166	183

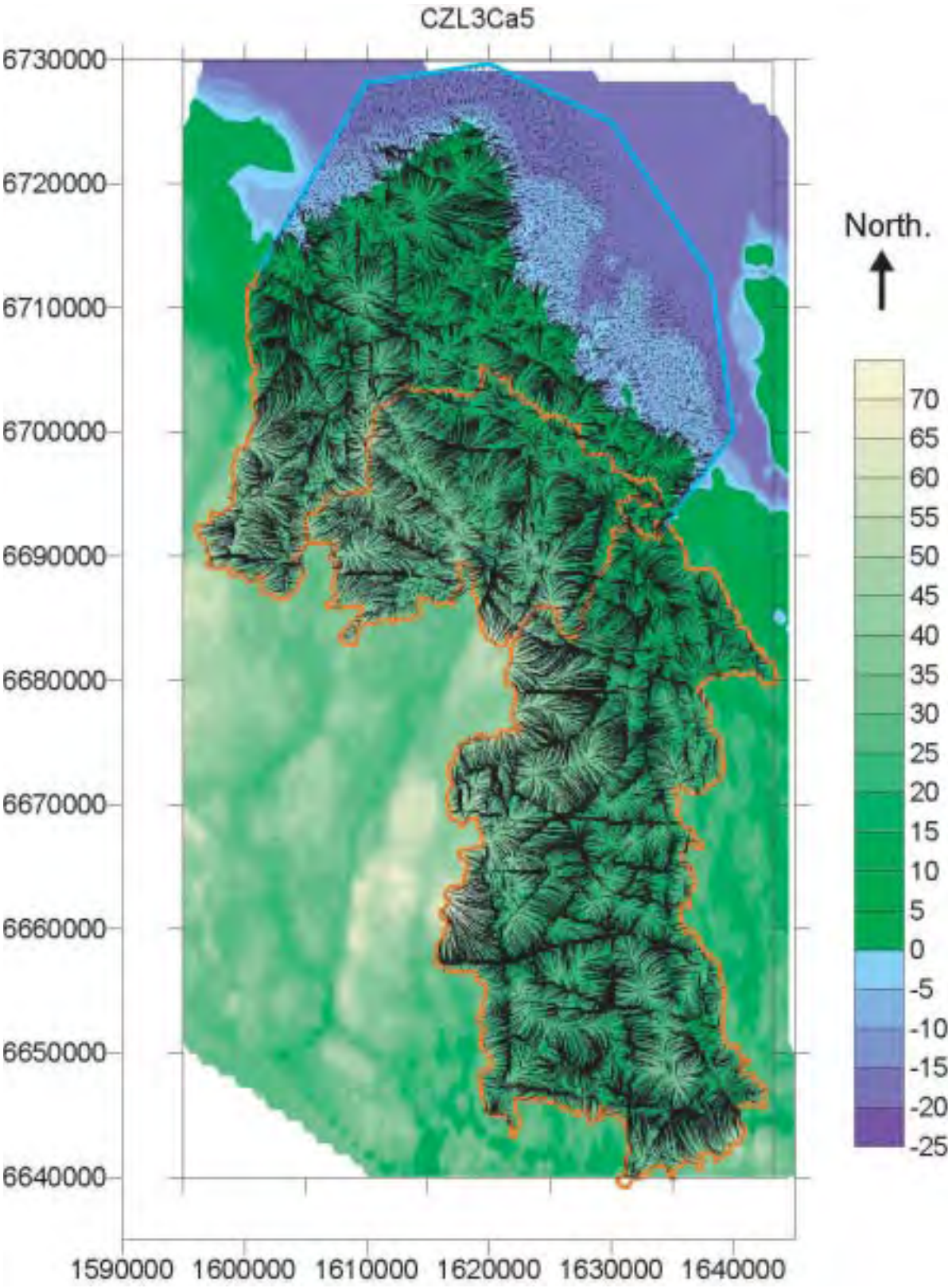

Figure 5-19. *Case 6. Flow paths released at repository depth (depth=490–540 m). The figure presents one path for each cell of the layer that represents repository depth, which gives 21 000 paths, plotted in the figure above.*

Considering flow paths from repository depth, approximately 70% of all paths will on their route to the ground surface use one or more of the regional vertical fracture zones (for a shorter or longer part). Considering flow paths from repository depth, but only paths released at a minimum distance of 660 m from a regional vertical fracture zone, for these paths approximately 50% will, on their route to the ground surface, use one or more of the vertical fracture zones (for some part of the route).

We have estimated the localisation of the repository positions with the longest flow paths and largest breakthrough times. Flow paths were released inside the shoreline and at depths between 490 m to 540 m, with the additional condition that the distance between a repository position and a vertical fracture zone has to be 660 m, or larger. The 500 and 100 positions with the longest flow paths or largest breakthrough time are given below in Figure 5-20 and Figure 5-21.

Repository positions inside the shoreline with long flow path lengths or long breakthrough times can be found at many different places within the domain studied. There is no general trend that the positions with large path lengths or breakthrough times are located as far as possible from the shoreline.

- For Case 6, the flow paths lengths of the paths from positions with the longest paths are as follows: For the 500 positions with longest paths the lengths are between 11 000 m and 4700 m, and for the 100 positions with the longest paths the lengths are between 11 000 and 6800 m. These results are rather similar for all the studied cases with undulating topography.
- For Case 6, the breakthrough times of the flow paths from the positions with the longest breakthrough times as follows: For the 500 positions with the longest breakthrough times, the times are between 650 000 and 41 000 years, and for the 100 positions with the longest breakthrough times, the times are between 650 000 and 130 000 years. The ten positions with the longest break through times are located close to the shoreline, or below islands. Paths from these positions extend below the Sea where the velocities are small.

The two criteria for selection of repository positions (flow path length and time) have created two ensembles of repository positions; these ensembles can be combined. Scanning for the repository positions that occur in each of the two ensembles does this. Considering the two ensembles of 500 positions each, 168 positions occur in both. These are positions that are among the 500 positions with the longest flow path lengths and among the 500 positions with the longest breakthrough times. Short flow paths with long breakthrough times and long flow paths with short breakthrough times will be excluded when combining the two ensembles. The resulting positions are given in Figure 5-22. For the combined ensemble, the flow paths lengths are between, 10 200 m and 4700 m, and the breakthrough times are between, 224 000 years and 47 000 years.

We conclude: With the addition of a discontinuous clay-layer on the surface of the model (the Case 6 model), path lengths from repository depth gets longer (10–25%) and the breakthrough times get longer as well (30–80%), compared to situation without the clay-layer. Repository positions with large flow path lengths or large breakthrough time can be found at many different places within the domain studied. This conclusion is not changed by the introduction of the clay-layer. The Case 6 models produce approximately the same repository positions as the other models with undulating topography, when considering the longest flow paths or the largest breakthrough times. In addition we have for this case also used a combined test that selects repository positions with regard to both path length and time. Also for the combined test the conclusion is that repository positions with large flow path lengths and large breakthrough time can be found at many different places within the domain studied. There is no general trend that positions with large path lengths and breakthrough times are found as far as possible from the Sea.

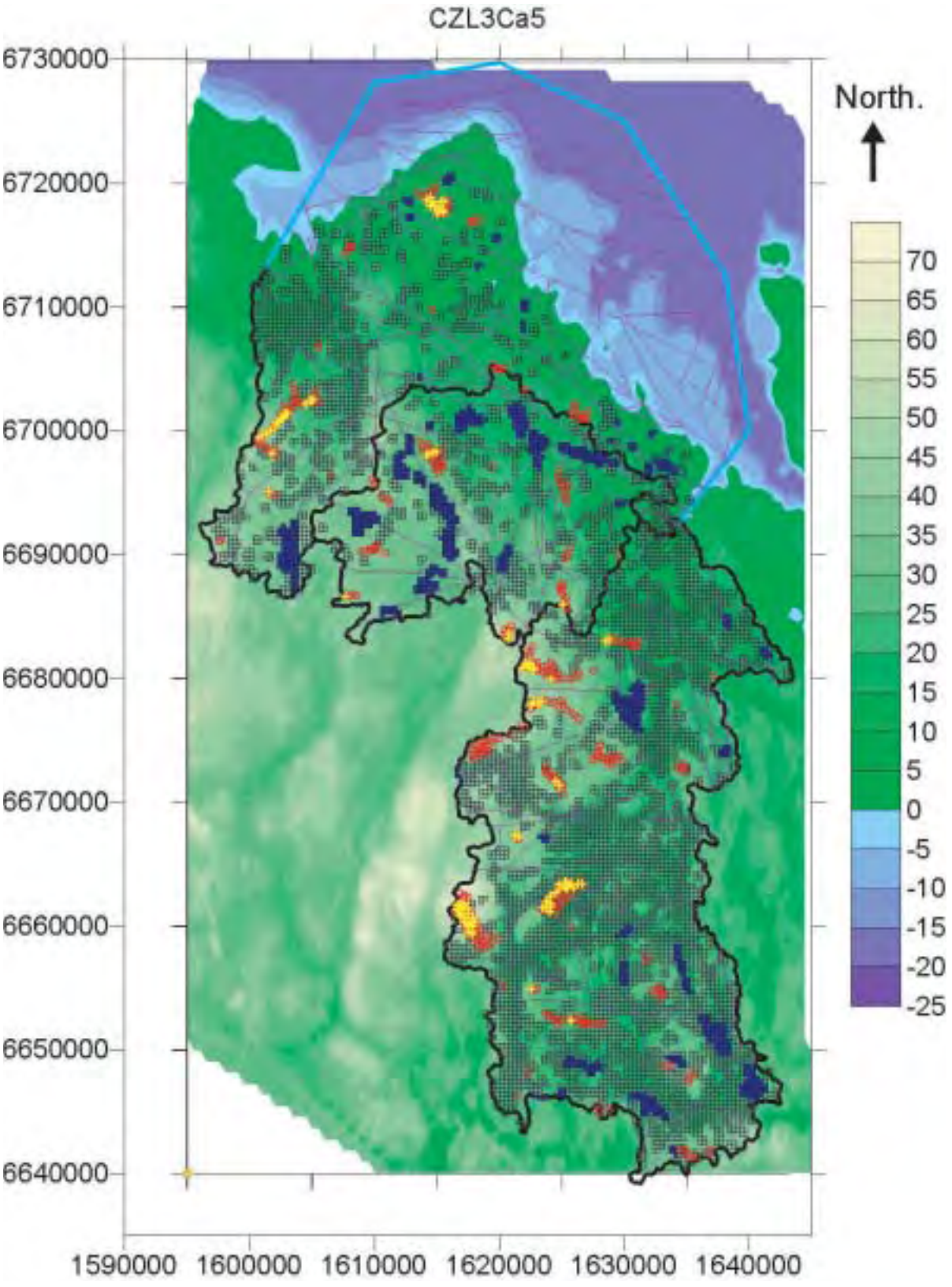

Figure 5-20. *Case 6. The 500 repository positions (Red dots) and the 100 positions (yellow dots) with the longest flow path lengths, from repository to ground surface (one position corresponds to an area of 330 × 300 m). All flow paths are released inside the shoreline (or below an island). The model includes: Undulating topography, vertical fracture zones, lakes, and areas with a confining surface clay.*

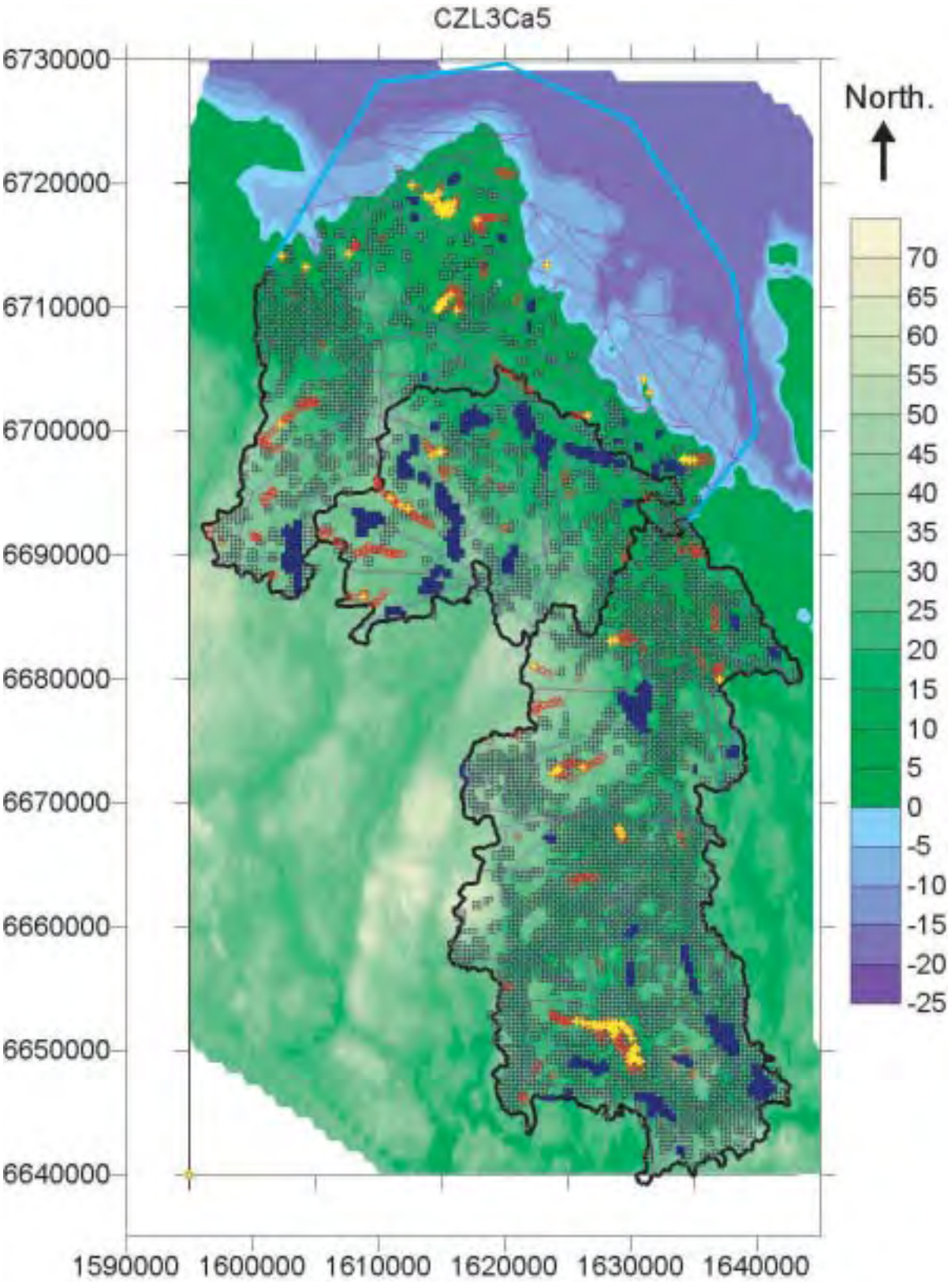

Figure 5-21. *Case 6. The 500 repository positions (Red dots) and the 100 positions (yellow dots) with the longest breakthrough times, for flow paths from repository depth to ground surface (one position corresponds to an area of 330 × 300 m). All flow paths are released inside the shoreline (or below an island). The model includes: Undulating topography, vertical fracture zones, lakes, and areas with a confining surface clay.*

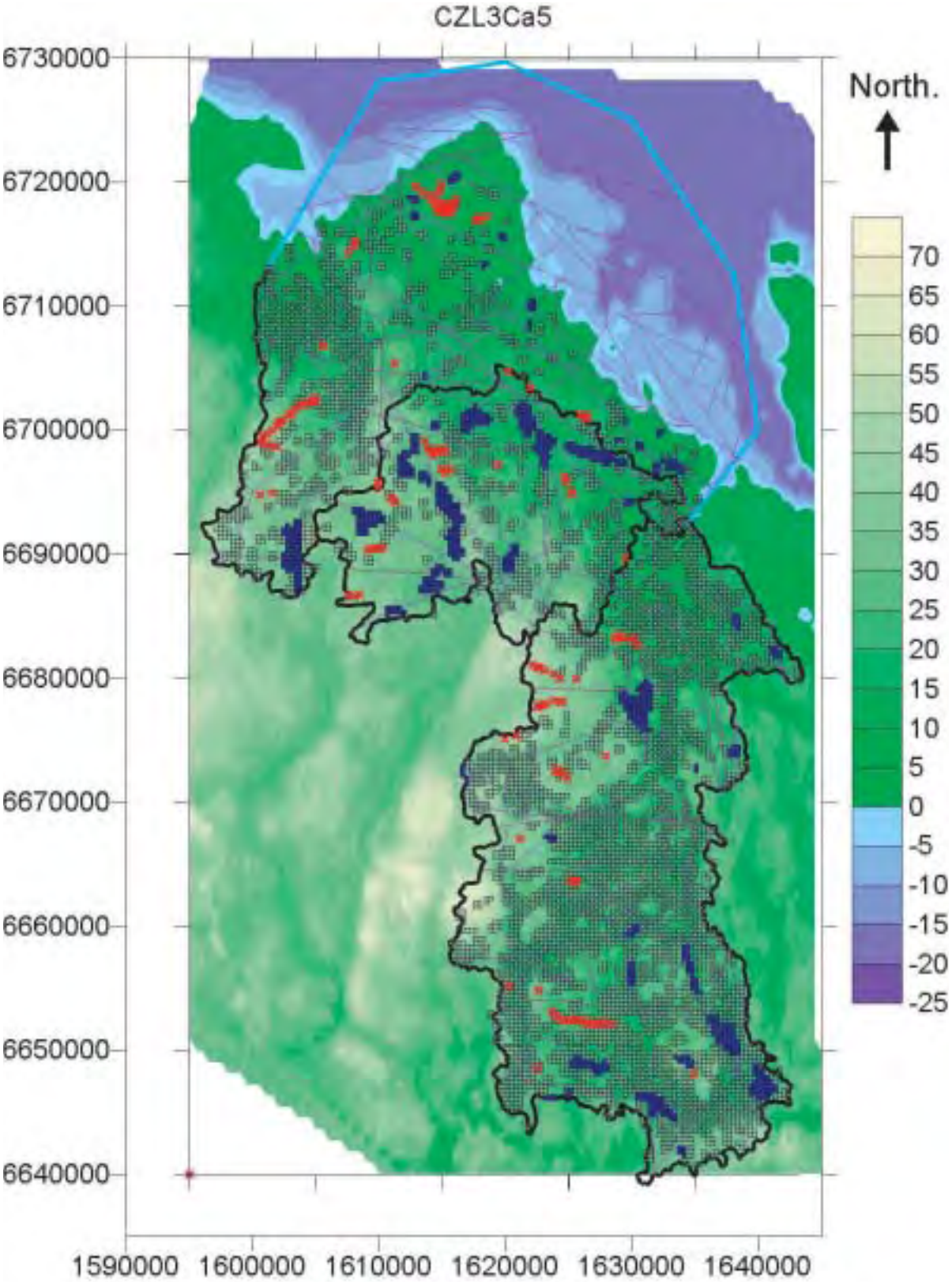

Figure 5-22. *Case 6. The repository positions (Red dots) that are among the 500 positions with the longest flow path lengths and among the 500 positions with the longest breakthrough times, from repository to ground surface. One position corresponds to an area of 330 × 300 m. All flow paths are released inside the shoreline (or below an island). The model includes: Undulating topography, vertical fracture zones, lakes, and areas with a confining surface clay.*

5.11.3 Distribution of discharge areas for groundwater from repository depth and size of groundwater recharge

Flow paths from repository depth discharges into different types of environment. Based on the boundary conditions of the model, we have divided discharge areas into three different types: (i) the lakes, (ii) the Sea and (iii) the rest (the rest includes all land above shoreline that is not defined as lakes). When considering all flow paths from repository depth, but only release positions inside of the shoreline (no release positions below the Sea), the following result was obtained: 23% of the paths discharged into lakes, 6% of the paths discharged into the Sea and 71% of the paths discharged on land (but not directly into lakes). Of the 100 repository positions with the longest path lengths, 35% discharged into lakes and 11% into the Sea. Considering the 100 repository positions with the longest path breakthrough times, 21% discharged into lakes and 36% into the Sea. For the domain studied, the model calculates the actual groundwater recharge to the rock mass as a part of the solution of the flow field (see Section 4.1.4); considering an average of the whole model (including the Sea), the actual recharge is 1.6 mm/year. Considering an average for the areas where the recharge takes place, the actual recharge is 5.7 mm/year.

The discontinuous clay layer will reduce the average actual recharge of the model of Case 6 (presented in this section), because at areas covered with clay the recharge is zero. The model of Case 3 carries no clay and no lakes, but has the same topography and vertical fracture zones as the model of Case 6, for the model of Case 3 the average actual recharge is 3.7 mm/year (in Case 6 it is 1.6 mm/year).

5.11.4 Distribution of flow with depth

The amount of water that is available to create groundwater is called the run off, or the potential recharge. It is equal to the precipitation minus the actual evapotranspiration. According to /Brandt et al, 1994/, for the period 1961–1990, the average precipitation in the Östhammar municipality, which is a part of the domain studied, is 600–700 mm/year; the average run off is 200–300 mm/year. For the province of Uppland, which includes the domain studied, Figure 3-7 presents the average run off, as measured and estimated by /SMHI, 1999/. The average run off (potential recharge), for the domain studied, is approximately 250 mm/year. Only a very small part of the potential recharge will, on the average, infiltrate into the fractured rock and create deep groundwater. In the fractured rock, on the average, the size of the groundwater flow decreases with depth. At great depth, the average specific groundwater flow is only a small fraction of the potential recharge, and an even smaller fraction of the precipitation. This is demonstrated in Figure 5-23, below. The figure presents the vertical component of the groundwater flow, calculated as the total amount of water that passes a layer in the model. The flow is given in mm/year; calculated as the flow that passes a studied layer divided by the horizontal area of the layer.

As can be seen in the figure above, the precipitation (650 mm/year) and the potential recharge (250 mm/year), is much larger than the actual amount of water that on the average infiltrates into the fractured rock of the model (average actual recharge is 1.6 mm/year). Hence, the amount of water that infiltrates into the fractured rock (the average actual recharge) is 0.25% of the precipitation and 0.64% of the potential recharge. The groundwater flow decreases with depth, and so does the downward component of the groundwater flow. At a depth of 500 m, the downward component of the groundwater flow is close to 0.3 mm/year, which is: (i) 0.046% of the precipitation, (ii) 0.12% of the potential recharge and (iii) 19% of the actual groundwater recharge. These results were obtained for a model in which the conductivity is constant with depth; a model with decreasing conductivity with depth will produce much smaller groundwater flows at great depth.

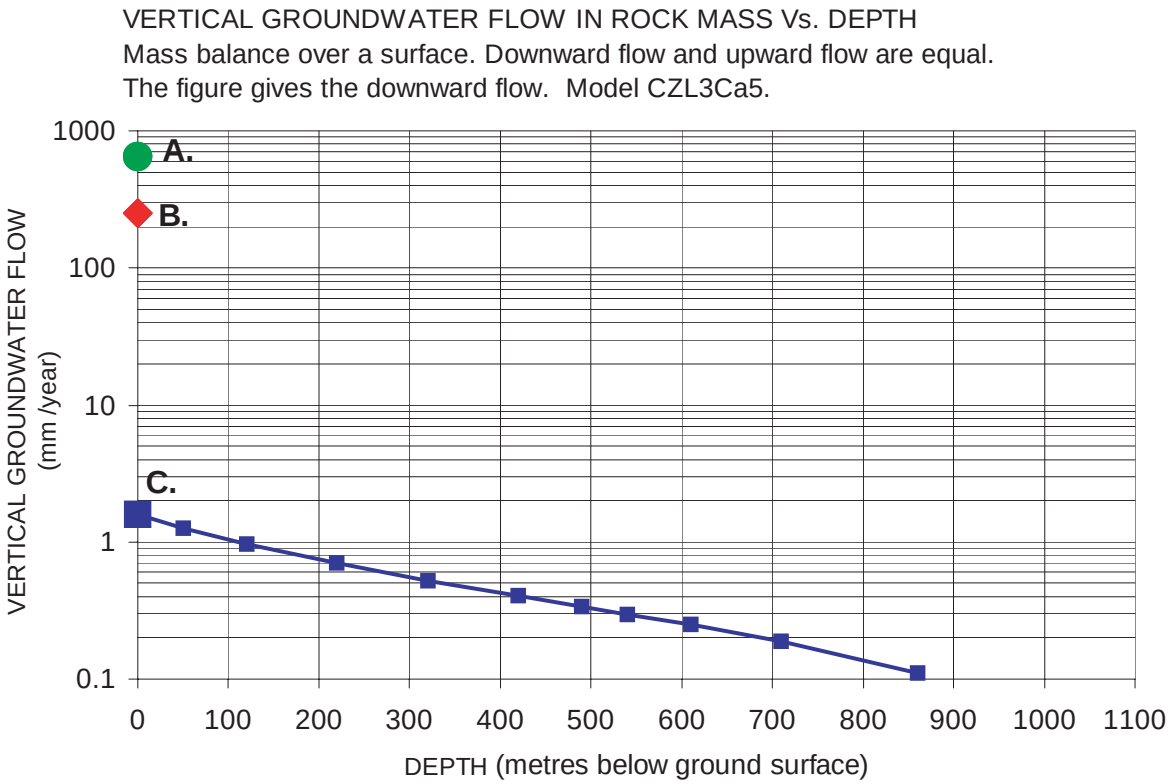

Figure 5-23. *Vertical groundwater flow in model versus depth.* **A** *denotes the precipitation (650 mm/year).* **B** *denotes the run off, which is equal to the potential groundwater recharge (250 mm/year) and* **C** *denotes the actual amount of water that infiltrates into the fractured rock of the model (1.6 mm/year). The blue curve denotes the vertical component of the groundwater flow in the model.*

It should also be noted that the figure above presents average values; at a local point the vertical component of the groundwater flow (and the average actual recharge) may diverge significantly from the average values given in the figure.

The specific flow is defined as a flow per unit area [$L^3 / (L^2\ T) = L / T$]. Because of the heterogeneous properties of the rock mass (i.e. the highly permeable fracture zones), and the undulating topography, the specific flow will vary in the model; this is illustrated in Figure 5-12 (above). The distribution of the specific flow is not symmetric, but biased because of the large flow in the small volumes of fracture zones, compared to the small flow in the large volumes of rock mass outside of the fracture zones. We have calculated the average specific flow in the model at different depths. As the distribution of specific flow values is not symmetric, different concept of mean will produce different results. We have used three different moments, arithmetic mean, volumetric mean and geometric mean. The geometric mean is close to the median of the distribution and therefore normally a better characterisation of a biased distribution than the arithmetic mean.

For each cell of the model we have calculated a specific flow, and for each layer of the model we have calculated mean values. As all cells in a layer is of equal size, the arithmetic mean and the volumetric mean is equal when considering a layer of cells. The resulting mean values versus depth are given below in Figure 5-24.

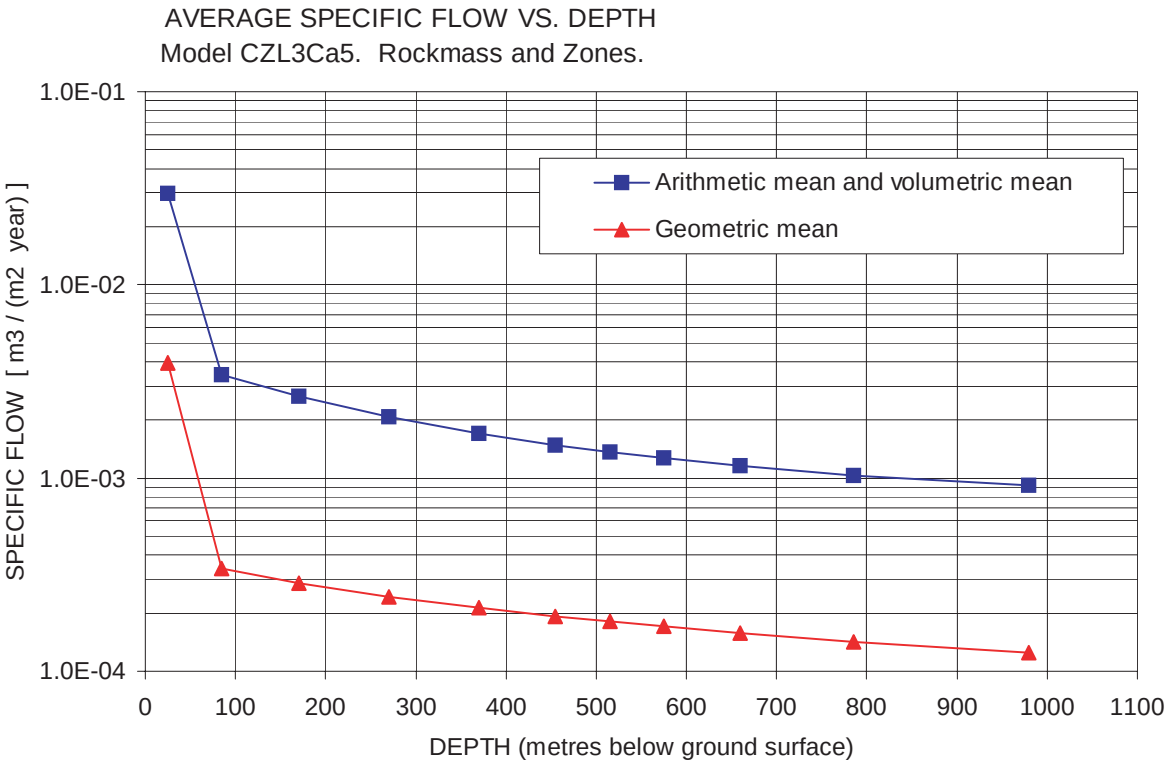

Figure 5-24. *Average specific flow versus depth.*

The large difference between the arithmetic mean and the geometric mean (see Figure 5-24 above) demonstrates that the distribution of specific flow is a very biased distribution. As can be seen in the figure, the flow at great depth is smaller than the flow close to the surface. The average specific flow at the top of the rock mass in the model is also given by the average actual recharge (see Figure 5-23, above) and it is 1.6 mm/year, which is the same as a specific flow of 1.6×10^{-3} $m^3/(m^2$ years). Comparing this value to the mean specific flow given above in Figure 5-24 demonstrates that the mean (arithmetic and geometric) specific flow at 25 metres depth is larger than the value given by the average actual recharge. This may look strange, but it is correct, because the mean values given above are moments of a distribution that is not symmetric, and the mean values at small depths are very much influenced by the very large specific flow (and recharge) that occur in the highly permeable fracture zones. Locally, the recharge to a fracture zone and the specific flow inside a fracture zone can be orders of magnitudes larger than 1.6×10^{-3} $m^3/(m^2$ years). It is well demonstrated by the figure above that the mean specific flow is much smaller at a depth of 100 metres than close to the ground surface. However, the figure should be interpreted with some care, as the specific flow at a local point may diverge a lot (order of magnitudes) from the mean values given in the figure.

We have also used a flow path analysis to characterise the distribution of flow versus depth. For this analysis all areas (cells) at which deep groundwater discharges were identified, the condition being that the discharge should be larger than the potential recharge (discharge > 250 mm/year), these cells are called the true discharge areas. From these cells a large number of flow paths were generated backwards (upstream). The number of paths released at a cell depended on the size of the discharge at that cell – a flow-weighted release (the total number of paths was approximately 150 000). The different layers of the model intersected by the flow paths were noted and statistically analysed. The result is a cumulative distribution of the depths reached by the flow paths. The distribution is

presented below in Figure 5-25. The figure also presents the vertical component of the groundwater flow in percent of the average actual recharge, i.e. the curve given in Figure 5-23, presented in percent of the average actual recharge. Both curves represent the same thing – the vertical distribution of the groundwater flow – and they should be very similar. The first curve is derived through particle tracking; the second curve is derived through mass balance calculations at different depths. As seen in Figure 5-23, they are very similar; the discrepancy at small depths comes from the definition of true discharge areas.

Figure 5-23 demonstrates the following: 50% of the water that infiltrates into the fractured rock will not reach any deeper than 180 metres and 90% will not reach any deeper than 750 metres; only 20% of the flow will reach below 500 metres. As for the previous figures concerning flow distribution with depth, we would like to point out that locally the flow distribution might diverge a lot from the average values given in the figure.

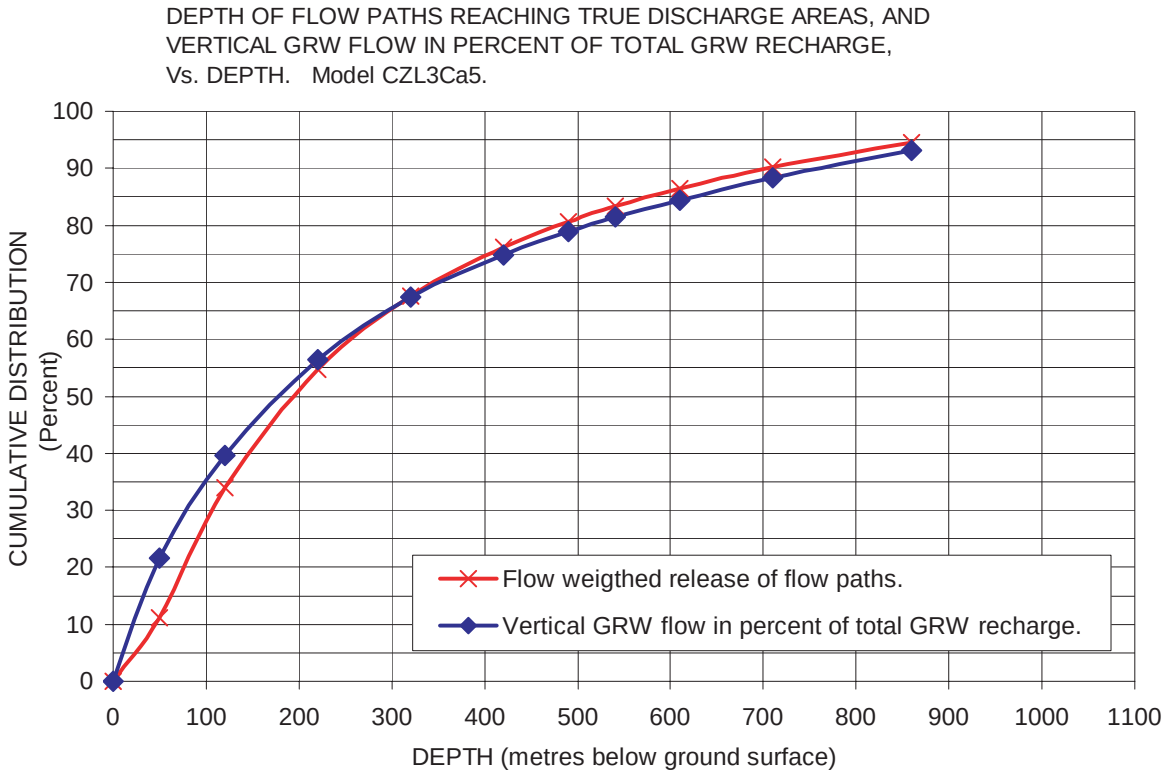

Figure 5-25. *Cumulative distribution of depth of flow paths.*

6 Cases with modified topography

The previously presented cases have demonstrated that the local topographic undulation is the most important parameter for the length and breakthrough times of flow paths from repository depths, when considering repository positions inside of the shoreline. The purpose of the following two cases (Case 7 and 8) is to demonstrate the importance of the relationship between the local topographic undulation and the regional topographic gradient. In the two cases presented below, we have modified the actual topography of the area studied. In Case 7, both the local and regional topographic gradients are increased. In Case 8, only the regional topographic gradient is increased while the local undulation remains the same.

6.1 Case 7 – Uniform rock mass plus regional vertical fracture zones. Undulating topography. Topography enhanced by increasing the topographic gradients

The model of Case 7 (presented below) is identical to the previous presented model of Case 4, except for the modification of the topography. (Cell size is 330 m × 330 m and model depth is 1100 m.) Case 7 is a purely hypothetical case, and its purpose is to demonstrate the effects of larger local topographic gradients. In Case 7, the relationship between local and regional topographic gradients is the same as for the actual topography, but the gradients are larger than for the actual topography.

The topography of Case 7 is given by an enhancement of the undulation of the topography, while keeping the relationship between local and regional trends. The topography of Case 7 will look the same as the actual topography, but elevations and topographic gradients will be larger. The topography will only be changed above the shoreline. The new topography is calculated as follows.

$$T_{NEW} = C\, T_{OLD}$$

T_{NEW} = *Modified topography (m)*
T_{OLD} = *Actual topography (m)*
C = *Constant*

The highest elevation of the actual topography is 72.6 masl. By use of a constant (*C)* equal to 5, the highest elevation of the modified topography becomes 363 masl. The topography of Case 7 is given in Figure 6-1.

The flow field of the model was investigated by use of flow paths. Flow paths were released at repository depth, between a depth of 490 m and 540 m. Putting all flow paths released inside the shoreline in one sample will produce the following distributions as regard length of flow paths (see Table 6-1).

The length of the flow paths of Case 4 and Case 7 are very much the same.

Breakthrough time for the flow paths from repository depth is given below in Table 6-2.

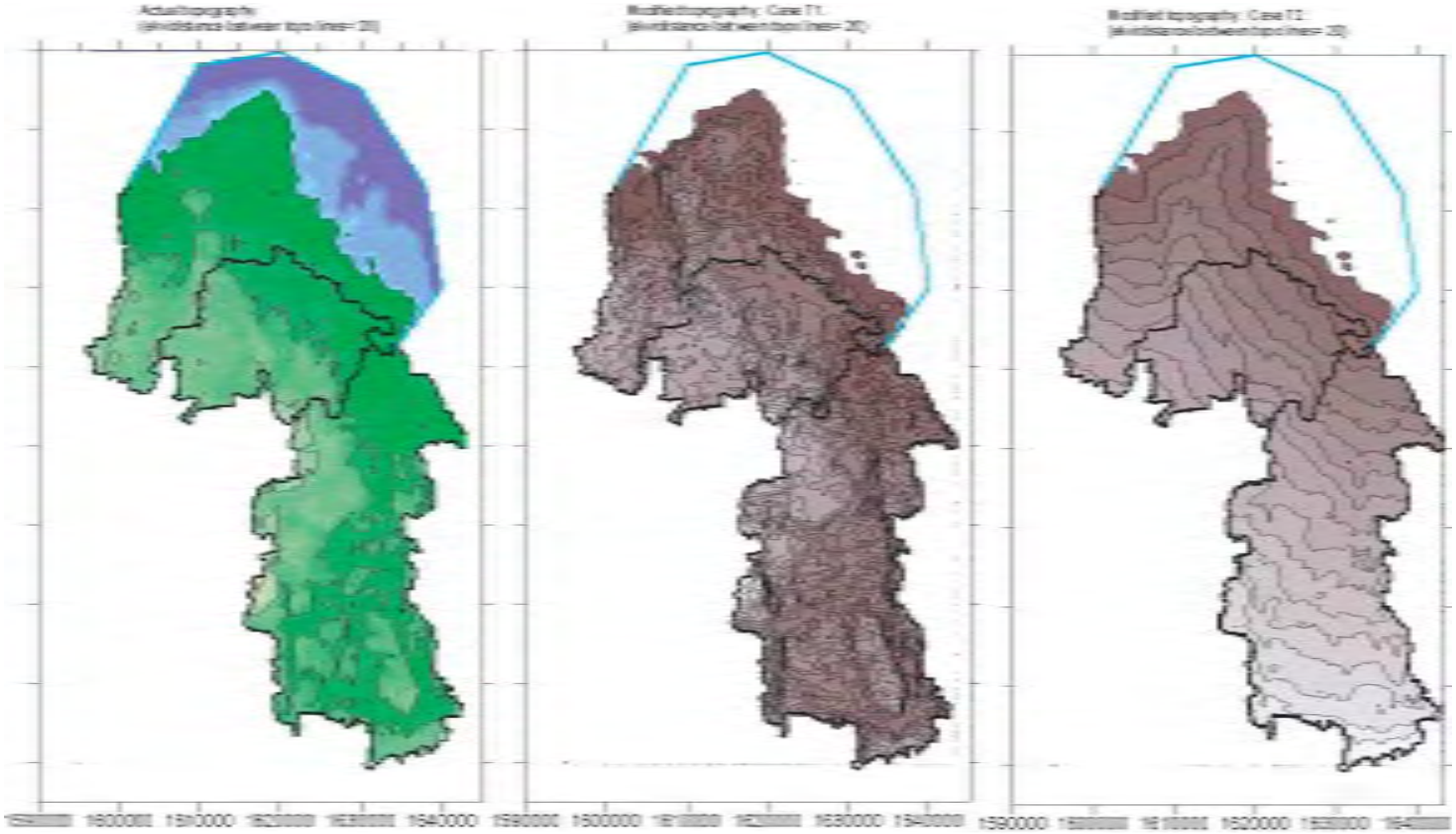

Figure 6-1. *The actual topography (Case 4) and that of the two cases with modified topography (Case 7 and 8). Below the Sea the topography is the same in all three cases. Distance between isolines is 20 m. Maximum elevation of actual topography is about 70 masl, for the modified cases maximum elevation is 363 masl.*

Table 6-1. Case 7. Percentiles of flow path length, all paths in one sample. Paths are from repository depth, no paths are released below the Sea. Case 4 and Case 7.

Case	Percentiles of flow path length (m)				
	90th	70th	50th	30th	10th
C4	3280	1860	1170	800	580
C7	3528	1963	1216	807	577
C7 in % of C4	108	106	104	101	99

Table 6-2. Case 7. Percentiles of breakthrough time for flow-paths from repository depth (490–540 m), all paths in one sample. *No* paths are released below the Sea. Case 4 and Case 7.

Case	Percentiles of breakthrough time (years)				
	90th	70th	50th	30th	10th
C4	4047	1591	770	225	19
C7	796	315	149	40	3
C7 in % of C4	20	20	19	18	18

Compared to the model of Case 4, the breakthrough times are much shorter for Case 7, the times are reduced to only 20% of the times of Case 4. This is because of the steeper topographic gradients, which will produce larger groundwater velocities.

We have estimated the localisation of the repository positions with the longest flow paths and largest breakthrough times. Flow paths were released a depth of 490 m to 540 m, with the additional condition that the distance between a repository position and a vertical fracture zone has to be 660 m, or larger. The 500 and 100 positions considering longest flow paths are given below in Figure 6-2.

Length of flow paths for the cells with longest paths:

- The 500 cells with the longest paths: 12 000 m to 4100 m.
- The 100 cells with the longest paths: 12 000 m to 6200 m.

We conclude: A comparison between cases 4 and 7 (the only difference between these to cases is the modified topography of Case 7) demonstrates that the enhanced topographic undulation of Case 7 does not change the lengths of the paths much, but the breakthrough times will be much shorter for Case 7, due to the increased groundwater velocities of this case. Repository positions with large flow path lengths or large breakthrough time can be found at many different places within the domain studied. This conclusion is not changed by the enhanced topographic undulation. The Case 7 models produce approximately the same repository positions as the model of Case 4, when considering the longest flow paths or the largest breakthrough times.

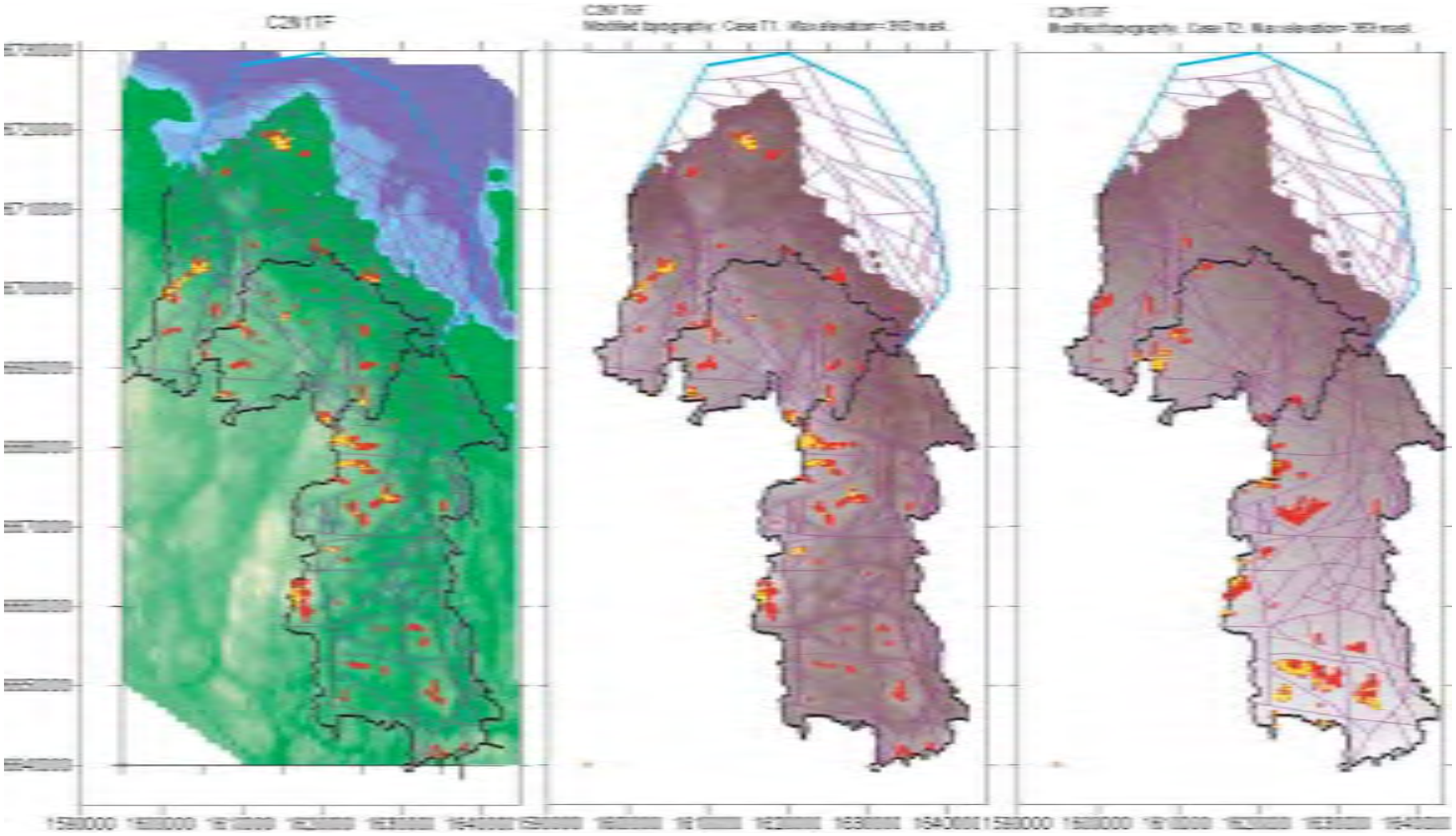

Figure 6-2. *Repository position considering longest flow paths for Case 4 (actual topo.), Case 7(modified topo.) and Case 8 (modified topo.). All cases have the same shoreline and vertical fracture zones. The red dots denotes the 500 positions and the yellow dots denoted the 100 positions, with the longest flow paths.*

6.2 Case 8 – Uniform rock mass plus regional vertical fracture zones. Undulating topography. Topography enhanced by increasing the regional topographic gradient

The model of Case 8 (presented below) is identical to the previous presented model of Case 4, except for the modification of the topography. (Cell size is 330 m × 330 m and model depth is 1100 m.) Case 8 is a purely hypothetical case; its purpose is to demonstrate the effects of larger regional topographic gradient, while keeping the local topographic undulation intact.

The topography of Case 8 is given by an introduction of a regional trend, which will increase the elevations with distance from the sea. The actual local topographic undulation is maintained in Case 8. However, for the case studied the new regional trend will come to dominate the topography and in general the modified topography of Case 8 will be a smooth lowering of the elevations towards the shoreline (more like an inclined plane than like the actual topography). The topography will only be changed above the shoreline. The new topography is calculated as follows:

$$T_{NEW} = T_{OLD} + C\,L$$

T_{NEW} = *Modified topography (m)*
T_{OLD} = *Actual topography (m)*
C = *Constant*
L = *Distance to shoreline*

The highest elevation of the actual topography is 72.6 masl. By use of a constant (*C)* equal to 0.005664, the highest elevation of the modified topography becomes 363 masl. The topography of Case 8 is given in Figure 6-1.

The flow field of the model was investigated by use of flow paths. Flow paths were released at repository depth, between a depth of 490 m and 540 m. Putting all flow paths released inside the shoreline in one sample will produce the following distributions considering length of flow paths (see Table 6-3).

The length of the flow paths in Case 4 and Case 8 are different. The introduction of the large regional topographic gradient of Case 8 will make the general topographic trends of Case 8 more similar to the inclined plane of Case 1 than to the undulating topography of the other cases. The flow path lengths of Case 8 are much larger for the longer paths, as these paths are much influenced by the regional trends of the topography (the 90th percentile of Case 8 is nearly 3 times as larger that that of Case 4). The shorter paths are not as much influenced by the regional topographic trend as the longer paths, as the repository depth is always the same in all models.

Table 6-3. Case 8. Percentiles of flow path length, all paths in one sample. Paths are from repository depth, no paths are released below the Sea. Case 4 and Case 8.

Case	Percentiles of flow path length (m)				
	90th	70th	50th	30th	10th
C4	3280	1860	1170	800	580
C8	9307	4395	2505	1467	823
C8 in % of C4	284	237	215	184	141

Breakthrough time for the flow paths from repository depth is given below in Table 6-4. Compared to the model of Case 4, the large breakthrough times are shorter for Case 8 than for Case 4, but the short breakthrough times of Case 8 are larger than those of Case 4.

We have estimated the localisation of the repository positions with the longest flow paths and largest breakthrough times. Flow paths were released a depth of 490 m to 540 m, with the additional condition that the distance between a repository position and a vertical fracture zone has to be 660 m, or larger. The 500 and 100 positions with the longest flow paths are given below in Figure 6-2.

Length of flow paths for the cells with the longest paths:

- The 500 cells with the longest paths: 30 000 m to 11 100 m.
- The 100 cells with the longest paths: 30 000 m to 18 200 m.

We conclude: A comparison between cases 4 and 8 (the only difference between these two cases is the modified topography of Case 8) demonstrate that the enhanced regional topographic gradient of Case 8 will change the lengths and the breakthrough times of the flow paths; because the introduction of the large regional topographic gradient of Case 8 will make the general topographic trends of Case 8 more similar to the inclined plane of Case 1, than to the undulating topography of the other cases. It should be noted that the increased regional gradient will make the paths longer, but it will also give rise to larger flow velocities, which will make the longest breakthrough times of Case 8 shorter than those of Case 4, in spite of the large lengths of the paths of Case 8. For Case 8, the repository positions with large flow path lengths or large breakthrough times are generally found far away from the Sea. However, due to the complex horizontal extension of the model and the local topographic undulation, even in Case 8 there are repository positions located as close as 12 km from the shoreline, among the positions with the largest path lengths.

Table 6-4. Case 8. Percentiles of breakthrough time for flow-paths from repository depth (490–540 m), all paths in one sample. *No* paths are released below the Sea. Case 4 and Case 8.

Case	Percentiles of breakthrough time (years)				
	90th	70th	50th	30th	10th
C4	4047	1591	770	225	19
C8	3010	1315	679	260	28
C8 in % of C4	74	83	88	116	150

7 Case with transient solution and without density dependent flow

The shore level progress was not included in the previously presented analyses. The shore level progress may however influence the flow situation and consequently the flow paths from repository depth. We have established a model (Case 9) with vertical fracture zones, but without lakes and clay, the model includes the shore level progress and is solved under transient conditions.

7.1 A qualitative assessment of the groundwater development and it's representation in the formal models

7.1.1 Introduction

The transient models need to be established in line with an assessment of the past and future development of the groundwater system. We assume that the shore level displacement has occurred and that it will continuvär e; hence we need to describe the past and future shore displacement and establish models that are time-dependent and capable of representing this phenomenon. It follows from the time-dependent models that we need an initial condition, this condition must be based on the assessment of the past groundwater system.

7.1.2 The shore level displacement – the land uplift

During the latest glacial period, large amounts of water were tied to the ice mass, which had a maximum thickness of about 3 km. When the ice began to melt both the levels of the land and the water levels of the seas became higher. The interplay between land, ice and the water has resulted in different water levels and different types of water in the Baltic Sea as well as in the Baltic shield rock. In some periods the Baltic Sea was a freshwater lake while in others it was a saline Sea. The sum of the ground level changes and the Sea level changes is called shore level displacement or shore level progress.

/Påsse, 1996/ presented a mathematical model of these phenomena. The shore level displacement in the transient models of this study, will be defined in line with the estimations given by /Påsse, 1996/, see Figure 7-1. The curve in Figure 7-1 is calculated based on a mathematical model given by /Påsse, 1996/, and by use of coefficients representing the geographical coordinates of the SFR (Forsmark) area.

In the models, the shore level displacement will be simulated as a lowering of the level of the seawater table, a lowering in relation to a fixed reference system. The topography and the different positions of the Sea are given in Figure 7-2 and in Figure 7-3.

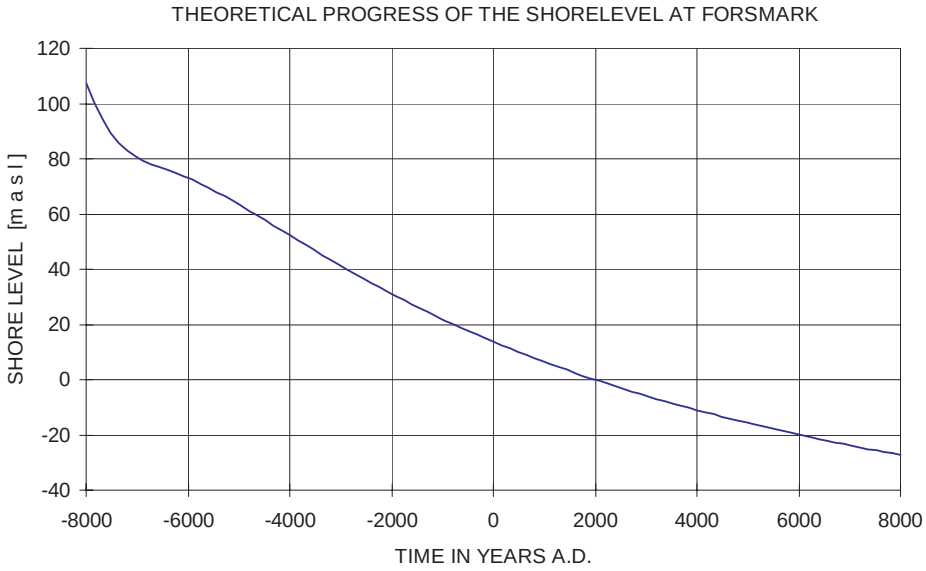

Figure 7-1. *The estimated shore level displacement as defined in the models of this study. The figure presents the estimated shore level displacement at the domain studied. The curve is based on a mathematical model presented by /Påsse, 1996/.*

7.1.3 Initial condition and studied time period

The models needs an initial condition, the initial condition is an assumed state of the studied system at the start of the time-dependent simulation. The actual condition of the system at past times is not known; consequently we will have to assume an initial condition. As a robust approach we will set the initial condition to a situation when the whole of the model is below the sea, and assume isostatic groundwater heads for this situation. Based on the analysis by /Påsse, 1996/ regarding the shore level displacement, we note that the whole of the domain included in the model, was below the seawater table at 6000 years before present (–4000 AD), except for islands close to Southwest boundary of the model (see Figure 7-2). We will set this time to the start point of the time-dependent simulation. For the start point (initial time) we will assign the model a generalised condition for the groundwater heads, everywhere in the models we will set the groundwater heads equal to the seawater level – this is the initial condition. Hence, the studied time period is from 6000 years before present (–4000 AD) and until present (2000 AD), length of period is 6000 years. The flow field of the model is analysed at time equal to 2000 AD.

7.1.4 Development of the groundwater flow field

From the initial condition, the shore level displacement will continue and as a consequence the land will successively rise from the sea. The groundwater heads will change and an increased groundwater flow will take place. Because of the land uplift and the moving shoreline, the groundwater flow will be increased close to the shoreline. Initially, below areas no longer covered by the sea, the main flow direction of the groundwater will be towards the ground surface and towards the retreating shoreline. With time, as the shoreline moves further away, the groundwater flow will develop into a steady-state-like situation, with recharge and discharge areas primarily controlled by the local topography.

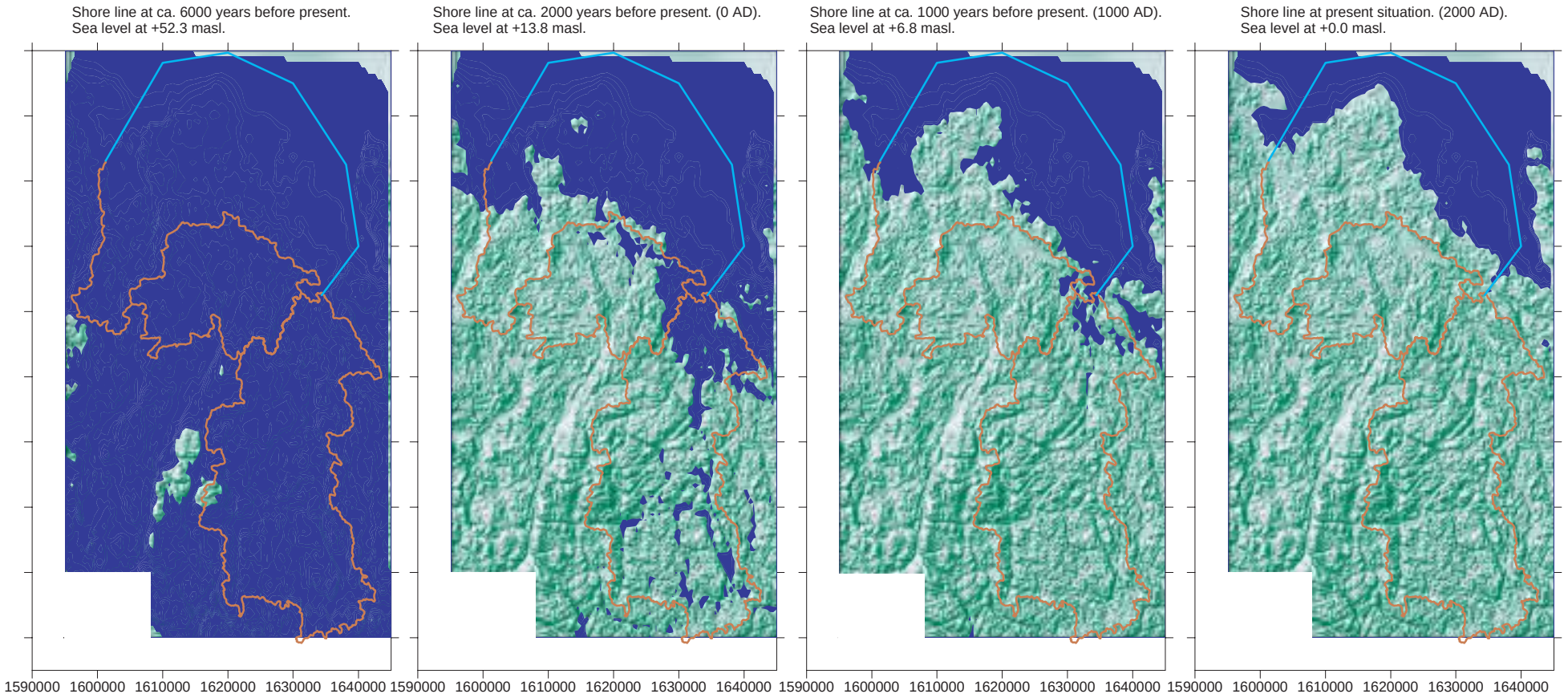

Figure 7-2. *The topography of the studied domain, the regional water divides and the shore level progress (land uplift), according to /Påsse, 1996/.*

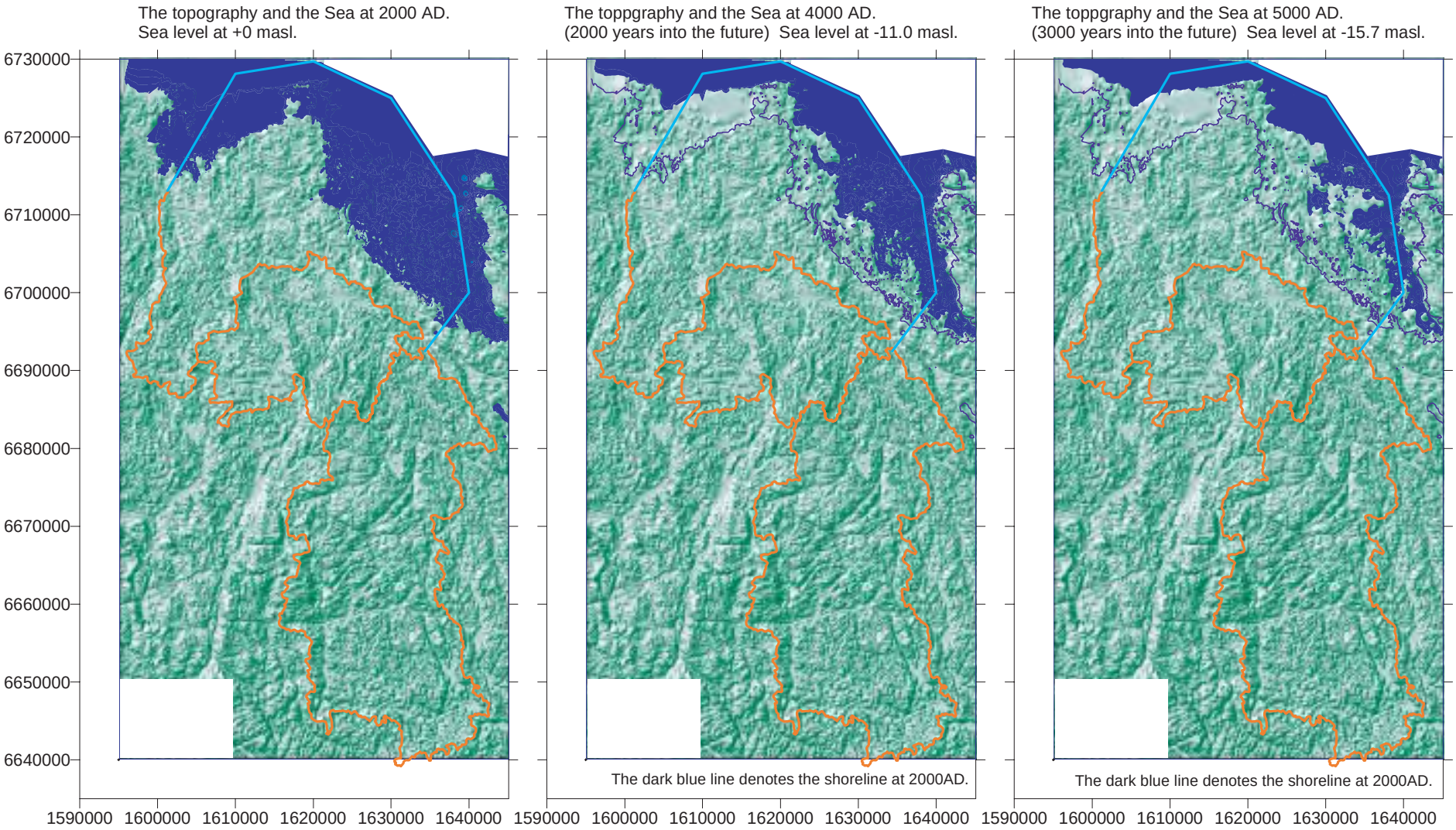

Figure 7-3. *The topography of the studied domain, the regional water divides and the shore level progress (land uplift), according to /Påsse, 1996/*

7.2 Case 9 – Uniform rock mass plus regional vertical fracture zones. Undulating topography. Transient solution

7.2.1 Model properties

The model of this case is identical to the model of Case 3. The difference is that the model of Case 9 is solved under transient conditions. The model includes the actual undulating topography and regional vertical fracture zones. The model does not include lakes or clay layers. Lakes and clay is not included as the creation and disappearance of such structures are a transient course in itself, and it is not known in detail. Cell size is 330 m × 330 m and model depth is 1100 m. The simulation was carried out by use of the GEOAN model.

7.2.2 Discretization of the time domain in the transient model

7.2.2.1 Size of timestep

To solve the differential equation with respect to time, we need to divide the time domain into discrete steps – time steps. The larger the number of time steps, the better the representation of the time-dependent course (presuming that the time step is not small enough to cause numerical difficulties). The drawback with a small time step is that the computational demands will be large if the time step is small. The size of the time step has to be balanced between acceptable accuracy and computational demands.

The numerical models are based on the finite difference method; this method replaces the original differential equation with a system of equations. The method for establishing the system of equations and the method for solving this system will have influence on the necessary size of the time step. The system of equations was established by use of the implicit method /Bear and Verruijt, 1987/, the system was solved by use of an iterative solver /Press et al, 1992/. The size of the selected time step was set equal to 25 years, which give 240 steps for a time period of 6000 years. The size of the time step was based on the sensitivity analysis (see below).

7.2.2.2 The excess head at SFR

During the siting investigations for the SFR repository (1980–1981), previous to the construction of the repository, boreholes were drilled from a floating platform at Sea (position of SFR is given in Figure 3-7 and Figure 7-9). In the boreholes falling head tests were performed and groundwater head was measured. /Hagconsult, 1982/ discusses these tests and the results of the tests. For the bore holes that intersected the H2 sub-horizontal fractures zone, the results of the head measurements demonstrated, in relation to the mean Sea water level, an excess head in the bore holes, which was between +0.11 meters and +0.61 meters /Hagconsult, 1982; Carlsson et al, 1987/. These head values are the excess head at SFR, and if they are correctly measured and interpreted they indicate the transient behaviour of the flow system, as caused by the shore level progress. From a theoretical point of view it is likely that there should be an excess head, but theoretical assessments gives no exact information of the size of the excess head, and the results of the actual measurements are uncertain. The size of the excess head in the rock mass depends on the velocity of the shore level displacement, compared to the velocity of the change of the heads in the rock mass. The velocity of the change of the heads in the rock mass depends on different factors like: (i) the conductivity and the storage properties of the rock mass, as well as (ii) the conductivity and the extension of previous and present quaternary deposits, and (iii) the effects of the movements of deep groundwater with a high density (relict salt water) as well as movements of near surface groundwater with a density higher than that of the present seawater.

7.2.2.3 Sensitivity analysis of size of time step and excess head

Using the initial condition discussed above as well as reasonable values of the conductivity and the storage properties of the flow media, the fresh water model of this study predicts values of the excess head at the SFR area, which are smaller than the measured and interpreted values (measured values are between +0.11 m and +0.61 m).

At steady state conditions, the models studied predict an excess head of about a 1 centimetre. The regional model of /Holmén and Stigsson, 2001/ also produced similar results, and /Carlsson et al, 1987/ made similar conclusions based on the results of their model.

Transient conditions have been analysed by use of a sensitivity analysis, in which results of different models with different time steps have been analysed (the only difference between the models was size of time step). The models did not include density-effects. The size of the time step and number of time steps were varied for the studied period of 6000 years (a period from 6000 years before present and until present, 2000 AD). The calculated head at SFR was checked for the different models (with different time steps), at time equal to present (2000 AD). The results are given in Figure 7-4, below. For a transient solution with a large number of time steps (i.e. size of step is small), the transient model predicts an excess head at SFR smaller than 0.1 metre (at 2000 AD).

A large excess head could nevertheless be an actual property of the system studied, as the models are simplified descriptions of the system studied. For the model that do not include density effects, we have selected a time step in a way that the model (for time equal to 2000 AD) will produce values of excess head at the SFR area, similar to the smallest of the actually measured and interpreted values of excess heads. The models will produce an excess head of 0.1 to 0.2 metres, dependent on depth. Hence, we have selected a time

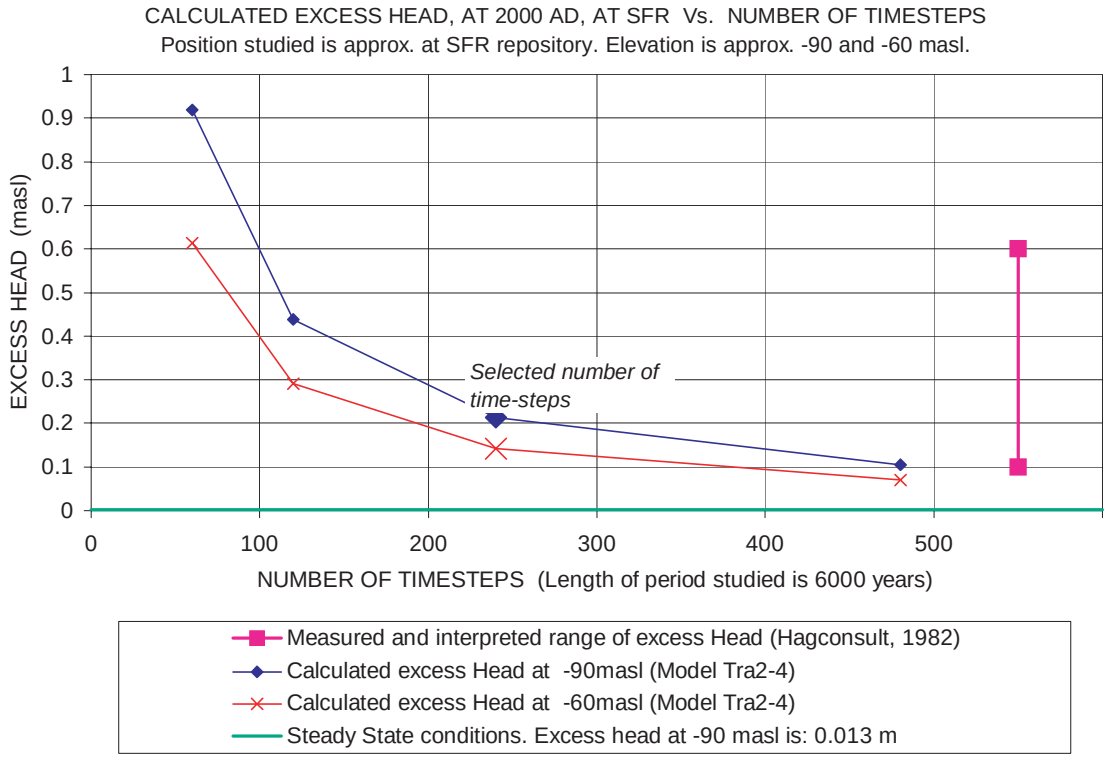

Figure 7-4. *Sensitivity analysis of time step used in model and the calculated (by use of models) excess head at SFR, and the measured and interpreted excess head at SFR.*

step for Case 9 (and Case 9b) that is larger than the numerically optimised time step; such a time step will delay the change of the head values of the model. Consequently for such time steps, large head values will remain at the SFR area for a longer period than for a time step selected based on a strictly numerical consideration. The use of this time step is a method of reproducing effects otherwise not included in the model. It is a conservative approach, as the models will produce larger flows (shorter breakthrough times) and shorter flow paths with this approach than if a numerically optimised time step was used.

7.2.3 Results at time equal to 2000 AD

The flow field of the model, representing the situation at time equal to 2000 AD, was investigated by use of flow paths. For this case we have simulated time-independent flow paths. The actual head field will change with time as the shore level retreats. Time-independent paths represent the flow system at a given moment, in this study at time equal to 2000 AD.

Examples of flow paths are given in Figure 7-5. This figure presents flow paths released between a depth of 490 m and 540 m. Figure 7-5 can be compared to Figure 5-19. Such a comparison demonstrates the difference in groundwater flow close to the shoreline. The flow field of the transient model is influenced by the shore level progress, included in the transient model, but not included in the steady state solution of the other model.

Putting all flow paths released inside the shoreline in one sample, the following distributions were obtained as regard length of flow paths (see Table 7-1).

Compared to the model of Case 3 the flow paths are shorter for Case 9. The lengths of Case 9 are about 92 to 97 percent of the lengths of Case 3. In the transient model, the head values at some depth below the ground surface are larger than in the model solved for steady state (excess head is discussed in Section 7.2.2). The excess head at depth follows from the transient mode and the shore level progress. In the transient model some of the flow cells will not reach the same depth as in the steady state model, because of the excess head at depth.

Breakthrough time for the flow paths from repository depth is given below in Table 7-2. Compared to the model of Case 3, the breakthrough times are shorter for Case 9. The times of Case 9 are about 54 to 93 percent of the times of Case 3. This follows from the shorter paths, but also from the somewhat larger flow velocities that takes place in the transient model.

Considering flow paths from repository depth, approximately 68% of all paths will on their route to the ground surface use one or more of the regional vertical fracture zones (for a shorter or longer part). Considering flow paths from repository depth, but only paths released at a minimum distance of 660 m from a regional vertical fracture zone, for these paths approximately 50% will, on their route to the ground surface, use one or more of the vertical fracture zones (for some part of the route).

We have estimated the localisation of the repository positions with the longest flow paths and largest breakthrough times. Flow paths were released inside the shoreline and at depths between 490 m to 540 m, with the additional condition that the distance between a repository position and a vertical fracture zone has to be 660 m, or larger. The 500 and 100 positions with the longest flow paths or largest breakthrough times are given below in Figure 7-6 and Figure 7-7. Repository positions inside the shoreline with large flow path lengths or large breakthrough times can be found at many different places within the domain studied. There is no general trend that the positions with large lengths or times are located as far as possible from the shoreline.

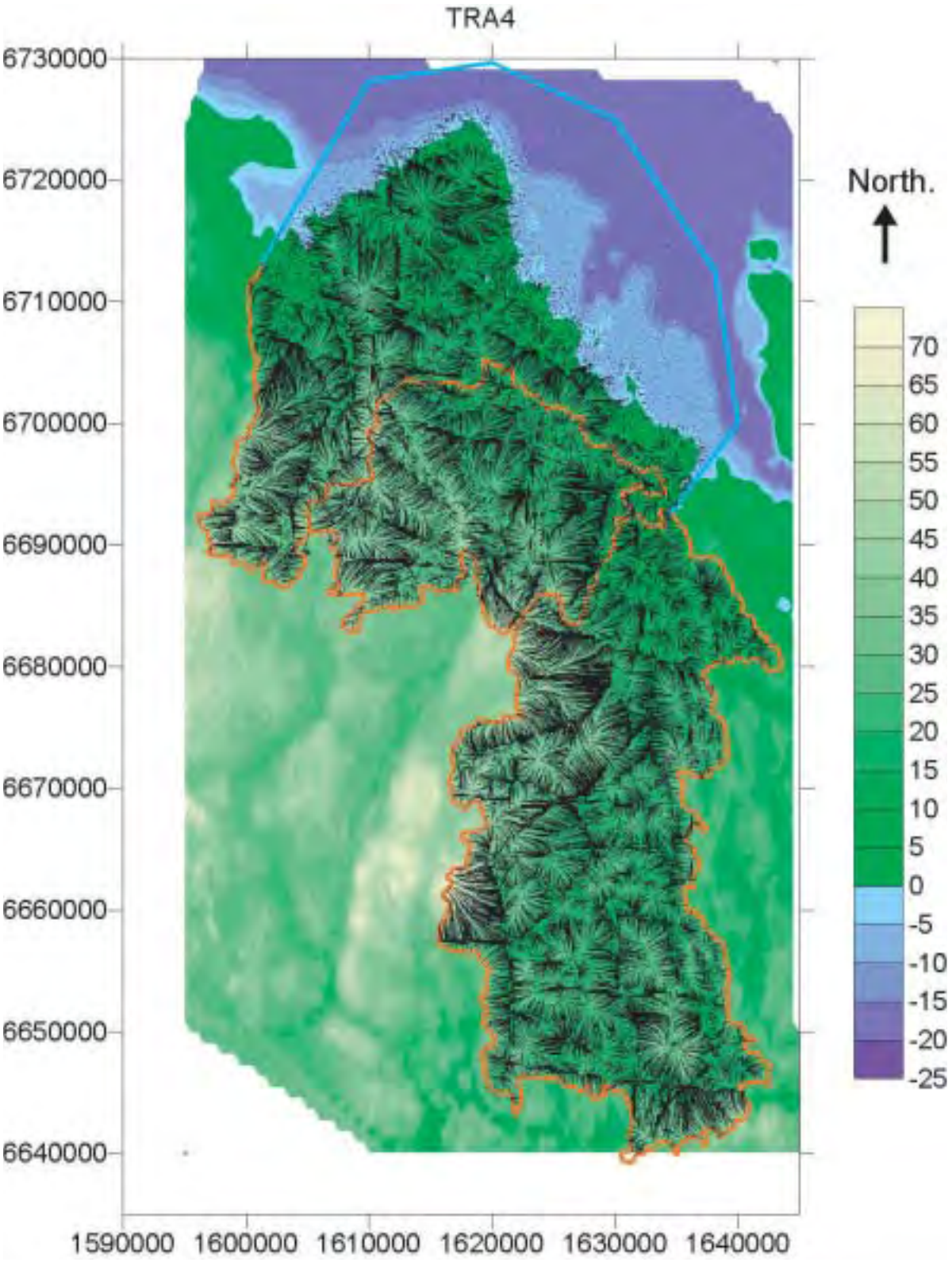

Figure 7-5. *Case 9. Time equal to 2000 AD. Flow paths released at repository depth (depth=490–540 m). The figure presents one path for each cell of the layer that represents repository depth, which gives 21 000 paths, plotted in the figure above. The model is solved for transient conditions and includes the undulating topography and vertical fracture zones.*

Table 7-1. Case 9. Time equal to 2000 AD. Percentiles of flow path length, all paths in one sample. Paths are from repository depth, no paths are released below the Sea. Case 3 and Case 9.

Case	Percentiles of flow path length (m)				
	90th	70th	50th	30th	10th
C3 (steady)	3302	1827	1132	773	571
C9 (transient)	3141	1700	1036	710	554
C9 in % of C3	95	93	92	92	97

Table 7-2. Case 9. Time equal to 2000 AD. Percentiles of breakthrough time for flow-paths from repository depth (490–540 m), all paths in one sample, no paths are released below the position of the Sea. Case 3 and Case 9.

Case	Percentiles of breakthrough time (years)				
	90th	70th	50th	30th	10th
C3 (steady)	6494	1542	731	198	14
C9 (transient)	3476	1358	674	184	13
C9 in % of C3	54	88	92	93	89

- For Case 9, the flow paths lengths of the paths from positions with the longest lengths are as follows: For the 500 positions with the longest paths the lengths are between 9080 m and 3770 m, and for the 100 positions with the longest paths the lengths are between 9080 and 5640 m. These results are rather similar for all the studied cases with undulating topography.
- For Case 9, the breakthrough times of the flow paths from the positions with the longest times as follows: For the 500 positions with the longest breakthrough times, the times are between 159 000 and 27 700 years, and for the 100 positions with the longest breakthrough times, the times are between 159 000 and 49 300 years. The ten positions with the longest break through times are not located very close to the shoreline, or below islands.

The two criteria for selection of repository positions (flow path length and time) have created two ensembles of repository positions; these ensembles can be combined. Scanning for the repository positions that occur in each of the two ensembles does this. Considering the two ensembles of 500 positions each, 209 positions occur in both. These are positions that are among the 500 positions with the longest flow path lengths and among the 500 positions with the longest breakthrough times. Short flow paths with long breakthrough times and long flow paths with short breakthrough times will be excluded by combining the two ensembles. The resulting positions are given in Figure 7-8. For the combined ensemble, the flow paths lengths are between, 9 080 m and 3 770 m, and the breakthrough times are between, 159 000 years and 27 800 years.

We conclude: With the transient solution, the flow paths from repository depth get shorter, and the breakthrough times get shorter as well (compared to the flow field of a steady state solution). Especially the very long paths and the paths with large breakthrough times will be reduced. Repository positions with large flow path lengths or large breakthrough time can nevertheless be found at many different places within the domain studied. This conclusion is not changed by the introduction of the transient solution. The Case 9 transient model

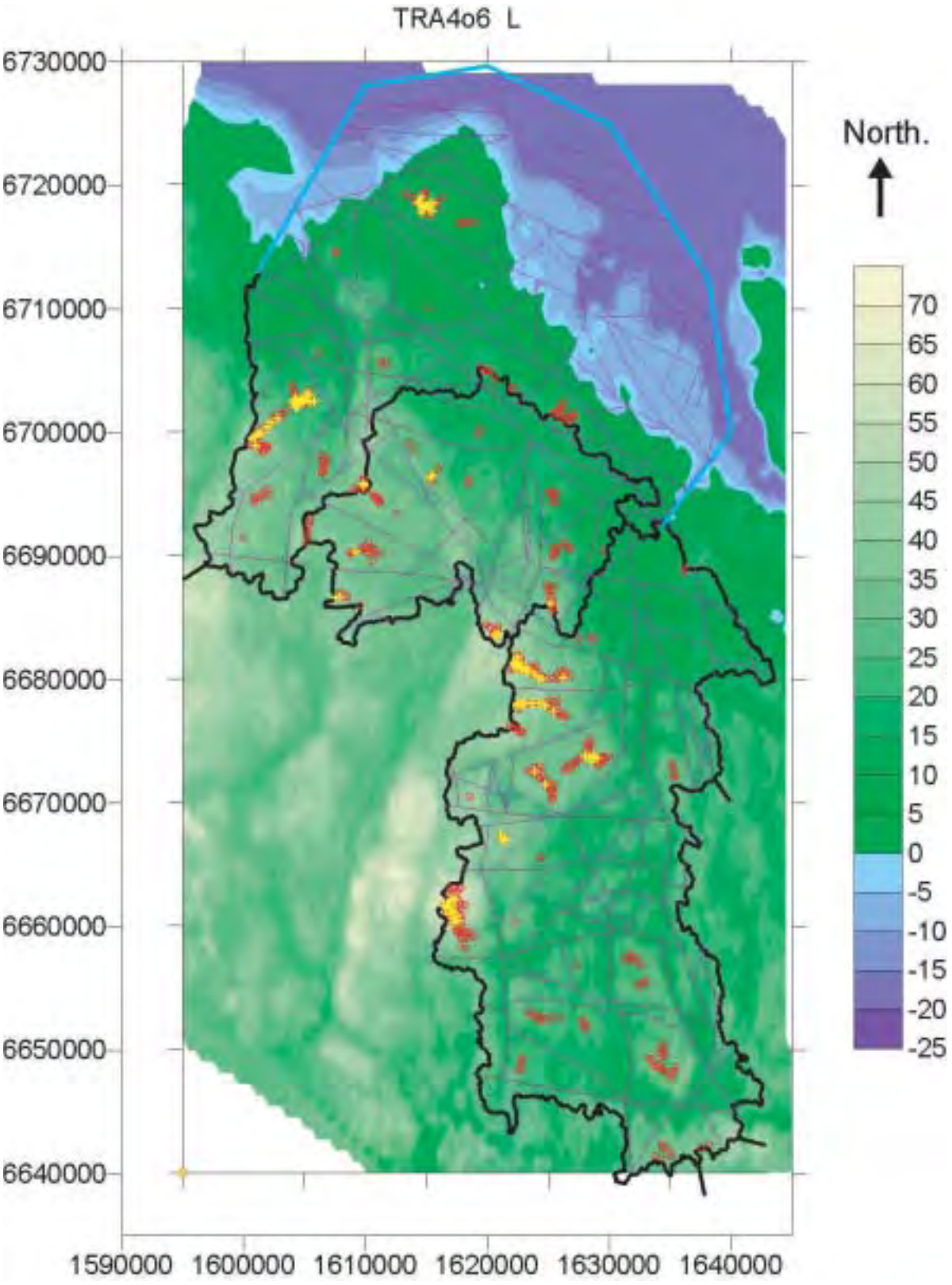

Figure 7-6. *Case 9. Time equal to 2000 AD. The 500 repository positions (Red dots) and the 100 positions (yellow dots) with the longest flow path lengths, from repository to ground surface (one position corresponds to an area of 330 × 300 m). All flow paths are released inside the shoreline (or below an island). The model is solved for transient conditions and includes the undulating topography and vertical fracture zones.*

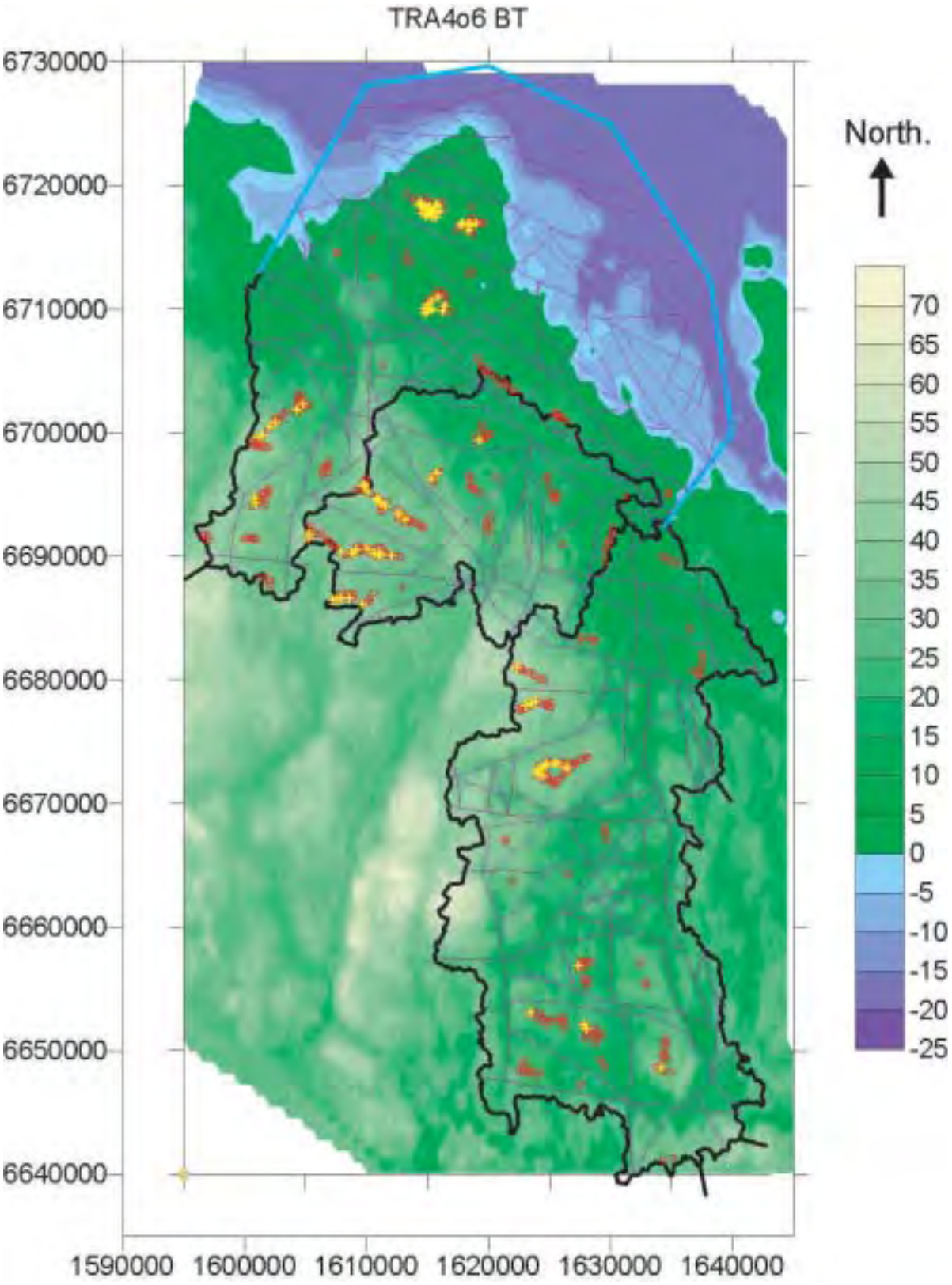

Figure 7-7. *Case 9. Time equal to 2000 AD. The 500 repository positions (Red dots) and the 100 positions (yellow dots) with the longest breakthrough times, for flow paths from repository depth to ground surface (one position corresponds to an area of 330 × 300 m). All flow paths are released inside the shoreline (or below an island). The model is solved for transient conditions and includes the undulating topography and vertical fracture zones*

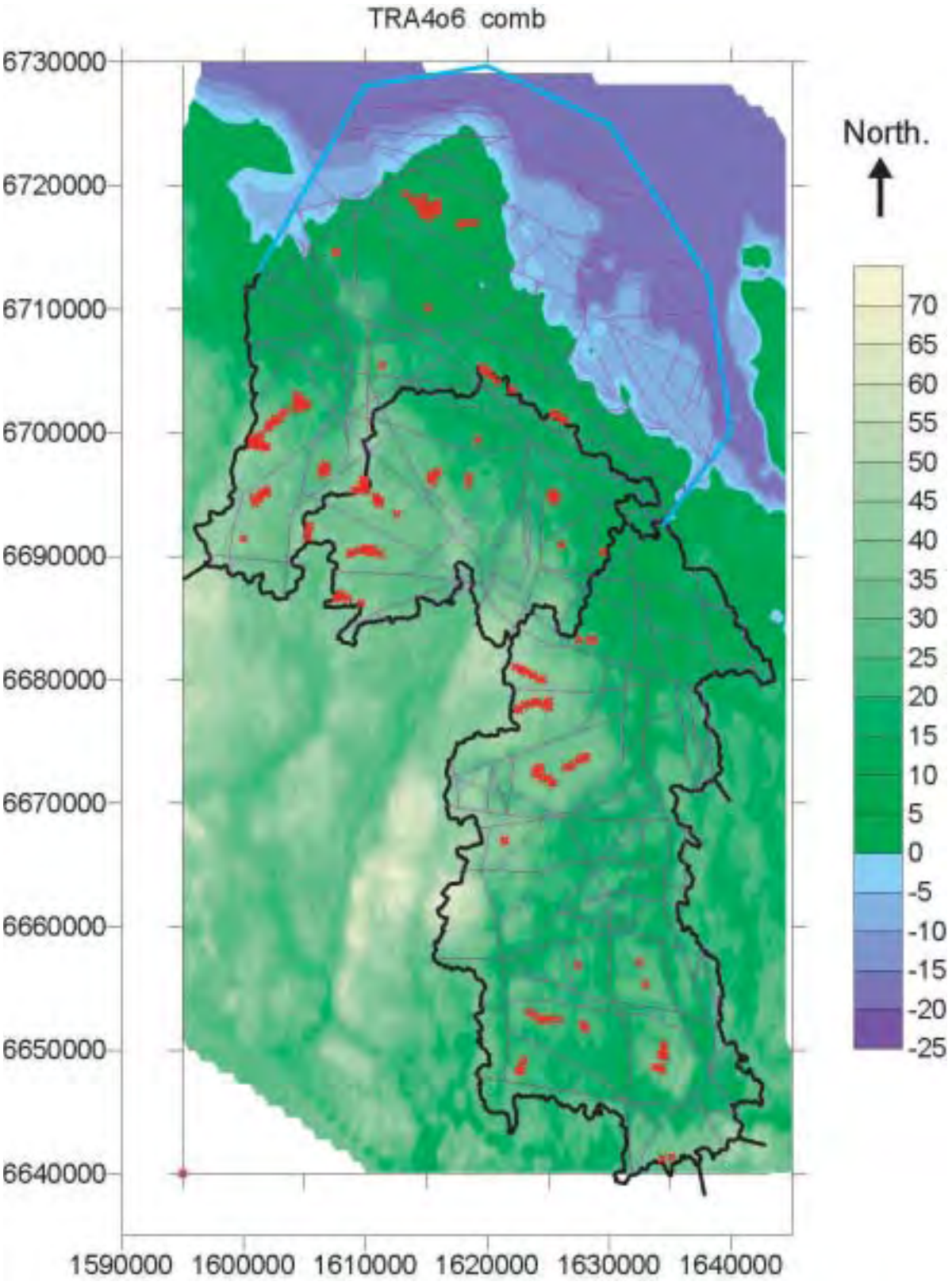

Figure 7-8. *Case 9. Time equal to 2000 AD. Repository positions (red dots) that take place within both ensembles of: (i) the 500 positions with the longest flow path lengths and (ii) the 500 positions with the largest breakthrough times. One position corresponds to an area of 330 × 300 m. All flow paths are released inside the shoreline (or below an island). The model is solved for transient conditions and includes the undulating topography and vertical fracture zones.*

produce approximately the same repository positions as the other models with undulating topography and steady state solution, when considering the longest flow paths or the largest breakthrough times.

However, the lengths and breakthrough times will be reduced due to transient effects. Considering breakthrough time, the repository positions very close to the shoreline and below islands are not as attractive with the transient solution as with the steady state solution. This is because of the excess head as created by the shore level progress. The excess head will increase the groundwater velocities below the Sea and therefore make the breakthrough times shorter for these positions in the transient solution, compared to the very long times found in the steady state solution.

In addition we have for this case also used a combined test that selects the repository positions that are among positions with both the longest paths and the longest breakthrough times. Also for the combined test the conclusion is that repository positions with large flow path lengths and large breakthrough time can be found at many different places within the domain studied. There is no general trend that positions with large path lengths and breakthrough times are found as far as possible from the Sea. Figure 5-9 presents the results of the combined test regarding a steady state solution (Case 6). Figure 7-8 presents the results of the combined test regarding a transient solution (Case 9). By comparing these two figures we note that the transient solution and the reduction of breakthrough times close to the shoreline that comes with it, will not have a large influence on the repository positions selected by the combined test. This is because repository positions close to the shoreline will not pass the combined test in either case, as the lengths of the flow paths from these positions are not long enough.

7.2.1 Results at time equal to 5000 AD

Flow paths released at 2000 AD have little relevance to an actual repository, since there will be practically no release to the geosphere the first thousands of years after the closure of the repository. In order to get more useful results we have also analysed a flow situation representing 5000 AD (i.e. 3000 years into the future).

The flow field of the model, presented in this section, represents the situation at time equal to 5000 AD. The flow field was investigated by use of flow paths; we have simulated time-independent flow paths. The actual head field/flow field will change with time as the shore level retreats. Time-independent paths represent the flow system at a given moment, for the results presented in this section that moment is 5000 AD.

For the flow path analysis presented in this section, as for the previous presented analyses, we have only analysed repository positions inside the 2000 AD shoreline (inside the present shoreline). The difference compared to the previous cases is that the flow field analysed in this section represents a situation (at 5000 AD) for which the shoreline has withdrawn from its present position. This can be looked upon as an analysis of possible repository positions inside the present shoreline, considering the flow situation that will take place at 5000 AD (3000 years into the future). Or in other words, an analysis of flow paths from possible repositories that are placed inside the present shoreline, and which starts to leak 3000 years into the future.

Putting all flow paths released inside the 2000 AD shoreline in one sample, the following distributions were obtained as regard length of flow paths (see Table 7-3).

Compared to the flow field at 2000 AD, the flow field at 5000 AD produces longer flow paths, considering repository positions inside the 2000 AD shoreline. The lengths of the paths at 5000 AD are about 103 to 113 percent of the lengths at 2000 AD.

Table 7-3. Case 9b. Time equal to 5000 AD. Percentiles of flow path length, paths are from repository depth (490–540 m). Release positions are inside the present shoreline (2000 AD), but the flow field studied is that of 5000 AD.

Case	Percentiles of flow path length (m)				
	90th	70th	50th	30th	10th
C9 (2000 AD)	3141	1700	1036	710	554
C9b (5000 AD)	3397	1902	1171	780	572
C9b in % of C9	108	112	113	110	103

Breakthrough time for the flow paths from repository depth is given above in Table 7-4. Compared to the flow field at 2000 AD, the flow field at 5000 AD produces somewhat larger break through times, considering repository positions inside the 2000 AD shoreline. The breakthrough times of the paths at 5000 AD are about 105 to 111 percent of the times at 2000 AD.

We have estimated the localisation of the repository positions with the longest flow paths and largest breakthrough times. Flow paths were released inside the 2000 AD shoreline and at depths between 490 m to 540 m, with the additional condition that the distance between a repository position and a vertical fracture zone has to be 660 m, or larger. The 500 positions with the longest flow paths or the largest breakthrough times have been calculated, each position representing an area of 330 m × 330 m.

The two criteria for selection of repository positions (longest flow path lengths and longest flow path breakthrough times) have created two ensembles of repository positions; these ensembles can be combined. Scanning for the repository positions that occur in each of the two ensembles does this. Considering the two ensembles of 500 positions each, 192 positions occur in both. These are positions that are among the 500 positions with the longest flow path lengths and among the 500 positions with the longest breakthrough times. Short flow paths with long breakthrough times and long flow paths with short breakthrough times will be excluded by combining the two ensembles. The resulting positions are given in Figure 7-9. For the combined ensemble, the flow paths lengths are between, 11 300 m and 4100 m, and the breakthrough times are between, 155 000 years and 29 100 years.

Table 7-4. Case 9b. Time equal to 5000 AD. Percentiles of breakthrough time for flow-paths from repository depth (490–540 m). Release positions are inside the present shoreline (2000 AD), but the flow field studied is that of 5000 AD.

Case	Percentiles of breakthrough time (years)				
	90th	70th	50th	30th	10th
C9 (2000 AD)	3476	1358	674	184	13
C9b (5000 AD)	3781	1492	715	193	14
C9b in % of C9	109	110	106	105	111

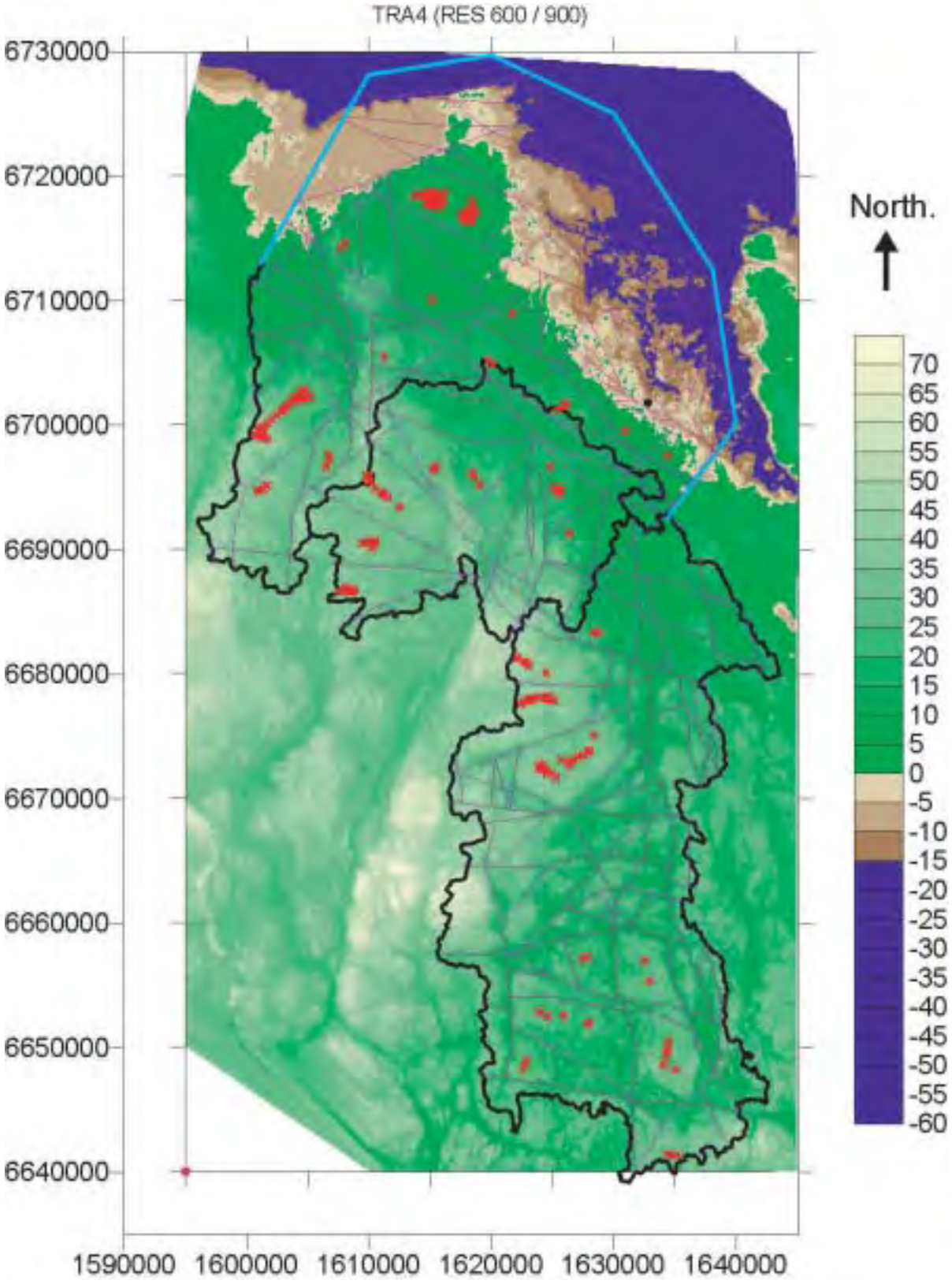

Figure 7-9. *Case 9b. Time equal to 5000 AD. Repository positions (red dots) that take place within both ensembles of: (i) the 500 positions with the longest flow path lengths and (ii) the 500 positions with the largest breakthrough times. One position corresponds to an area of 330 × 300 m. All flow paths are released inside the shoreline. The model is solved for transient conditions and includes undulating topography and vertical fracture zones. The topography is denoted as follows: Green colours are above the present shoreline, brown colours are above the shoreline of 5000 AD, and blue denotes the Baltic Sea at 5000 AD. A black dot denotes the position of the SFR repository.*

Repository positions with large flow path lengths or large breakthrough time can be found at many different places within the domain studied. This conclusion is the same as for the previous cases studied, and not changed by the flow field of 5000 AD. The transient flow field of 5000 AD produce approximately the same repository positions as the other models with undulating topography, when considering the longest flow paths or the largest breakthrough times. Interesting results at 5000 AD are the new repository positions close to the 2000 AD shoreline – positions that passed the combined test when considering the flow field of 5000 AD. When comparing Figure 7-8 (2000 AD) and Figure 7-9 (5000 AD), we note three new repository positions close to the 2000 AD shoreline; two positions are located only a few kilometres from the SFR-repository (SFR is denoted by a black dot in Figure 7-9). These repository positions did not qualify at time equal 2000 AD, because of the very close vicinity of the shoreline at 2000 AD and the short flow paths that follows from that situation; but at time equal to 5000 AD, the shoreline is at some distance and these positions are among the 192 positions that have the longest paths and the longest breakthrough times, considering the whole domain studied.

We conclude: Repository positions close to the present shoreline, which for the present situation may not produce the longest flow path lengths and longest breakthrough times, may in the future be among the repository positions that produce the longest paths and breakthrough times; this is due to the changed flow field that will be created by the retreat of the shoreline.

8 Case with transient solution and density dependent flow

The groundwater at the domain studied is of different origin, and at repository depth it is not unlikely that the groundwater is saline, the salinity may be close to that of the present Baltic Sea, but higher and lower levels of salinity may also be found. Different levels of salinity correspond to different values of density. Density dependent flow was however not included in the previously presented cases. To be able to evaluate the importance of density dependent flow we have included a model (Case 10) with vertical fracture zones, but without lakes and clay, the model includes the shore level progress and density dependent flow, and is solved under transient conditions. The produced flow fields are analysed at time equal to 2000 AD, 5000 AD and 7000 AD.

8.1 Case 10 – Uniform rock mass plus regional vertical fracture zones. Undulating topography. Transient solution. Density dependent flow using NAMMU

8.1.1 Introduction

In order to investigate the influence of density dependent flow on the distribution of flow paths from repository depth, a number of transient calculations using the NAMMU computer code were performed. NAMMU (Numerical Assessment Method for modelling Migration Underground) is a finite-element software package for modelling groundwater flow and transport in porous media /Cliffe et al, 1998/. In SR 97 NAMMU was used for regional studies. It produced boundary conditions for site-scale modelling of two sites, Beberg /Gylling et al, 1999/ and Ceberg /Walker et al, 1999/. In addition, NAMMU was used to model a land-rising scenario including salinity /Hartley et al, 1998/ for the Beberg site, which is based on data from Finnsjön located within the domain studied. Using NAMMU, the Beberg site was modelled again to verify simulation results, and to study modelling concepts by /Marsic and Hartley, 2000/. Recently, NAMMU has been developed even further by work of /Marsic et al, 2001/.

8.1.2 Model properties

An effort has been made to set up the NAMMU model as similar as possible to the GEOAN model. This was ensured by importing a grid file produced by GEOAN and using the same data set. The data set contains e.g. topography, fracture zones and water divides. In addition, a shore level displacement, i.e. the sum of changes of ground level and Sea level by time, is included in the concept. Similar to the transient calculations in GEOAN, the shore level displacement is addressed by using a mathematical model presented by /Påsse, 1996/.

The GEOAN model used a grid with a cell size of 330–330 m in the X and Y directions respectively and contained 11 layers. All layers are defined in relation to the surface topography, and layer 5 is at repository depth (490–540 m below surface). The depth of the GEOAN model (from ground surface) was 1100 m. It was decided that the grid used for salt transport calculations with NAMMU had to be extended down to –2000 masl in order to accommodate the saline water and the transient evolution of it. The argument for

not extending the model even further was the presence of “shield-brine” at large depths in the bedrock. This “shield-brine” will effectively act as a flow barrier and therefore make a further extension of the model unnecessary.

The imported GEOAN grid was used down to –800 masl which corresponds to the top 9 layers of the existing 11 layers in the GEOAN model. Beneath the uppermost 9 layers imported from GEOAN, another 11 layers were added. For simplicity reasons these added layers were kept horizontal. The vertical discretisation of the NAMMU model is presented in Table 8-1.

The permeability (k) of the rock mass was calculated as $k = 1.02\times10^{-7}$–K, where $K = 5\times10^{-9}$ m/s, which gives $k = 5.1\times10^{-16}$ m2. The effective porosity through out the entire model was set to 1×10^{-3}. The same value was used both for calculating the salt transport as well as the flow paths.

The conductivity field of the NAMMU model was defined in line with that of the GEOAN model. As in the GEOAN model a number of 614 vertical fracture zones were defined. In the NAMMU model this was done by use of the IFZ (Implicit Fracture Zone) method, see /Marsic et al, 2001/. As in the GEOAN model , the fracture zones were assumed to have a thickness of 30 m, a conductivity of K = 8×10–7 m/s, a porosity of 1×10–3 and continuously defined. No depth dependence was used in the model, neither for the fractures nor the bedrock matrix (as in the GEOAN model). A deterministic permeability field was generated, i.e. no variability of the rock mass or the fracture zones are used, using the IFZ routine. As a variant, a horizontal fracture zone with the same properties as the other zones was added. The large horizontal zone covers the entire model at a depth of –250 masl. A plan view of the generated effective permeability field for the NAMMU model is shown in Figure 8-1.

Table 8-1. Vertical discretisation of the NAMMU model.

Layer	Lower boundary [m below surface]	Thickness [m]
20	50	50
19	120	70
18	220	100
17	320	100
16	420	100
15	490	70
14	540	50
13	610	70
12	710	100
11	800 masl	100
10	900 masl	100
9	1000 masl	100
8	1100 masl	100
7	1200 masl	100
6	1300 masl	110
5	1400 masl	120
4	1550 masl	130
3	1700 masl	140
2	1850 masl	140
1	2000 masl	150

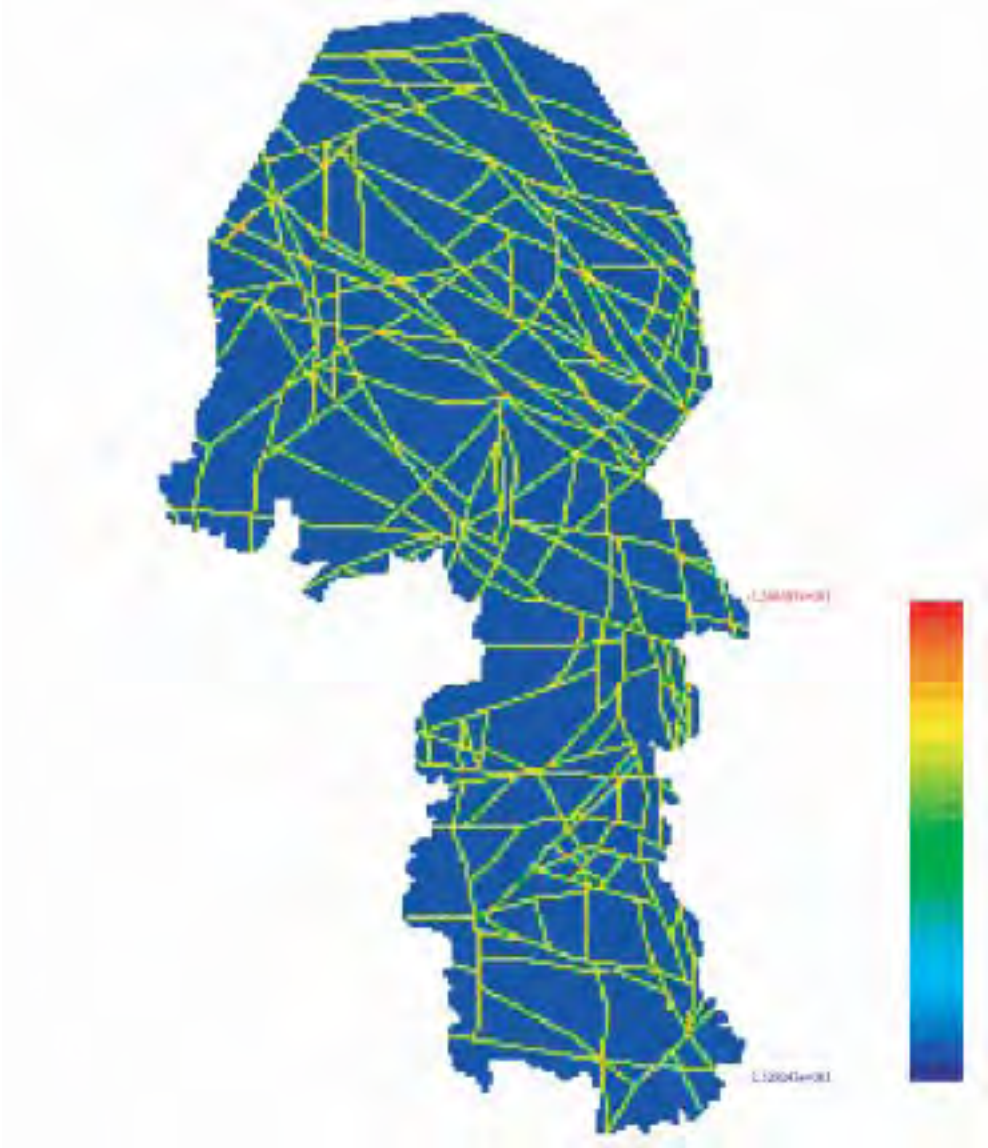

Figure 8-1. *Plan view of the effective permeability field for the NAMMU model. The elements are coloured according to the logarithm of permeability (K_{ZZ}). Red showing higher values and blue lower.*

The density of freshwater was set to 998.3 kg/m^3, and for underground saltwater the density varies with time, see section describing the boundary conditions. The longitudinal dispersion length was set to be 300 m and the transversal 150 m.

The same set of flow path starting positions as in the GEOAN was used, i.e. one starting position in each element in the layer at approximately 500 m depth. However, for the statistical evaluations only starting positions corresponding to locations on-shore (above the shore level) were used while particles started below the Sea were removed. The present day situation and shore level was used sorting the starting positions in groups of onshore and offshore positions respectively. Hence, 16 913 starting positions were used to release flow paths from a typical repository depth varying between from –540 to –490 masl. As an additional analysis (to show the effect of excluding particles started below the sea), particles started below the Sea were included in the population at time equal to 2000 AD. This means that the ensemble of 20 794 flow paths was released in the second analysis. Both results are presented in the text.

A summary of the used values of the physical parameters is given in Table 8-2.

Table 8-2. Values of physical parameters used in the NAMMU model.

Rock name	Permeability k_{xx} k_{yy} k_{zz} (m^2)	Salt diffusion coefficient (m^2/s)	Disperivity (m)	Flow porosity, Φ	Specific Storage Coefficient (m^{-1})
'BGR1'	5.1×10^{-16}	2×10^{-9}	150	10^{-3}	5×10^{-6}

8.1.2.1 Boundary conditions and initial conditions

Various types of boundary conditions were used in the transient groundwater calculations. It was assumed that the regional water divides remained valid over the transient considered. This motivated the use of no-flow boundaries for the vertical sides of the model. As the bottom boundary of the model was at –2000 masl it was assumed that no vertical groundwater flow or salinity flux existed over the bottom of the model. Hence, no-flow and no-flux boundary conditions were used.

For the top surface, the topography was used as a specified head boundary condition for areas above the Sea level. For offshore domains the head caused by the saline Baltic water, above the Sea bottom was included. For the salt, a Dirichlet boundary condition was used. In places above the Sea level where flow was inward the salinity was set to zero (fresh-water). At places where flow was outwards an advective flux of salinity was taken out of the model.

Since the start of the simulation was set to –4000 AD it was possible to choose a simple initial condition for the salinity of the model. At this time the Lithorina Sea covered the entire area of interest; consequently the entire model was initially filled with saltwater of a density equal to 1009.4 kg/m^3. This corresponds to a normalised concentration of C=1. However, since the concentration of salt in the seawater has been decreasing with time some correction had to be made. The following assumption was made: At a time equal to –4000 AD the density of saline water was set to 1009.4 kg/m^3 (1.5% salt). At present time (2000 AD) the density of saline water was set to 1001.9 kg/m^3 (0.5% salt). For the time between these to points a linear relation was assumed for the density of the saltwater. For times greater than 2000 AD a constant value of 1001.9 kg/m^3 was used.

This has the effect that the maximum value of the normalised concentration, C, will be decreasing with time, from C=1 (at time=–4000 AD) to C=0.32 (at time=2000 AD). This will effect the colour scale of the presented pictures including salinity, especially on the top boundary where it will clearly show off as a different colour in the Sea as the time changes. On the other hand, this also makes it possible to identify the age of the saline water deep down in the model, since old Lithorina water, where present, will still have a salt concentration close to 1. A more thorough explanation regarding the boundary conditions is presented in /Marsic et al, 2001/ and /Marsic et al, 2002/.

8.1.2.2 Discretisation of time

In order to obtain the appropriate discretisation of time a sensitivity analysis was performed gradually refining the time stepping. For each analysis the time steps were halved compared to the previous run. When the changes in the performance measures (flow path length, breakthrough time, canister flux and excess head) between to runs were sufficiently low (less than 10%) it was considered that the time steps were appropriate.

A fully implicit Crank-Nicholson time stepping scheme was used. In total 476 time steps were used per run. Initially, small time steps were used to resolve early fast transients.

Time-step sizes were then gradually increased until a final constant step of 50 years was used, see Table 8-3. Even though the simulations were run to a time equal to 8000 AD, results are only presented for a maximum time equal to 7000 AD.

8.1.2.3 Modelled variants

Two variants were set up with NAMMU, Case 10v1 and Case 10v2. These variants are identical in all aspects but one. The only difference between the variants is that a horizontal fracture zone at z=–250 masl was added to the model of Case 10v2, see section above.

As an additional study, two freshwater variants were set up in NAMMU, FWCv1 and FWCv2. These two variants correspond to the two salt variants described above, with the exception that no salt was included in the model. Also, the shore level displacement was not addressed in the freshwater variants, which were consequently modelled as steady state simulations. The topography used in the freshwater variants corresponds to the present day situation (2000 AD). The results from the freshwater variants (FWCv1 and FWCv2) were used in comparison with the salt variants (Case 10v1 and Case 10v2) to determine the effects caused by the presence of saline groundwater in the model. The comparison was only made for a time equal time 2000 AD since the freshwater variants were not transient simulations.

8.1.3 Case 10v1. Transient results

8.1.3.1 Evolution of pressure and salt on the top boundary

The transient simulation is started at a time equal to –4000 AD and continued 11000 years to 7000 AD. The start time corresponds to a situation when the Lithorina Sea covered the entire area of interest. Thus, the initial condition for both the pressure and the salt-water density is clearly defined. The initial head equals zero and the entire model domain is filled with water with a salt concentration equal to one which is a normalised value corresponding to the density of Lithorina water (1009.4 kg/m^3).

The evolution in time of the residual pressure at the top boundary of the model is shown in Figure 8-2 for selected times. Since the top boundary condition is the same in the two variants, Case 10v1 and Case 10v2, the figure is applicable to both variants. It is clear that the top pressure boundary condition is working correctly. The initial pressure equals zero over almost the entire area except for a small area in the south-west which corresponds to the highest topography in the studied region. As the time increases more land rises above the Sea due to the land uplift. At a time equal to 7000 AD practically the entire area is above sea-level (even though this might be difficult to see due to the colour scale).

Table 8-3. Time steps used for the transient simulations with the NAMMU model. Times given in years counted from the start of the simulation, i.e. –4000 AD.

Time interval [yr]	Time step size [yrs]	Nr of time steps
0–16	0.5	32
16–40	1	24
40–200	2.5	64
200–400	5	40
400–1800	12.5	112
1800–12000	50	204

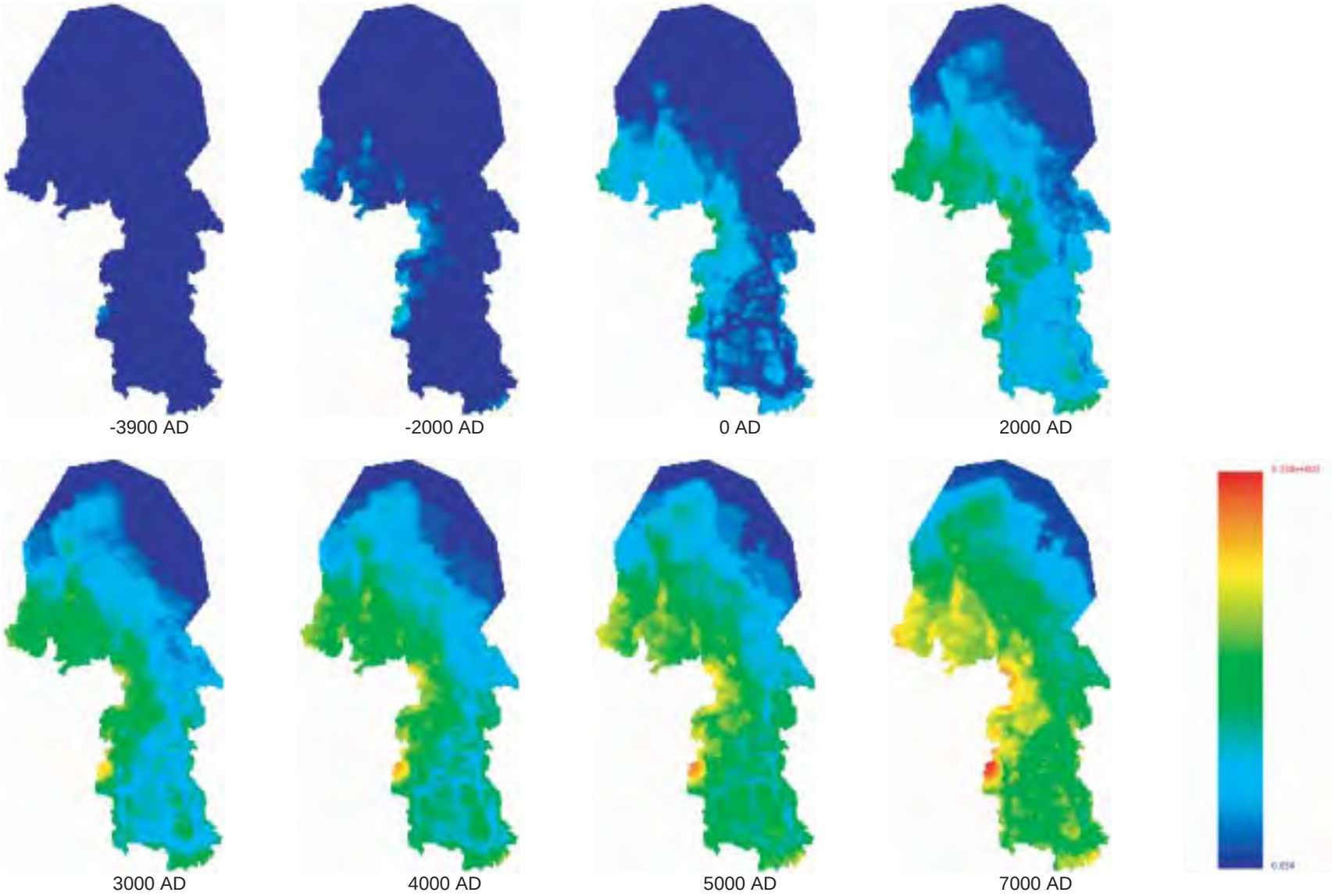

Figure 8-2. *Cases 10v1 and 10v2. Evolution in time of the residual pressure at the top boundary of the model. Range in head values shown is from 0 (blue) to 85 m (red).*

In Figure 8-3, the evolution in time of the salt concentration at the top boundary of the model is shown for Case 10v1. The selected times correspond to the ones used in Figure 8-2. Initially much of the model is saline but as the time increases the salt concentration on the top boundary decreases in the areas where the land rises above the sea. This is an effect of the freshwater infiltrating the system through the exposed surface. The freshwater flushes the salt water from the model out through local discharge areas and the sea. By 2000 AD most of the near-surface is fresh and apart from the Sea are up north, there are only a few places where weak saline water discharges to the surface. Here it is also clearer that the entire model area is above the Sea level at the end of the simulation (7000 AD).

Another point worth noting is the change in salt concentration in the Sea with time. This is an effect of the applied top boundary condition discussed in section 0. The decrease of density with time in the top boundary condition is apparent in the first three pictures (–3900, –2000 and 0 AD) in Figure 8-3. Remember that this follows from the need to change the maximum density from the value corresponding to the Lithorina water (1.5% salt in the Sea water) to the present day situation (0.5% salt in the Sea water).

8.1.3.2 Salt concentration profile as a function of depth

In Figure 8-4 to Figure 8-6, the salt concentration at different depths in the model is presented for three different times, 2000 AD, 5000 AD and 7000 AD respectively for Case 10v1. For the present day situation (2000 AD) shown in Figure 8-4, the more shallow salt water has already been flushed out and much of the model above 500 masl, apart from some small discharge areas, is filled with freshwater. It is also clear that older Lithorina water is still present at larger depths (–1000 down to –2000 masl) in the model where salt concentrations close to 1 can be found. It can also be seen that the salt water in the fracture zones is flushed out faster than the water in the surrounding bedrock. Another effect worth pointing out is the fact that the salt concentration in some areas at the bottom of the model reaches slightly above 1, which is the maximum. This is probably due to numerical problems likely caused by the coarse grid refinement or the time stepping. The fact that the numerical equations for pressure and salt are not fully coupled can also have an impact on the observed effects. The problem is not stationary but moves around as the groundwater situation evolves with time, also see Figure 8-5 and Figure 8-6.

Figure 8-5 and Figure 8-6 present the same views of the salinity profiles as shown in Figure 8-4 but at later times, 5000 AD and 7000 AD respectively. The continuous flushing of saltwater out of the model is more apparent at larger depths. At time equal to 7000 AD the major part of the salt water is present beneath –1000 masl, see Figure 8-6.

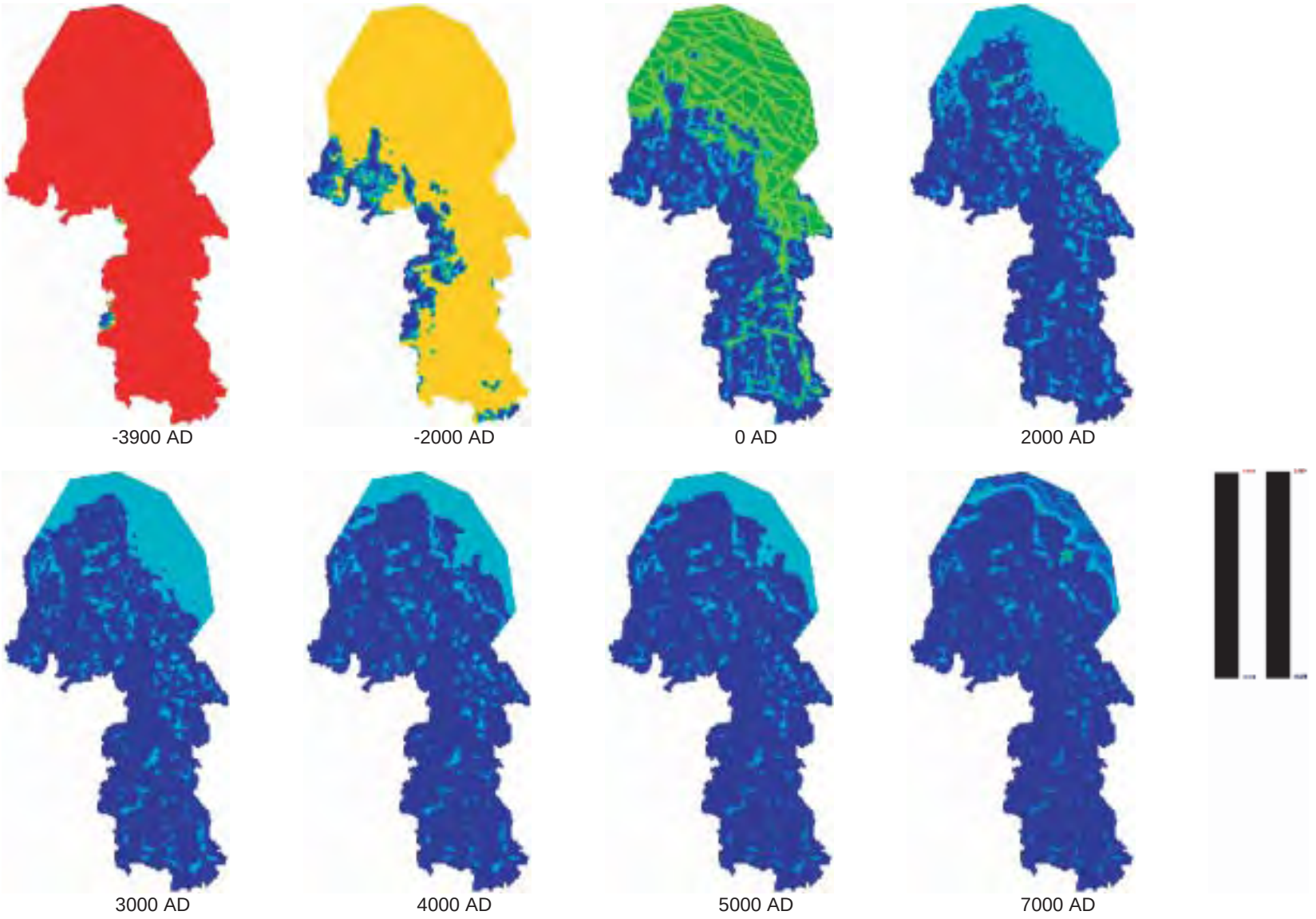

Figure 8-3. *Case 10v1. Evolution in time of the salt concentration at the top boundary of the model. Range in concentration values shown is from 0 (blue) to 1 (red).*

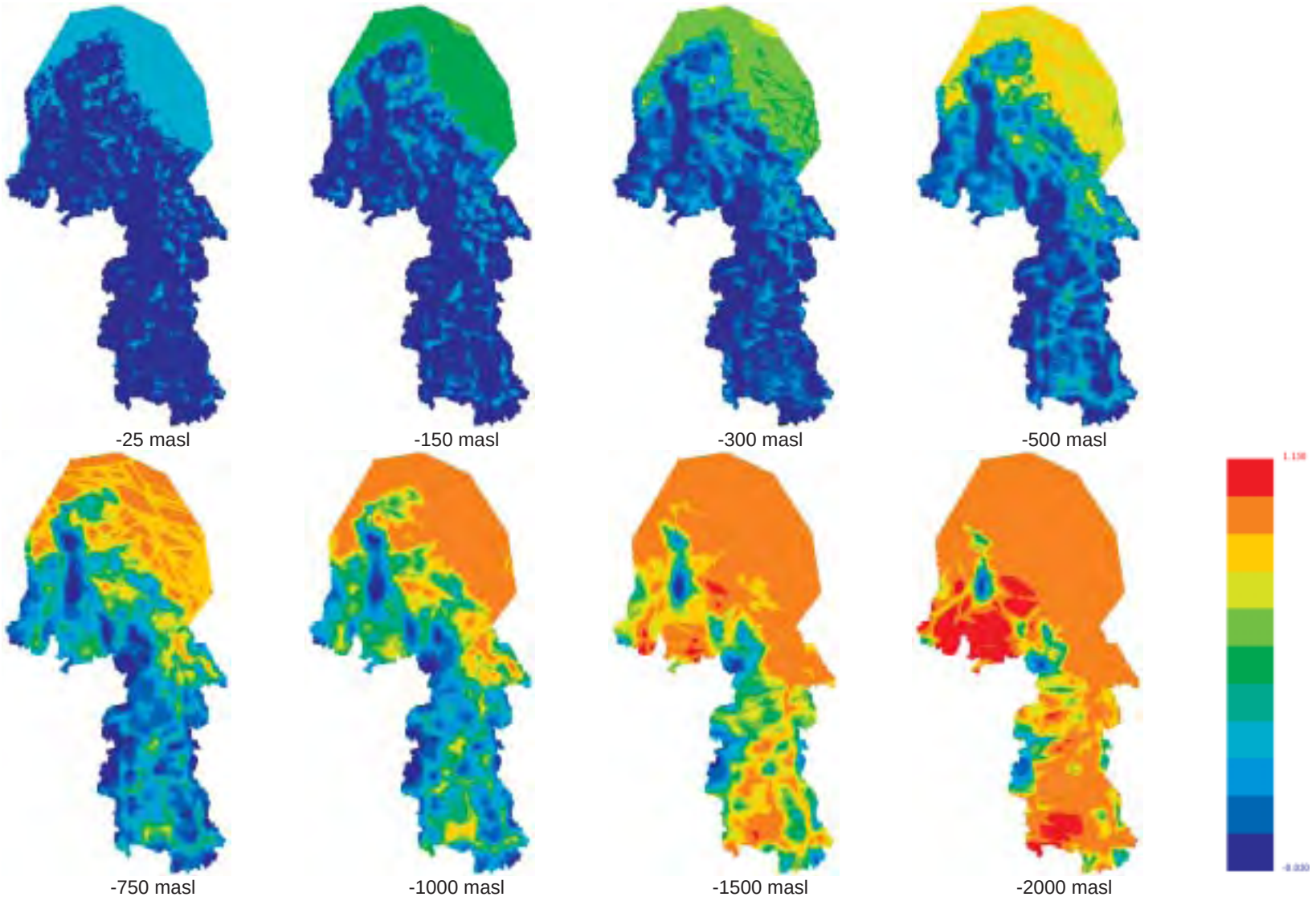

Figure 8-4. *Case 10v1. Time equal to 2000 AD. Salt concentration at different depths in the model. Range in concentration values shown is from 0 (blue) to 1 (red).*

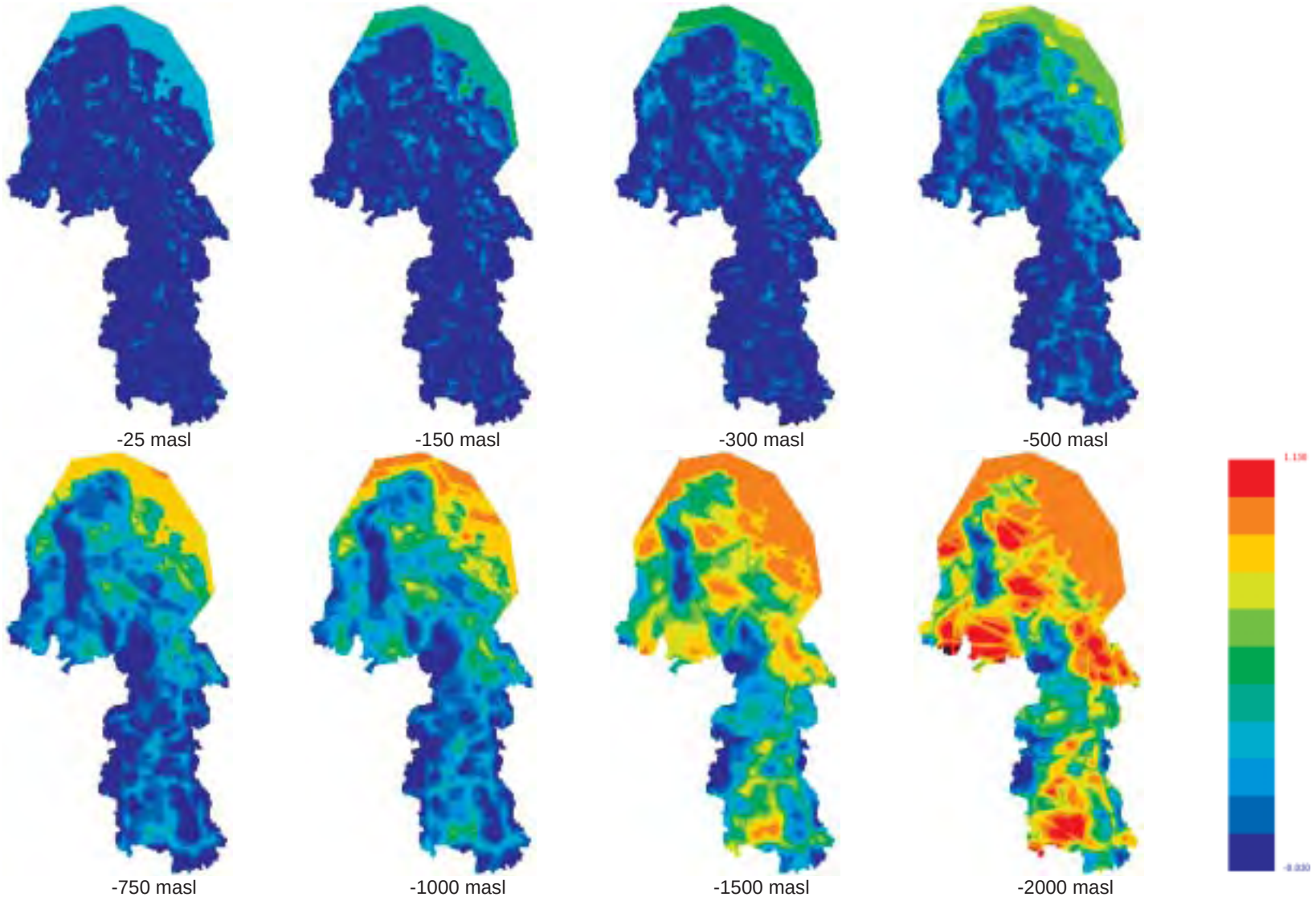

Figure 8-5. *Case 10v1. Time equal to 5000 AD. Salt concentration at different depths in the model. Range in concentration values shown is from 0 (blue) to 1 (red).*

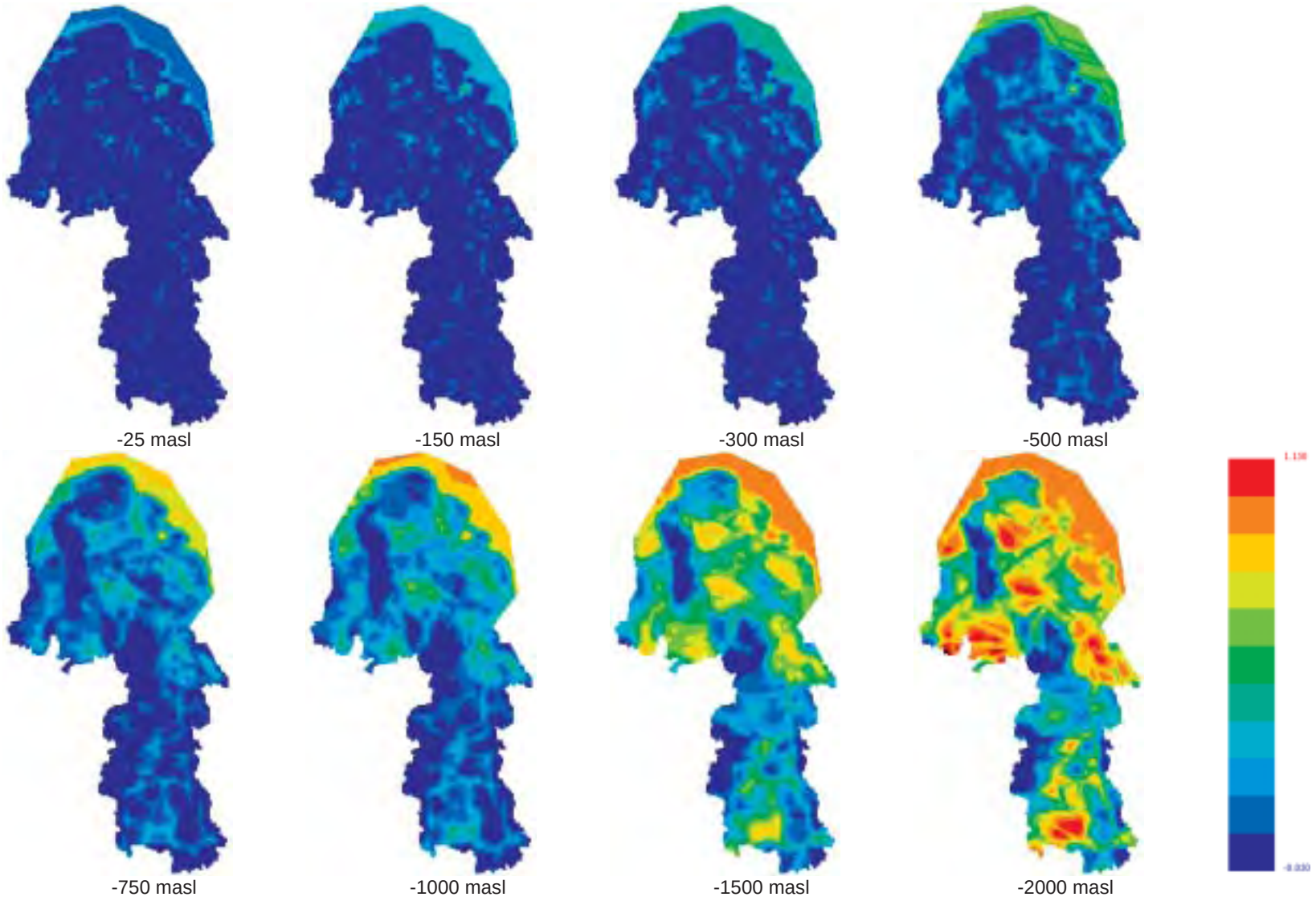

Figure 8-6. *Case 10v1. Time equal to 7000 AD. Salt concentration at different depths in the model. Range in concentration values shown is from 0 (blue) to 1 (red).*

8.1.3.3 Flow paths released at repository depth

In order to study the calculated flow field of the model, a number of 20 794 paths were released at repository depth (depth=490–540 m). The flow paths were released at different times in fixed pressure fields (snapshots), or in other words as the system looked at the time of the release. Figure 8-7 presents a plan view of flow-paths released at three different times (2000 AD, 5000 AD and 7000 AD respectively). The figure presents one path for each cell of the layer that represents repository depth, which gives in total 20 794 paths. The paths are coloured according to the logarithm of time.

Releasing flow paths at different times has little effect on the results. There is practically no difference in the patterns comparing the three pictures in Figure 8-7. Even if the colour scales are not identical in the pictures, it is still clear that longest breakthrough times are obtained from the flow paths started underneath the Sea and of course this constantly shrinking area is moving north as the shore level displacement evolves in time. The presence of fracture zones is clearly visible in the flow path pattern. The flow paths tend to follow the permeable fracture zones and discharge where there is an appropriate local low point in the topography. It is also possible to see that the flow paths are not very long in general, the exit locations are often located just a few kilometres from the release point. Thus, the flow paths are generally located to rather local flow cells. This will later on be confirmed in the statistical analysis of the flow paths.

In Figure 8-8 and Figure 8-9 an attempt is made to illustrate the discussion above in more detail by showing close-up views of the northern part of the model domain. The top picture of Figure 8-8 shows a plan view of the flow paths at a time equal to 2000 AD and the bottom picture of the same figure shows the permeability filed in exactly the same area. It is easy to see how the released flow paths find their ways through the bedrock to the nearest fracture zone and follow the zone to a suitable exit location. Of course, the flow paths are highly three-dimensional features in reality, which is never easy to visualise in two dimensions. However, some of the flow paths tend to go quite deep into the model before they eventually turn back up and exit through the top surface.

In Figure 8-9 only the exit locations for the generated flow paths are shown for the same time as in Figure 8-8. In the top picture of the figure the exit locations are superimposed on a slice coloured according to permeability and here it is very clear that practically all the exit locations are associated with the location of the fracture zones. In the bottom picture of the same figure the exit locations are superimposed on a slice coloured according to the calculated residual pressure at a depth of –50 masl. As expected, the picture shows that the exit locations are also located in areas with low elevation. Another noteworthy result is that many of the released flow paths exit in the Baltic Sea, which is of course the lowest topographic point in the area. These are also the flow paths with the longest breakthrough times.

8.1.3.4 Flux direction at repository depth

Groundwater flux at the starting positions for the flow paths were also studied. The starting positions are located about 500 m below Sea level. In Figure 8-10, the vertical flux directions are shown (up or down) for Case 10v1. Here, the flux contours are plotted for three times, 0 AD (about 2000 before present time), 2000 AD (about present time) and 5000 AD (about 3000 years after present time).

Seemingly, there is no dramatic difference in the direction of the flow field, especially for the first two times shown, i.e. times equal to 0 AD and 2000 AD. In the pattern for the time equal to 5000 AD some minor differences may be seen, compared to the other patterns shown, traces of fracture zones may also be seen in the flow fields.

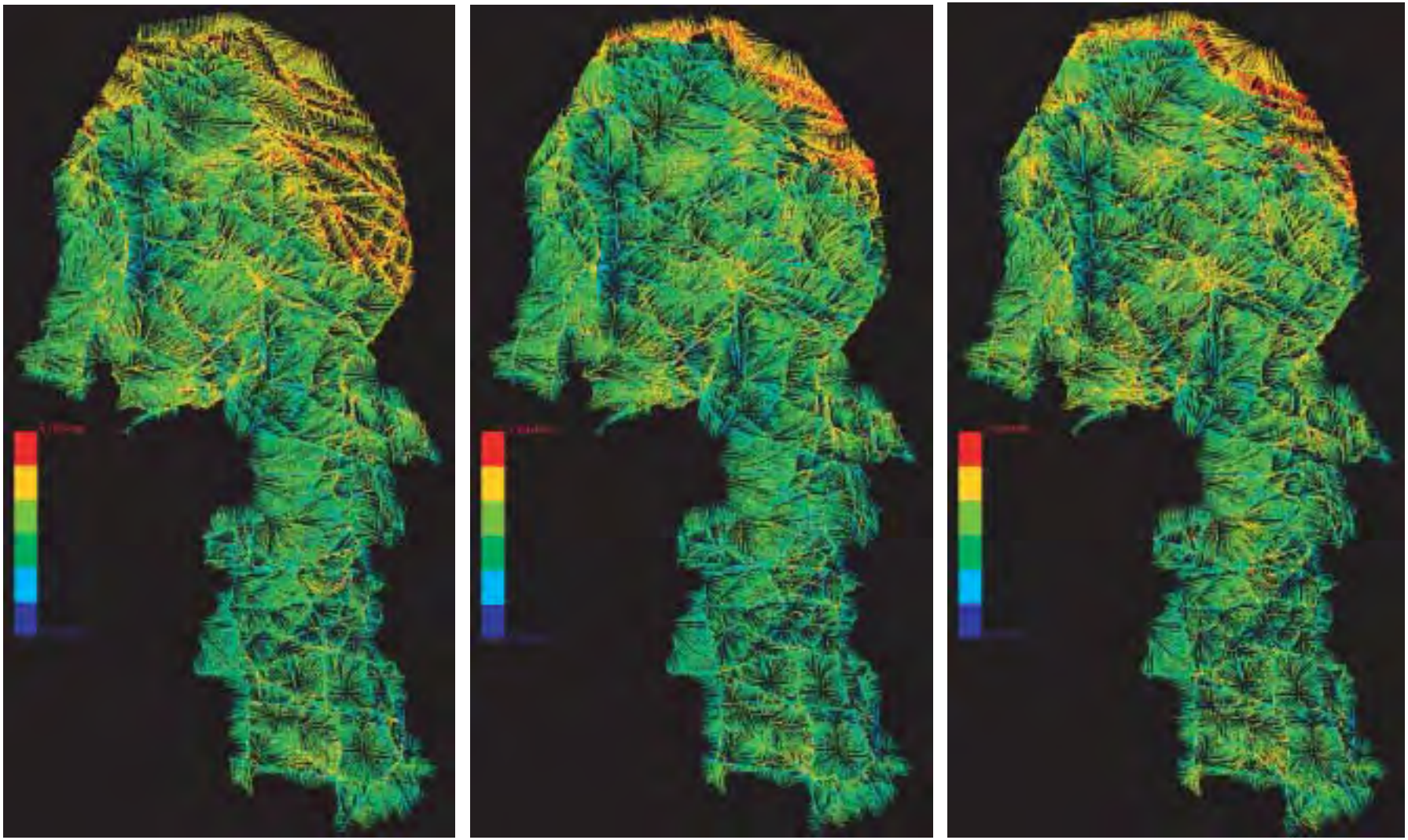

Figure 8-7. *Case 10v1. Plan view of flow-paths released at repository depth (depth=490–540m) in a fixed pressure field at three different times (2000 AD, 5000 AD and 7000 AD respectively). The figure presents one path for each cell of the layer that represents repository depth, which gives 20 794 paths. The paths are coloured according to the logarithm of time. Note that the colour scales are not identical in the different pictures.*

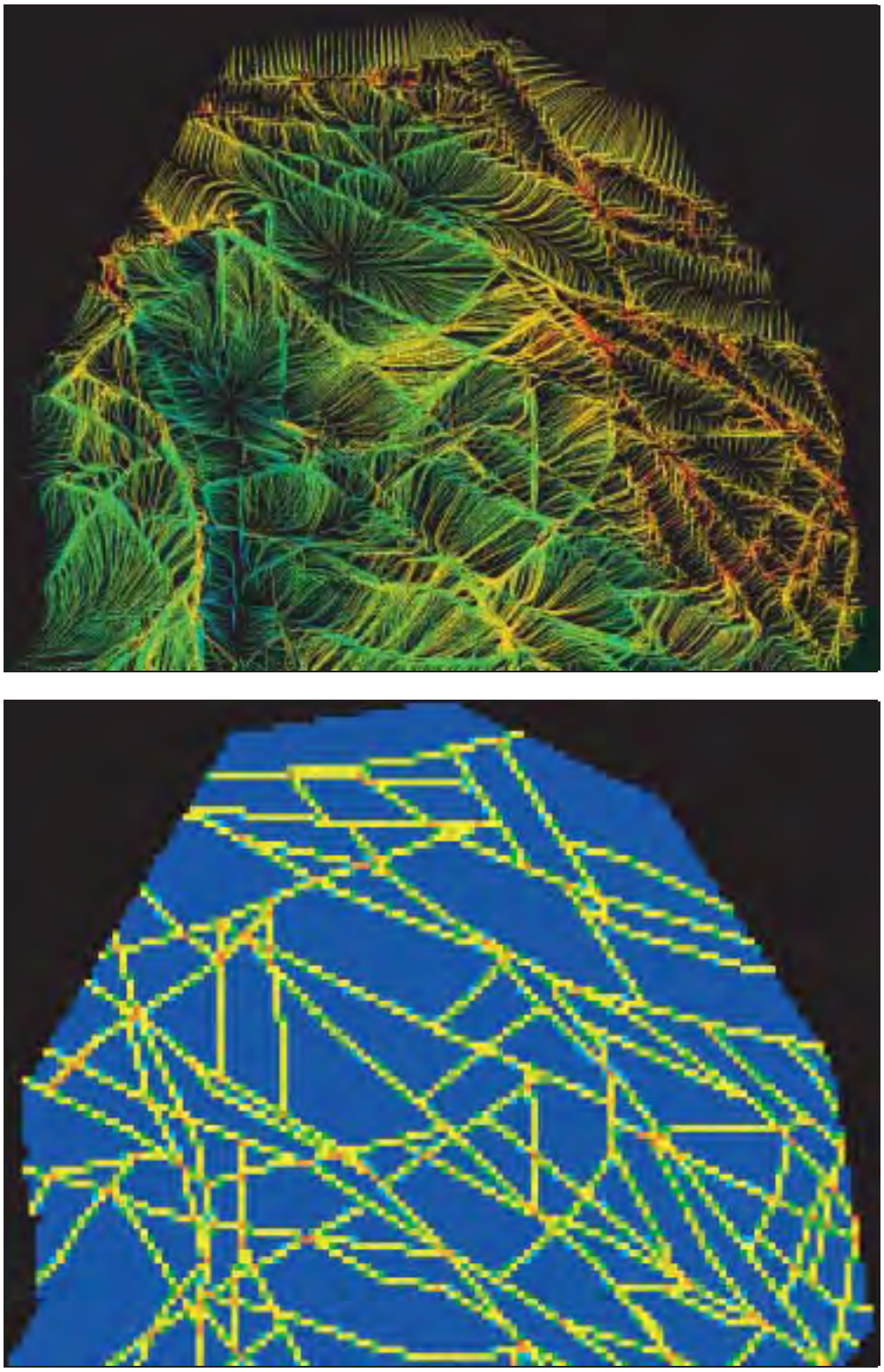

Figure 8-8. *Case 10v1. Top: Close-up view of the northern part of the model showing flow-paths released at repository depth (depth=490–540 m) in a fixed pressure field at time equal to 2000 AD. The paths are coloured according to time. Bottom: Same view as above but showing the effective permeability field for comparison.*

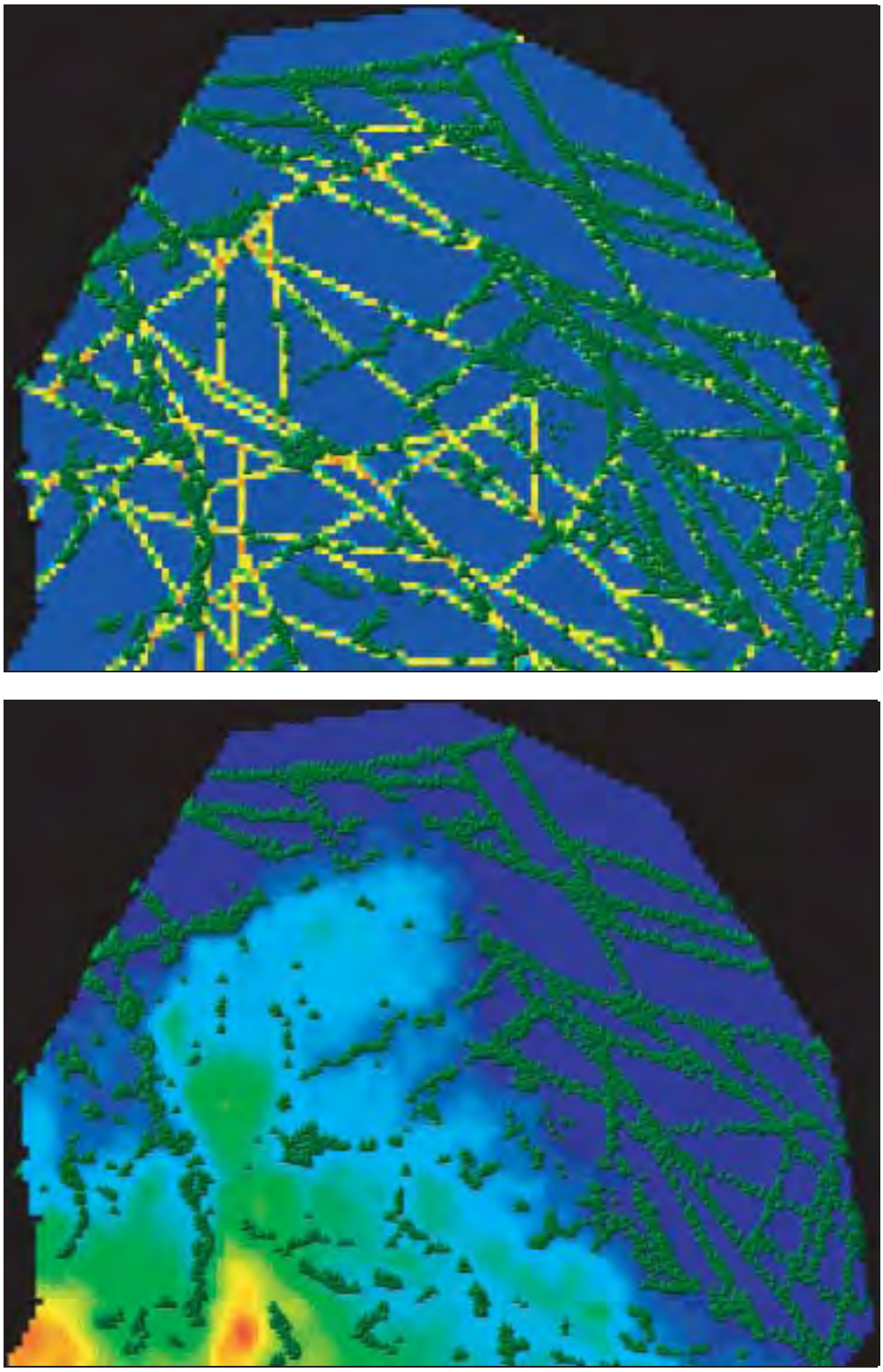

Figure 8-9. *Case 10v1. Top: Close-up view of the northern part of the model showing exit-locations for the flow-paths released at repository depth (depth=490–540 m) in a fixed pressure field at time equal to 2000 AD. The exit-locations are superimposed on a slice z=–50 masl coloured according to permeability. Bottom: Same view as above but with the slice showing the residual pressure at z=–50 masl.*

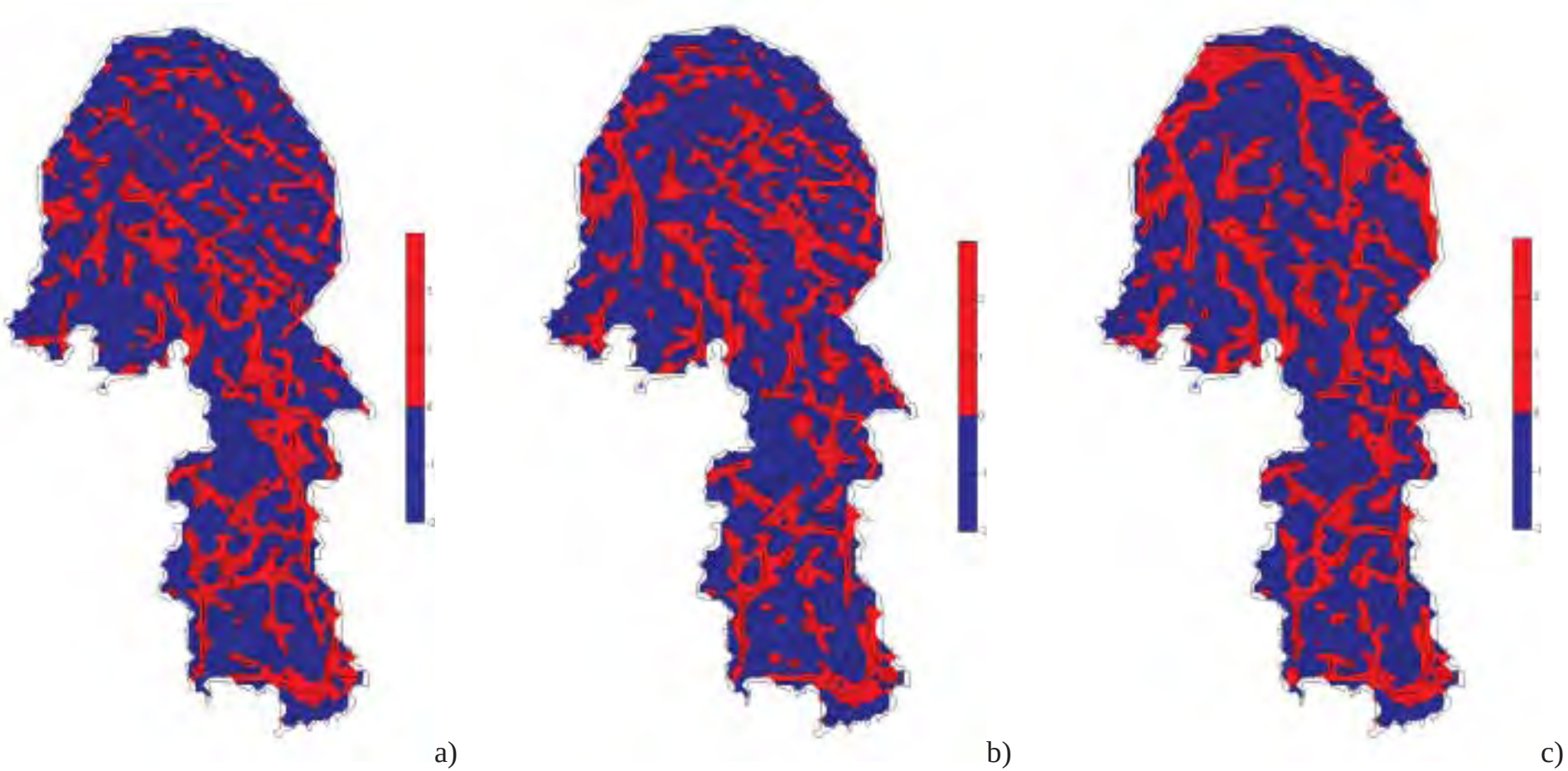

Figure 8-10. *Case 10v1. Groundwater flux at the starting positions for the pathlines for three selected times, a) 0 AD, b) 2000 AD, and c) 5000 AD. Negative values, here marked with blue, indicate that the z-component of the flux is downward.*

8.1.3.5 Results at time equal to 2000 AD

Transient simulations are performed in NAMMU. Within the simulated time period, performance measures are obtained for any time chosen. A statistical analysis was performed for the released flow-path ensemble based on the performance measures: flow path lengths and breakthrough time, considering the flow situation at time equal 2000 AD. A number of 16 913 flow paths were released at repository depth, i.e. at a depth of 490–540 m, the flow paths were released inside the shoreline, i.e. starting positions situated below the Sea were not included. Flow paths that for some reason (e.g. numerical problems in the particle tracking algorithm) were stuck inside the model and did not reach a horizontal plane at –50 masl were also removed from the ensemble results in order not to skew the results. As an additional analysis also particles released outside of the shoreline (below the Sea) were included in the analysis, see Table 8-5. The number of flow paths in the entire ensemble corresponds to the number of elements in each layer of the grid so that one flow path is released from the centre of each element. This means that 20 794 flow paths were released in the second analysis.

In Table 8-4, the percentiles of flow path length for flow paths released from repository depth are presented at a time equal to 2000 AD. The median path length is close to 2000 m. Given that the flow paths are released about 500 m below Sea level, it follows that that the flow paths generally do not reach very far sideways from the starting position. This confirms previous statements that the flow paths are controlled by the local topography. This is a result of the topography, the structural representation and the rather fine grid discretisation. Even the longest flow paths stay within approximately 10 km.

Table 8-4. Case 10v1. Time equal to 2000 AD. Percentiles of flow path lengths, for two different populations of flow paths: (i) 20 794 paths released inside and outside of the 2000 AD shoreline, and (ii) 16913 paths released inside the 2000 AD shoreline. For comparison the results from the corresponding NAMMU freshwater case (FWCv1) are also presented. All paths start at repository depth (490–540 m).

2000 AD		Percentiles of flow path length (m)				
		95th	75th	50th	25th	5th
Case 10v1	20 794 flow paths	10 561	3 981	1 912	1 023	637
	16 913 flow paths	11 402	4 036	1 826	983	620
FWCv1	20 794 flow paths	4 378	2 245	1 188	712	555

Table 8-5. Case 10v1. Time equal to 2000 AD. Percentiles of flow path breakthrough times, for two different populations of flow paths: (i) 20 794 paths released inside and outside of the 2000 AD shoreline, and (ii) 16913 paths released inside the 2000 AD shoreline. For comparison the results from the corresponding NAMMU freshwater case (FWCv1) are also presented. All paths start at repository depth (490–540 m).

2000 AD		Percentiles of breakthrough time (years)				
		95th	75th	50th	25th	5th
Case 10v1	20 794 flow paths	100 046	18 014	3 605	880	137
	16 913 flow paths	39 838	8 557	2 148	666	117
FWCv1	20 794 flow paths	249 345	4 797	1 738	663	117

In order to determine the effects that the presence of saline groundwater has on the groundwater flow, results from the corresponding steady state freshwater variant, FWCv1, is also presented in Table 8-4. The freshwater variant however does not include salt or the shore level displacement. Nevertheless the difference between the variants for the median of the flow path length is only about 60%. Introducing salt in the model gives longer flow paths but the change is not dramatic.

Table 8-5 presents the percentiles of breakthrough time for flow paths released from repository depth at a time equal to 2000 AD. The median breakthrough time is approximately 3600 years for the entire ensemble and 2100 years when the flow paths started underneath the Sea are removed. This difference is expected since the flow paths started underneath the Sea move very slow due to the small hydraulic gradients below the Sea. There are in the population of flow paths also paths that are faster and exit the model in a few hundred years. These flow paths correspond to starting positions located within fracture zones possibly in combination with low elevation areas and therefore more or less go straight up to the top surface. Again, the presence of saline groundwater has an effect on the groundwater flow giving a factor two longer breakthrough times in the saline case compared to the freshwater case.

The excess head was also calculated at two different positions corresponding to the location of SFR (see previous discussions in Sections 7.2.2.2 and 7.2.2.3). The calculated excess head at –60 masl is 0.03 m and 0.04 m at –90 masl. These values are smaller than the measured values, but in line with the results produced by the GEOAN model (see Section 7.2.2.3). It is important to remember the large uncertainties that are associated with the measurements of the excess head. This is also why no further effort was put into the calibration of calculated excess head.

8.1.3.6 Repository positions

By analysing the flow paths, released evenly over the modelling region, repository positions producing the longest flow paths and longest breakthrough times may be indicated. The flow paths were sorted with respect to path lengths and breakthrough times. The starting positions with the 500 longest breakthrough times and 500 longest path lengths were recorded indicating favourable repository locations.

The starting positions with the 500 longest breakthrough times and 500 longest path lengths were recorded. The repository positions that produced the 500 fastest breakthrough times and the 500 shortest path lengths were also recorded. These positions are shown in Figure 8-11 for the entire ensemble of 20 794 flow paths (including flow paths started underneath the sea). Figure 8-13 presents the corresponding selection but with no flow paths started underneath the sea, i.e. 16 913 released flow paths.

As may be seen in Figure 8-11, the longest breakthrough times do not always correlate to longest flow paths. Many of the starting positions resulting in long breakthrough times are located under the Baltic Sea, whereas many of the starting positions with long flow paths are located further inland. However, there seems to be a clear correlation between regions of starting positions with short breakthrough times and short flow paths. The less favourable starting positions seem to be located in regions near and with close contact with areas with low elevation, i.e. potential discharge areas.

Considering Case 10v1 and time equal to 2000 AD, Figure 8-12 gives the 500 starting positions with the longest breakthrough time and the 500 positions with the longest flow path lengths. Figure 8-14 presents the corresponding selection but with no flow paths started underneath the sea, i.e. 16 913 released flow paths.

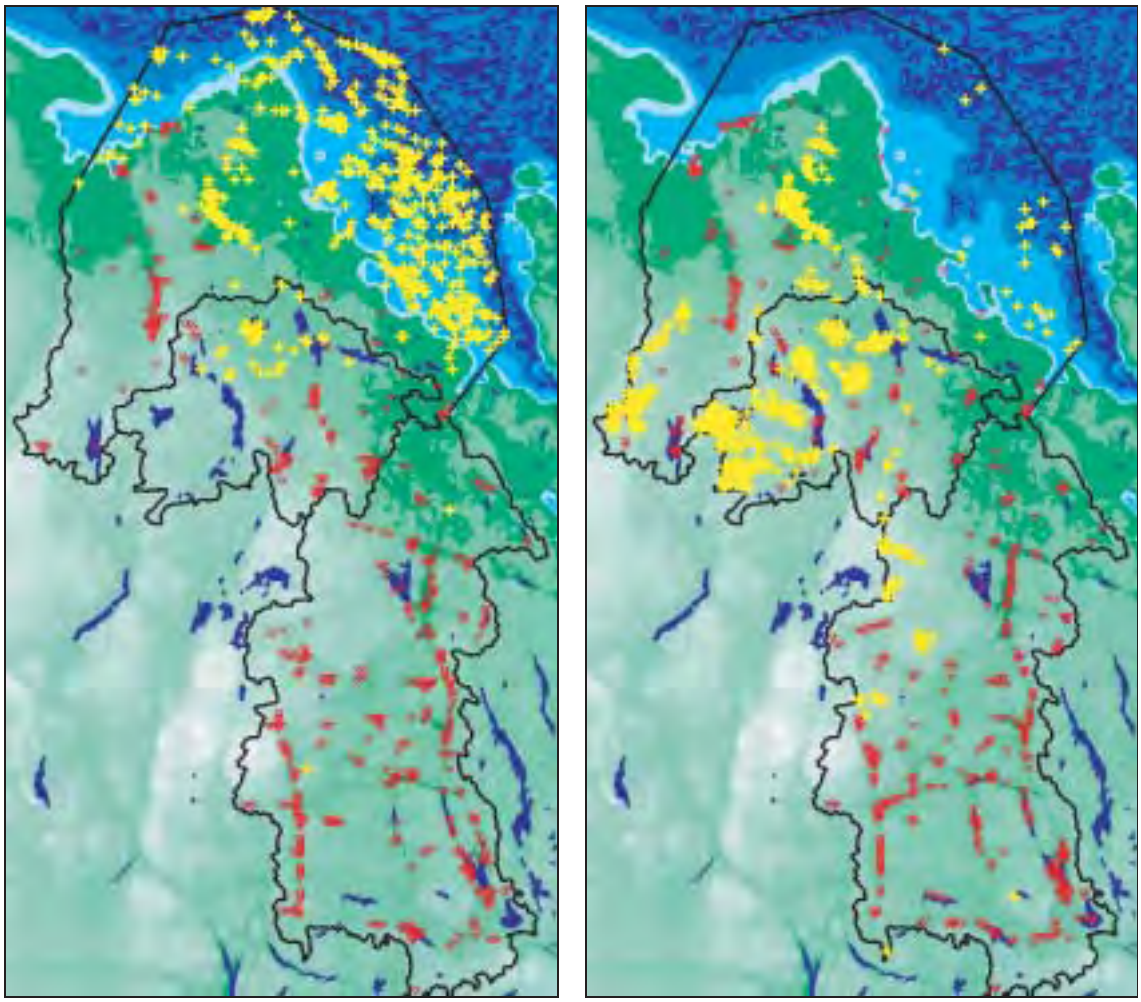

Figure 8-11. *Case 10v1. Time equal to 2000 AD, for the ensemble of exiting flow paths (including flow paths started underneath the sea). To the left: projected starting positions resulting in the 500 shortest breakthrough times marked red dots and the 500 longest breakthrough times marked with yellow symbols (+). To the right: projected starting positions for flow paths with the 500 shortest flow paths (red dots) and the 500 longest flow paths (yellow +).*

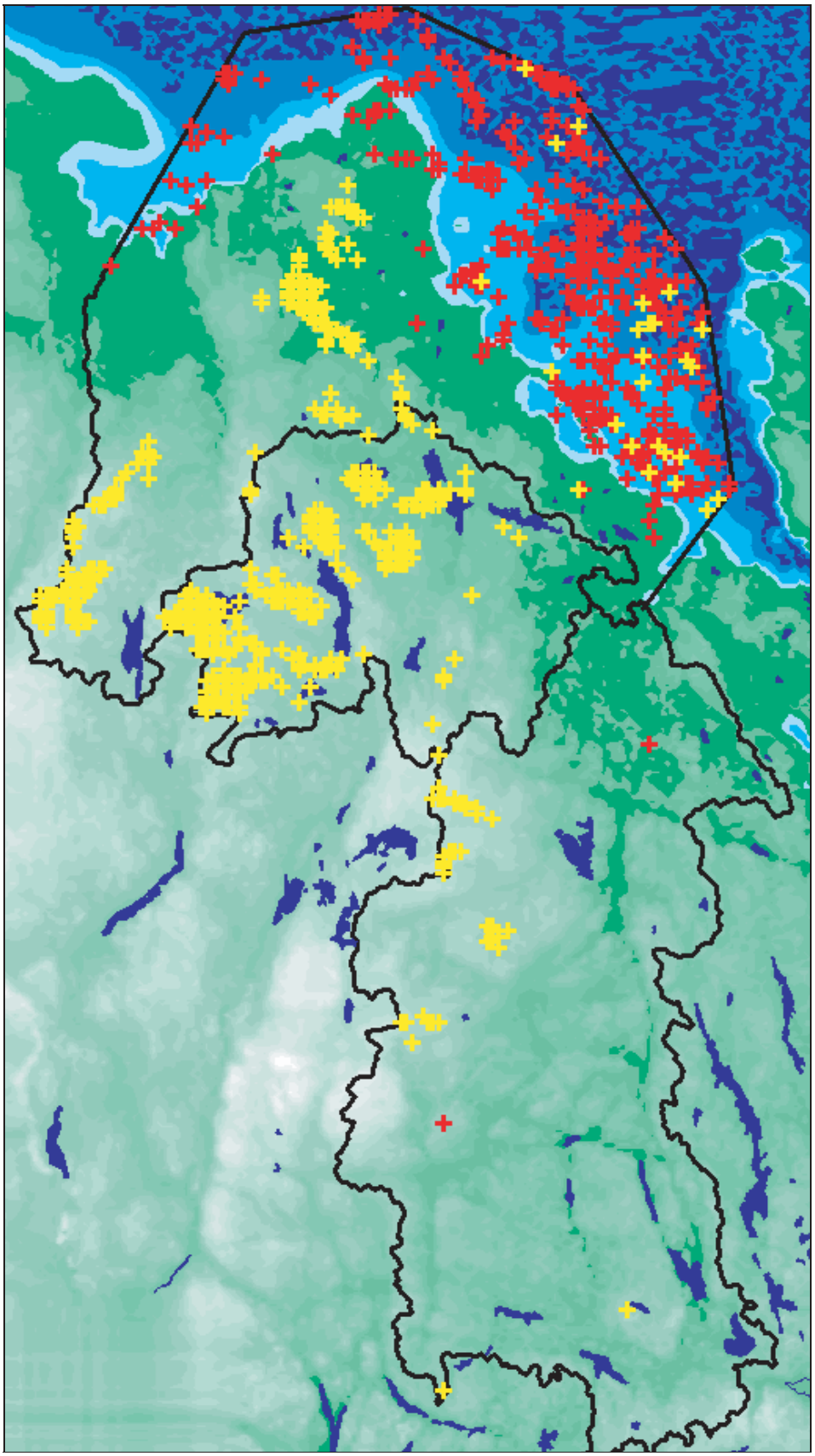

Figure 8-12. *Case 10v1. Time equal to 2000 AD, for the ensemble of exiting flow paths (including flow paths started underneath the sea). The 500 repository positions with the longest flow paths (yellow markers) and the 500 longest breakthrough times (red markers), considering flow paths from repository to the ground surface.*

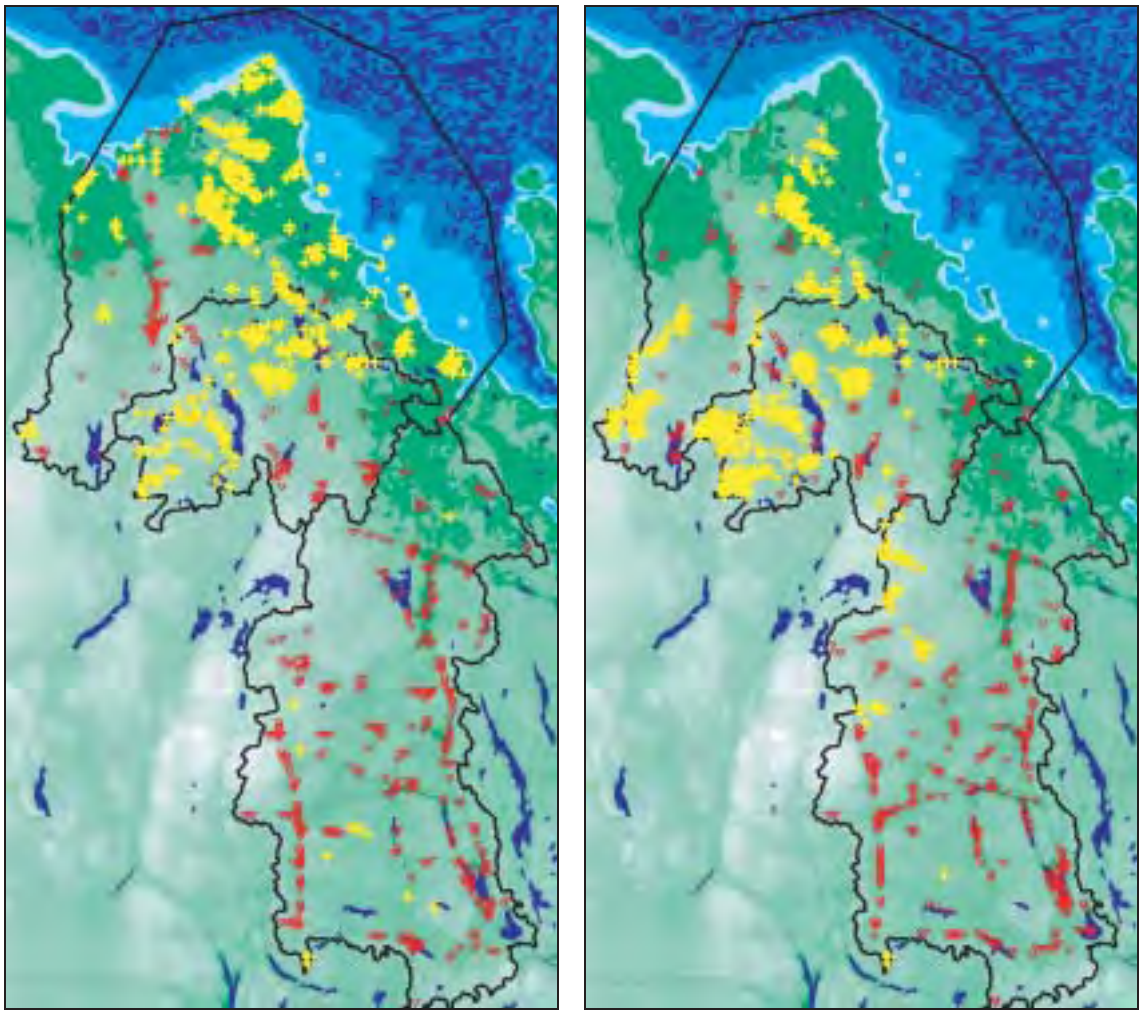

Figure 8-13. *Case 10v1. Time equal to 2000 AD, with no flow paths started underneath the sea. To the left: projected starting positions resulting in the 500 shortest breakthrough times marked red dots and the 500 longest breakthrough times marked with yellow symbols (+). To the right: projected starting positions for flow paths with the 500 shortest flow paths (red dots) and the 500 longest flow paths (yellow +).*

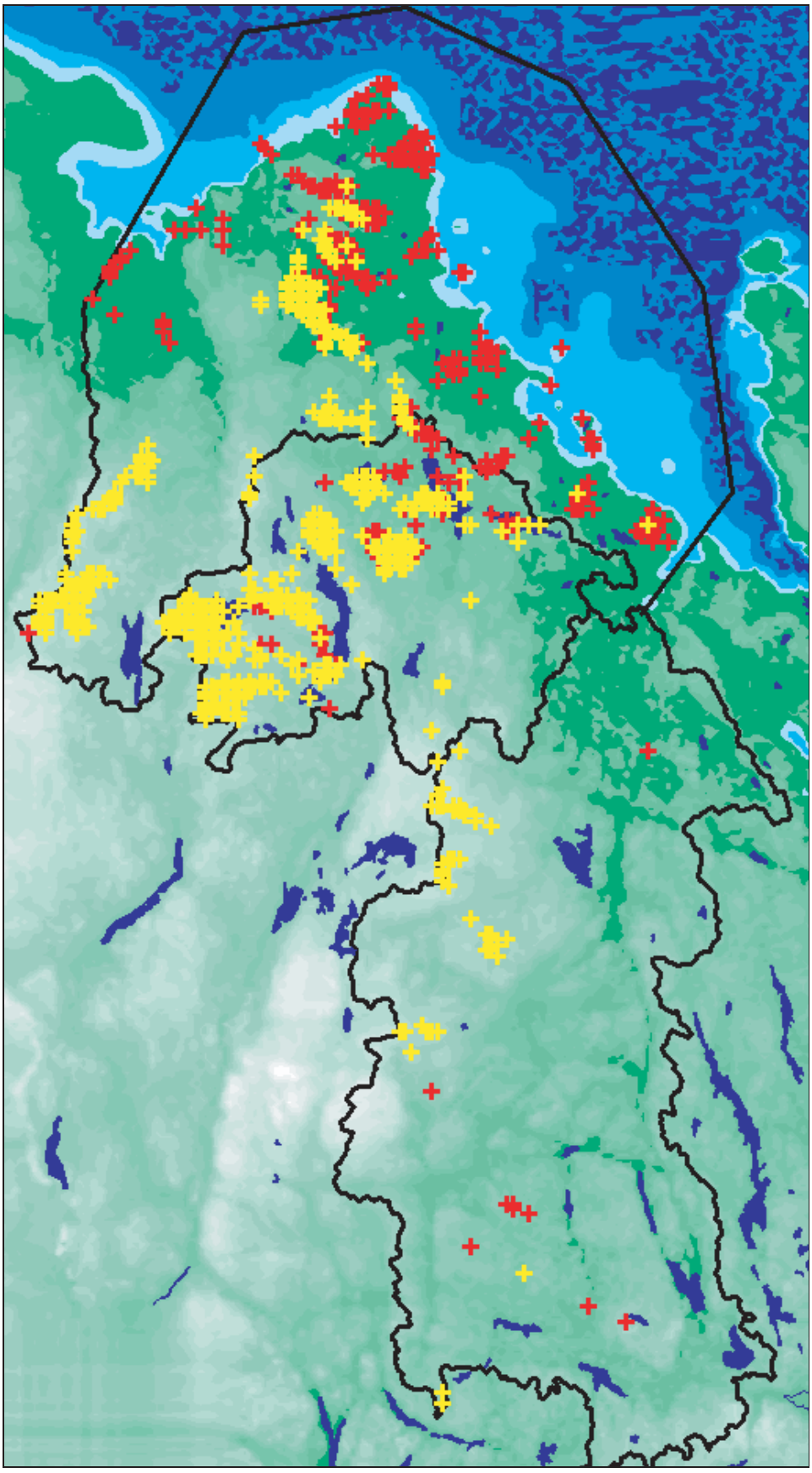

Figure 8-14. *Case 10v1. Time equal to 2000 AD, with no flow paths started underneath the sea. The 500 repository positions with the longest flow paths (yellow markers) and the 500 longest breakthrough times (red markers), considering flow paths from repository to the ground surface.*

8.1.3.7 Results at time equal to 5000 AD and 7000 AD

For times equal to 5000 AD and 7000 AD statistical results are only presented for flow paths corresponding to starting positions inside the present shoreline (hence inside the shoreline of 2000 AD), i.e. a total number of 16 913 flow paths.

In Table 8-6, the percentiles of flow path length for flow paths released from repository depth are presented at times equal to 5000 AD and 7000 AD respectively. The median path lengths are approximately 1500 to 1700 m, which is slightly shorter than for the flow paths released at a time equal 2000 AD. The evolution of the shore level progress and out-flushing of saline water could explain this decrease of length with time. On the other hand the 95th percentile for 5000 AD is somewhat longer compared to 2000 AD. It is important to remember that these statistics are based on a large ensemble of released flow paths and that it would be necessary to study the evolution of specific flow paths in order to give a thorough explanation to the change in statistics. However, in general the lengths of the flow paths still remain rather short.

Table 8-7 presents the percentiles of breakthrough time for flow paths released from repository depth at times equal to 5000 AD and 7000 AD respectively. The median breakthrough times are approximately 1600 to 1800 years. This is about half of the value for 2000 AD.

Table 8-6. Case 10v1. Time equal to 5000 AD and 7000 AD. Percentiles of flow path length, considering starting positions inside the present shoreline. All paths start at repository depth (490–540 m).

Case 10v1	Percentiles of flow path length (m)				
	95th	75th	50th	25th	5th
5000 AD	12 159	3 723	1 661	902	598
7000 AD	10 755	3 415	1 557	863	588

Table 8-7. Case 10v1. Time equal to 5000 AD and 7000 AD. Percentiles of breakthrough time, considering starting positions inside the present shoreline. All paths start at repository depth (490–540 m).

Case 10v1	Percentiles of breakthrough time (years)				
	95th	75th	50th	25th	5th
5000 AD	31 842	5 365	1 772	619	106
7000 AD	25 310	4 623	1 675	603	103

8.1.3.8 Location of repository

Similar to time equal to 2000 AD, repository positions with long and short flow paths may be indicated based on the results of the flow path analysis (paths were released evenly over the modelling region). Again, the starting positions were sorted with respect to flow path lengths and breakthrough times. For the extreme values, projections of the starting positions are shown in Figure 8-15. Note that the topography in this figure is representing present time and that no flow paths are started underneath the sea, i.e. a total of 16 913 released flow paths.

Also for this selected time (5000 AD), as may be seen in Figure 8-15, the longest breakthrough times do not always correlate to longest flow paths. Again, there seems to be a clear correlation between regions of starting positions with short breakthrough times and short flow paths. Compared to 2000 AD, the starting positions with the longest breakthrough times seem to have shifted to the north-east, which may be an effect of the shore level displacement and the resulting change in the flow field.

Considering Case 10v1 and time equal to 5000 AD, Figure 8-16 gives the 500 starting positions with the longest breakthrough times and the longest flow path lengths.

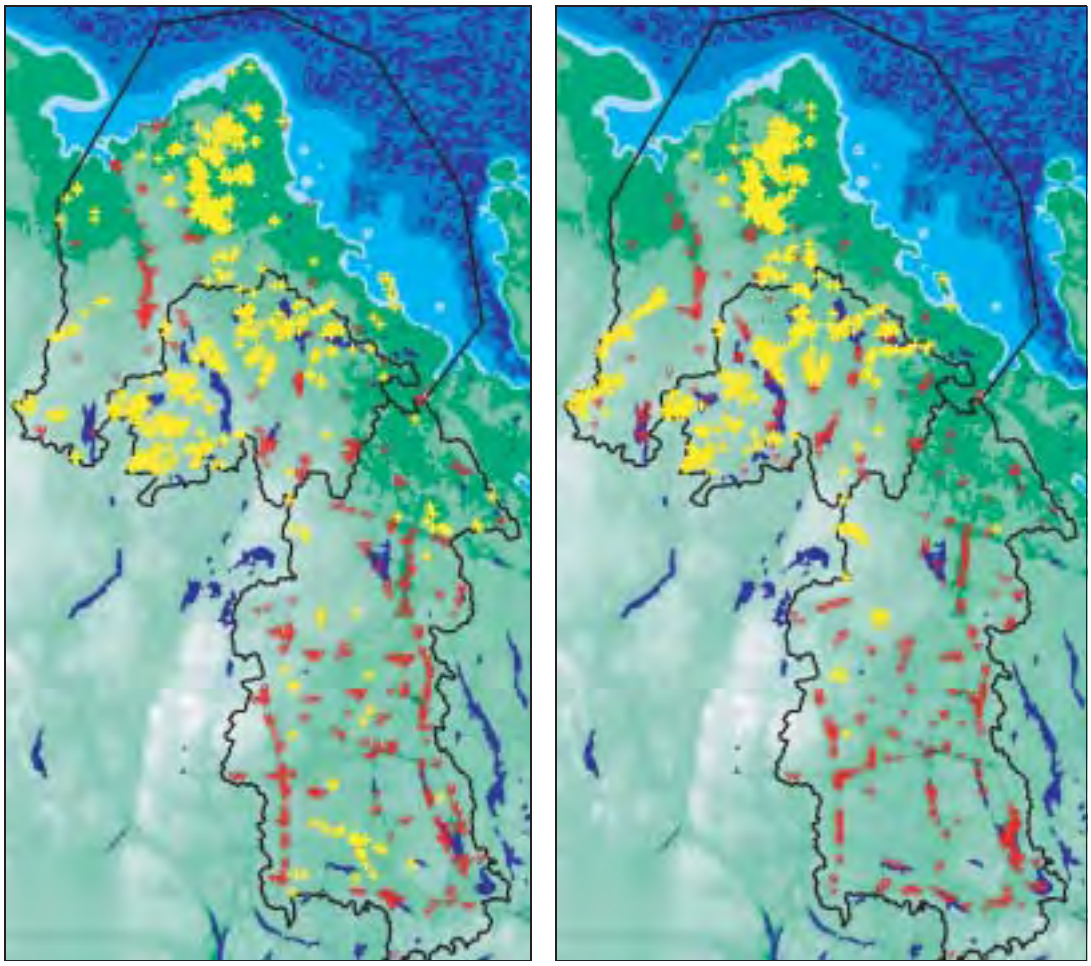

Figure 8-15. *Case 10v1. Time equal to 5000 AD, with no flow paths started underneath the sea. To the left: starting positions resulting in the 500 shortest breakthrough times marked with red dots and the 500 longest breakthrough times marked with yellow symbols (+). To the right: starting positions for flow paths with the 500 shortest flow paths (red dots) and the 500 longest flow paths (yellow +). Note that the topography is representing present time for reference.*

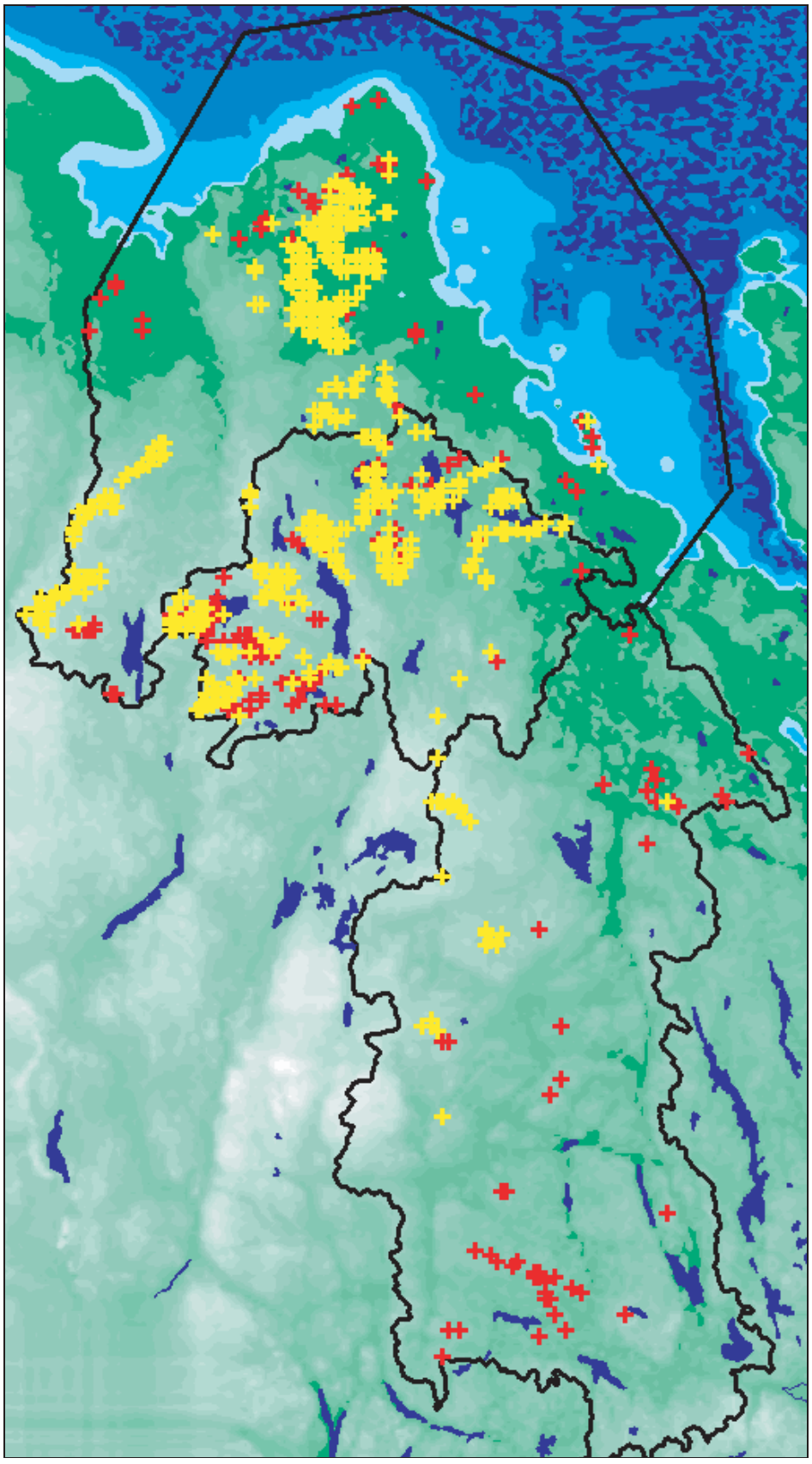

Figure 8-16. *Case 10v1. Time equal to 5000 AD, with no flow paths started underneath the sea. The 500 repository positions with the longest flow paths (yellow markers) and the 500 longest breakthrough times (red markers), considering flow paths from repository to the ground surface. Note that the topography represents the present time for reference.*

8.1.4 Case 10v2. Transient results

8.1.4.1 Evolution of pressure and salt on the top boundary

Since Case 10v2 is a variant of Case 10v1 with the only difference of having a horizontal fracture zone added at –250 masl, the top pressure boundary condition will be the same in both variants. Therefore see Figure 8-2 for the evolution of the residual pressure at the top boundary of the model.

In Figure 8-17, the evolution in time of the salt concentration at the top boundary of the model is shown for Case 10v2. The changes with time are practically the same as for Case 10v1, see Figure 8-3.

Initially much of the model is saline, but as the time increases the salt concentration on the top boundary decreases in the areas where the land rises above the sea. This is an effect of the freshwater infiltrating the system through the exposed surface. The freshwater flushes the salt water from the model out through local discharge areas and the sea. By 2000 AD most of the near-surface groundwater is fresh, saline water will discharges to the surface only at a few large and strong discharge areas.

Compared to Case 10v1, there are some differences indicating that less saline groundwater is discharging through the top surface of the model. This can be seen as brighter spots on the top surface of the later times in Figure 8-3. These brighter spots, indicating the presence of saline groundwater, are not present to the same extent in Figure 8-17. Since the only difference between Case 10v1 and Case 10v2 is the horizontal fracture zone the explanation of course has to be found there. The horizontal fracture zone covers the entire model and therefore connects all the vertical fractures with a highly permeable path. The zone deflects the groundwater flow and enhances the flow in the horizontal direction. The effect is that saline groundwater is flushed out from the near-surface bedrock faster than in Case 10v1. The horizontal zone probably also acts as a shield for the groundwater coming from larger depths in the model and redirects some of the saline groundwater out towards the sea. These effects will be shown and confirmed later on when the flow paths are presented.

8.1.4.2 Salt concentration profile as a function of depth

In Figure 8-18 to Figure 8-20, the salt concentration at different depths in the model is presented for three different times, 2000 AD, 5000 AD and 7000 AD respectively for Case 10v2. The profiles resembles the ones in Case 10v1, see Figure 8-4 to Figure 8-6. For the present day situation (2000 AD) shown in Figure 8-18, the more shallow saline water has already been flushed out and much of the model above 500 masl, apart from some small discharge areas, is filled with freshwater. However, these discharge areas are not as frequently present here as they were in Case 10v1. It is also clear that older Lithorina water is still present at larger depths (–1000 down to –2000 masl) in the model where salt concentrations close to 1 can be found. It can also be seen that the salt water in the fracture zones is flushed out faster than the water in the surrounding bedrock. Figure 8-19 and Figure 8-20 present the same views of the salinity profiles as shown in Figure 8-18 but at later times, 5000 AD and 7000 AD respectively. The continuous flushing of saltwater out of the model is more apparent at larger depths. At 7000 AD the major part of the salt water is present beneath –1000 masl, see Figure 8-20.

The differences compared to Case 10v1 are most obvious above –500 masl where the effect of the horizontal fracture zone can be seen as generally lower salt concentrations. At the bottom of the model the differences are smaller. The effects remain the same as the time increases.

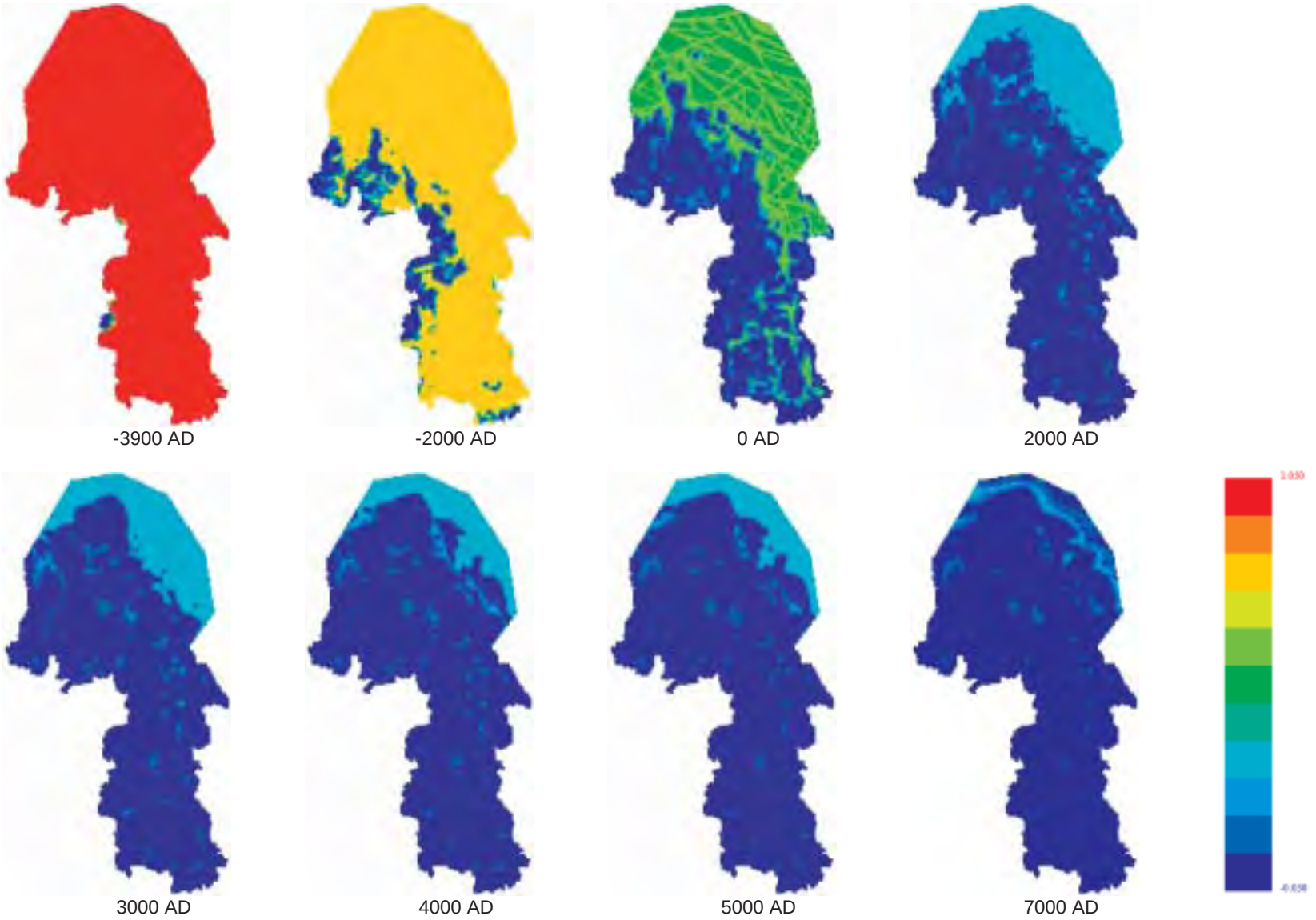

Figure 8-17. *Case 10v2. Evolution in time of the salt concentration at the top boundary of the model. Range in concentration values shown is from 0 (blue) to 1 (red).*

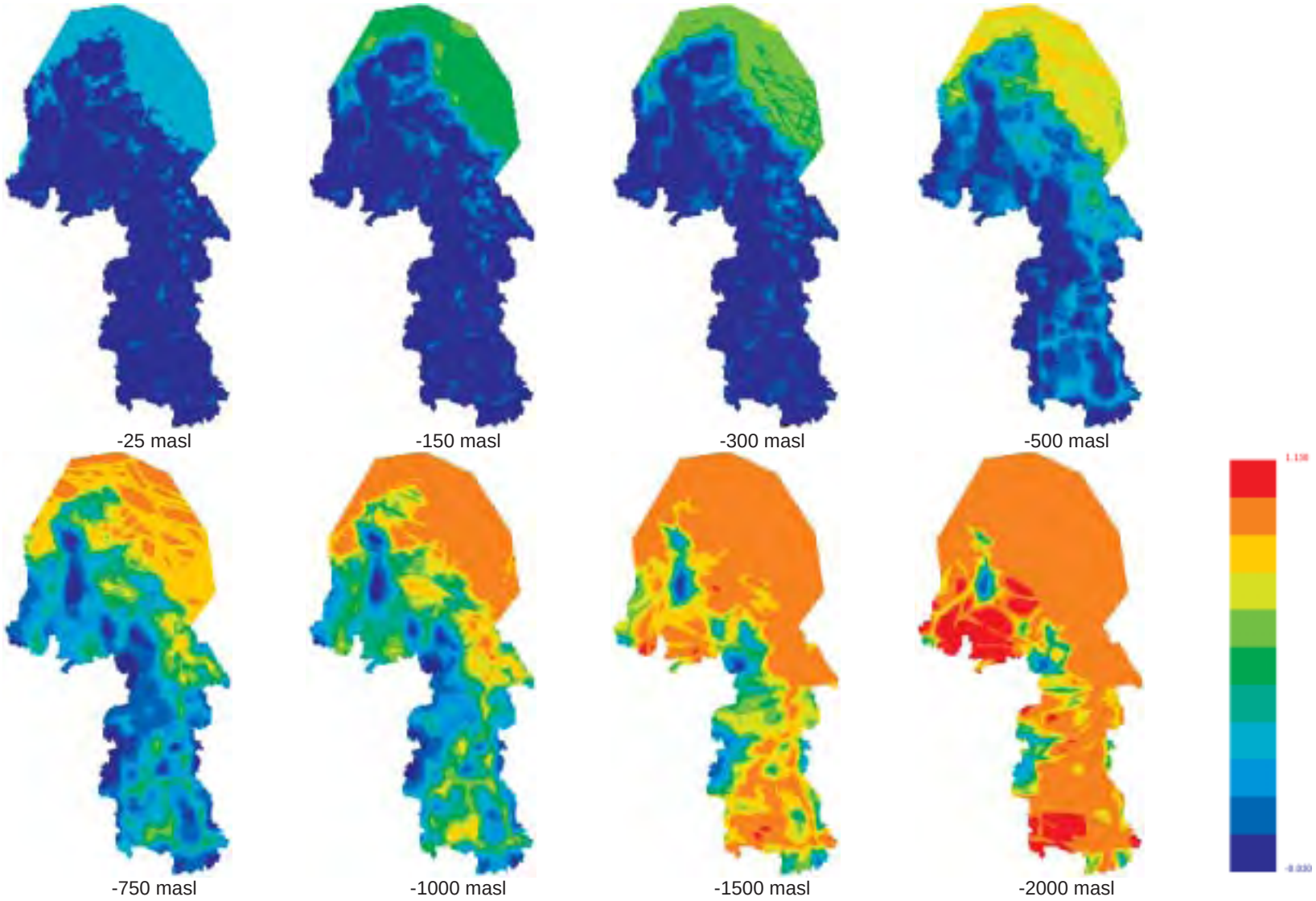

Figure 8-18. *Case 10v2. Time equal to 2000 AD. Salt concentration at different depths in the model. Range in concentration values shown is from 0 (blue) to 1 (red).*

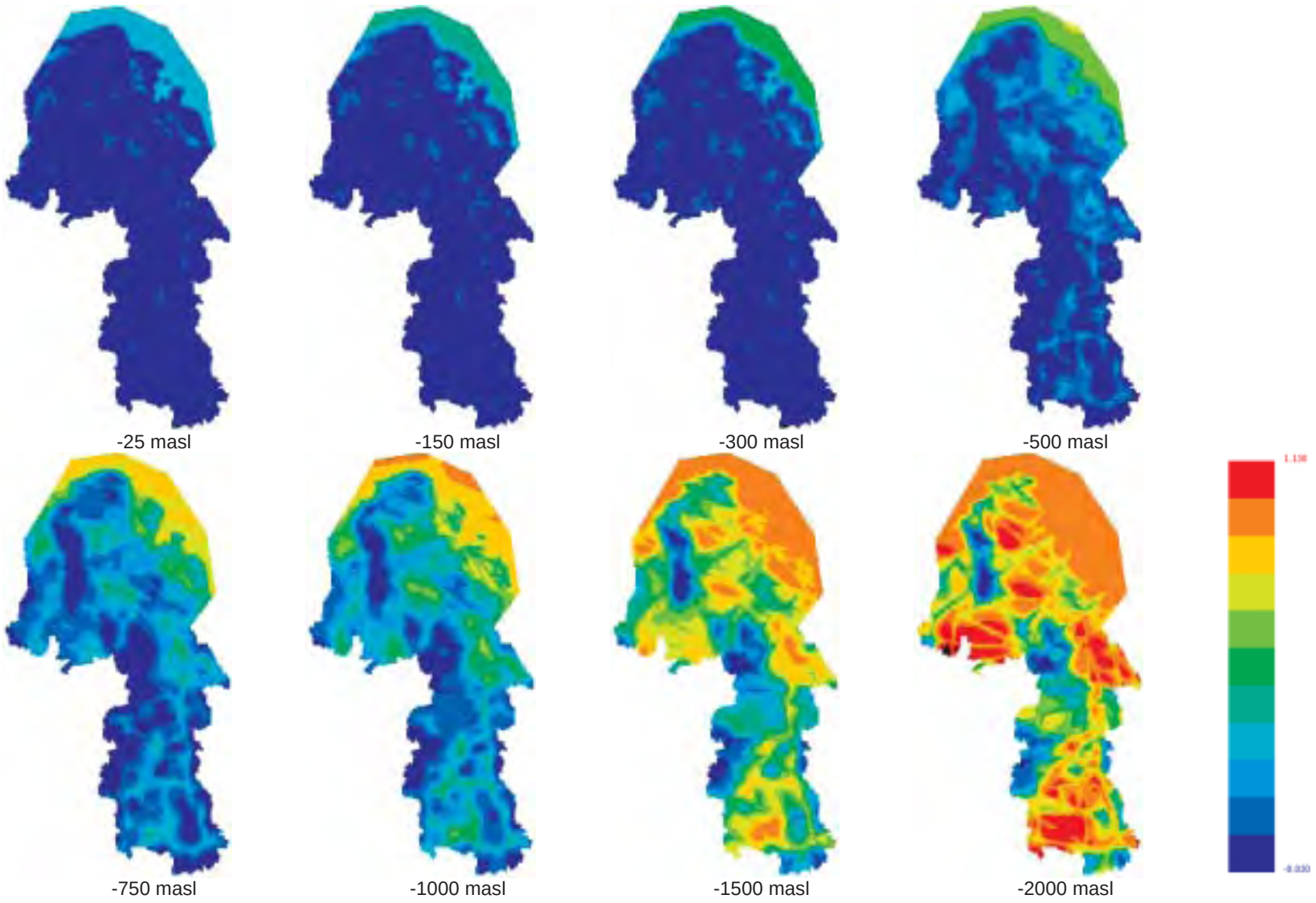

Figure 8-19. *Case 10v2. Time equal to 5000 AD. Salt concentration at different depths in the model. Range in concentration values shown is from 0 (blue) to 1 (red).*

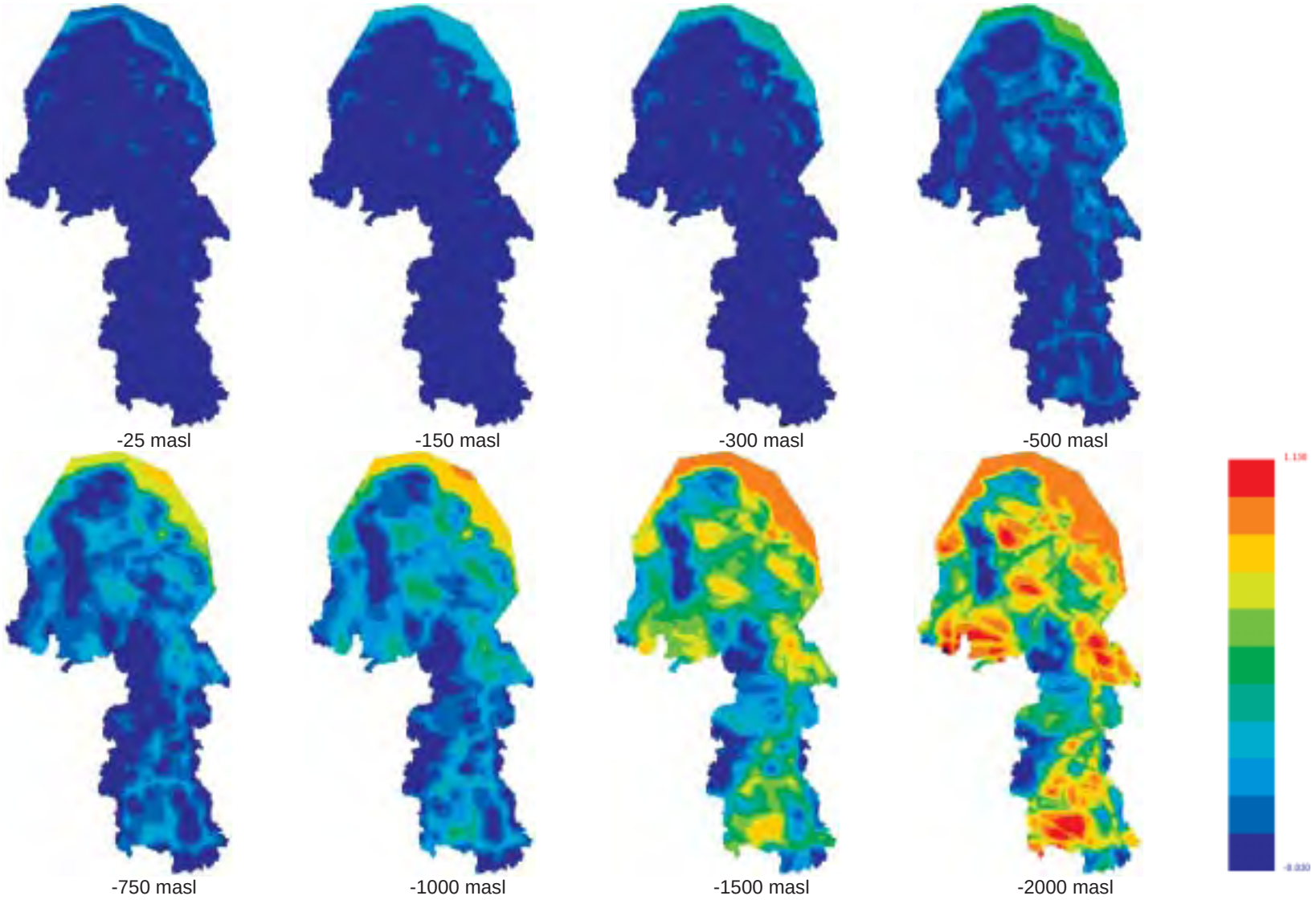

Figure 8-20. *Case 10v2. Time equal to 7000 AD. Salt concentration at different depths in the model. Range in concentration values shown is from 0 (blue) to 1 (red).*

8.1.4.3 Flow paths released at repository depth

The same flow path analysis (paths from repository depth) was performed for Case 10v2 as for Case 10v1. The flow paths were released at different times in fixed pressure fields. Figure 8-21 presents a plan view of flow-paths released at three different times (2000 AD, 5000 AD and 7000 AD respectively). The figure presents one path for each cell of the layer that represents repository depth. The paths are coloured according to the logarithm of time. As stated before, releasing flow paths at different times has little effect on the results. There are only small differences in the patterns comparing the three pictures in Figure 8-21. Even if the colour scales are not identical in the pictures, it is clear that longest breakthrough times are obtained from the flow paths started underneath the sea.

Comparing the flow path patterns with the results from Case 10v1, it is clear that the presence of the horizontal fracture zones has a great effect on the results. Since the fracture is located between the repository depth, from where the flow paths are released, and the top surface, the flow paths have more options to choose easier ways on their way up to the surface. This can be seen from above as an increased horizontal movement, which occurs at the depth of the horizontal fracture zone, i.e. –250 masl. The presence of the vertical fracture zones is still clearly visible in the flow path pattern. As before, the flow paths tend to follow the permeable fracture zones and discharge where there is an appropriate local low point in the topography. The flow paths are somewhat longer in this case compared to Case 10v1. The reason is that the horizontal fracture makes it possible for the flow paths to reach further and discharge in a more favourable area. Still though, the flow paths are generally located to rather local flow cells.

8.1.4.4 Flux direction at repository depth

Also for Case 10v2, groundwater flux at starting positions for pathlines were studied. Case 10v2 is identical to Case 10v1 except the additional horizontal fracture zone. Again, the starting positions are located about 500m below Sea level. In Figure 8-22, the vertical flow directions (up or down) are shown. Here, the flux contours are plotted for three selected times, 0 AD, 2000 AD, and 5000 AD respectively.

Seemingly, there is no dramatic difference in the direction of the flow field, especially for the first two times shown, i.e. times equal to 0 AD and 2000 AD. In the pattern for time equal to 5000 AD some minor differences may be seen, compared to the other patterns shown.

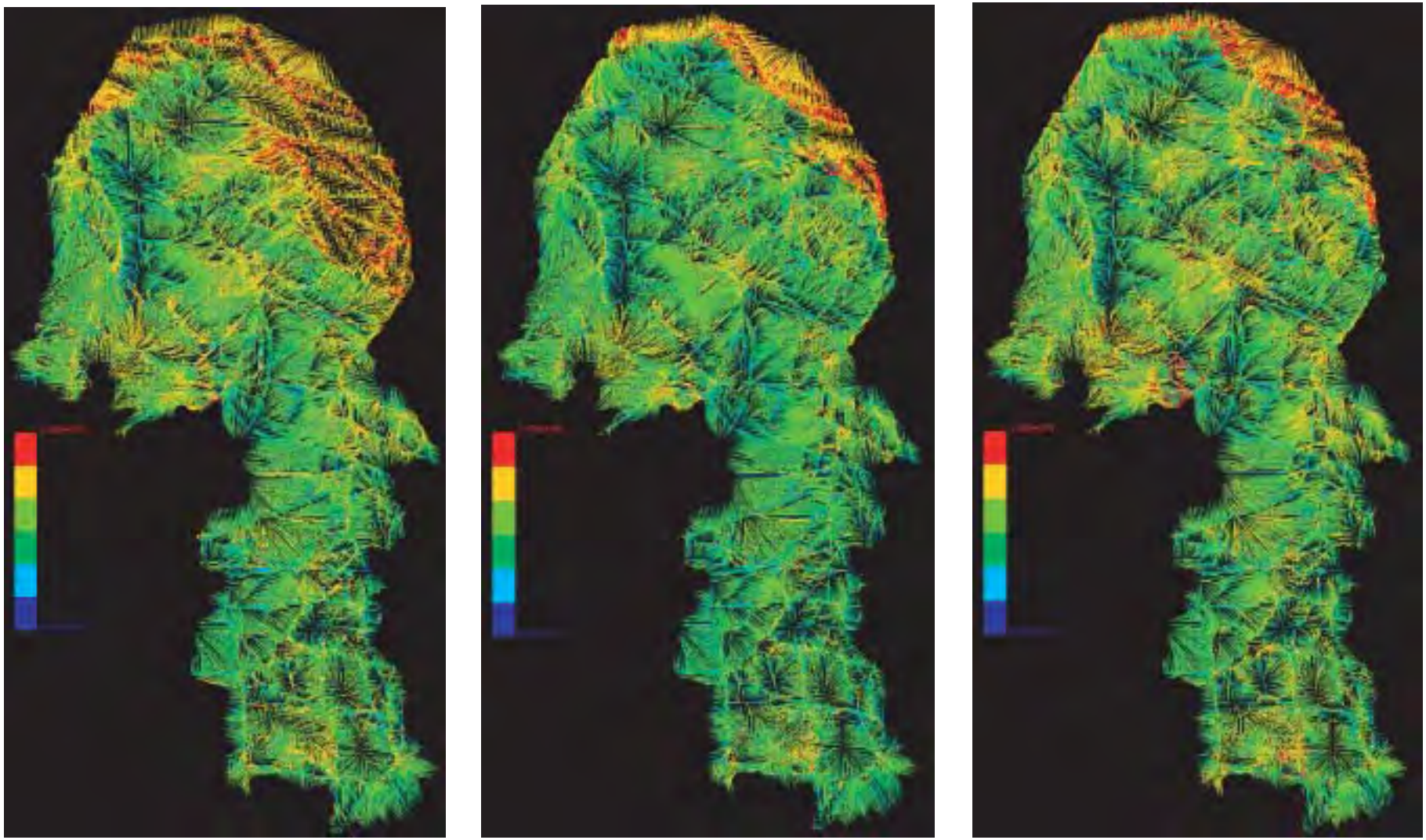

Figure 8-21. *Case 10v2. Plan view of flow-paths released at repository depth (depth=490–540 m) in a fixed pressure field at three different times (2000 AD, 5000 AD and 7000 AD respectively). The figure presents one path for each cell of the layer that represents repository depth, which gives 20 794 paths. The paths are coloured according to the logarithm of time. Note that the colour scales are not identical in the different pictures.*

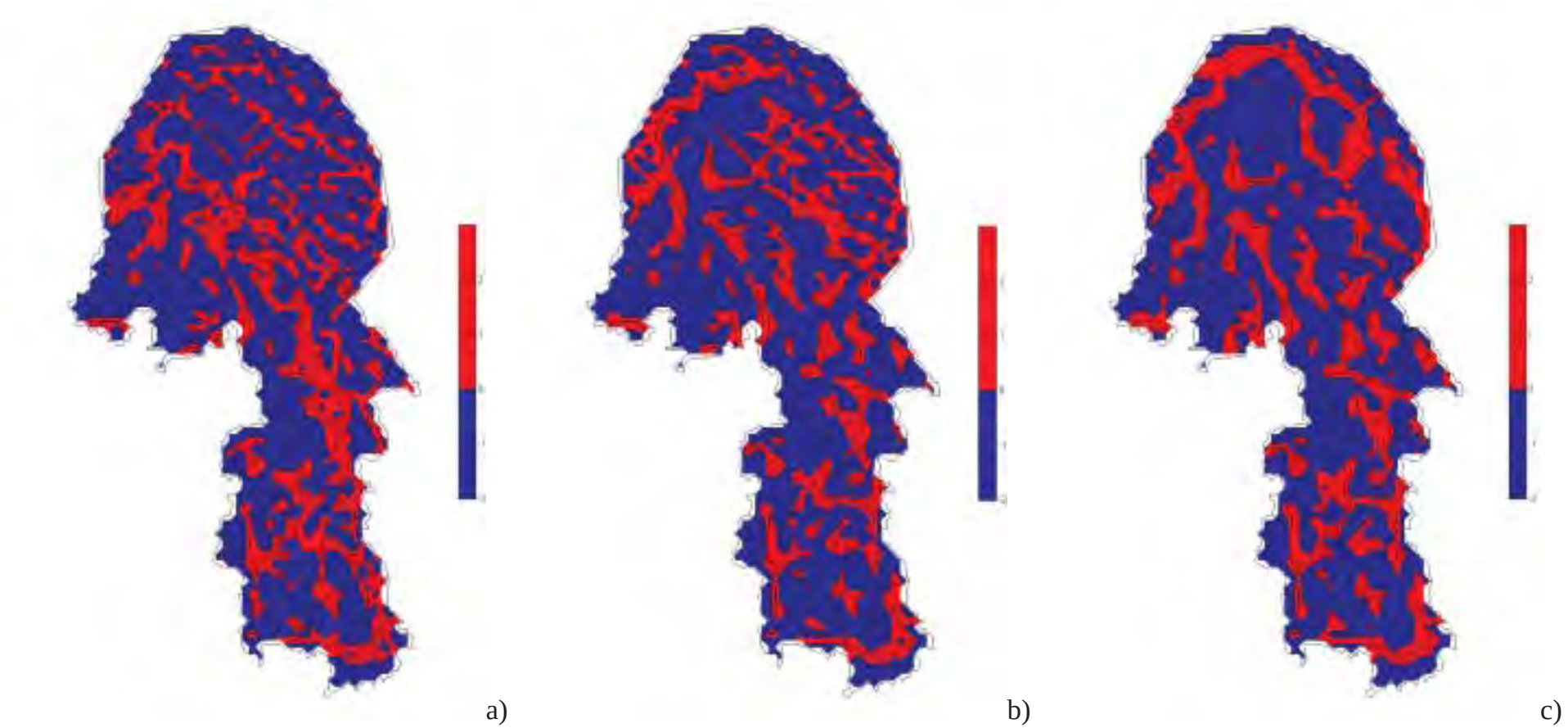

Figure 8-22. *Case 10v2. Groundwater flux at starting positions for pathlines for three selected times, a) 0 AD, b) 2000 AD, and c) 5000 AD. Negative values, here marked with blue, indicate that the z-component of the flux is downward.*

8.1.4.5 Results at time equal to 2000 AD

A statistical analysis was performed for the released flow-path ensemble based on the performance measures: flow path lengths and breakthrough time, considering the flow situation at time equal 2000 AD. A number of 16 913 flow paths were released at repository depth, i.e. 490–540 m below Sea level. These starting positions correspond to locations inside the present shoreline (shoreline of 2000 AD), i.e. starting positions situated below the Sea are removed. Flow paths that for some reason (e.g. numerical problems in the particle tracking algorithm) were stuck inside the model and did not reach a horizontal plane at –50 masl were also removed from the ensemble results in order not to skew the results. As an additional analysis, particles started below the Sea were included in the population, see Table 8-9. The number of flow paths in the entire ensemble corresponds to the number of elements in each layer of the grid so that one flow path is released from the centre of each element. This means that 20 794 flow paths were released in the second analysis. As was also seen in Case 10v1, removing these flow paths has an effect on the breakthrough times where the 95th percentile is very high for the entire ensemble (20 794 flow paths) whereas it is considerably lower for the population of 16 913 flow paths, see Table 8-9. The flow paths started underneath the sea, where the groundwater flow is very small due to the small hydraulic gradients, result in very long breakthrough times. Note that these extremely long breakthrough times do not necessarily correspond to long flow paths.

In Table 8-8, the percentiles of flow path length for flow paths released from repository depth are presented at a time equal to 2000 AD. The median path length is approximately 2600–2700 m. Compared to Case 10v1, this is slightly longer showing that the flow paths tend to follow the horizontal fracture zone and exit a bit further away from the starting positions. The flow paths are 35% longer in Case 10v2 but still the flow paths are located in rather small local groundwater flow cells. Removing the flow paths started underneath the Sea does not have as much effect on the flow path length as it had on the breakthrough times. In order to investigate the effects that the presence of saline groundwater has on the groundwater flow, results from the corresponding steady state freshwater variant, FWCv2, is also presented in Table 8-8. The freshwater variant however does not include salt or the shore level displacement. The difference between the variants for the median of the flow path length is only about 30%. Introducing salt in the model gives slightly longer flow paths but the change is not dramatic.

Table 8-9 presents the percentiles of breakthrough time for flow paths released from repository depth at a time equal to 2000 AD. The median breakthrough time is approximately 5400 years for the entire ensemble and 3800 years when the flow paths started underneath the Sea are removed. (This difference is expected since the flow paths started underneath the Sea move very slow due to the small hydraulic gradient.) The median breakthrough time is almost a factor two longer than for Case 10v1 and the explanation is the same as discussed above. There are some flow paths that are much faster and exit the model in a few hundred years. These flow paths correspond to starting positions located within fracture zones possibly in combination with low elevation areas and therefore flows more or less straight up to the top surface. Again, the presence of saline groundwater has a small effect on the groundwater flow giving less than factor two longer breakthrough times in the saline case compared to the freshwater case.

The excess head was also calculated for Case 10v2 at two different positions corresponding to the location of SFR (see previous discussion). The calculated excess head at –60 masl is 0.03 m and 0.04 m at –90 masl, which is the same as for Case 10v1. These values are lower than the measured values. The presence of a horizontal fracture zone does not seem to have an effect on the calculated excess head. The same discussion regarding the excess head as for Case 10v1 is valid here.

Table 8-8. Case 10v2. Time equal to 2000 AD. Percentiles of flow path length for two different populations of flow paths: (i) 20 794 paths released inside and outside of the 2000 AD shoreline, and (ii) 16913 paths released inside the 2000 AD shoreline. For comparison the results from the corresponding NAMMU freshwater case (FWCv2) are also presented. All paths start at repository depth (490–540 m).

2000 AD		Percentiles of flow path length (m)				
		95th	75th	50th	25th	5th
Case 10v2	20 794 flow paths	12 179	5 000	2 595	1 386	715
	16 913 flow paths	13 002	5 389	2 718	1 471	765
FWCv2	20 794 flow paths	6 347	3 304	1 986	1 204	687

Table 8-9. Case 10v2. Time equal to 2000 AD. Percentiles of flow path breakthrough times for two different populations of flow paths: (i) 20 794 paths released inside and outside of the 2000 AD shoreline, and (ii) 16913 paths released inside the 2000 AD shoreline. For comparison the results from the corresponding NAMMU freshwater case (FWCv2) are also presented. All paths start at repository depth (490–540 m).

2000 AD		Percentiles of breakthrough time (years)				
		95th	75th	50th	25th	5th
Case 10v2	20 794 flow paths	81 433	19 866	5 368	1 353	174
	16 913 flow paths	44 658	13 119	3 799	1 033	145
FWCv2	20 794 flow paths	423 058	9 043	3 088	1 082	155

8.1.4.6 Location of repository

Repository positions with long and short flow paths may be indicated based on the results of the flow path analysis (paths were released evenly over the modelling region). Again, the starting positions were sorted with respect to flow path lengths and breakthrough times. For the extreme values, projections of the starting positions are shown in Figure 8-23. Figure 8-24 presents the corresponding selection but with no flow paths started underneath the sea, i.e. 16 913 released flow paths.

Similar to Case 10v1 and as may be seen in Figure 8-23, the longest breakthrough times do not always correlate to longest flow paths. Many of the starting positions resulting in long breakthrough times are located under the Baltic Sea, whereas many of the starting positions with long flow paths are located further inland. However, there seems to be a correlation between regions of starting positions with short breakthrough times and short flow paths.

For Case 10v2 and time equal to 2000 AD, Figure 8-24 presents the 500 starting positions with the longest breakthrough time and the 500 positions with the longest flow path lengths. Figure 8-26 presents the corresponding selection but with no flow paths started underneath the sea, i.e. 16 913 released flow paths.

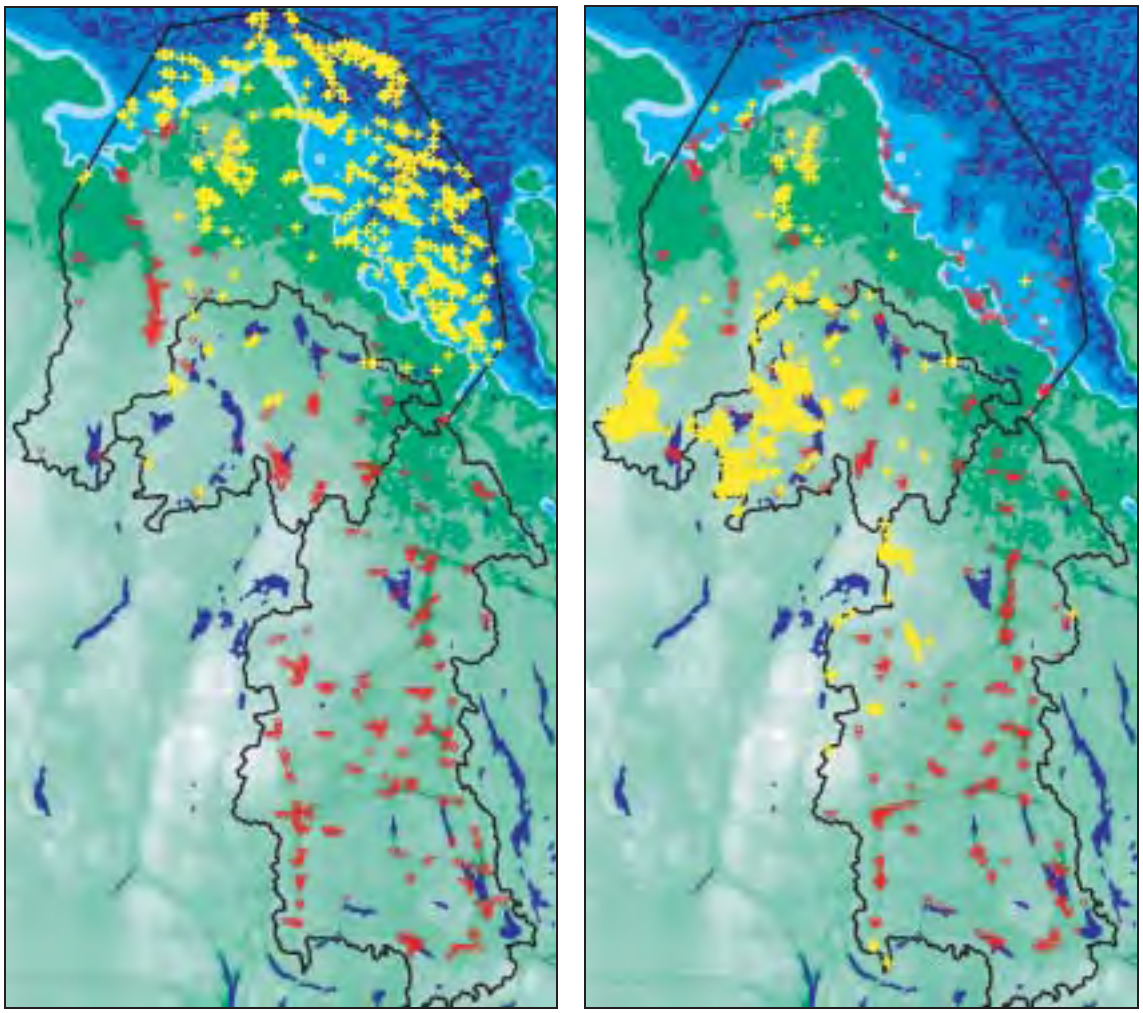

Figure 8-23. *Case 10v2. Time equal to 2000 AD. To the left: projected starting positions resulting in the 500 shortest breakthrough times marked red dots and the 500 longest breakthrough times marked with yellow symbols (+). To the right: projected starting positions for flow paths with the 500 shortest flow paths (red dots) and the 500 longest flow paths (yellow +).*

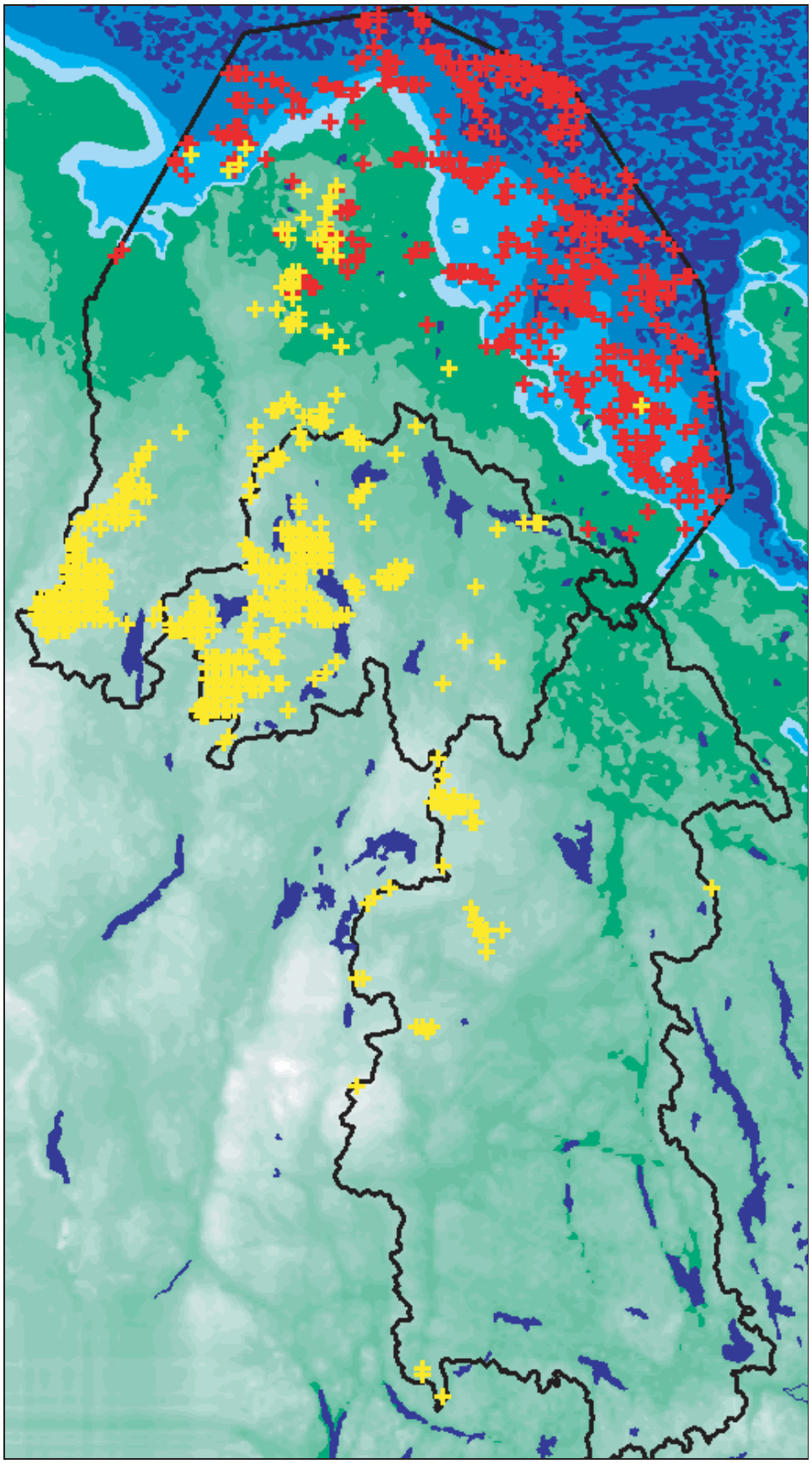

Figure 8-24. *Case 10v2. Time equal to 2000 AD. The 500 repository positions with the longest flow paths (yellow markers) and the 500 longest breakthrough times (red markers), considering flow paths from repository to the ground surface.*

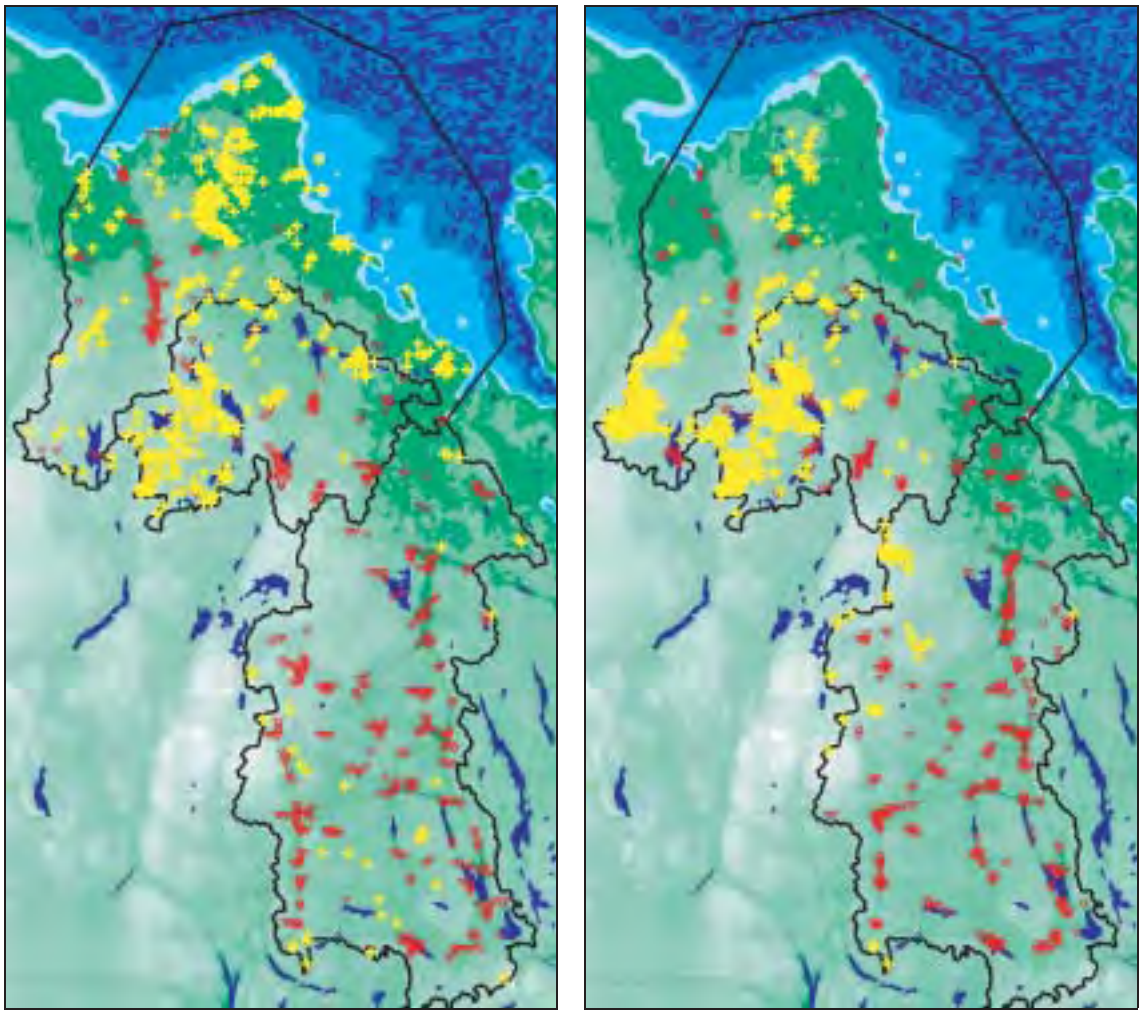

Figure 8-25. *Case 10v2. Time equal to 2000 AD, with no flow paths started underneath the sea. To the left: projected starting positions resulting in the 500 shortest breakthrough times marked red dots and the 500 longest breakthrough times marked with yellow symbols (+). To the right: projected starting positions for flow paths with the 500 shortest flow paths (red dots) and the 500 longest flow paths (yellow +).*

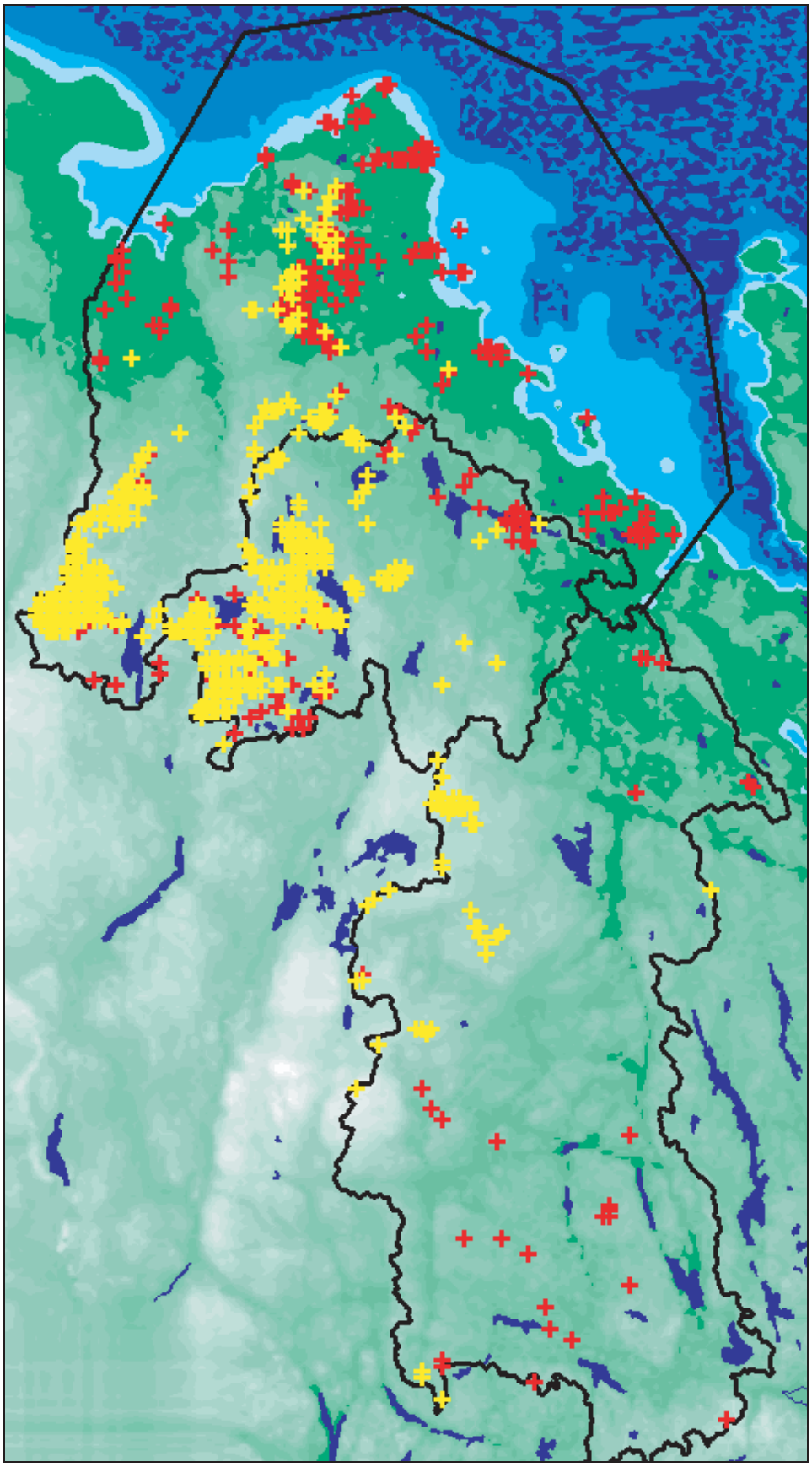

Figure 8-26. *Case 10v2. Time equal to 2000 AD, with no flow paths started underneath the sea. The 500 repository positions with the longest flow paths (yellow markers) and the 500 longest breakthrough times (red markers), considering flow paths from repository to the ground surface*

8.1.4.7 Results at time equal to 5000 AD and 7000 AD

For times equal to 5000 AD and 7000 AD statistical results are only presented for flow paths corresponding to starting positions inside of the present shoreline (the shoreline of 2000 AD), i.e. a total number of 16 913 flow paths.

In Table 8-10, the percentiles of flow path length for flow paths released from repository depth are presented at times equal to 5000 AD and 7000 AD respectively. The median path lengths are approximately 2600 to 2700 m, which is about the same as for 2000 AD. The flow path lengths do not seem to be as sensitive for the selected time as is the case with the breakthrough times when the horizontal fracture zone is present. Again, it is important to remember that these statistics are based on the entire ensemble of released flow paths and that it would be necessary to study the evolution of specific flow paths in order to give more thorough explanations to the change in statistics.

Table 8-11 presents the percentiles of breakthrough time for flow paths released from repository depth at times equal to 5000 AD and 7000 AD respectively. The median breakthrough times are approximately 2800 to 3100 years. This is approximately 20–25% shorter than for 2000 AD.

Table 8-10. Case 10v2. Time equal to 5000 AD and 7000 AD. Percentiles of flow path length, considering starting positions inside the 2000 AD shoreline. All paths start at repository depth (490–540 m).

Case 10v2	Percentiles of flow path length (m)				
	95th	75th	50th	25th	5th
5000 AD	15 531	5 668	2 729	1 468	740
7000 AD	14 710	5 284	2 618	1 410	725

Table 8-11. Case 10v2. Time equal to 5000 AD and 7000 AD. Percentiles of flow path breakthrough times, considering starting positions inside the 2000 AD shoreline. All paths start at repository depth (490–540 m).

Case 10v2	Percentiles of breakthrough time (years)				
	95th	75th	50th	25th	5th
5000 AD	44 198	9 927	3 103	945	130
7000 AD	41 248	8 845	2 839	909	127

8.1.4.8 Location of repository

To characterise different regions of the model, starting positions were sorted with respect to flow path lengths and breakthrough times. The starting positions with the 500 longest breakthrough times and 500 longest flow paths were recorded, also the starting positions resulting in the 500 fastest breakthrough times and the 500 shortest flow paths were recorded. These starting positions are shown in Figure 8-27.

Also for this selected time, as may be seen in Figure 8-27, the longest breakthrough times do not always correlate to longest flow paths. There seems to be some correlation between regions of starting positions with short breakthrough times and short flow paths. The less favourable starting positions seem to be located in regions near and with close contact with discharge areas. Compared to 2000 AD, the starting positions with the longest breakthrough times seem to have shifted to the north-east, which may be an effect of the shore level displacement.

Considering Case 10v2 and time equal to 5000 AD, Figure 8-28 presents the 500 starting positions with the longest breakthrough times and the 500 positions with the longest flow path lengths.

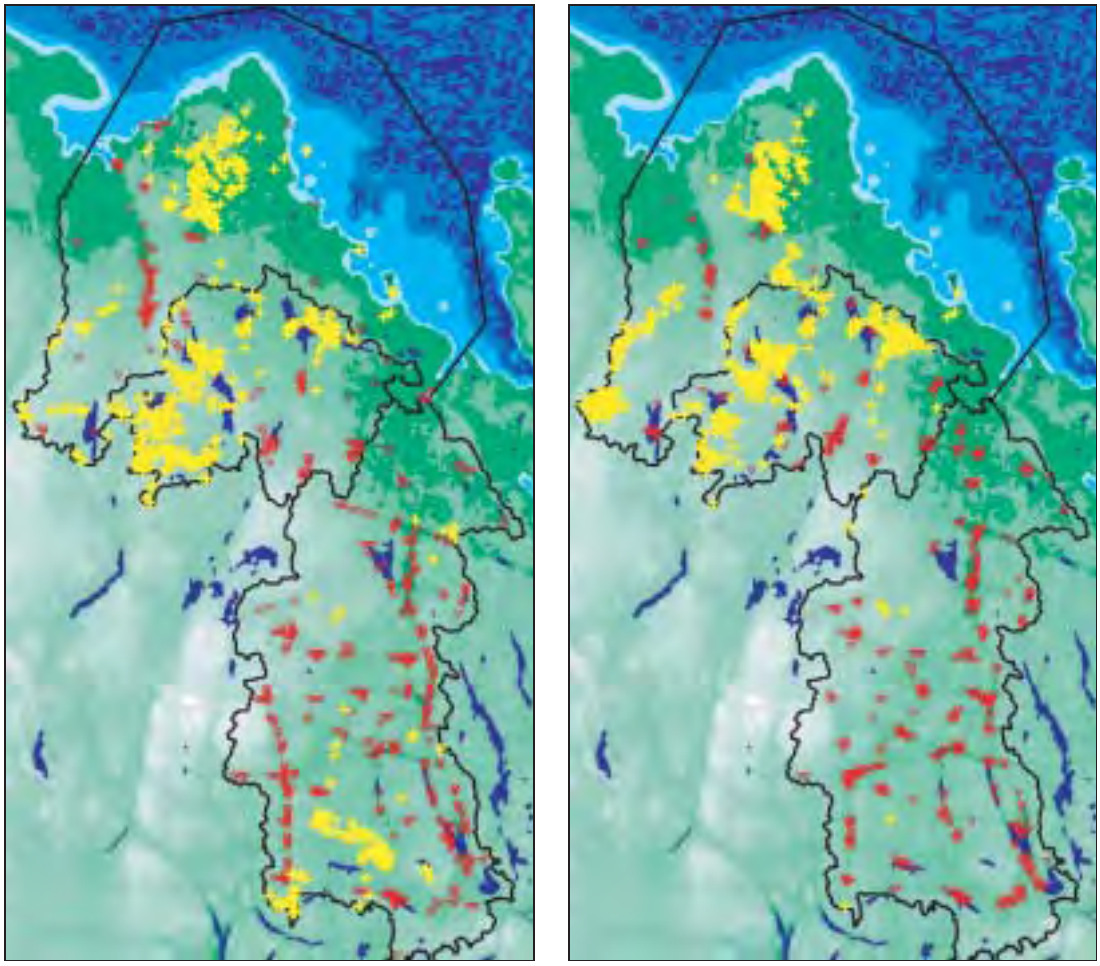

Figure 8-27. *Case 10v2. Time equal to 5000 AD, with no flow paths started underneath the sea. To the left: starting positions resulting in the 500 shortest breakthrough times marked with red dots and the 500 longest breakthrough times marked with yellow symbols (+). To the right: starting positions for flow paths with the 500 shortest flow paths (red dots) and the 500 longest flow paths (yellow +). Note that the topography is representing present time for reference.*

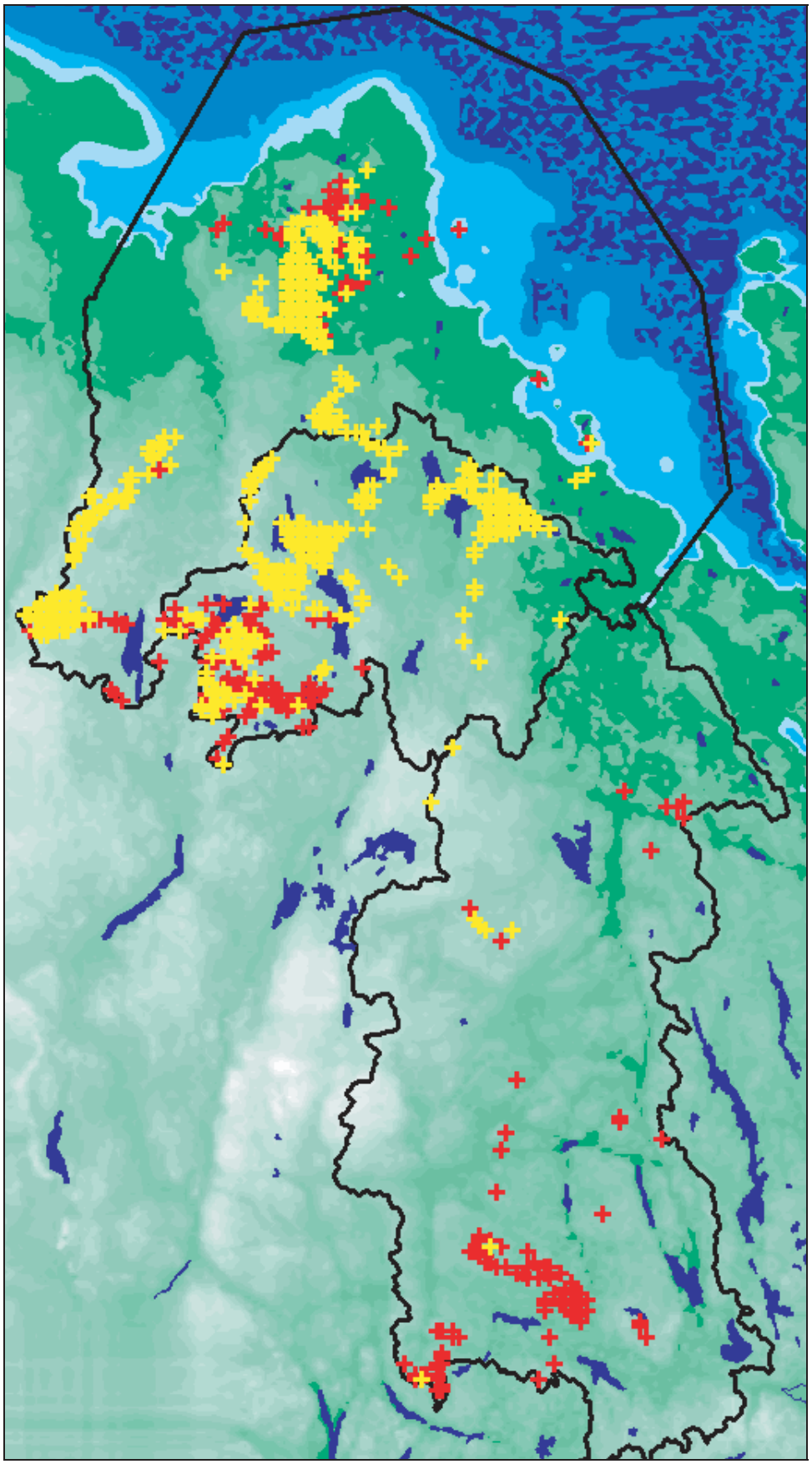

Figure 8-28. *Case 10v2. Time equal to 5000 AD, with no flow paths started underneath the sea.*

The 500 repository positions with the longest flow paths (yellow markers) and the 500 longest breakthrough times (red markers), considering flow paths from repository to the ground surface. Note that the topography is representing present time for reference.

8.1.5 Conclusions Density Dependent Flow

In order to investigate the impact of density dependent flow on the distribution of flow paths from repository depth (a depth of approximately 500 m), a number of transient calculations using NAMMU were performed. An effort has been made to set up the NAMMU model as similar as possible to the GEOAN model used for previously presented fresh water cases.

A time dependent shore-level displacement was included in the simulations. As initial conditions, the models were fully filled with salt water of the highest relative concentration. Due to the shore level displacement and the infiltration of freshwater saline water was transported in the model, and as expected the saline water was eventually flushed out of the model. All fracture zones were modelled as vertical entities. In one variant, a horizontal fracture zone was added. The same rock and fracture zone properties, such as conductivity (NAMMU uses permeability) and porosity, as in the GEOAN model were used. The starting positions for the analysed flow paths were the same in the NAMMU and in the GEOAN models.

Within the simulated time period, performance measures were obtained for several selected times. Results are mainly presented for the simulated times representing 2000 AD (present time), 5000 AD and 7000 AD. A statistical analysis was performed for the released flow-path ensembles based on the performance measures flow path length and breakthrough time. A number of 16 913 flow paths were released at repository depth, i.e. 490–540 m, inside of the 2000 AD shoreline. These starting positions correspond to locations on-shore (inside the shore line).

A median path length close to 2000 m with the 95th percentile at approximately 10 km indicates that the flow paths are located in rather small local groundwater flow cells. This is a result of the local topographic undulation, the structural representation and the rather fine grid discretisation. It should be noted that the long breakthrough times do not necessarily correspond to long flow paths. Not surprisingly, most released flow paths will find a fracture zone at some point during the migration.

The effect that the presence of salt has on the groundwater flow in the model was studied by comparing the results of the density dependent flow model with a fresh-water steady state model. The changes in the performance measures studied (flow path length and breakthrough time) stays within a factor of two when introducing salt in the model. The presence of salt results in longer flow paths and longer breakthrough times. However, the effect is not significant compared to other uncertainties in the model (as e.g. the porosity or the permeability).

Based on the results of the flow path analysis repository positions with the longest flow paths and longest breakthrough times were identified. The starting positions with the 500 longest breakthrough times and 500 longest flow paths were recorded, also the starting positions resulting in the 500 shortest breakthrough times and the 500 shortest flow paths were recorded. Repository positions with long flow paths lengths and long breakthrough times, considering paths from repository to the ground surface, can be found all over the studied domain.

9 Conclusions

The general purpose of this study is to estimate the groundwater flow for a large regional domain by use of groundwater models; and to do that with such a resolution (degree of detail) that important local properties of the flow system studied is represented in the established models. Based on the results of the groundwater modelling, we have compared different theoretical locations of a repository for nuclear waste, considering length and breakthrough time (advective flow) for flow paths from such a repository.

Considering flow path lengths and breakthrough times from a theoretical repository, we have evaluated the following:

- Importance of the local and regional topography.
- Importance of cell size in the numerical model.
- Importance of depth of domain represented in the numerical model.
- Importance of regional fracture zones.
- Importance of local lakes.
- Importance of areas covered by a clay layer.
- Importance of a modified topography.
- Importance of the shore level progress and the transient behaviour of the regional flow.
- Importance of density dependent flow.

Importance of the local and regional topography

The topography of the area studied is not very dramatic; it is a smooth lowering of the elevations of the ground surface, with some local topographic undulation, towards the shoreline (the topography is given in Figure 3-2, page 27). A simplification of the studied system by ignoring, or strongly reducing, the local topographic undulation may not seem like a change that is very important for the groundwater flow – but it is. Without the local topographic undulation the topography will follow the regional topographic gradient and the topography will be like that of an inclined plane (Case 1). And for such a situation the groundwater flow field is primarily controlled by the regional topographic gradient, and with little regard for the complex horizontal shape of the area studied, most flow paths (about 70%) from repository depth will flow towards the shoreline and discharge below the Sea or close to the shoreline. For such a situation, the repository positions with the longest flow paths and breakthrough times are positions as far as possible from the shoreline, because on the average flow paths length (and breakthrough time) increases with distance from the Sea (see Figure 5-3, page 49).

With the inclusion of the local undulation of the topography (Case 2) the groundwater flow situation changes dramatically, the groundwater flow field at repository depth and above it (above a depth of approximately 500 m) will primarily be controlled by the local topographic undulation. Regardless of distance to the Sea, most flow paths will be shorter than 3 km (90% of the paths are shorter than 3 km and 99% of the paths are shorter than 10 km). The flow field is illustrated in Figure 5-6 (page 52), it is demonstrated by the figure that it is the local topographic undulation that controls the flow paths from repository depth.

With inclusion of the local topographic undulation, the repository positions with the longest flow paths are not necessarily far away from the Sea. Repository positions with long flow paths are found at many different positions within the domain studied and at different distances to the Sea (see Figure 5-7, page 54). The positions with long paths are however all located below local topographic heights. Considering breakthrough time, a more complex situation arises. If flow paths are released both inside of the shoreline and outside of the shoreline, the longest breakthrough times will take place for the flow paths released outside of the shoreline (below the sea), because of the small hydraulic gradient below the Sea (see Figure 5-8, page 56). If only release positions inside of the shoreline are considered, repository positions with long breakthrough times are found at many different positions within the domain studied and at different distances to the Sea (Figure 5-9, page 57). Nevertheless, many of the repository positions with long breakthrough times are close to the shoreline or outside of the shoreline, below islands, because of the small hydraulic gradient below the Sea. By comparing the repository positions with the longest paths and the positions with the longest breakthrough times we note that these positions are not the same. Positions below local heights will produce long flow paths, but the gradients could be large at such places, which may produce short break through times. The shoreline will not stay the same in the future. Due to the shore level progress, the Sea will retreat and positions that today are outside of the shoreline or close to the shoreline may in the future be inside of the shoreline; and this will change the flow paths from these repository positions

The analysis of the flow situations with local topographic undulation demonstrates that above the shoreline, the local undulation of the topography creates local flow cells for the groundwater, and these local flow cells will come to dominate the general flow pattern of the groundwater, even below repository depth. It should however be noted that this flow situation (as seen in Figure 5-6, page 52) follows not only from the local undulation of the topography, but also from the size of the permeability of the flow medium and the size of the groundwater recharge. For this flow situation to occur it is necessary that: (i) the permeability (length/time) of the flow medium is small compared to the potential groundwater recharge (length/time), or that (ii) the potential recharge is large compared to the permeability. Considering a fractured crystalline rock mass and the climate of North Europe, both the above discussed conditions are fulfilled: the permeability is small and the potential recharge is large.

Importance of cell size in the numerical model

The smaller the cells of the computational grid, the better the representation of the local topography. It follows that the cell size is important, and that it will influence the lengths of the calculated flow paths. Our modelling demonstrates that the larger the cell size, the longer the flow paths. The largest acceptable cell size depends on the amount of local topographic undulation and the purpose of the study. For the analyses carried out in this study (modelling on a super regional scale), Figure 5-15 (page 64) demonstrates that the horizontal cell size should be smaller than about 700 m. The horizontal cell size used in this study is 330 m.

Importance of depth of domain represented in the numerical model

By using models of different depth, we have demonstrated that it is primarily the flow paths with very large lengths that are influenced by the vertical extension of the model, in general only the longest 10% (see Figure 5-16, page 66).

In addition to the flow pattern induced by the topography, in reality also heavy saline groundwater at great depth and decreasing conductivity with depth may limit the vertical extension of flow paths starting at repository depth. The models of this study do not include decreasing conductivity or heavy saline groundwater at great depth (i.e. the Shield brine). The vertical extension of the applied models should represent the rock mass above the heavy saline groundwater. Based on this study it is not possible to conclude if a model of depth 1100 m is a better representation than a model of depth 2200 m (or even 4000 m). However, the analysed fresh water cases demonstrate that the uncertainty in depth of model will only influence length and breakthrough time for the longest flow paths, but it will not influence the localisation of the repository positions that produce the longest flow paths or the longest breakthrough times, these positions are in general the same regardless of vertical extension of model.

Importance of regional fracture zones

With the addition of vertical fracture zones (Case 3), the flow path lengths from repository depth gets somewhat longer and the breakthrough times get somewhat shorter (compared to situation without zones). Repository positions with large flow path lengths or large breakthrough times can be found at many different places within the domain studied; this conclusion is not changed by the introduction of the fracture zones. A model with fracture zones (Case 3) produces approximately the same repository positions as a model without fracture zones (Case 2), when considering the longest flow paths or the largest breakthrough times. The introduction of the vertical fracture zones will not cause a large change in the overall flow paths distribution (considering paths from repository depth); because fracture zones typically takes place along low lying parts of the topography, i.e. along valleys; and these areas are, with or without the fracture zones, discharge areas for the flow paths from repository depth. With or without fracture zones, the groundwater flows towards the lowest potential.

Keeping the vertical fracture zones in the model and adding a continuous sub-horizontal fracture zone at a depth of 250 m (Case 5), will produce path lengths from repository depth that are longer and breakthrough times that are shorter, compared to situation without the sub-horizontal zone. The model with both vertical zones and a sub-horizontal zone produces approximately the same repository positions as a model without fracture zones (Case 2), when considering the longest flow paths or the longest breakthrough times. The studied large sub-horizontal fracture zone will not separate the groundwater flow system into a lower system with long flow paths (below the sub-horizontal zone), and an upper system with short paths (above the zone).

Importance of local lakes

Considering groundwater flow from repository depth, the analyses of the cases with lakes and without lakes demonstrate that the addition of lakes will in general not cause a large change in magnitude and direction of the groundwater flow. The lakes will not cause a large change in the regional flow pattern because (as for the fracture zones) lakes typically takes place along low lying parts of the topography; and these areas are, with or without the lakes, discharge areas for the flow paths from repository depth. Repository positions with large flow path lengths or large breakthrough time can be found at many different places within the domain studied. This conclusion is not changed by the introduction of the lakes. A model with lakes and fracture zones (Case 4) produce approximately the same repository positions as a model with fracture zones, but without lakes (Case 2), when considering the longest flow paths or the longest breakthrough times.

Importance of areas covered by a clay layer

With the addition of areas covered with clay on the surface of the model (Case 6), path lengths from repository depth get longer and the breakthrough times get longer as well (compared to situation without the clay-areas). The addition of areas covered with clay will influence the regional flow pattern, because in the model the groundwater flow cannot penetrate the clay; but the clay areas are discontinuously distributed over the area studied and therefore (on a regional scale) the influence of the clay areas is limited. Repository positions with large flow path lengths or large breakthrough time can be found at many different places within the domain studied. This conclusion is not changed by the introduction of the clay-areas. The model containing regional fracture zones, lakes and some areas covered by clay (Case 6), produce approximately the same repository positions as a homogeneous model with undulating topography (Case 2), when considering the longest flow paths or the longest breakthrough times (Compare Figure 5-7, page 54 and Figure 5-20, page 76).

In addition we have for this case also used a combined test that selects repository positions with both long path lengths and long breakthrough times. Also for the combined test the conclusion is that repository positions with large flow path lengths and large breakthrough times can be found at many different places within the domain studied. There is no general trend that the positions with both large path lengths and breakthrough times are found as far as possible from the Sea (see Figure 5-22, page 78).

Groundwater flow versus depth

When analysing the regional flow pattern and the spatial distribution of flow paths from repository depth, it is also of interest to study the variation of size of flow with depth. Only a very small part of the potential groundwater recharge will, on the average, infiltrate into the fractured rock and create deep groundwater. For the domain studied, the model calculates the actual groundwater recharge to the rock mass as a part of the solution of the flow field. Considering a model that includes fracture zones, lakes and areas covered with clay (Case 6), and considering an average value of the whole model (including the Sea), the actual groundwater recharge is 1.6 mm/year. In the fractured rock, on the average, the size of the groundwater flow decreases with depth. At great depth, the average specific groundwater flow is only a small fraction of the potential groundwater recharge, and an even smaller fraction of the precipitation. This is demonstrated in Figure 5-23 (page 80) and in and Figure 5-25 (page 82). Considering a model with fracture zones, lakes and areas covered with clay (Case 6), the amount of water that infiltrates into the fractured rock is 0.25% of the precipitation and 0.64% of the potential recharge. The groundwater flow decreases with depth. At a depth of 500 m, the downward component of the groundwater flow is close to 0.3 mm/year, which is: (i) 0.05% of the precipitation, (ii) 0.12% of the potential recharge and (iii) 19% of the groundwater recharge at ground surface. These results were obtained for a model in which the conductivity is constant with depth; a model with decreasing conductivity with depth will produce much smaller groundwater flows at great depth. It should also be noted that at a local point the vertical component of the groundwater flow (and the average actual recharge) might diverge significantly from the average values discussed above. The specific groundwater flow is defined as a flow per unit area; because of the heterogeneous properties of the rock mass (i.e. the highly permeable fracture zones), and the undulating topography, the specific flow will vary in the model; this is illustrated in Figure 5-12 (page 60).

Distribution of discharge areas for groundwater from repository depth

Flow paths from repository depth discharges into different types of environment. Based on the boundary conditions of the model, we have divided discharge areas into three different types: (i) the lakes, (ii) the Sea and (iii) the rest (the rest includes all land above shoreline that is not defined as lakes). The analyses was carried out for Case 6, which is the model with the most realistic properties at ground surface (lakes and clay is included) When considering all flow paths from repository depth, but only release positions inside of the shoreline (no release positions below the Sea), the following result was obtained: 23% of the paths discharged into lakes, 6% of the paths discharged into the Sea and 71% of the paths discharged on land (but not directly into areas defined as lakes). Of the 100 repository positions with the longest path lengths, 35% discharged into lakes and 11% into the Sea. Considering the 100 repository positions with the longest path breakthrough times, 21% discharged into lakes and 36% into the Sea.

Modified topography

The importance of the topography was also demonstrated by a sensitivity analysis of the relationship between the regional and the local topographic gradients (Cases 7 and 8). If the regional gradient is increased, but the local undulation is not changed, the resulting distribution of flow path lengths will converge towards the distribution produced by the model without any local undulation. If both the regional gradient and the local gradients are increased in proportion, the local flow cells will remain in the flow system and continue to dominate the flow system; and if the increases in gradients are within reasonable values, the lengths of the flow paths from repository depth will not change much. For both sensitivity cases, the breakthrough times will decrease, because of the increase in gradients and flow velocities.

Importance of the shore level progress and the transient behaviour of the regional flow

The shore level progress was not included in the previously presented analyses. The shore level progress may however influence the flow situation and consequently the flow paths from repository depth. We have established a model (Case 9) with vertical fracture zones, but without lakes and clay, the model includes the shore level progress and is solved under transient conditions. The produced flow fields are analysed at time equal to 2000 AD and at time equal to 5000 AD.

With the transient solution, the flow paths from repository depth get somewhat shorter, and the breakthrough times get shorter as well (compared to the flow field of a steady state solution). Especially the very long paths and the paths with large breakthrough times will be reduced. Repository positions with large flow path lengths or large breakthrough time can nevertheless be found at many different places within the domain studied, this conclusion is not changed by the introduction of the transient solution. The transient model produce approximately the same repository positions as the other fresh water models with undulating topography and steady state solution, when considering the longest flow paths or the largest breakthrough times.

The transient solution for 2000 AD demonstrates that the repository positions very close to the present shoreline and below islands are not as attractive with the transient solution as with the steady state solution. This is because of the excess head as created by the shore level progress. The excess head will increase the groundwater velocities below the Sea and therefore make the breakthrough times shorter for these positions in the transient solution,

compared to the very long times found in the steady state solution. It should however be noted that the model is set up in a way that it reproduces values of the excess head, as measured and interpreted at SFR (see Section 7.2.2), these measured values of the excess head are however very uncertain.

We have for this case also used a combined test that selects the repository positions with regard to both the longest path lengths and longest path breakthrough times. Also for the combined test the conclusion is that repository positions with large flow path lengths and large breakthrough time can be found at many different places within the domain studied. There is no general trend that the positions with long paths and long breakthrough times are found as far as possible from the Sea. Figure 5-9 (page 57) presents the results of the combined test regarding a steady state solution (Case 6); and Figure 7-8 (page 100) presents the results of the combined test regarding a transient solution at 2000 AD (Case 9). By comparing these two figures we note that the reduction of breakthrough times for repository positions close to the shoreline that comes with the shore level progress (and transient solution), will not have a large influence on the repository positions selected by the combined test. This is because repository positions close to the shoreline will not be selected by the combined test, not for the steady state solution and not fore the transient solution, as the lengths of the flow paths from these positions are not long enough.

Flow paths released at 2000 AD have little relevance to an actual repository, since there will be practically no release to the geosphere the first thousands of years after the closure of the repository. In order to get more useful results we have also analysed a flow situation representing 5000 AD (i.e. 3000 years into the future). Only repository positions inside of the present shoreline (the shoreline of 2000 AD) were included in the flow path analysis. Repository positions with large flow path lengths or large breakthrough time can be found at many different places within the domain studied, this conclusion is the same as for the previous cases studied, and not changed by the transient flow field of 5000 AD. The transient flow field of 5000 AD produce approximately the same repository positions as the other models with undulating topography, when considering the longest flow paths or the largest breakthrough times. There are also new and interesting results produced by the flow field of 5000 AD, a few repository positions close to the 2000 AD shoreline have been selected by the combined test, these are repository positions selected by the combined test when considering the flow field of 5000 AD. These positions were not selected at time equal to 2000 AD. When comparing Figure 7-8 (page 100) representing 2000 AD and Figure 7-9 (page 103) representing 5000 AD, we note three new repository positions close to the 2000 AD shoreline; two positions are located only a few kilometres from the SFR-repository. These repository positions did not qualify at time equal 2000 AD, because of the very close vicinity of the shoreline at 2000 AD and the short flow paths that follows from that situation; but at time equal to 5000 AD, the shoreline is at some distance and these positions are among the positions that have the longest paths and the longest breakthrough times, considering the whole domain studied. Hence, repository positions close to the present shoreline, which for the present situation may not produce the longest flow path lengths and longest breakthrough times, may in the future be among the repository positions that produce the longest paths and longest breakthrough times; this is due to the changed flow field that will be created by the retreat of the shoreline.

Importance of density dependent flow

The groundwater at the domain studied is of different origin, and at repository depth it is not unlikely that the groundwater is saline, the salinity may be close to that of the present Baltic Sea, but higher and lower levels of salinity may also be found. Different levels of salinity correspond to different values of density. Density dependent flow was however

not included in the previously presented analyses. To be able to evaluate the importance of density dependent flow we have included a model (Case 10) with vertical fracture zones, but without lakes and clay, the model includes the shore level progress and density dependent flow, and is solved under transient conditions.

The studied model (Case 10) is a transient and density dependent model, simulated by use of the NAMMU finite element code. The results of the density dependent model demonstrate a general groundwater flow pattern that is not very different to that of the previously presented transient fresh water model (Case 9). However, the flow paths from repository depth are longer and breakthrough times are also longer in the density dependent model. The differences between the freshwater models and the density dependent model are probably an effect of both the density dependent flow and the different mathematical approaches of the applied codes (see Section 5.5, page 60). The differences are however not very large.

Comparing the density dependent model (NAMMU Case 10) with the corresponding freshwater model (GEOAN Case 9), the lengths of the flow paths from repository depth are for the 50^{th} percentile 1.8 times larger in the density dependent model (Case 10) than in the freshwater model (Case 9); and when considering the breakthrough times for flow paths from repository depth, the 50^{th} percentile three times larger in the density dependent model. The effect that the presence of saline water and density dependent flow has on the groundwater flow in the model was also studied by comparing the results of the density dependent flow model with the same model simulating a freshwater steady state situation (both were NAMMU models). The changes in the performance measures studied (flow path length and breakthrough time) stays within a factor of two when introducing saline water, density dependent flow and a transient solution.

These results demonstrate that the introduction of density dependent flow will cause an increase in both the lengths and breakthrough times of the flow paths from repository depth, however the increase is not necessarily significant when considering the combined uncertainty in hydraulic conductivity and porosity of the flow domain.

Repository positions with large flow path lengths and large breakthrough time can be found at many different places within the domain studied; this conclusion is not changed by the introduction of the transient and density dependent solution. However, when considering the 500 repository positions with the longest path lengths and the longest breakthrough times, the distribution of the positions in the density dependent model is not the same as for the other cases studied. Compared to the other cases studied, the density dependent model (Case 10) predicts that a large amount of the 500 positions with long path lengths are located in the Northwest part of the domain studied (see Figure 8-14. page 126).

A case was also studied in which a horizontal fracture zone was added to the transient and density dependent model (Case 10v2), the zone was defined at a depth of 250 m. This zone had the same permeability and porosity as the vertical fracture zones. Considering the flow situation at 2000 AD, this model (Case 10v2) demonstrates no large differences compared to the model without the horizontal zone. The flow pattern of the paths from repository depth is in general similar to the paths of the model without the horizontal zone, except that the flow path lengths and breakthrough times are larger.

As stated above, flow paths released at 2000 AD have little relevance to an actual repository, since there will be practically no release to the geosphere the first thousands of years after the closure of the repository. In order to get more useful results we have also analysed the flow field of the transient and density dependent model (Case 10) considering a flow situation representing 5000 AD. Only repository positions inside of the present shoreline

(the shoreline of 2000 AD) were included in the flow path analysis. The length and the breakthrough times of the flow paths from repository depth are approximately the same at 2000 AD and at 5000 AD. The difference is that at 5000 AD the median of the path lengths is about 10% shorter compared to at 2000 AD, and at 5000 AD the median of the path breakthrough time is about 20% shorter compared to at 2000 AD. The evolution of the shore level progress and out-flushing of saline water may be the explanation for the somewhat shorter path lengths and shorter breakthrough times at 5000 AD. The general conclusion, that repository positions with large flow path lengths or large breakthrough time can be found at many different places within the domain studied, is not changed by the flow field of 5000 AD. There are however some local changes in the distribution of the repository positions with the longest paths, in comparison to positions produced by the flow field of 2000 AD; at 5000 AD many of the positions with the longest flow paths have moved closer to the shoreline of 2000 AD (this is in line with the results of the transient fresh water model, Case 9); and many of the positions with the longest breakthrough times have moved away from the shoreline of 2000 AD (see Figure 8-16, page 129).

Flow path length and breakthrough time, relation between different cases

The hydrogeological complexity of the models representing the domain studied was increased gradually; step by step different hydrogeological entities were added to the model: local topographic undulation, regional fracture zones, lakes, clay-areas, shore-level progress, and density dependent flow. For all the studied cases, the conductivity and the porosity of the rock mass between fracture zones were the same and not changed. Considering flow paths from repository depth, the result of this procedure is presented in Figure 9-1 (page 157), as well as in Table 9-1 (page 158). As a reference case we have selected a homogeneous model that includes the local topographic undulation (Case 2). The reference case model is based on the present topography and includes the present shoreline (2000 AD). Table 9-1 presents a comparison between (i) path lengths and breakthrough times produced by the reference case, and (ii) path lengths and breakthrough times produced by other cases with increasing complexity. It is well demonstrated by Table 9-1 that the most important parameter is the local topographic undulation; without the local topographic undulation the simulated groundwater flow field will be very different. The addition of the other hydraulic entities will in comparison be of less importance.

The case without local topographic undulation is very different from the other cases, therefore in the following discussion it is not considered as a part of the chain of cases representing increasing complexity. Considering the cases with undulating topography, the path lengths tend to increase with increasing model complexity. The largest lengths take place with density dependent flow. With density dependent flow and considering the median of the flow path length distributions, the increase in median value, compared to the reference case, is within a factor of 2.0. Considering the cases with undulating topography and the models with a larger complexity than the reference case, the breakthrough times tend to be smaller than the times produced by the reference case; except for the model that includes density dependent flow. With density dependent flow and considering the median of the breakthrough time distributions, the increase in median value, compared to the reference case, is within a factor of 1.5. A comparison between the results produced by the density dependent case and an identical case solved without density dependence (both models were defined with the NAMMU code) produces an increase in the median path length by a factor of 1.5 and an increase in the median breakthrough time by a factor of 1.2 (the increase took place for the density dependent model). It should be noted that the models studied are regional models, and they do not include parameter heterogeneity on a detailed scale, such heterogeneity will increase the variance presented in Table 9-1.

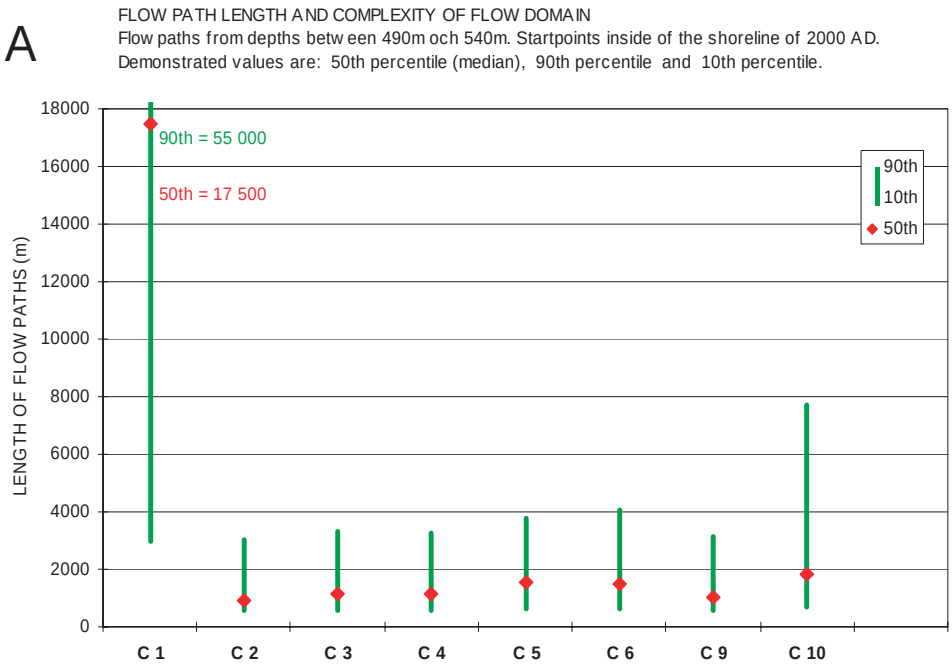

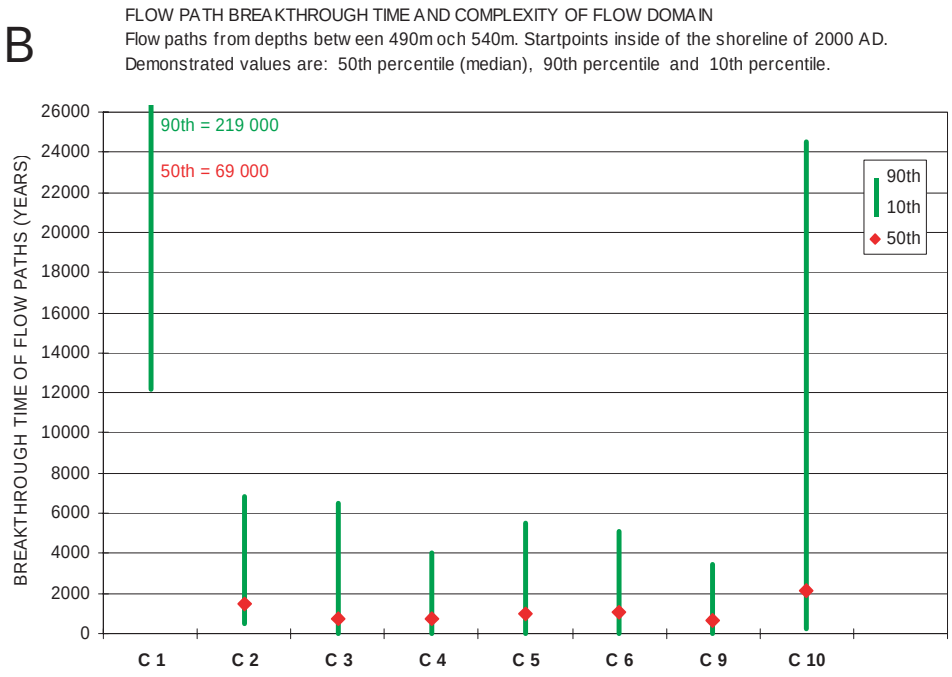

THE DIFFERENT CASES

C1 = Uniform flow medium, topography as an inclined plane.
C2 = Uniform flow medium and an undulating topography.
C3 = Uniform rock mass plus regional vertical fracture zones and undulating topography.
C4 = Uniform rock mass plus regional vertical fracture zones, undulating topography and Lakes.
C5 = Uniform rock mass plus regional vertical fracture zones and a regional sub-horizontal zone everywhere in the model at a depth of 250 m. Undulating topography.
C6 = Uniform rock mass plus regional vertical fracture zones, undulating topography, lakes and clay.
C9 = Uniform rock mass plus regional vertical fracture zones and undulating topography. Analysis of flow field at 2000 AD. Uniform density flow
C10 = Uniform rock mass plus regional vertical fracture zones and undulating topography. Analysis of flow field at 2000 AD. Density dependent flow (NAMMU).

Figure 9-1. *Flow path lengths (**A**) and breakthrough time (**B**) for different cases, the different cases represent increasing levels of complexity of the flow domain.*

Table 9-1. Comparison of path lengths and breakthrough times for the different cases.

Case [2]	Flow paths from repository depth Length distribution Factor for increase [1] Median	90th percentile	Breakthrough time distribution Factor for increase [1] Median	90th percentile
Without local topographic undulation (C1)	18.7	18.2	46.8	31.9
Reference case (C2)				
Homogeneous model.	1.0	1.0	1.0	1.0
With regional fracture zones (C3)	1.22	1.09	0.49	0.95
With regional fracture zones and 0.59 lakes (C4)	1.25	1.08	0.52	
With regional vertical fracture zones lakes and clay areas (C6)	1.59	1.34	0.70	0.75
With regional fracture zones and shore level progress (C9)	1.11	1.04	0.46	0.51
With regional fracture zones and shore level progress, and density dependent flow (C10)	1.96	2.55	1.45	3.6

[1] Factor = Parameter_of_Studied_Case / Parameter_of_Reference_Case

[2] For all the studied cases, the conductivity and the porosity of the rock mass between fracture zones were the same and not changed

Comparison of:		
- NAMMU freshwater case and	Path length distribution	Path breakthrough time distribution
- NAMMU density dependent case	Increase of the Median value of the density dependent case (2000 AD)	Increase of the Median value of the density dependent case (2000 AD)
	Factor = 1.5	Factor = 1.2

When studying the variation in path lengths and breakthrough times presented in Table 9-1, it is necessary to keep in mind the uncertainty in the parameters defining the system studied, (e.g. the uncertainty in conductivity and in porosity). The range of variation given in the table is not necessarily significant when considering the combined uncertainty of the parameters defining the system studied.

Thus, considering a regional scale and the spatial distribution of flow paths from repository depth, the most important parameters are the topography and the position of the Sea. A model used for prediction of flow path distribution needs to include the local topographic undulation, and the topography needs to be included in such detail that the model is capable of reproducing the influence that the local topographic undulation has on the groundwater flow field.

The studied models also demonstrate that repository positions at a depth of about 500 m below ground surface, with long flow path lengths and long breakthrough times for the groundwater flow from the repository to the ground surface, such repository positions may be found at many different places within the domain studied. This conclusion is based on all the different cases studied. There is no general trend that the positions with the longest paths or the longest breakthrough times are found as far as possible from the Sea.

10 References

Bear J, Verruit A, 1987. “Modeling groundwater flow and pollution”. D. Reidel publishing company, P.O.Box 17, 3300 AA Dorfrecht, Holland. ISBN 1-55608-014-X.

Bear J, Bachmat Y, 1990. “Introduction to Modeling of Transport Phenomena in Porous Media.” Kluwer Academic Publishers, Dordrecht, The Netherlands. ISBN 0-7923-0557-4

Brandt M, Jutman T, Alexanderson H, 1994. “Sveriges vattenbalans, Årsmedelvärden 1961–1990 av nederbörd, avdunstning och avrinning”, SMHI Hydrologi 49, Sveriges Meterologiska och Hydrologiska Institut, Norrköping. (In Swedish).

Carlsson L, Gustafsson G, 1984. “Provpumpning som geohydrologisk undersöknings-metod”, Rapport R41: 1984, Byggforskningsrådet. (In Swedish).

Carlsson, 1986. s 44

Carlsson L, Winberg A, Arnefors J, 1986. “Hydraulic modelling of the final repository for reactor waste (SFR). “Compilation and conceptualization of available geological and hydrological data” SKB PR SFR 86-03, Svensk Kärnbränslehantering AB.

Carlsson L, Grundfelt B, Winberg A, 1987. “Hydraulic modelling of the final repository for reactor waste (SFR). Evaluation of the groundwater flow situation at SFR“, SKB Progress Report SFR 86-07, May 1987. Svensk Kärnbränslehantering AB.

Cliffe K A, Morris S T, Porter J D, 1998. “Assessment Model Validity Document; NAMMU: A program for calculating groundwater flow and transport through porous media, SKB R-99-51”, Svensk Kärnbränslehantering AB.

Darcy H, 1856. “Les Fontaines Publiques de la Ville de Dijon”, Dalmont, Paris, France.

Fetter C W, 1993. ”Contaminant Hydrogeology”, Macmillan Publishing Company. 866 Third Avenue, New York, NY 10022 ISBN 0-02-337135-8

Gustafson G, Stanfors R, Wikberg P, 1989. “Swedish hard rock laboratory evaluation of 1988 year preinvestigations and description of the target area, the island of Äspö”. SKB TR 89-16, June 1989. Svensk Kärnbränslehantering AB.

Gylling B, Walker D, Hartley L, 1999. “Site-scale groundwater flow modelling of Beberg”, SKB TR-99-18, Svensk Kärnbränslehantering AB.

Hagconsult, 1982. “Geologiska undersökningar och utvärderingar för lokalisering av SFR till Forsmark” SFR 81-13 Del 1. Hagconsult AB, Stockholm Sweden (In swedish).

Hartley L, Boghammar A, Grundfelt B, 1998. Investigation of the large-scale regional hydrogeological situation at Beberg**,** SKB TR-98-24, Svensk Kärnbränslehantering AB.

Holmén J G, 1992. “A three-dimensional finite difference model for calculation of flow in the saturated zone”, Department of quaternary geology, Uppsala University, Uppsala, Sweden, ISBN 91-7376-119-2, ISSN 0348-2979.

Holmén J G, 1997. ”On the flow of groundwater in closed tunnels. Generic hydrogeological modelling of nuclear waste repository, SFL 3-5”, TR 97-10, Svensk Kärnbränslehantering AB.

Holmén J G, Stigsson M, 2001. “Modelling of Future Hydrogeological Conditions at SFR, Forsmark”, SKB R-01-02, Svensk Kärnbränslehantering AB.

Marsic N, Hartley L, 2000. “Modelling of the Site Scale Hydrogeological situation at Beberg Using NAMMU”, SKB R-00-14, Svensk Kärnbränslehantering AB.

Marsic N, Hartley L, Jackson C P, Poole M, 2001. “Development of Hydrogeological Modelling Tools Based on NAMMU”, SKB R-01-49, Svensk Kärnbränslehantering AB.

Marsic N, Hartley L, Jackson C P, Sanchez-Friera P, 2002. “Embedded regional/local-scale model of natural transients in saline groundwater flow illustrated using the Beberg Site”, SKB R-02-22, Svensk Kärnbränslehantering AB.

Pollock D W, 1989. “Documentation of computer program to compute and display path lines using results from the U.S. Geological survey modular three-dimensional finite difference groundwater flow model”, (Modpath manual). US Geological survey, 411 National Centre Reston, VA 22092, USA.

Press W, Teukolsky S, Vetterling W, Flannery B, 1992. “Numerical recipes in fortran. The art of scientific computing” (second edition), Cambridge University Press, ISBN 0-521-43064-X.

Påsse T, 1996. “A mathematical model of the shore level displacement in Fennoscandia”, SKB TR 96-24, Svensk Kärnbränslehantering AB.

SKB, 1993. “Slutförvar för radioaktivt driftavfall – SFR2. Slutlig säkerhetsrapport. Reviderad utgåva – Maj 1993”, (SKB Final repository for radioactive waste – SFR1. Final safety report. Revised edition – May 1993) SKB, Svensk Kärnbränslehantering AB.

SMHI, 1999. Data provided by SMHI through the internet:
http://www.smhi.se/sgn0102/n0205/index.htm
June 2, 1999, SMHI – the Swedish Meteorological and Hydrological Institute, Norrköping.

Stigsson M, Follin S, Andersson J, 1998. “On the simulation of variable density flow at SFR, Sweden” SKB R-98-08, Svensk Kärnbränslehantering AB.

Voss C I, Andersson J, 1993. “Regional flow in the Baltic Shield During Holocene Coastal Regression. Ground Water, Vol 31, No 6.

Walker 1997. s 65

Walker D, Rhen I, Gurban I, 1997. “Summary of the hydrogeological conditions at Aberg, Beberg and Ceberg.” SKB TR-97-23, Svensk Kärnbränslehantering AB.

Walker D, Gylling B, 1999. Site-scale groundwater modelling of Ceberg, SKB TR-99-13, Svensk Kärnbränslehantering AB.

Walker et al, 1999. s 105

Wikberg P (ed). Gustafson G, Rhén I, Stanfors R, 1991. “Äspö Hard Rock Laboratory. Evaluation and conceptual modelling based on the pre-investigations 1986–1990”. SKB TR 91-22, June 1991. Svensk Kärnbränslehantering AB.

Appendix A

Regional topographic surface water divides and flow paths from repository depth

For this analysis, the model of Case 3 was used, as presented in Section 5.8. This analyses focus on a limited catchment area that is within the modelled domain. Regional topographic water divides define the boundaries and extension of catchment area studied. A part of the boundary of the catchment area studied (25%), is along the outer boundary of the modelled domain. Hence, no flow will take place across this boundary as it is defined as a no-flow boundary in the model. The rest of the boundary of the catchment area (75%) is fully inside the model domain, and the cells along this part of the boundary are defined as continuous, and the flow directions of these cells are not restricted by any boundary condition.

In the fist analysis, flow paths were released in all cells at repository depth, inside the catchment area studied. The release was area weighted; hence the number of paths released per unit area is constant. The resulting flow paths are presented below in FigureA.1.

Figure A-1 demonstrates that very few flow paths will cross the regional topographic water divides.

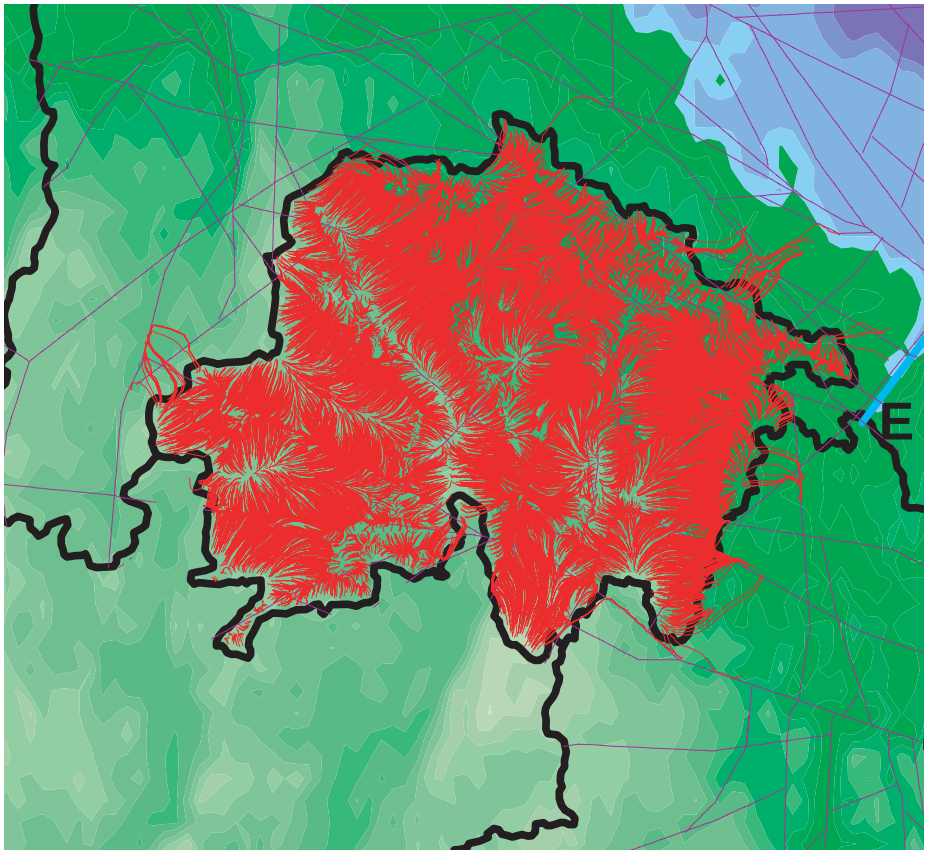

Figure A-1.

In the second analysis flow paths were released, at repository depth, in all cells along the boundary of the catchment area studied (along regional topographic water divides). The release was area weighted; hence the number of paths released per unit area is constant. The resulting flow paths are presented below in Figure A-2.

Figure A-2 demonstrates the following. Flow paths released along the regional topographic water divides are not bounded by the catchment area, such flow paths can be directed into or out of the catchment area.

We conclude. For the analysed model and when considering groundwater flow paths from repository depth, regional topographic water divides are efficient boundaries for these flow paths. Only a very small amount of the studied groundwater flow paths crosses the water divides and leaves the catchment area as a groundwater flow.

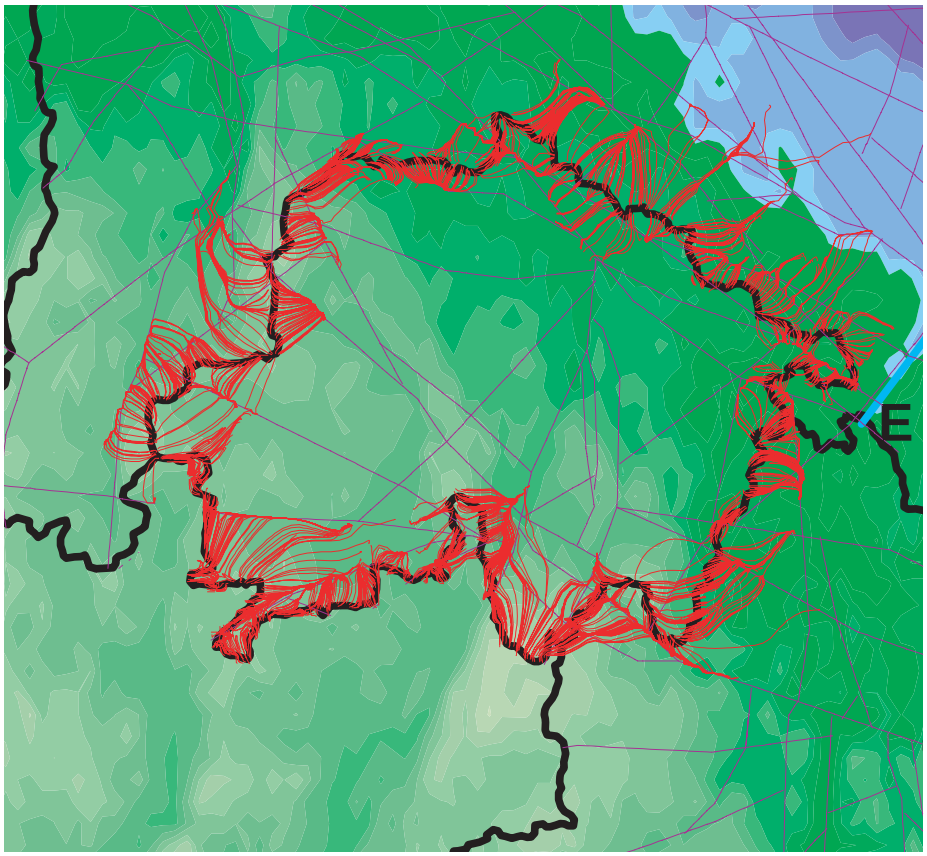

Figure A-2.